

NTIS # PB2015-

SSC-472

**SURVIVABILITY OF HULL GIRDER
IN DAMAGED CONDITION**



This document has been approved
For public release and sale; its
Distribution is unlimited

SHIP STRUCTURE COMMITTEE
2015

Ship Structure Committee

RDML Paul F. Thomas
U. S. Coast Guard Assistant Commandant,
for Prevention Policy
Co-Chair, Ship Structure Committee

Mr. H. Paul Cojeen
Society of Naval Architects and Marine Engineers

Mr. Kevin Kohlmann
Director, Office of Ship Construction
Maritime Administration

Mr. Kevin Baetsen
Director of Engineering
Military Sealift Command

Mr. Jeffrey Lantz,
Director, Commercial Regulations and Standards
U.S. Coast Guard

Mr. Albert Curry
Deputy Assistant Commandant for Engineering and
Logistics – U.S. Coast Guard

RDML Bryant Fuller
Chief Engineer and Deputy Commander
For Naval Systems Engineering (SEA05)
Co-Chair, Ship Structure Committee

Mr. Howard Fireman
Senior Vice President
American Bureau of Shipping

Ms. Julie Gascon
Executive Director, Domestic Vessel Regulatory
Oversight and Boating Safety, Transport Canada

Dr. Neil Pegg
Group Leader - Structural Mechanics
Defence Research & Development Canada - Atlantic

Mr. Matthew Garner
Director, Structural Integrity and Performance Division
Naval Sea Systems Command

Dr. Paul Hess
Director, Ship Systems and Engineering Research
Division
Office of Naval Research

SHIP STRUCTURE SUB-COMMITTEE

AMERICAN BUREAU OF SHIPPING (ABS)

Mr. Craig Bone
Mr. Daniel LaMere
Mr. Richard Delpizzo

MARITIME ADMINISTRATION (MARAD)

Mr. Chao Lin
Mr. Richard Sonnenschein
Mr. Todd Ripley
Mr. Todd Hiller

NAVSEA/NSWCCD

Mr. David Qualley
Mr. Gerard Mercier
Mr. Dean Schleicher

UNITED STATES COAST GUARD (CVE)

CAPT Ben Hawkins
Mr. Jaideep Sirkar
Mr. Charles Rawson

UNITED STATES COAST GUARD (ELC)

CAPT
Mr. Timothy McAllister
Mr. Chris Cleary

DEFENCE RESEARCH & DEVELOPMENT CANADA

ATLANTIC (DRDC)

Mr. Malcolm Smith
Mr. Cameron Munro
Dr. Layton Gilroy

MILITARY SEALIFT COMMAND (MSC)

TRANSPORT CANADA

Mr. Bashir Ahmed Golam

SOCIETY OF NAVAL ARCHITECTS AND MARINE ENGINEERS (SNAME)

Mr. Rick Ashcroft
Dr. Roger Basu
Dr. Robert Sielski
Mr. Paul H. Miller

OFFICE OF NAVAL RESEARCH (ONR)

Dr. Paul Hess
Dr. Roshdy Barsoum

Member Agencies:

*American Bureau of Shipping
Defence Research and Development Canada
Maritime Administration
Military Sealift Command
Naval Sea Systems Command
Office of Naval Research
Society of Naval Architects & Marine Engineers
Transport Canada
United States Coast Guard*



Address Correspondence to:

COMMANDANT (CG-ENG-2/SSC)
ATTN (EXECUTIVE DIRECTOR/SHIP
STRUCTURE COMMITTEE)
US COAST GUARD
2703 MARTIN LUTHER KING JR. AVE SE
WASHINGTON DC 20593-7509
Website: <http://www.shipstructure.org>

SSC – 472
SR – 1473

November 17, 2015

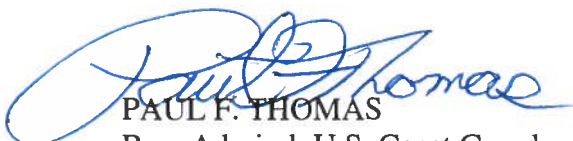
SURVIVABILITY OF HULL GIRDER IN DAMAGED CONDITION

Catastrophic hull girder collapse is considered to be one of the most critical failure modes for many ship types. It usually occurs suddenly with severe consequences such as loss of life, environmental pollution, and significant financial losses. While intact hull girder ultimate strength has been well studied, advanced analysis of damaged condition residual strength is scarce.

This project assesses the hull girder vertical bending moment ultimate capacity in a large number of systematically varied damage conditions due to collision or grounding, using state-of-the-art nonlinear finite element analysis (NLFEA), as well as identifies the most suitable modeling and analysis techniques. NLFEA is generally considered as the most sophisticated and time-consuming method for ultimate strength calculations. It accounts for material and geometric nonlinearities and has the ability to correctly represent the load redistribution in the structure undergoing collapse. NLFEA is very challenging due to the number of different parameters that have to be accurately controlled during the analysis in order to achieve a stable solution. In this study, the two-hold computer aided design (CAD) and finite element (FE) models of four vessels were generated: floating production, storage, and offloading vessel (FPSO), tanker, bulk carrier, and containership.

A total of eight intact and 266 residual strength analyses were conducted on the two hold models of the four selected vessels for systematically varied damage type, damage size, damage location, and the vertical bending moment direction. The guidance provided in this report is useful for avoiding needless repetition of the NLFE analyses. This very large collection of ultimate strength results can be used to calibrate the Rule residual strength requirements, or to validate more efficient methods. It can also be used to quickly estimate the ultimate strength reduction factor of a vessel, based on its type and damage parameters.

We thank the authors and Project Technical Committee for their dedication and research toward completing the objectives and tasks detailed throughout this paper and continuing the Ship Structure Committee's mission to enhance the safety of life at sea.



PAUL F. THOMAS
Rear Admiral, U.S. Coast Guard
Co-Chairman, Ship Structure Committee



L. BRYANT FULLER
Rear Admiral, U.S. Navy
Co-Chairman, Ship Structure Committee

1. Report No. SSC - 472	2. Government Accession No.	3. Recipient's Catalog No.	
4. Title and Subtitle SURVIVABILITY OF HULL GIRDER IN DAMAGED CONDITION		5. Report Date 11/17/2015	
		6. Performing Organization Code	
7. Author(s) Martin Petričić		8. Performing Organization Report No. SR-1473	
9. Performing Organization Name and Address American Bureau of Shipping 16855 Northchase Drive, Houston, TX 77060 USA		10. Work Unit No. (TRAIS)	
		11. Contract or Grant No.	
12. Sponsoring Agency Name and Address COMMANDANT (CG-ENG-2/SSC) ATTN (SHIP STRUCTURE COMMITTEE) US COAST GUARD 2703 MARTIN LUTHER KING, JR. AVE. SE STOP 7509 WASHINGTON DC 20593-7509		13. Type of Report Final Report	
		14. Sponsoring Agency Code CG- 5P	
15. Supplementary Notes Sponsored by the Ship Structure Committee and its member agencies. Reviewed by designated Project Technical Committee.			
16. Abstract Nonlinear finite element analysis (NLFEA) has been used to investigate the reduction of ultimate vertical bending moment capacity of a vessel following damage due to collision and grounding. Two-hold (2-H) computer aided design (CAD) and finite element (FE) models of four vessels have been generated: single hull floating production, storage, and offloading (FPSO) vessel, double hull Suezmax tanker, 180,000 DWT bulk carrier, and 8500 TEU containership. One bay (1-B) FE model of the FPSO has also been generated and used in the sensitivity study with respect to model and analysis parameters. A total of eight intact and 266 residual strength analyses have been conducted on the 2-H models of the four selected vessels for systematically varied damage type, damage size, damage location, and the vertical bending moment direction. On average, one such analysis took 15 hours to complete on a cluster with 20 processor cores. The guidance provided in this report is useful for avoiding needless repetition of NLFE analyses because of the modeling that did not fit the problem. All the NLFEA results have been presented in graphic and tabular fashions. This very large collection of ultimate strength results can be used to calibrate the Rule residual strength requirements, or to validate more efficient methods. It can also be used to quickly estimate the ultimate strength reduction factor of a vessel, based on its type and damage parameters.			
17. Key Words Nonlinear finite element analysis, residual strength, ultimate strength, collision, grounding, FPSO, tanker, bulk carrier, containership, beam theory, idealized structural unit method, Smith Method		18. Distribution Statement National Technical Information Service U.S. Department of Commerce Springfield, VA 22151 Ph. (703) 487-4650 / www.ntis.gov	
19. Security Classif. (of this report) Unclassified	20. Security Classif. (of this page) Unclassified	21. No. of Pages 146	22. Price

CONVERSION FACTORS
(Approximate conversions to metric measures)

To convert from	to	Function	Value
LENGTH			
inches	meters	divide	39.3701
inches	millimeters	multiply by	25.4000
feet	meters	divide by	3.2808
VOLUME			
cubic feet	cubic meters	divide by	35.3149
cubic inches	cubic meters	divide by	61,024
SECTION MODULUS			
inches ² feet	centimeters ² meters	multiply by	1.9665
inches ² feet	centimeters ³	multiply by	196.6448
inches ³	centimeters ³	multiply by	16.3871
MOMENT OF INERTIA			
inches ² feet ²	centimeters ² meters ²	divide by	1.6684
inches ² feet ²	centimeters ⁴	multiply by	5993.73
inches ⁴	centimeters ⁴	multiply by	41.623
FORCE OR MASS			
long tons	tonne	multiply by	1.0160
long tons	kilograms	multiply by	1016.047
pounds	tonnes	divide by	2204.62
pounds	kilograms	divide by	2.2046
pounds	Newtons	multiply by	4.4482
PRESSURE OR STRESS			
pounds/inch ²	Newtons/meter ² (Pascals)	multiply by	6894.757
kilo pounds/inch ²	mega Newtons/meter ² (mega Pascals)	multiply by	6.8947
BENDING OR TORQUE			
foot tons	meter tons	divide by	3.2291
foot pounds	kilogram meters	divide by	7.23285
foot pounds	Newton meters	multiply by	1.35582
ENERGY			
foot pounds	Joules	multiply by	1.355826
STRESS INTENSITY			
kilo pound/inch ² inch ^{1/2} (ksi ^{1/2} /in)	mega Newton MNm ^{3/2}	multiply by	1.0998
J-INTEGRAL			
kilo pound/inch	Joules/mm ²	multiply by	0.1753
kilo pound/inch	kilo Joules/m ²	multiply by	175.3

TABLE OF CONTENTS

TABLE OF CONTENTS	I
LIST OF FIGURES	III
LIST OF TABLES	VII
1. INTRODUCTION.....	1
1.1 Project Background	1
1.2 Scope of Work.....	2
1.3 Scope of the Report	3
2. ULTIMATE STRENGTH CALCULATIONS	5
2.1 Available Methods	5
2.1.1 Simple Beam Theory Method.....	5
2.1.2 Presumed Stress Distribution Method	6
2.1.3 Idealized Structural Unit Method (ISUM) and Smith Method	8
2.1.4 Intelligent Supersize FEM (IS FEM).....	11
2.1.5 Nonlinear Finite Element Analysis (NLFEA)	11
2.2 HGUS under Combined Loads	13
3. RULE REQUIREMENTS FOR RESIDUAL STRENGTH	15
3.1 IACS Requirements.....	15
3.1.1 Damage Extent.....	16
4. NLFEA.....	19
4.1 Iterative Solution Process for Static NLFEA	19
4.1.1 The Newton-Raphson (N-R) Iteration Algorithm.....	20
4.1.2 Riks Iteration Algorithm (Arc Length Method).....	22
4.2 Types of NLFEA for the Ultimate Strength Calculations.....	23
4.2.1 Static Analysis	23
4.2.2 Quasi-Static Analysis	24
4.2.3 Dynamic Analysis.....	25
4.3 Iterative Solution Algorithms.....	25
4.4 Incremental Loading Process	25
4.4.1 Curvature Control	26
4.4.2 Moment Control.....	26

4.5	Loads and Boundary Conditions	27
4.6	Geometric Imperfections.....	29
4.7	Material Properties	30
4.8	Fracture Modeling.....	31
4.9	Meshing.....	32
4.10	Element Types	33
4.11	3-D CAD Modeling.....	34
5.	SENSITIVITY STUDY	38
5.1	Analysis Type and Time Integration Scheme Sensitivity	38
5.2	Load Control	40
5.3	Iteration Algorithm and Element Type Sensitivity	43
5.4	Conclusion and Final Choice of Analysis Parameters	43
6.	PHASE II RESULTS.....	46
6.1	Damage Cases	46
6.2	Results of NLFEA.....	53
6.2.1	Intact Condition	53
6.2.2	Damage Cases.....	56
6.2.3	A Note on the Buckling Capacity of Stiffeners	75
6.2.4	The Ultimate Strength Reduction Factor	77
6.2.5	Effect of the Longitudinal Damage Extent.....	92
6.2.6	Effect of the Longitudinal Position of the Damage	94
6.2.7	Effect of the Transverse Position of the Damage	95
7.	SUMMARY AND CONCLUSIONS	96
7.1	Recommendations for Future Work.....	97
8.	REFERENCES.....	98
9.	APPENDIX.....	100
9.1	FPSO – Collision Damage (Sagging)	100
9.2	FPSO – Collision Damage (Hogging).....	102
9.3	FPSO – Grounding Damage (Hogging).....	104
9.4	FPSO – Grounding Damage (Sagging).....	106
9.5	Tanker – Collision Damage (Sagging - 1WF)	108
9.6	Tanker – Collision Damage (Sagging - 3WF)	110
9.7	Tanker – Collision Damage (Sagging - ALL WF).....	112
9.8	Tanker – Collision Damage (Hogging - 3WF).....	114

9.9	Tanker – Grounding Damage (Hogging)	116
9.10	Tanker – Grounding Damage (Sagging)	118
9.11	Bulk Carrier – Collision Damage (Sagging)	120
9.12	Bulk Carrier – Collision Damage (Hogging)	122
9.13	Bulk Carrier – Grounding Damage (Hogging).....	124
9.14	Bulk Carrier – Grounding Damage (Sagging).....	126
9.15	Containership – Collision Damage (Sagging).....	128
9.16	Containership – Collision Damage (Hogging).....	130
9.17	Containership – Grounding Damage (Hogging)	132
9.18	Containership – Grounding Damage (Sagging).....	134

LIST OF FIGURES

Figure 1: Caldwell’s presumed bending stress distribution at the ultimate limit state. N.A. is the neutral axis and D_B is the double bottom extent. Collapsed section is in compression, while the yielded section is in tension. Figure has been taken from [7].....	6
Figure 2: Presumed bending stress distribution at the ultimate limit state according to Paik and Mansour. The subscripts U , Y , E denote the ultimate strength, yielding, and elastic region, respectively. Figure has been taken from [7].	7
Figure 3: An example of structural discretization of the cross section into idealized stiffener element and hard corner units. Figure has been taken from [2].	9
Figure 4: An example of a load-end shortening curve for beam column buckling. Figure has been taken from [2].....	9
Figure 5: Flow chart of the incremental-iterative procedure. Figure has been taken from [2].....	10
Figure 6: Screenshot from the ALPS/Hull software based on IS FEM. Figure has been taken from http://www.maestromarine.com/alps-hull.php	11
Figure 7: Interframe collapse of a single hull FPSO in sagging condition analyzed using NLFEA.....	12
Figure 8: IACS CSR damage extent for collision and grounding	17
Figure 9: Schematic of the Newton-Raphson iteration (Figure taken from [7]).	21
Figure 10: Schematic of the Quasi Newton-Raphson iteration (Figure taken from [7]).	22
Figure 11: Schematic of the Riks iteration (Figure taken from [7]).	23
Figure 12: Boundary conditions for moment control.	28
Figure 13: Boundary conditions for curvature control.	29
Figure 14: Details of the geometric imperfections applied on the FPSO (magnification = 94x)	30
Figure 15: Bilinear isotropic hardening material model.....	31
Figure 16: Transition between finer and coarse mesh (Suezmax tanker).....	33

Figure 17: 2-H CAD model of the FPSO	34
Figure 18: 2-H CAD model of the Suezmax tanker	34
Figure 19: 2-H CAD model of the bulk carrier	35
Figure 20: 2-H CAD model of the containership	35
Figure 21: 1-B CAD models.....	36
Figure 22: TBHD submodel illustrating many intersecting plates and beams (encircled with red). Geometric consistency and accuracy has to be maintained while modeling. ..	36
Figure 23: Assembly of the 2-H model	37
Figure 24: Sensitivity of NLFEA results with respect to analysis type. Curvature control has been applied in all three runs.....	39
Figure 25: Ratio of kinetic and internal energies for implicit and explicit analyses	40
Figure 26: Von Mises stresses in $[N/cm^2]$ at the last increment of the static analysis	41
Figure 27: Deck stiffener tripping and “pitched roof” plate configuration	41
Figure 28: Sensitivity of time integration scheme and loading control for S4 shell elements	42
Figure 29: Sensitivity of time integration scheme and loading control for S4R shell elements	42
Figure 30: Sensitivity of iteration algorithm and element type. All simulations have been performed using quasi-static implicit analysis with curvature control.	43
Figure 31: Comparison between the quasi-static explicit NLFEA and the linear static analysis (intact bulk carrier in hogging 2-H model)	44
Figure 32: Transverse damage extents for the FPSO	50
Figure 33: Transverse damage extents for the Suezmax tanker	51
Figure 34: Longitudinal damage extents	51
Figure 35: Longitudinal variation of the damage on a tanker with D10 collision damage	52
Figure 36: Transverse variation of the damage on a tanker with grounding damage.....	52
Figure 37: FPSO intact moment-curvature curves	54
Figure 38: Tanker intact moment-curvature curves.....	54
Figure 39: Bulk carrier intact moment-curvature curves.....	55
Figure 40: Containership intact moment-curvature curves.....	55
Figure 41: Intact FPSO in sagging.....	64
Figure 42: FPSO with D3 collision damage in sagging. Two narrow failure domains stemming from the damage corners can be observed.	65
Figure 43: FPSO with D3 collision damage in sagging. Deck is viewed from below. ...	65
Figure 44: Intact tanker in hogging. The model has been cut to reveal the damage to bottom and inner bottom stiffened panels.....	66
Figure 45: Tanker with D14 grounding damage in hogging.	66
Figure 46: Tanker with D16 grounding damage in hogging.	67
Figure 47: Tanker with D5 collision damage in sagging.....	67
Figure 48: The interframe collapse mode of the intact bulk carrier in hogging	68
Figure 49: The interframe collapse mode of the bulk carrier with D8 grounding damage in hogging	68
Figure 50: The interframe collapse mode of the containership with D10 grounding damage in hogging.....	68

Figure 51: The interframe collapse mode of the containership with D5 collision damage in sagging.....	69
Figure 52: Tanker with D2 collision damage in sagging. Overall deck buckling can be observed.....	70
Figure 53: Tanker with D2 collision damage in sagging. Damaged deck web has tripped.....	70
Figure 54: Tanker with D4 collision damage in sagging. There is no overall deck buckling.....	71
Figure 55: Tanker with D4 collision damage in sagging. Damaged deck webs are completely unstressed.....	71
Figure 56: Tanker with D4 collision damage in sagging. Two types of interframe collapse are shown: stiffener tripping and gross panel buckling.....	72
Figure 57: Failure modes on damaged and intact sides of a bulk carrier with grounding damage in hogging.....	73
Figure 58: Non-interframe (left) and interframe (right) failure modes on a bulk carrier in hogging with two different damage heights.....	73
Figure 59: Non-interframe failure mode on a bulk carrier (left) and interframe failure mode on a containership (right) with grounding damage. Both damage heights are 75% of the double bottom height.....	74
Figure 60: Interframe collapse modes of the bulk carrier with collision damage in sagging.....	74
Figure 61: Failure modes on damaged and intact sides of a bulk carrier with collision damage in sagging when the damage length spans across the entire model.....	75
Figure 62: Comparison of the ultimate strength of the containership in hogging and its total Rule hogging bending moment.....	76
Figure 63: Longitudinal stresses in the x direction in the bottom of the containership at the Rule value of the total bending moment.....	76
Figure 64: Longitudinal stresses in the x direction in the bottom of the containership at the onset of buckling and yielding.....	77
Figure 65: Containership D14 (a) and D13 (b) collision cases at the sagging ultimate strength point.....	78
Figure 66: Ultimate strength reduction factor vs. damage size ratios for the FPSO.....	81
Figure 67: Ultimate strength reduction factor vs. damage size ratios for the Tanker.....	81
Figure 68: Ultimate strength reduction factor vs. damage size ratios for the Bulk Carrier.....	83
Figure 69: Ultimate strength reduction factor vs. damage size ratios for the Containership.....	85
Figure 70: FPSO – ultimate strength reduction factor vs. section modulus reduction factor.....	90
Figure 71: Tanker – ultimate strength reduction factor vs. section modulus reduction factor.....	90
Figure 72: Bulk Carrier – ultimate strength reduction factor vs. section modulus reduction factor.....	91
Figure 73: Containership – ultimate strength reduction factor vs. section modulus reduction factor.....	91
Figure 74: Tanker – Collision Damage - The effect of longitudinal damage extent.....	92

Figure 75: Tanker – D6 Collision Damage - The effect of longitudinal damage extent (each damage has sharp corners at its ends)	93
Figure 76: Tanker – D10 Collision Damage - The effect of longitudinal position of the damage	94
Figure 77: Tanker – D10 Collision Damage - The effect of longitudinal position of the damage	95
Figure 78: FPSO – Collision Damage D1-D4 (Sagging)	100
Figure 79: FPSO – Collision Damage D5-D8 (Sagging)	100
Figure 80: FPSO – Collision Damage D9-D12 (Sagging)	101
Figure 81: FPSO – Collision Damage D13-D16 (Sagging)	101
Figure 82: FPSO – Collision Damage D1-D4 (Hogging).....	102
Figure 83: FPSO – Collision Damage D5-D8 (Hogging).....	102
Figure 84: FPSO – Collision Damage D9-D12 (Hogging).....	103
Figure 85: FPSO – Collision Damage D13-D16 (Hogging).....	103
Figure 86: FPSO – Grounding Damage D1-D4 (Hogging).....	104
Figure 87: FPSO – Grounding Damage D5-D8 (Hogging).....	104
Figure 88: FPSO – Grounding Damage D9-D12 (Hogging).....	105
Figure 89: FPSO – Grounding Damage D13-D16 (Hogging).....	105
Figure 90: FPSO – Grounding Damage D1-D4 (Sagging).....	106
Figure 91: FPSO – Grounding Damage D5-D8 (Sagging).....	106
Figure 92: FPSO – Grounding Damage D9-D12 (Sagging).....	107
Figure 93: FPSO – Grounding Damage D13-D16 (Sagging).....	107
Figure 94: Tanker – Collision Damage D1-D4 (Sagging - 1WF longitudinal extent) ..	108
Figure 95: Tanker – Collision Damage D5-D8 (Sagging - 1WF longitudinal extent) ..	108
Figure 96: Tanker – Collision Damage D9-D12 (Sagging - 1WF longitudinal extent)	109
Figure 97: Tanker – Collision Damage D13-D16 (Sagging - 1WF longitudinal extent)	109
Figure 98: Tanker – Collision Damage D1-D4 (Sagging - 3WF longitudinal extent) ..	110
Figure 99: Tanker – Collision Damage D5-D8 (Sagging - 3WF longitudinal extent) ..	110
Figure 100: Tanker – Collision Damage D9-D12 (Sagging - 3WF longitudinal extent)	111
Figure 101: Tanker – Collision Damage D13-D16 (Sagging - 3WF longitudinal extent)	111
Figure 102: Tanker – Collision Damage D1-D4 (Sagging - ALL WF longitudinal extent)	112
Figure 103: Tanker – Collision Damage D5-D8 (Sagging - ALL WF longitudinal extent)	112
Figure 104: Tanker – Collision Damage D9-D12 (Sagging - ALL WF longitudinal extent)	113
Figure 105: Tanker – Collision Damage D13-D16 (Sagging - ALL WF longitudinal extent)	113
Figure 106: Tanker – Collision Damage D1-D4 (Hogging - 3WF longitudinal extent)	114
Figure 107: Tanker – Collision Damage D5-D8 (Hogging - 3WF longitudinal extent)	114
Figure 108: Tanker – Collision Damage D9-D12 (Hogging - 3WF longitudinal extent)	115

Figure 109: Tanker – Collision Damage D13-D16 (Hogging - 3WF longitudinal extent)	115
Figure 110: Tanker – Grounding Damage D1-D4 (Hogging)	116
Figure 111: Tanker – Grounding Damage D5-D8 (Hogging)	116
Figure 112: Tanker – Grounding Damage D9-D12 (Hogging)	117
Figure 113: Tanker – Grounding Damage D13-D16 (Hogging)	117
Figure 114: Tanker – Grounding Damage D1-D4 (Sagging)	118
Figure 115: Tanker – Grounding Damage D5-D8 (Sagging)	118
Figure 116: Tanker – Grounding Damage D9-D12 (Sagging)	119
Figure 117: Bulk Carrier – Collision Damage D1-D4 (Sagging)	120
Figure 118: Bulk Carrier – Collision Damage D5-D8 (Sagging)	120
Figure 119: Bulk Carrier – Collision Damage D9-D12 (Sagging)	121
Figure 120: Bulk Carrier – Collision Damage D13-D16 (Sagging)	121
Figure 121: Bulk Carrier – Collision Damage D1-D4 (Hogging)	122
Figure 122: Bulk Carrier – Collision Damage D5-D8 (Hogging)	122
Figure 123: Bulk Carrier – Collision Damage D9-D12 (Hogging)	123
Figure 124: Bulk Carrier – Collision Damage D13-D16 (Hogging)	123
Figure 125: Bulk Carrier – Grounding Damage D1-D4 (Hogging)	124
Figure 126: Bulk Carrier – Grounding Damage D5-D8 (Hogging)	124
Figure 127: Bulk Carrier – Grounding Damage D9-D12 (Hogging)	125
Figure 128: Bulk Carrier – Grounding Damage D13-D16 (Hogging)	125
Figure 129: Bulk Carrier – Grounding Damage D1-D4 (Sagging)	126
Figure 130: Bulk Carrier – Grounding Damage D5-D8 (Sagging)	126
Figure 131: Bulk Carrier – Grounding Damage D9-D12 (Sagging)	127
Figure 132: Containership – Collision Damage D1-D2 (Sagging)	128
Figure 133: Containership – Collision Damage D5-D6 (Sagging)	128
Figure 134: Containership – Collision Damage D9-D10 (Sagging)	129
Figure 135: Containership – Collision Damage D13-D14 (Sagging)	129
Figure 136: Containership – Collision Damage D1-D2 (Hogging)	130
Figure 137: Containership – Collision Damage D5-D6 (Hogging)	130
Figure 138: Containership – Collision Damage D9-D10 (Hogging)	131
Figure 139: Containership – Collision Damage D13-D14 (Hogging)	131
Figure 140: Containership – Grounding Damage D1-D4 (Hogging)	132
Figure 141: Containership – Grounding Damage D5-D8 (Hogging)	132
Figure 142: Containership – Grounding Damage D9-D12 (Hogging)	133
Figure 143: Containership – Grounding Damage D13-D16 (Hogging)	133
Figure 144: Containership – Grounding Damage D1-D4 (Sagging)	134
Figure 145: Containership – Grounding Damage D5-D8 (Sagging)	134
Figure 146: Containership – Grounding Damage D9-D12 (Sagging)	135

LIST OF TABLES

Table 1: Summary of IACS CSR PSFs for damaged ships	16
Table 2: IACS CSR collision and grounding damage extent parameters	16

Table 3: Material properties	31
Table 4: Ultimate limit states for three analysis types	38
Table 5: DOF of the 2-H FE models in intact condition (in millions).....	46
Table 6: Analyzed cases.....	47
Table 7: Damaged case classification by damage size, vessel, damage type, and vertical bending moment direction	47
Table 8: Summary of NLFEA results for FPSO	56
Table 9: Summary of NLFEA results for Tanker	58
Table 10: Summary of NLFEA results for Bulk Carrier	60
Table 11: Summary of NLFEA results for Containership	62
Table 12: Summary of ultimate bending moment capacity in [GNm] for FPSO	85
Table 13: Summary of ultimate strength reduction factor (<i>USRF</i>) for FPSO	86
Table 14: Summary of ultimate bending moment capacity in [GNm] for Tanker	87
Table 15: Summary of ultimate strength reduction factor (<i>USRF</i>) for Tanker.....	87
Table 16: Summary of ultimate bending moment capacity in [GNm] for Bulk Carrier..	88
Table 17: Summary of ultimate strength reduction factor (<i>USRF</i>) for Bulk Carrier	88
Table 18: Summary of ultimate bending moment capacity in [GNm] for Containership	89
Table 19: Summary of ultimate strength reduction factor (<i>USRF</i>) for Containership.....	89
Table 20: Ultimate strength values for the three variations in the longitudinal extent of the D6 collision damage.....	93
Table 21: Ultimate strength values for the three variations in the longitudinal position of the collision damage	94
Table 22: Ultimate strength values for the three variations in the transverse position of the collision damage	95

1. INTRODUCTION

1.1 Project Background

Global hull girder collapse is considered to be one of the most critical failure modes for many ship types. It usually occurs suddenly with severe consequences such as loss of life, environment pollution, and big financial losses. Catastrophic hull girder failures can happen due to:

- Severe environmental loads such as waves in a big storm
- Human error such as overloading of the ship structure with cargo
- Poor maintenance and occurrence of excessive corrosion and cracks on critical parts in the ship structure
- Collision or grounding damage after which the hull girder ultimate capacity can be severely diminished
- Inadequate hull design
- Any combination of the aforementioned causes.

Although the hull girder ultimate strength in the intact condition has been extensively studied by numerous authors, the residual strength calculations using the most advanced analysis techniques are still scarce.

The goal of this project is to assess the hull girder vertical bending moment ultimate capacity in a damaged condition (residual strength) due to collision or grounding using the state-of-the-art nonlinear finite element analysis (NLFEA). Accurate calculation of the residual strength is very important for a number of reasons including:

- Calibration of rules governing the residual strength requirements of ship hulls;
- Establishing a matrix of residual strength values for most common damage types and extents which can be used in emergency situations for rapid residual strength estimates of severely damaged ship hulls;
- Better understanding of the hull girder progressive collapse sequence;
- Validation of simple methods such as the Smith method [1].

Although the same calculation techniques can be used in both intact and damaged cases, calculation of the hull girder residual strength presents more challenges than the intact ultimate strength calculation. First, it is necessary to establish relevant damage case scenarios which include damage parameters such as damage type, size, and location. In certain cases, hydrostatic and stability analysis of the damaged vessel has to be performed in order to calculate the additional hull girder loads due to flooding and listing. Usually, the listing of the ship can be neglected as the ships will be ballasted after an accident to minimize the listing. Another difficulty associated with the residual strength calculations is the rotation of the neutral plane of the damaged cross section due to asymmetry of the structure and the loading. The neutral axis of an intact symmetric structure loaded only by the vertical bending moment is always parallel to the baseline and can only shift in the

vertical direction. However, if the structure is geometrically asymmetric (e.g. due to damage), and/or if the loading is asymmetric (e.g. horizontal bending moment is also applied along with the vertical bending moment), the neutral axis of the cross section will shift and rotate. This has to be taken into account by the analysis method. Finally, damage to the transverse structure providing support for the longitudinal structural members must be appropriately modeled.

Better understanding of the progressive collapse sequence of the damaged hull is even more important now that the new Harmonized Common Structural Rules (CSR) [2] for tankers and bulk carriers require the residual strength check.

1.2 Scope of Work

The initial work on this project started in 2014 (Phase I). It included the following tasks:

Phase I

1. Initial literature review;
2. Computer aided design (CAD) and finite element (FE) modeling of the single hull floating production, storage, and offloading (FPSO) vessel;
3. Initial ultimate strength calculations in the intact condition.

Phase I served as a starting point for a much more comprehensive current phase of the project (Phase II) which consists of the following tasks:

Phase II

Milestone	Est. Date	Status
Project Start Date	1-Sep-14	Completed
Literature review of NLFEA	15-Sep-14	Completed
Literature survey on databases of ship accidental damages	30-Sep-14	Completed
Categorize accidental damages	15-Oct-14	Completed
Select the ships for NLFEA and associated damage parameters	31-Oct-14	Completed
Build FE models of selected ships (four ships)	28-Feb-15	Completed
Perform sensitivity study of the model parameters and identify the best analysis practices	31-Mar-15	Completed
Perform NLFEA for selected ships, damage parameters, and model parameters	31-May-15	Completed
Post-process the results and assess the residual strength for each damage case	31-Jul-15	Completed
Generate the report and submit it to SSC	31-Aug-15	Completed
Project End Date	31-Aug-15	

Original project plan was to analyze three ships (single hull FPSO, double hull Suezmax tanker, and 180,000 DWT bulk carrier). However, a fourth vessel, 8500 TEU containership, has also been selected for the analysis.

1.3 Scope of the Report

- Section 1 contains basic information about the project, its background and its scope.
- Section 2 presents details about available methods for hull girder ultimate strength (HGUS) calculations in both intact and damaged conditions.
- Section 3 contains the IACS CSR Rule requirements for residual strength calculations.
- Section 4 contains an introduction to residual strength calculations using the nonlinear finite element analysis with the detailed description of various model and analysis parameters.
- Section 5 presents the results of the sensitivity study aimed at determining the best model and analysis parameters for performing the NLFEA.
- Section 6 contains the Phase II results of eight intact and 266 different damage cases for the FPSO, tanker, bulk carrier, and the containership.
- Section 7 summarizes the results and draws important conclusions.

2. Ultimate Strength Calculations

2.1 Available Methods

Currently available methods for ultimate strength calculations can be categorized in the increasing order of accuracy and complexity, as follows:

- Simple Beam Theory;
- Presumed Stress Distribution Methods [3], [4];
- Idealized Structural Unit Method [5] and Smith Method [1];
- Intelligent Supersize Finite Element Method [6];
- Nonlinear Finite Element Analysis (NLFEA) [7], [8] [9].

All of the foregoing methods will be briefly described in the subsequent subsections.

2.1.1 Simple Beam Theory Method

This method assumes that a ship hull will reach the ultimate collapse state when the maximum stress in the outermost fiber reaches the ultimate compressive strength of the compressed flange (deck in sagging or bottom in hogging). It gives the first-failure hull girder strength (e.g. the bending moment at which the first yielding or buckling of a longitudinal structural member occurs) rather than the ultimate strength.

The relationship between the bending moment and the maximum stress in the outermost fiber is assumed linear, hence

$$(1)$$

where M_U is the ultimate vertical bending moment, Z is the section modulus of the outermost fiber in question, σ_U is the ultimate compressive strength of the fiber, and k is the calibration coefficient.

Advantages:

- Extremely straight forward and computationally efficient.

Disadvantages:

- Gives the first-failure hull girder strength, rather than the true ultimate strength;
- Requires calibration against more sophisticated methods to get the k factor;
- Cannot account for complex interactions between local and global failure modes or load redistribution.

2.1.2 Presumed Stress Distribution Method

The stress distribution at the ultimate limit state is presumed over the hull cross section. Caldwell [3] first proposed such a procedure for determining the HGUS. He assumed that all the material in compression has buckled and that all the material in tension has yielded - see Figure 1.

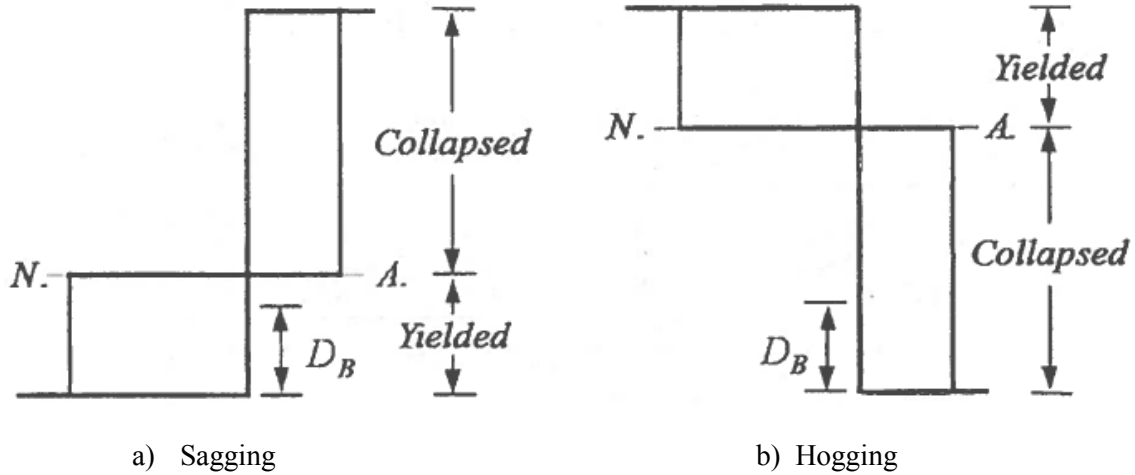


Figure 1: Caldwell's presumed bending stress distribution at the ultimate limit state. N.A. is the neutral axis and D_B is the double bottom extent. Collapsed section is in compression, while the yielded section is in tension. Figure has been taken from [7].

Paik and Mansour [4] proposed a more realistic stress distribution at the ultimate collapse state. Two stress regions were proposed for the material in tension and two for the material in compression. The outermost fiber in tension has just reached the yielding point while the rest of the material in tension is still in the elastic region. In compression there is material that is still in the elastic stage and the material that has buckled - see Figure 2.

The buckling extent can be determined by making sure the axial force on the cross section is equal to zero for pure bending

$$\int_A \sigma_x dA = 0 \quad (2)$$

The distance of the neutral axis from the baseline at collapse can then be obtained using

$$g_u = \frac{\sum_{i=1}^n |\sigma_{xi}| a_i z_i}{\sum_{i=1}^n |\sigma_{xi}| a_i} \quad (3)$$

σ_{xi} is the longitudinal stress at the i -th element of the cross section, a_i is the cross-sectional area of the i -th element, and z_i is the distance of the i -th element from the baseline. The ultimate bending moment is then calculated as the first moment of the bending stresses about the N. A.

2.1.3 Idealized Structural Unit Method (ISUM) and Smith Method

The previous two methods cannot account for the progression of hull girder failure. They can only indicate the point of first failure or the ultimate strength itself. In 1974 Ueda and Rashed [5] first proposed the Idealized Structural Unit Method capable of representing the nonlinear collapse sequence of the hull cross section. However, the method has first been applied to analyze the ultimate strength behavior of deep girders in ultimate transverse strength calculations.

ISUM assumes that the ship cross-section section can be divided into a number of idealized structural units, such as plate-stiffener and plate-plate assemblies, that behave independently. The nonlinear behavior of each idealized unit is formulated explicitly using direct force-displacement or stress-strain relationships in matrix form. The ultimate and post ultimate strength analysis is carried by summing the nonlinear behavior of each individual idealized unit as the applied force (or displacement) incrementally increases.

In 1977 Smith [1], in almost parallel development, proposed a very similar method to ISUM. Many authors do not make a distinction between the two methods; however, small differences do exist. With the Smith method, the nonlinear behavior of each unit is defined using analytical stress-strain relationships, otherwise known as load-end shortening curves, instead of direct matrix formulations. This method is otherwise known as the Incremental Iterative Method.

Almost all classification societies use Incremental Iterative Method (IIM) as one alternative to calculating the HGUS due to the vertical bending moment. Figure 3 has been taken from the new IACS CSR Rules and shows the cross-section discretization into idealized structural units. Figure 4 has also been taken from CSR Rules and shows an example of the stress-strain (load-end shortening) curve for beam column buckling. Every failure mode of the idealized structural unit has to be represented with its own load-end shortening curve. Figure 5 shows a flowchart of the Incremental Iterative Method.

Advantages:

- Computationally efficient;
- Can effectively take into account the damage to longitudinal structural members;
- Can be modified to account for the effect of the neutral axis rotation due to asymmetric loading and/or damage.

Disadvantages:

- Cannot take into account the damage to transverse structure;
- The load-end shortening curves are difficult to obtain in the closed form, especially if the effects of initial imperfections, corrosion, residual stresses, and in-service damage are to be accounted for.
- Always assumes the inter-frame failure mode.
- Cannot account for complex interactions between local and global failure modes or load redistribution.

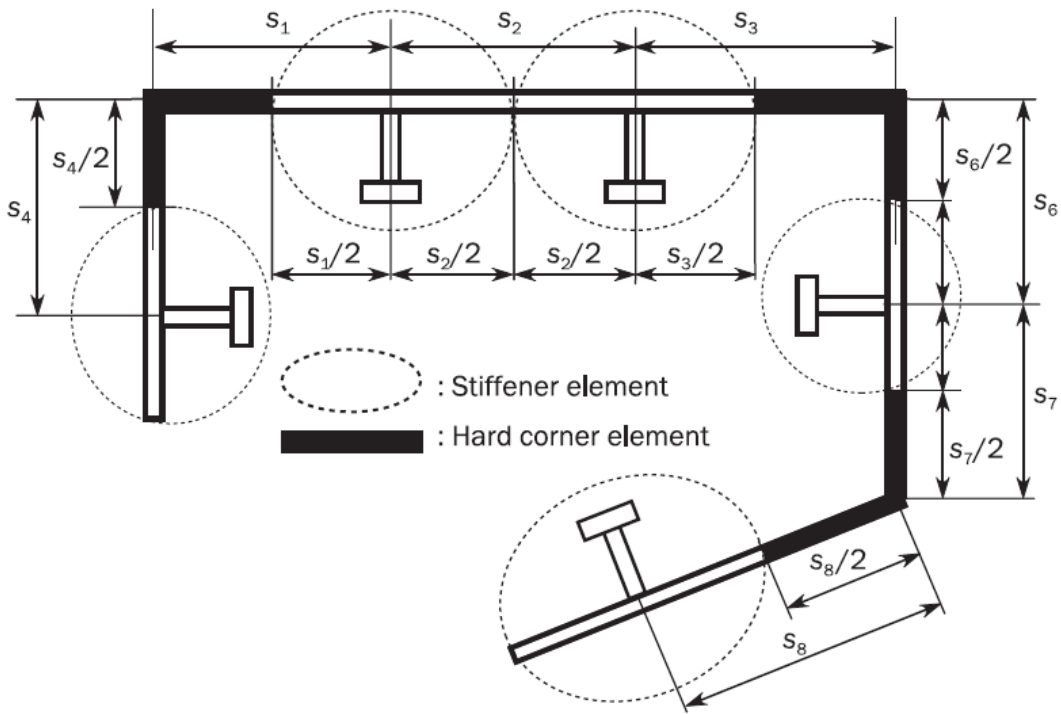


Figure 3: An example of structural discretization of the cross section into idealized stiffener element and hard corner units. Figure has been taken from [2].

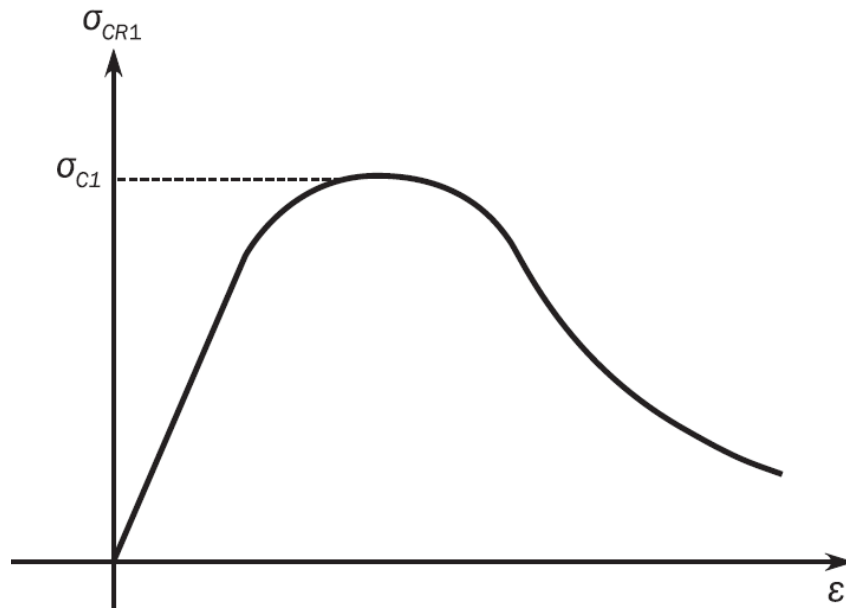


Figure 4: An example of a load-end shortening curve for beam column buckling. Figure has been taken from [2].

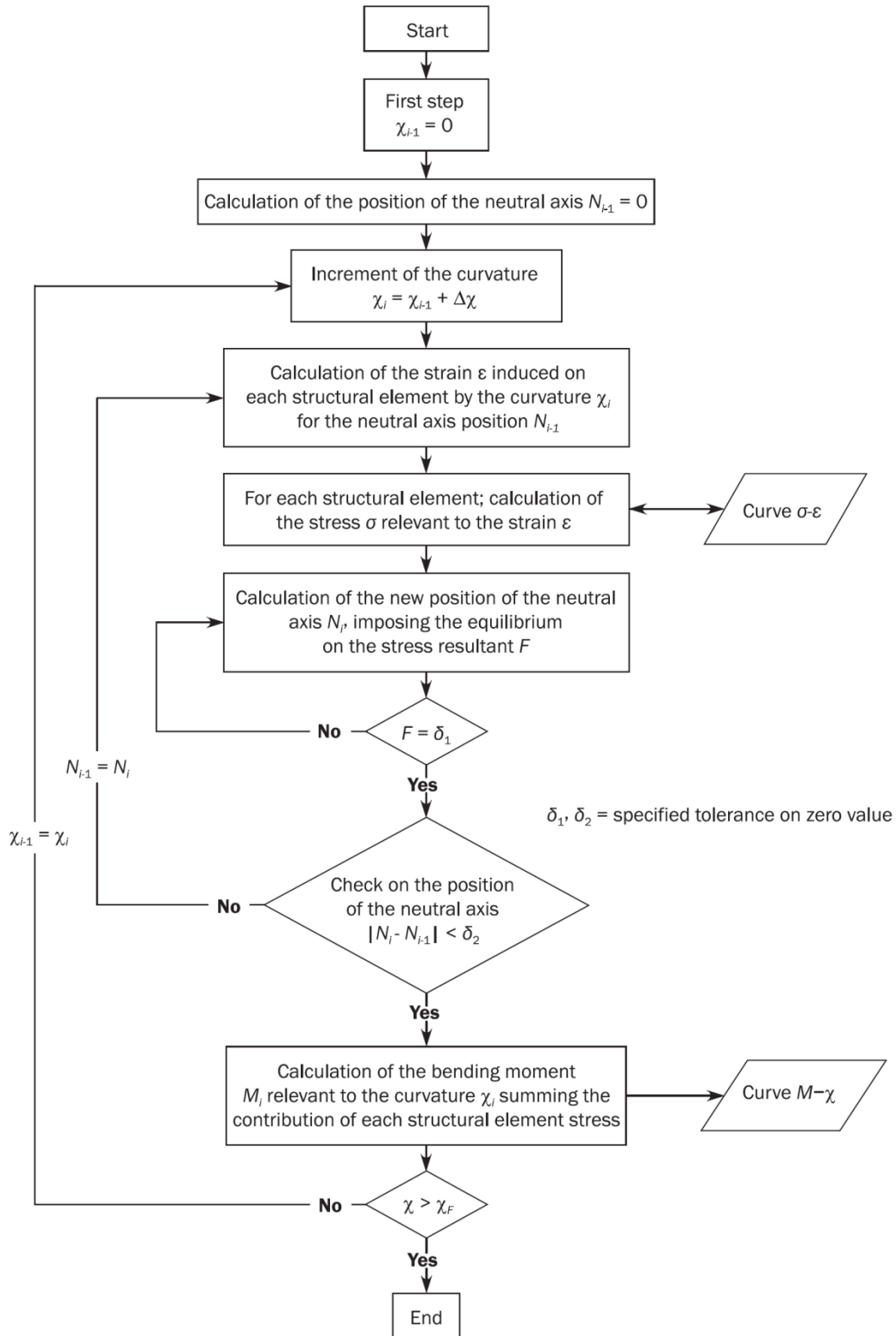


Figure 5: Flow chart of the incremental-iterative procedure. Figure has been taken from [2].

2.1.4 Intelligent Supersize FEM (IS FEM)

This numerical finite element approach, proposed by Paik [6], is similar to the NLFEA (see below) with the exception that the supersize plate and stiffener elements already include the geometric nonlinear effects of all possible failure modes depending on the geometric proportions of the elements. It accounts for the complex interactions between structural members during progressive collapse of the structure. Compared to the NLFEA, this method is much more computationally efficient, but less accurate. Figure 6 shows the screenshot from the ALPS/Hull software that implements IS FEM.

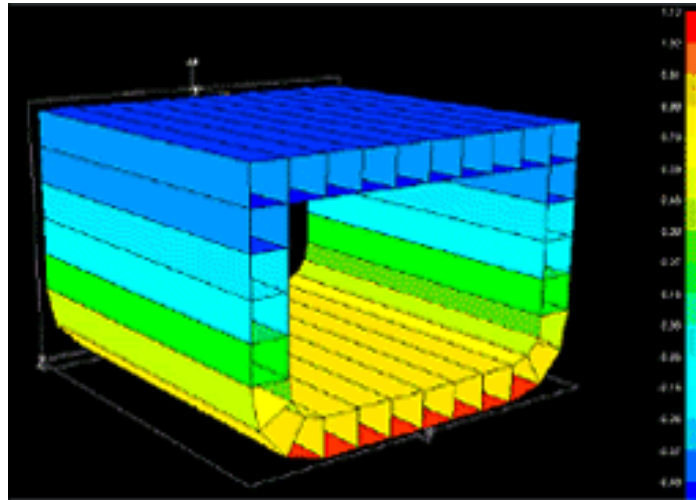


Figure 6: Screenshot from the ALPS/Hull software based on IS FEM. Figure has been taken from <http://www.maestromarine.com/alps-hull.php>

Advantages:

- It accounts for the complex interactions between structural members during progressive collapse of the structure and the load redistribution;
- Is computationally more efficient than the NLFEA;
- Can account for the damage to the hull transverse members;
- Any combination of hull girder load components can be applied.

Disadvantages:

- Less accurate than the NLFEA;
- Geometric imperfections are dealt with as parameters of influence;
- Accident induced structural damages caused by collision, grounding, fire, and explosion are dealt with as parameters of influence.

2.1.5 Nonlinear Finite Element Analysis (NLFEA)

NLFEA is the most advanced analysis technique for ultimate strength calculations (intact and residual) available today.

When using the NLFEA, it is very important to assess the adequacy of the applied modeling techniques, since the results can be very misleading if inadequate models or analysis parameters are used. Aspects of the NLFEA that have to be specially considered are:

- Fine mesh modeling of the hull outer flanges (deck or bottom);
- Modeling of potential structural damage;
- Applied loading (curvature control, moment control);
- Boundary conditions;
- Longitudinal extent of the model (full ship model, three hold model, two hold model, one hold model, two bay model, and one bay model between two transverse frames);
- Geometric imperfections;
- Type of analysis (static, dynamic – quasi-static);
- Integration scheme for quasi static analysis (implicit, explicit);
- Numerical algorithm (Newton-Raphson, quasi-Newton, Riks);
- Numerical stabilization.

All of these aspects will be described in detail in Section 4.

Sometimes the transverse frames can fail or deform significantly before the collapse of longitudinally stiffened panels between them. In that case, at least one cargo hold FE model must be used. If the effects of rotational restraints at transverse bulkheads are to be analyzed, then the three or two hold FE models have to be used.

Figure 7 shows a typical result of the NLFEA where yielding and buckling of the structural members can be observed.

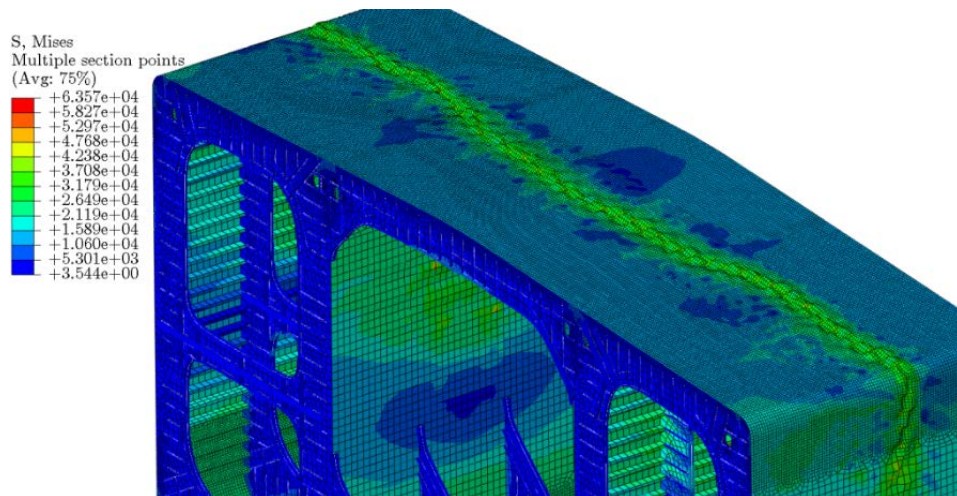


Figure 7: Interframe collapse of a single hull FPSO in sagging condition analyzed using NLFEA.

Advantages:

- It enables a refined computation of the progressive collapse behavior;
- It accounts for the interaction between the local and global failure modes;
- It accounts for both geometric and material nonlinearities.

Disadvantages:

- Requires a large effort to prepare the FE model and correctly set up the analysis parameters;
- It is very computationally intensive;
- Convergence of the analysis is not guaranteed.

2.2 HGUS under Combined Loads

Hull girder loads interact and this interaction will affect the ultimate limit state of the structure. The effects of lateral pressure should also be included where applicable (see Paik and Thayamballi [8], Paik and Thayamballi [10], Gordo and Guedes Soares [11]). Ultimate strength of the hull girder under combined loading can be represented using the so-called interaction formulae of the form

$$\left(\frac{M^v}{M_u^v F_1}\right)^{c_1} + \left(\frac{M^h}{M_u^h F_2}\right)^{c_2} = 1 \quad (5)$$

where

$$F_1 = \left[1 - \left(\frac{F^v}{F_u^v}\right)^{c_4}\right]^{\frac{1}{c_3}} \quad (6)$$

$$F_2 = \left[1 - \left(\frac{F^v}{F_u^v}\right)^{c_5}\right]^{\frac{1}{c_6}} \quad (7)$$

M_u^v, M_u^h, F_u^v are the ultimate strengths under the vertical bending moment, horizontal bending moment, and vertical shear force acting on their own. M^v, M^h, F^v are the applied vertical bending moment, horizontal moment, and vertical shear force, respectively. Big scatter in the coefficients c_1 to c_6 can be observed, depending on the author.

Interaction formulae between vertical bending moment and torsion also exist, but the interaction formulae that include the horizontal shear force have not been found in the literature.

3. Rule Requirements for Residual Strength

3.1 IACS Requirements

Only vertical bending moment is considered in residual strength calculations. Because damage usually occurs in coastal waters and the exposure time is short compared to ship's lifetime, the residual strength criteria is rarely governing for the design of the hull. The probability of failure due to capsizing or sinking is usually much greater than the probability of failure due to the progressive collapse of the hull. However, the residual strength criteria could become governing if the extent of damage is significant. That is why IACS requires residual strength assessment in the new CSR rules [2].

Two types of damage are to be considered as per IACS CSR Rules: collision and grounding. Consequently, only these two types of damage have been considered in the present study. In principle, any of the aforementioned methods for ultimate strength calculations (see Section 2) can be used to calculate the residual strength of the hull as long as the damaged structure is properly accounted for in the analysis. There is an issue of loss of support for the longitudinal members due to damaged transverse structure in which case they are no longer 100% effective. Only IS FEM and NLFEM can take into account the damage to the transverse structural members.

The residual strength is only considered with respect to the vertical bending moment. IACS Technical Background report summarizes the technical details of calculating the residual hull girder strength and of the calibration procedure for determining the partial safety factors (PSF) for the Rule residual strength calculations. It appears that only one ship has been selected to demonstrate the procedure. Ideally, more ships should be considered before proper calibration of the PSF can take place.

The residual strength criteria in the new CSR Rules is very similar to the criteria for the ultimate strength in the intact condition and is as follows

$$\gamma_{SD}M_{SW-D} + \gamma_{WD}M_{WV} \leq \frac{M_{UD}}{\gamma_{RD}C_{NA}} \quad (8)$$

where M_{SW-D} is the permissible still water bending moment (SWBM) in damaged condition, M_{WV} is the Rule defined vertical wave bending moment (WBM), M_{UD} is the ultimate vertical bending moment capacity in the damaged condition; γ_{SD} is the PSF for the still water bending moment in the damaged condition, γ_{WD} is the PSF for the vertical wave bending moment in the damaged condition, and γ_{RD} is the PSF for the vertical hull girder ultimate bending capacity in damaged condition. C_{NA} is the neutral axis coefficient. It is equal to 1.0 for grounding and 1.1 for collision. The purpose of this coefficient is to account for the translation and rotation of the neutral axis for asymmetric damage cases.

SWBM can increase or decrease due to damage. Since M_{SW-D} is equal to M_{SW} , as per CSR Rules, the value of γ_{SD} controls whether the SWBM will increase or decrease due to

damage. CSR Rules conservatively specify a single value of $\gamma_{SD} = 1.1$ regardless of the damage case (a 10% increase of the SWBM due to damage).

WBM for the residual strength analysis is usually much lower than for the intact ultimate strength analysis because damage usually occurs in the coastal areas and the exposure time is much shorter (usually one week) compared to the life of the vessel. This is controlled by $\gamma_{WD} = 0.67$ (33% reduction of the Rule defined WBM).

Partial safety factor associated with the vertical hull girder ultimate capacity in the damaged condition is to be taken as $\gamma_{RD} = 1.0$.

Table 1 summarizes the PSFs specified in the IACS CSR Rules for residual strength calculations.

Table 1: Summary of IACS CSR PSFs for damaged ships

		IACS CSR	
		Grounding	Collision
Hogging	\mathcal{G}_{SD}	1.10	1.10
	\mathcal{G}_{WD}	0.67	0.67
	\mathcal{G}_{RD}	1.00	1.00
	C_{NA}	1.00	1.10
Sagging	\mathcal{G}_{SD}	1.10	1.10
	\mathcal{G}_{WD}	0.67	0.67
	\mathcal{G}_{RD}	1.00	1.00
	C_{NA}	1.00	1.10

3.1.1 Damage Extent

When using Equation (8), M_{UD} has to be calculated for strictly defined damage cases as shown in Table 2 and Figure 8.

Table 2: IACS CSR collision and grounding damage extent parameters

	Single side	Double side		Bulk carriers	Tankers
Height: h/D	0.75	0.60	Height: h	$\min(B/20,2)$	$\min(B/15,2)$
Depth d/B	0.06	0.06	Breadth: b/B	0.60	0.60

a) Collision

b) Grounding

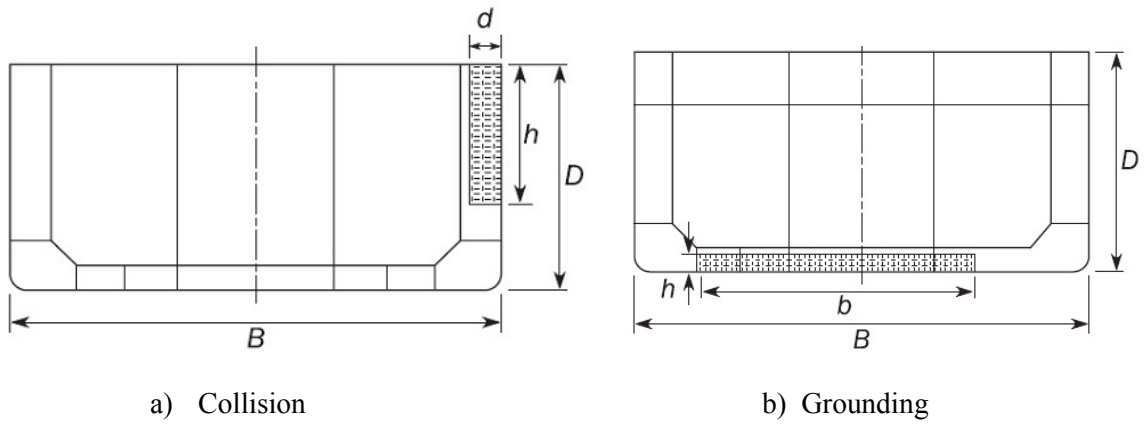


Figure 8: IACS CSR damage extent for collision and grounding

4. NLFEA

Modeling of continuum mechanics problems often leads to partial differential equations, many of which are nonlinear. A powerful tool to solve these differential equations is the finite element method which was developed over the last 50 years. Nonlinear finite element analysis (NLFEA) is considered mature enough today to be applied in daily structural design and analysis.

There are a number of different types of nonlinearities associated with structural mechanics. The main types are as follows:

- **Geometric nonlinearity** occurs in problems with large displacements and rotations where the loading on the structure becomes dependent on its response.
- **Finite deformations** can occur when the strains, as well as displacements, become large. This usually happens with materials such as rubber.
- **Material nonlinearity** occurs when the behavior of the material, characterized by its stress-strain relationship, is nonlinear.
- **Nonlinear boundary conditions** occur in problems when two bodies come into contact, or the applied loading is deformation dependent.

All of these types of nonlinearity can be addressed by the NLFEA. However, the two most important types relevant to residual strength analysis are the geometric and material nonlinearities.

The following section briefly describes the solution process for time-independent NLFEA and highlights the differences between nonlinear and linear methods. Time-dependent NLFEA that has also been used during this project will not be covered in this brief overview of the NLFEA. However, similar iterative algorithms can be used to solve time-dependent problems when implicit time integration scheme is used. Another time integration scheme that can be used to solve the time-dependent problems, called explicit scheme, does not require iterative solution process.

4.1 Iterative Solution Process for Static NLFEA

A time-independent (static) problem in finite element analysis is typically expressed by the following matrix equation

$$[K][U] = [R] \quad (9)$$

where $[K]$ is the stiffness matrix of the structure, $[U]$ is the nodal displacement vector, and $[R]$ is the nodal load vector. The stiffness matrix is a function of a structure's geometry and material properties, and if it is a constant, the problem is linear. However, if the stiffness matrix is dependent on either the displacement vector or the load vector, the problem is nonlinear and will require an iterative algorithm to solve it. That is why

the load vector has to be applied incrementally during the NLFEA and the respective stiffness matrix and displacement vector need to be calculated iteratively at each load increment. A typical residual strength analysis with post ultimate-strength analysis on a 2-hold FE model might require 400 load increments with an average of four iterations per increment. Each iteration is computationally equivalent to performing a linear FEA. This means that the NLFEA requires 1600x the CPU time of a linear FEA.

In order to describe the iterative solution process required in NLFA, one can look at a simple example of nonlinear spring loaded with axial force P . The relationship between the force P and displacement u can be given by

$$P = (k_0 + k_N)u \quad (10)$$

where $k = k_0 + k_N$ = stiffness of the nonlinear spring, k_0 = constant stiffness term, and $k_N = f(u)$ = nonlinear stiffness term that is a function of the displacement. Because Equation (10) is nonlinear in u , solving it requires an iterative process such as the Newton-Raphson method

4.1.1 The Newton-Raphson (N-R) Iteration Algorithm

This algorithm requires an incremental load application to search for the displacement solution. The increment form of Equation (10) is given by

$$\frac{dP}{du} = \frac{d}{du} [(k_0 + k_N)u] = k_0 + \frac{d}{du} (k_N u) \equiv k_t \quad (11)$$

where k_t is the tangent stiffness (see Figure 9). Point A represents the start of the load increment and point B represents its end. Points 1, 2, ... are the iterations needed to find the displacement u_B at the end of the load increment. At point A, the load can be calculated as follows

$$P_A = [k_0 + (k_N)_A]u_A \quad (12)$$

where $(k_N)_A = k_N$ at $u = u_A$.

The applied load can be linearized using the Taylor series expansion around point A

$$f(u_A + \Delta u_1) = f(u_A) + \left(\frac{dP}{du}\right)_A \Delta u_1 \quad (13)$$

where $(dP/du)_A \equiv (k_t)_A \equiv (k_t)_0$ = tangent stiffness at initial point A. Displacement increment Δu_1 at the first iteration can be computed from

$$\Delta u_1 = (k_t)_0^{-1}(P_B - P_A) \quad (14)$$

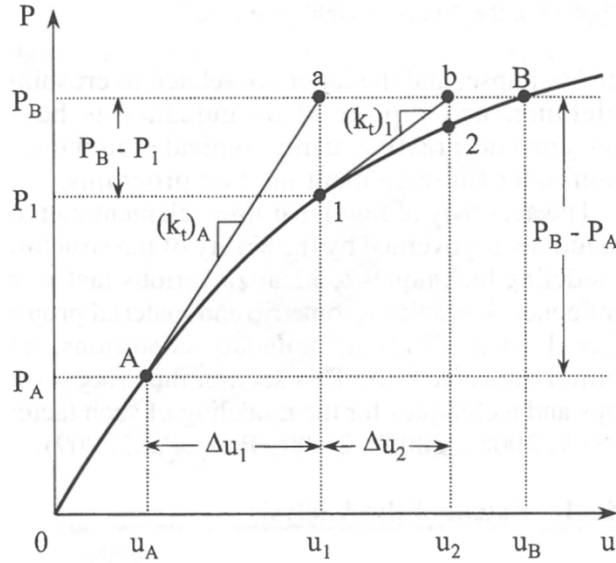


Figure 9: Schematic of the Newton-Raphson iteration (Figure taken from [7]).

with $P_B = f(u_A + \Delta u_1)$ and $P_A = f(u_A)$. The displacement after the first iteration can be determined from the following expression

$$u_1 = u_A + \Delta u_1 \quad (15)$$

Since the real force at Point 1 is P_1 , not P_B , the unbalanced force is equal to $P_B - P_1$ and further iteration is required to eliminate it. A new tangent stiffness at Point 1, $(k_t)_1$, can be obtained from Equation (11) at $u=u_1$ and the next displacement increment is then

$$\Delta u_2 = (k_t)_1^{-1}(P_B - P_1) \quad (16)$$

Iterations are repeated until the unbalanced force is less than the acceptable limit. After the i -th iteration, the displacement increment is equal to

$$\Delta u_i = (k_t)_{i-1}^{-1}(P_B - P_{i-1}) \quad (17)$$

The final displacement at the end of the load increment is computed as follows.

$$u_B = u_{i-1} + \Delta u_i \quad (18)$$

Since every iteration requires the calculation of the updated stiffness matrix, $(k_t)_i$, and its inverse, N-R method is very computationally intensive. Therefore, the Modified N-R method, also called the Quasi N-R method, does not require the tangent stiffness matrix to be updated. Instead, it uses the tangent stiffness matrix calculated at the beginning of the load increment. However, the total number of iterations needed to achieve a certain level of accuracy will be higher compared to the original N-R method. Figure 10 shows the Quasi N-R method.

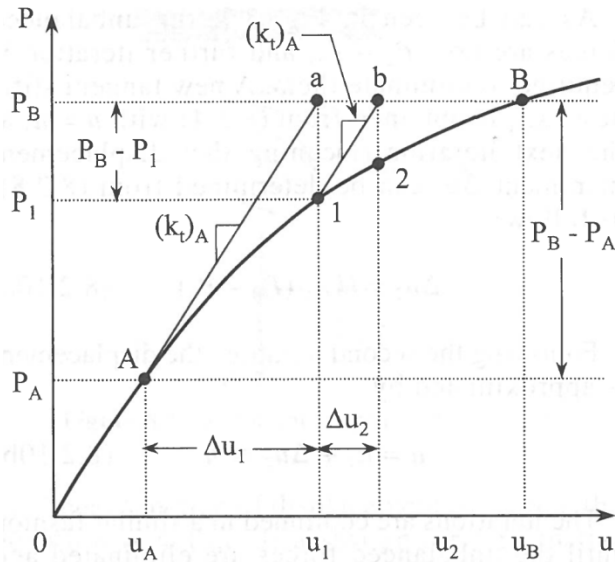


Figure 10: Schematic of the Quasi Newton-Raphson iteration (Figure taken from [7]).

4.1.2 Riks Iteration Algorithm (Arc Length Method)

In cases where the slope of the load-displacement curve becomes negative, such as in “snap through” problems, N-R algorithm breaks down and fails to converge. In such cases, Riks algorithm [12], also called the Arc Length method might provide convergence. It considers the load increment, ΔP , as another variable during the iteration process to eliminate the unbalanced forces

$$\Delta P = \lambda_i \Delta P_0 \quad (19)$$

where ΔP_0 = initial load increment and λ_i = load magnification factor at the i -th iteration (see Figure 11). The quantity that is actually being incremented is the arc length along the load displacement curve defined as

$$\Delta L = \sqrt{[\Delta u]_i^T [\Delta u]_i} \quad (20)$$

where $[\Delta u]_i$ is the incremental nodal displacement vector at the i -th iteration. Figure 11 shows how ΔL and λ_i are related.

Riks method is capable of solving highly nonlinear problems involving global instabilities. In cases where local instabilities exist, such as local stiffened panel buckling during the hull girder collapse sequence, Riks method might not converge.

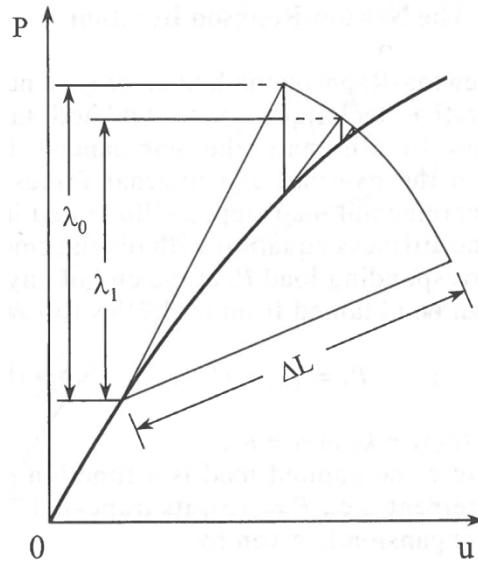


Figure 11: Schematic of the Riks iteration (Figure taken from [7]).

4.2 Types of NLFEA for the Ultimate Strength Calculations

The ultimate bending capacity in the damaged and intact conditions can be analyzed using three main types of FEA:

1. Static analysis
2. Quasi-static analysis
3. Dynamic analysis.

Most authors use general static or quasi-static analysis for ultimate strength calculations. However, the ultimate strength of the hull girder is often reached in highly dynamic conditions when the ship is in a severe sea state with dynamic pressure and inertia forces acting on it. Although dynamic effects could have a significant impact on the sequence of progressive collapse of the hull girder, this topic is beyond the scope of this report.

In the following subsections all three types of NLFEA will be described.

4.2.1 Static Analysis

During the static analysis, load or displacements are applied incrementally. At each load increment, static equilibrium is found using iterative numerical algorithm, e.g. N-R or Riks, as described in Sections 4.1.1 and 4.1.2. This type of analysis can be numerically unstable due to sudden local or global geometric and/or material instabilities (buckling and/or yielding). The instability comes from the fact that the displacements or strains at the onset of instability become very large, even though the load increment is kept relatively small. Using numerical stabilization techniques can help to eliminate this problem. Such techniques are based on the introduction of artificial damping elements at

the nodes where the displacement to load ratio is very high. If damping is not excessive, it should not significantly affect the final static equilibrium.

The amount of damping needed to stabilize a certain problem is not known apriori. Experience with a similar type of problem and some trial and error simulations can help to determine the right amount of damping. Too much damping can lead to unrealistically stiff structures and will affect the final static equilibrium. It is important to verify that the dissipated stabilization energy is a sufficiently small fraction (e.g. less than 5%) of the total strain energy (internal energy) of the model. The proper amount of damping also depends on the mesh size and the extent of the model.

Numerical stabilization using artificial damping can only be used with the N-R and quasi N-R algorithms.

Some static analysis problems with strong nonlinearities cannot be stabilized using the numerical stabilization techniques. In these cases quasi-static analysis can offer better convergence properties.

Static calculations of the hull girder ultimate strength have been performed using ABAQUS/Standard [13] FE software.

4.2.2 Quasi-Static Analysis

This is a dynamic analysis in which the loading is applied over a certain time period. There are three ways to minimize the inertia effects and to achieve a quasi-static equilibrium using dynamic analysis:

1. Loads are applied over a long time period.
2. Density of the structural material is deliberately lowered by an order of magnitude. This is called “reversed mass scaling”.
3. The structure is heavily dampened.

Dynamic analysis uses either implicit or explicit time integration schemes also known as Backward Euler and Forward Euler schemes, respectively.

Implicit method requires an iterative solution (using the N-R algorithm, for example) of the nonlinear system of equations for each time increment which can be very CPU intensive. For linear problems, or linear portions of the nonlinear problem, implicit method has an unconditionally stable time increment which means that the solution can be achieved in only one time step.

On the other hand, explicit method does not require iterations at each time increment because the solution at a particular time step depends only on the solutions at previous time steps and can be calculated explicitly. However, the stable time step is much smaller compared to the implicit method. Therefore, the solution time using the explicit method can become comparable with that of the implicit method, depending on the type of the problem. Explicit method can usually achieve convergence in cases where implicit method fails since it does not require iteration.

Both schemes can help in obtaining a stable quasi-static solution in cases where static analysis fails. However, one has to check that the quasi-static solution has, indeed, been obtained. This can be done by comparing the kinetic and internal energies of the system throughout the solution sequence. Kinetic energy has to be below a very small percentage of the internal energy of the system (e.g. 5%).

In this work, ABAQUS/Standard has been used for furnishing the implicit quasi-static solutions and ABAQUS/Explicit for the explicit quasi-static solutions.

4.2.3 Dynamic Analysis

Purely dynamic solution can be obtained using the methods mentioned in Section 4.2.2. However, the loading is usually applied over a much shorter period of time, there is no reverse mass scaling, and minimum amount of damping is applied in order to stabilize the solution, if necessary.

Although dynamic effects could have an impact on the sequence of progressive collapse of the hull girder, as mentioned before, only dynamic quasi-static solutions have been used in this project. This has been done mainly because it is very difficult to predict the dynamic loading at the ultimate capacity point. Using realistic dynamic loading would not give consistent results that can be compared with other methods or other NLFEA results available in the literature.

4.3 Iterative Solution Algorithms

The three most important iterative solution algorithms that can be used in NLFEA are:

1. Newton-Raphson algorithm (Section 4.1.1);
2. Quasi Newton-Raphson algorithm (Section 4.1.1);
3. Riks Algorithm (Section 4.1.2)

These algorithms have been described in the previous sections. It is important to mention that N-R and quasi N-R algorithms can be used either with the static or dynamic implicit analysis, while the Riks algorithm can only be used in the static analysis. Dynamic explicit analysis does not require an iterative solution algorithm.

4.4 Incremental Loading Process

As mentioned in Section 4.1, the loading on the FE model has to be applied incrementally during the NLFEA. There are two main types of load control in order to achieve an ultimate vertical bending limit state of the hull girder:

- Curvature (displacement) control;
- Moment control.

4.4.1 Curvature Control

This loading approach consists of incrementally increasing the curvature (rigid body rotation of the model end cross sections). It is used by many authors primarily because it is easy to track the behavior of the structure in the post-collapse region. However, it requires special post processing of the stress results in order to find the equivalent bending moment at the cross section of interest. Another issue of pre-imposing a curvature on the FE model was pointed out by Lehman, [14] who stated that the real world behavior of the ship structure is not controlled by pathways, but by forces (moments), and the input of the curvature does not accurately represent the failure process. During the complex global failure process, ships' cross sections do not necessarily remain plane, and they do not rotate uniformly around the initial neutral axis.

Curvature control, when applied to asymmetric cross sections, will result in the development of the horizontal bending moment in addition to the vertical bending moment, if the neutral axis of the model is not allowed to rotate. No such horizontal bending moment will develop in symmetric structures where curvature control in the vertical plane is equivalent to moment control in the vertical plane.

However, if boundary conditions applied at the ends of a sufficiently long FE model (e.g. two-hold (2-H)) prevent the development of internal axial forces, then the neutral axis of the hull away from the ends will be allowed to shift and rotate. This has been confirmed in many NLFEA analyses conducted at ABS with curvature control in the vertical plane only. Such prescribed curvature has led to the development of only the vertical bending moment in the middle of the model which indicates that the neutral axis must have rotated. This observation has also been made by Amlashi and Moan [15].

4.4.2 Moment Control

This loading approach consists of incrementally increasing the vertical bending moment. The major drawback of this approach is that it is very difficult to obtain the negative slope portion of the load-deflection curve when using static analysis, which puts some uncertainty on the calculated ultimate strength value, i.e., how can one be sure that the ultimate capacity of a structure has been reached unless the peak in the moment-curvature curve has been identified. Another difficulty arises in situations when the moment-curvature curve of the hull has more than one peak. The loss of convergence during static analysis will, of course, occur just as the first peak is being reached. Therefore, unless the first peak is also the highest, it will usually be impossible to find the ultimate bending moment of the hull using the moment control during a static analysis.

In theory, Riks iteration algorithm has the ability to track the static solution into the post ultimate strength region. In practice, however, for complex structures such as ships, the Riks algorithm usually fails to converge as soon as local instabilities start to occur.

When dynamic analysis is used, the static equilibrium between the applied moments at the end of the model and the internal cross-sectional moments no longer exists. In other words, if the end moment exceeds the ultimate bending capacity, the FE model is allowed

to collapse in accelerated manner. That is why the post ultimate strength region of the moment-curvature curve can be analyzed.

As the difference between the applied bending moment and the internal moments taken up by the hull increases in the post ultimate strength regime, the dynamic effects will increase as well. However, if the applied moment is gradually increased using a smooth step function, the ultimate bending capacity of the hull will be unaffected by the inertial effects.

4.5 Loads and Boundary Conditions

The ship hull in still water is a free body in equilibrium with perfectly balanced loading. When using a partial model of the hull to calculate the ultimate strength, it is important to prescribe realistic boundary conditions at the ends of the model. In the case of nonlinear analysis, this is a very difficult task since the simple beam theory assumptions might not hold anymore. In particular, the assumption that the cross sections remain plain will probably not hold when the structure is nearing its ultimate capacity. Unfortunately, when using a partial model of the ship hull, there is no way of knowing what the exact boundary conditions will be when simple beam theory assumptions cease to hold. Therefore, the end cross sections are usually assumed to remain plane, even during the nonlinear analysis. The boundaries of a 2-H FE model are fairly far from the failure region which usually occurs in the middle of the center hold. In that case the assumption of plain end cross sections is still reasonable. For a one-bay model this assumption might become less valid.

The need to place the model boundaries away from the damage prevents the use of model aft/forward symmetry. Also, the FE models with damage have no ports side/starboard side symmetry as the damage is always placed on one side of the vessel in the transverse sense.

When using moment control, cantilever boundary conditions have been prescribed with one end fixed and the other one free (see Figure 12). Pure vertical bending moment has been applied on the free end using kinematic coupling in ABAQUS. In other words, moment has been applied on an imaginary reference point at the intersection of the free cross section and the ship neutral axes (see Figure 12). Then, all degrees of freedom (DOF) of the reference point have been kinematically coupled with the corresponding DOF of all the nodes on the free cross section. However, similar to the curvature control, a sufficiently long FE model ensures that the neutral axis of the hull away from the ends will be allowed to freely shift and rotate. Identical load applications have also been used by Notaro et al. [16] and by Amlashi and Moan [15].

When using curvature control, no load is prescribed at the ends of the model. Rather, rotation of the cross sections around the horizontal transverse axis is symmetrically incremented at both ends of the model at the reference points (see Figure 13). All DOFs of the reference point have been kinematically coupled with the corresponding DOFs of all the nodes on the two end cross sections. The two reference points have been placed at

the neutral axis level. At the aft end of the model the vertical and transverse translations of the reference point have been restricted, while at the forward end all translations (U1, U2, and U3) of the reference point have been restricted as well as the rotation around the longitudinal axes (UR1). Rotation around the transverse axis has been prescribed at the reference points on both ends of the model. Such constraints prevent the rigid body motion of the model and the kinematic coupling ensures that the end cross sections remain plain. These boundary conditions have also been used by Amlashi and Moan [15].

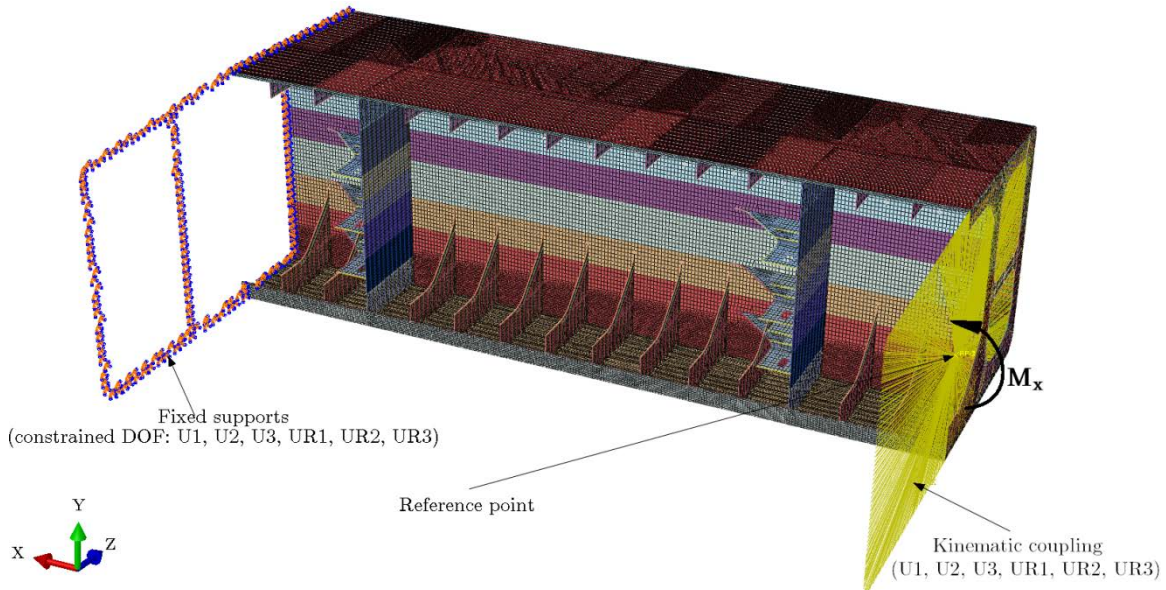


Figure 12: Boundary conditions for moment control.

In order to achieve a pure bending loading with either load control method, it is important that one end of the model is not restrained in the longitudinal direction. This eliminates the axial forces throughout the model.

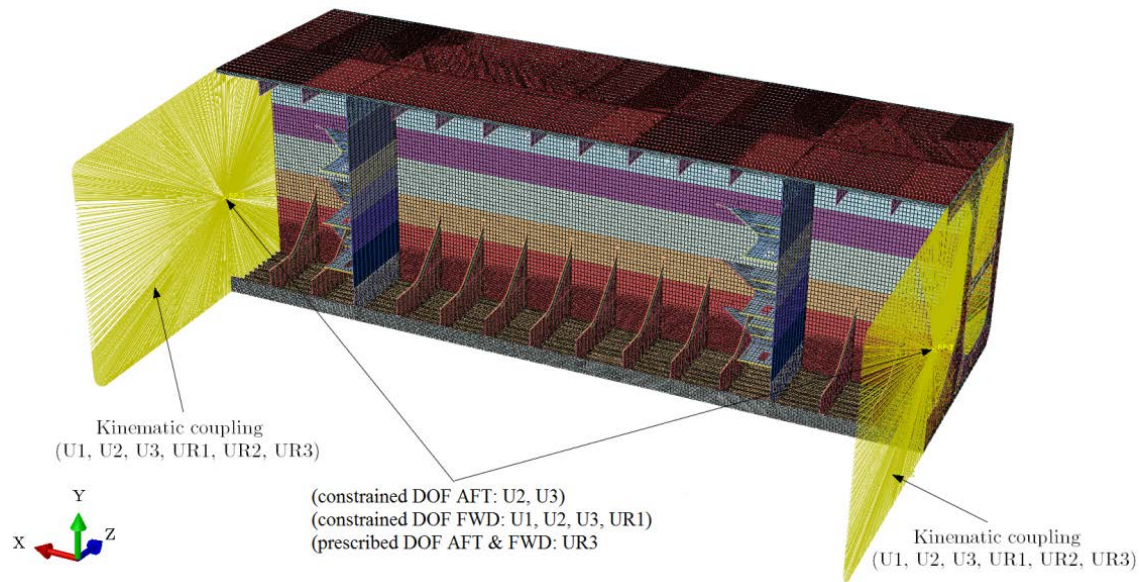


Figure 13: Boundary conditions for curvature control.

4.6 Geometric Imperfections

During fabrication of thin-walled structures (metal cutting, rolling, forming, welding, and heat treatment) some geometric imperfections (nonuniformities in shape, eccentricities, and local imperfections) and residual stresses are inevitably introduced into the structures and can affect the ultimate strength of thin-walled structures. NLFEA usually considers only the geometric imperfections which can also help avoid the numerical instabilities during the solution process.

The most accurate approach to treating the geometric imperfections would be to impose the measured initial deformation pattern onto the FE model. However, these kinds of measurements on real ship structures are usually not available. Furthermore, real imperfections are inherently random in nature and never repeat. Therefore, other geometric imperfection shapes are used. They can be applied through one of the following three methods:

1. Linear superposition of buckling eigenvalue modes from the eigenvalue buckling analysis;
2. Direct shape definition through the specification of nodal coordinates;
3. Using the deformation shape from a linear static analysis.

The first method is usually the most convenient one. Only a first couple of eigenmodes are linearly combined and scaled to obtain the imperfection pattern with amplitudes that are consistent with Class Rules or measurements. This method usually produces the most severe imperfection pattern which partially offsets the exclusion of residual stresses from the analysis.

Direct shape definition uses measurements or deformation patterns based on trigonometric functions to describe the initial imperfections by manually offsetting all the

nodes in the structure. This can be a very cumbersome process. Additionally, the user needs to ensure that the deformation pattern is consistent at each boundary between separately treated regions of the ship structure.

Using the deformed shape from the linear static analysis to prescribe initial geometric imperfections is only applicable to simple structures which are not sensitive to the imperfection shapes.

The eigenmodes superposition method is widely used on more complex structures that are sensitive to the imperfection forms and has been used in this project. First, a buckling perturbation analysis has been conducted with many eigenmodes calculated. The aim has been to select those modes that will cover the compression outer flange of the model with imperfections, both plates and stiffeners. The modes have previously been scaled so that the largest plate out-of-plane deformation is equal to $b/200$ where b is the width of the plate between the stiffeners. This imperfection magnitude is also used in [15], [17], and the DnV PULS code [18]. Figure 14 shows details of the applied imperfections in the deck and bottom flanges of the FPSO. Both plate and stiffener imperfections have been applied.

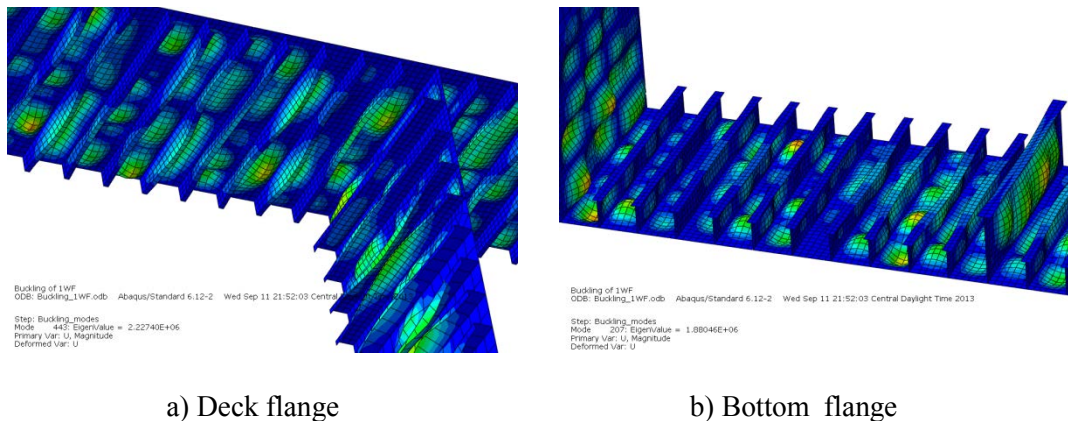


Figure 14: Details of the geometric imperfections applied on the FPSO (magnification = 94x)

Imperfections have been applied over the three web spacings in the center hold of the 2-H models and over the entire length of the 1-B models.

Since the main purpose of this work is to analyze the hull ultimate bending capacity reduction after damage, there was no need to analyze the effect of different imperfection shapes as long as the same imperfections are applied to damaged and intact models.

4.7 Material Properties

In order to conduct the NLFEA, nonlinear material stress-strain curves must be available for all the materials used in the FE model. Properties of the same material can vary significantly between two different steel mills. For that reason and the fact that the actual

stress-strain curves are rarely published by the steel manufacturers, a standard bilinear isotropic hardening model, like the one described in [15], has been used in this project. The use of the bilinear model presents numerical difficulties since it contains discontinuity of the first derivative at the point of slope change. Using material's actual smooth stress-strain curve might improve convergence and shorten the analysis time.

The material properties are given in Table 3, while Figure 15 shows the adopted stress-strain curves for all three materials.

Table 3: Material properties

	MS	AH32	AH36
Density [kg/m ³]	7850	7850	7850
Young's Modulus [MPa]	2.0608E+05	2.0608E+05	2.0608E+05
Poisson's Ratio	0.3	0.3	0.3
Shear Modulus [MPa]	7.9262E+04	7.9262E+04	7.9262E+04
Yield Strength [MPa]	235	313.6	352.8
Tangent Modulus [MPa]	825	625	675

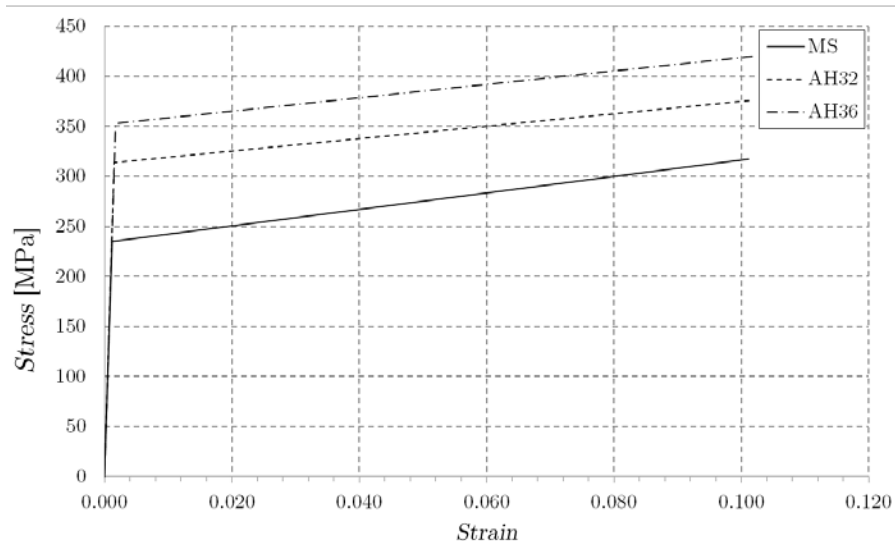


Figure 15: Bilinear isotropic hardening material model

4.8 Fracture Modeling

The impact of material fracture on the value of ultimate bending capacity has been taken into account using the material failure criteria based on forming limit diagrams combined with finite element deletion. The strain values at which the material fractures occur when the structure is far into the post ultimate strength point. Therefore, material fracture has no impact on the ultimate strength calculations.

4.9 Meshing

Mesh size and quality are even more important for the NLFEA compared to the linear FEA. If the elements undergo significant change in shape during the large deflection nonlinear analysis, the reliability of the solution may be reduced. Therefore, special attention has been given to element quality (ratio of element edge lengths and angles inside the element). The usage of triangular shell elements has been kept to a minimum.

Before performing a large NLFEA analysis, mesh convergence studies have to be performed. The regions of the model that are expected to have high compressive stresses should have a mesh that is fine enough to be able to capture the main buckling failure modes of structural members. Away from the hull compression outer flanges, the fine mesh should be gradually transitioned into a coarser mesh in order to minimize the computation time. The mesh size and distribution adopted in the present study are based on [19] and [15].

The following mesh characteristics have been applied to 2-H and 1-B models:

- Only the compression outer flange has been modeled using finer mesh with an element size of approximately 130 mm.
- Other parts of the model have been meshed using element size equal to the spacing of longitudinals (approximately 800 mm).
- At least two shell elements across the flange of the longitudinals have been used in the region of finer mesh.
- The finer mesh has been carefully transitioned into the coarse mesh regions.
- The longitudinal extent of the finer mesh is approximately equal to five web frame spacings on the 2-H models and one web frame spacing on the 1-B models.
- All longitudinals in the finer mesh region have been meshed using shell elements.
- The flanges of the longitudinals outside the finer mesh region have been modeled using beam elements, while their webs have been modeled using shell elements.
- Stiffeners on the transverse structural members have been modeled with beam elements.
- Containership model has been entirely meshed using only shell elements.

Figure 16 shows a typical finer mesh in the double bottom of the Suezmax tanker. The mesh transition can be observed.

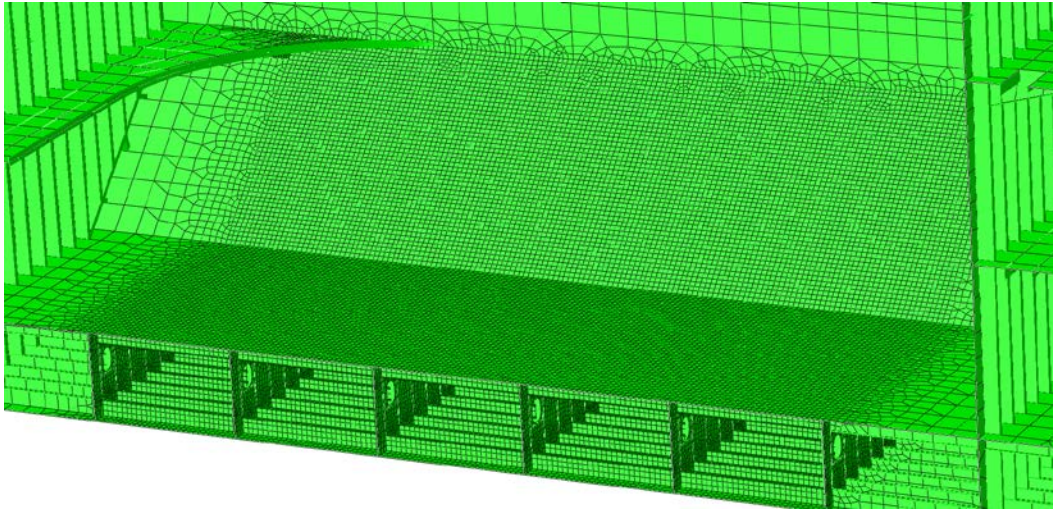


Figure 16: Transition between finer and coarse mesh (Suezmax tanker)

4.10 Element Types

ABAQUS B31 beam elements have been used in certain areas of the models (see Section 4.9). These are ABAQUS default beam elements for nonlinear analysis. Each element has two nodes with six DOF. These elements allow for transverse shear deformation (Timoshenko beam).

All plates have been meshed using ABAQUS shell quadrilateral and triangular elements. Two main types of shell elements have been tested in this work:

- Full integration quadrilateral and triangular elements S4 and S3.
- Reduced integration quadrilateral and triangular elements S4R and S3R.

All of these elements are well-suited for NLFEA of thick and thin shells, as well as for small and large strain applications. Integration scheme using Simpson's rule with five integration points across the thickness of the plate element has been used.

Element type S4 is a fully integrated, general-purpose, finite-membrane-strain shell element. The element's membrane response is treated with an assumed strain formulation that gives accurate solutions to in-plane bending problems, is not sensitive to element distortion, and avoids parasitic locking [13].

Element type S4 does not have hourglass modes in either the membrane or bending response of the element; hence, the element does not require hourglass control. The element has four integration locations per element compared with one integration location for S4R, which makes the element computationally more expensive. S4 can be used for problems prone to membrane- or bending-mode hourglassing, in areas where greater solution accuracy is required or for problems where in-plane bending is expected. In all of these situations S4 will outperform element type S4R [13]. It is also worth noting that the S3 and S3R elements in ABAQUS are identical.

4.11 3-D CAD Modeling

In order to generate a good quality mesh, it is important to have a detailed 3-D model of the hull geometry. For that purpose 2-H and 1-B 3-D CAD models have been generated for all four vessels. The models have been generated using ABAQUS/CAE's powerful CAD engine.

Figure 17 through Figure 20 show the 2-H models of all vessels, while Figure 21 shows the 1-B models of the FPSO and tanker vessels.

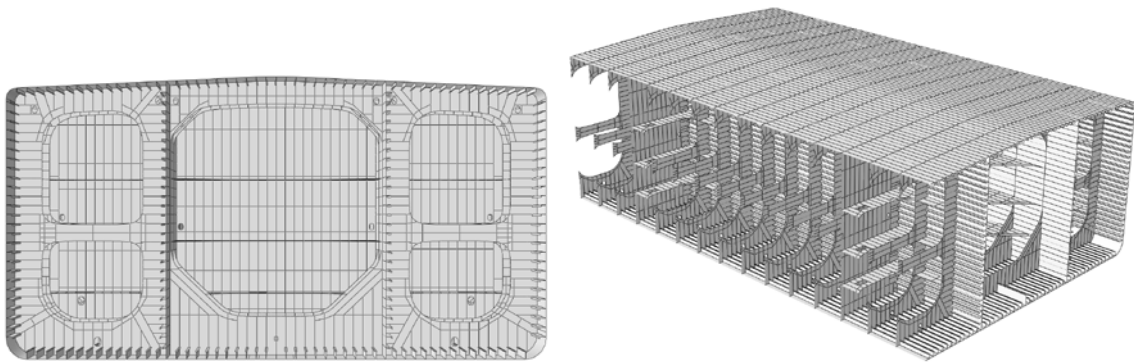


Figure 17: 2-H CAD model of the FPSO

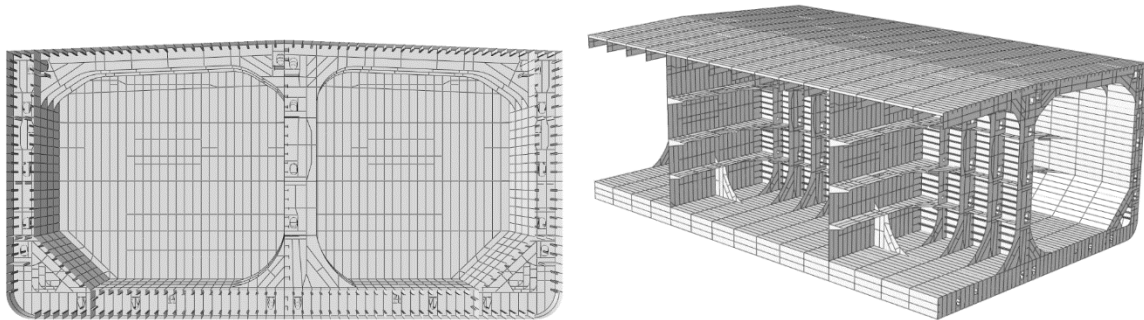


Figure 18: 2-H CAD model of the Suezmax tanker

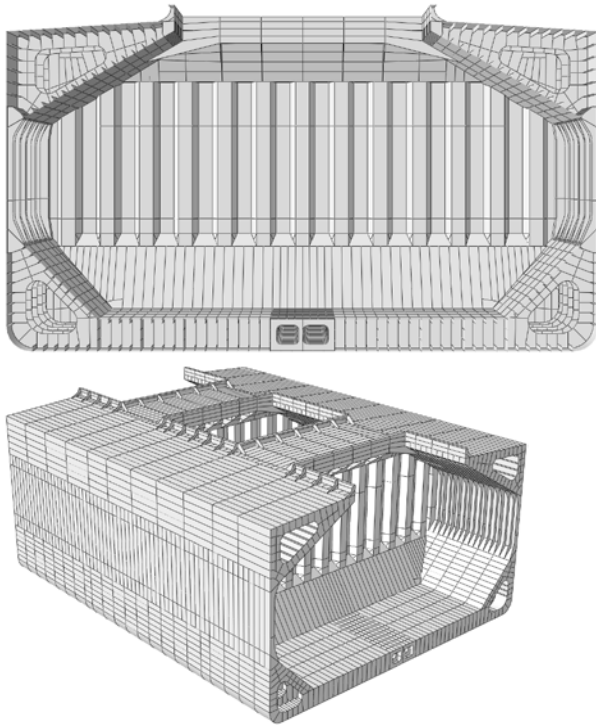


Figure 19: 2-H CAD model of the bulk carrier

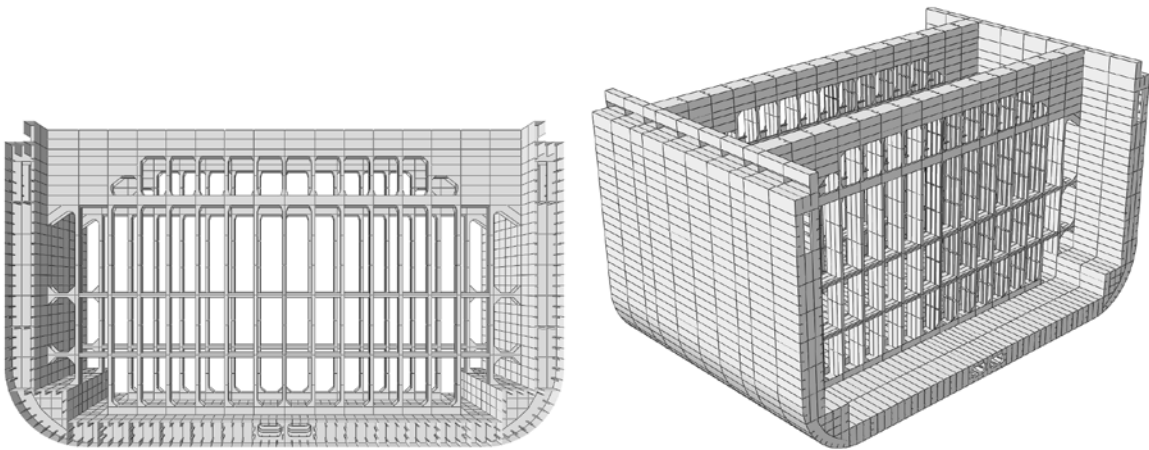


Figure 20: 2-H CAD model of the containership

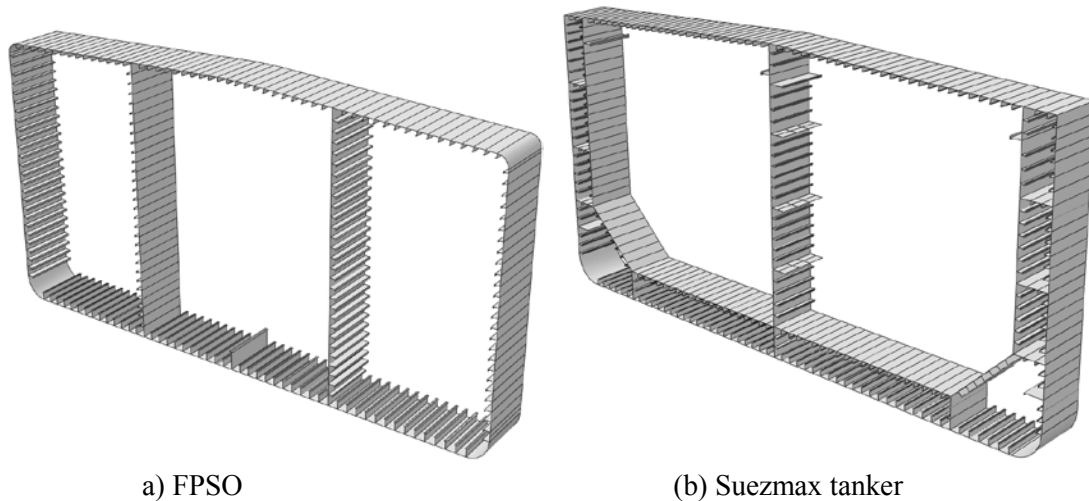


Figure 21: 1-B CAD models

The 3-D modeling of a complex structure such as the 2-H model of the hull is not an easy task. Great attention has to be paid to ensuring the geometric conformity between different parts of the structure. For example, in the case of the FPSO, vertical stiffeners on the transverse bulkhead (TBHD) have to be perfectly aligned with the horizontal stiffeners on each of the three horizontal stringers that support the TBHD, with stiffeners on the web frames, as well as with the longitudinals on the shell (see Figure 22). Any geometric inconsistency, such as a short edge, a sliver or a small face will cause meshing issues. Perfect alignment of the intersecting elements (especially line elements) has been achieved through multiple projections of lines onto surfaces in all three directions.

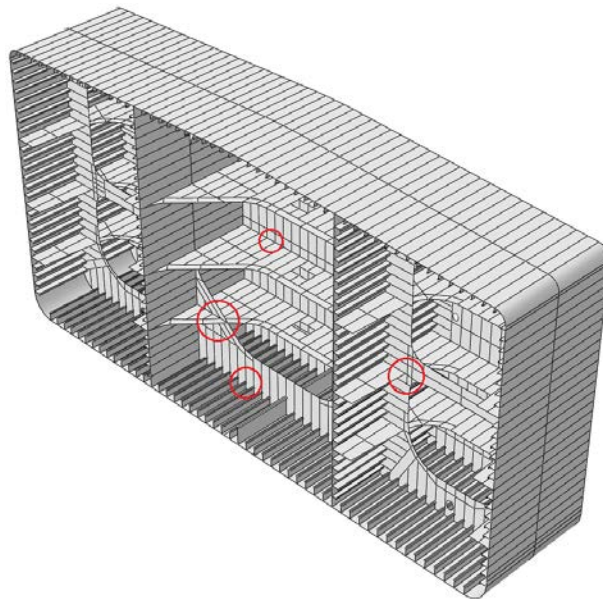


Figure 22: TBHD submodel illustrating many intersecting plates and beams (encircled with red). Geometric consistency and accuracy has to be maintained while modeling.

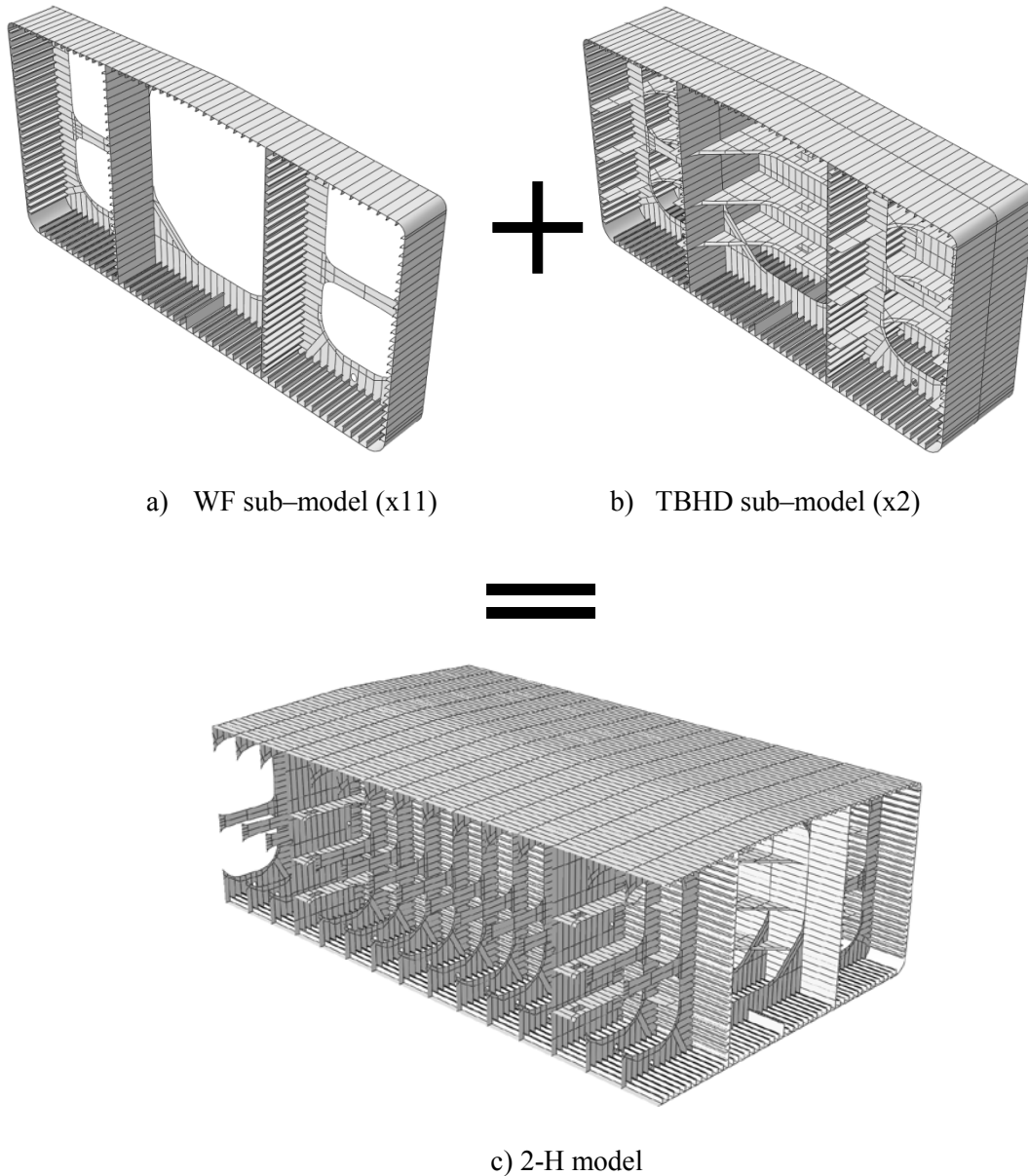


Figure 23: Assembly of the 2-H model

The 2-H model is actually $\frac{1}{2}$ -H + 1-H + $\frac{1}{2}$ -H model that consists of the midship hold plus one half hold on each side of the midship hold.

The 2-H models have been assembled using two major sub models: TBHD submodel and a web frame (WF) submodel. The final assembly of the 2-H model of the FPSO is shown in Figure 23 using two TBHD sub-models and 11 WF submodels.

5. Sensitivity Study

When performing large scale NLFEA, it is very important to conduct the sensitivity study of various model and analysis parameters in order to find the best possible compromise between accuracy and efficiency. In the present study, the following sensitivity studies have been performed using the intact 1-B FPSO model:

- Analysis type (static vs. dynamic quasi-static);
- Time integration scheme (implicit vs. explicit);
- Loading control (curvature control vs. moment control);
- Numerical algorithm (Quasi-N-R vs. N-R);
- Shell element type (reduced integration quadrilaterals - S4R vs. full integration quadrilaterals – S4);
- Mesh sensitivity study (see Section 4.9).

To illustrate the effects of the above mentioned parameters on the ultimate strength and the post ultimate strength behavior of the hull girder, 17 NLFE analyses have been performed for pure sagging condition using the intact 1-B model of the FPSO. The initial imperfections have been applied using the superposition of buckling modes. The results are summarized in the following sections.

5.1 Analysis Type and Time Integration Scheme Sensitivity

Figure 24 shows the moment-curvature curves for two different types of NLFEA: static and quasi-static. The latter one has been used with two different time integration schemes: implicit and explicit. All other analysis parameters have been kept the same (element type, loading control, etc.). The moment has always been measured at the middle of the FE model in the longitudinal sense. The moment has been post-processed based on the nodal forces in the middle cross section using an ABAQUS subroutine. It can be seen in Figure 24 that there are some differences between these three analyses in the post-elastic response of the hull. Table 4 shows the ultimate sagging bending limit states for the three analyses. The maximum difference in the value of the ultimate sagging bending moment, $M_{u, sag}$, is about 2%, while the differences in the curvature at which the ultimate limit state is reached are quite significant. For example, the limit state curvature in the static or quasi-static explicit analysis is twice as large as the limit state curvature in the quasi-static implicit analysis.

Table 4: Ultimate limit states for three analysis types

Ultimate limit state	Static	Q-S Implicit	Q-S Explicit
$M_{u, sag}$ [GNm]	8.848	8.909	9.035
Curvature [rad/m]	1.888E-04	9.583E-05	1.958E-04

The behavior of the structure in the post-elastic region is quite sensitive to small differences in the numerical solution process. This slightly changes the sequence of

collapse of structural members and load redistribution within the structure which, in turn, has an impact on the moment-curvature curve away from the elastic region.

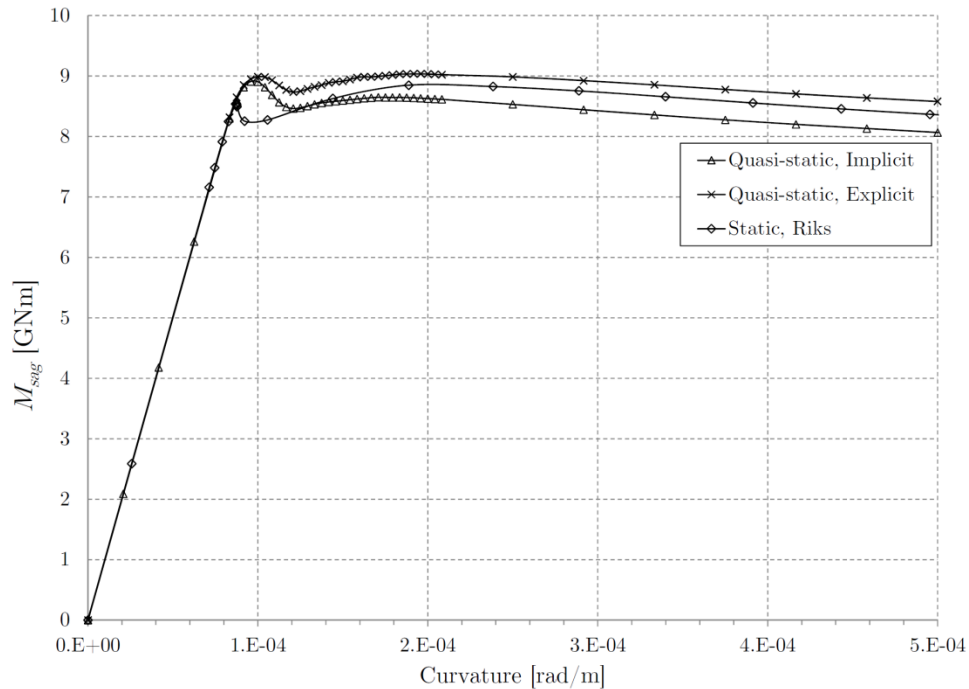


Figure 24: Sensitivity of NLFEA results with respect to analysis type. Curvature control has been applied in all three runs.

For quasi-static analyses, it is important to verify that the effect of inertial forces is small. This is checked by looking at the ratio of total system kinetic energy (KE) to total system internal energy (IE). If this ratio is smaller than 5%, then it is safe to assume that the quasi-static solution has, indeed, been obtained. Figure 25 shows this ratio for both implicit and explicit quasi-static analyses. It is seen that this ratio is well below 1% for both quasi-static analyses. It has also been confirmed that this ratio is below 1% in all other quasi-static analyses when curvature control has been used.

The main difference between implicit and explicit quasi-static analysis, apart from the different time integration scheme, is the fact that the implicit analysis is heavily dampened by default, while explicit analysis is not. As a consequence, the inertial effects at the beginning of the analysis are a little bigger for explicit analysis, but still very low. Explicit analysis yielded consistently higher bending moment capacities at corresponding curvatures in the inelastic region of the moment-curvature curve compared to the static analysis and quasi-static implicit analysis.

Figure 26 shows the 1-B FE model at the last increment of the static analysis. The von Mises equivalent stresses at the deck are well above the yield stress. Stiffener tripping across the entire deck and shear strake can be observed. This is a very common failure mode for open stiffener sections and plates of intermediate slenderness such as these. Local stiffener tripping occurs first. The plate between stiffeners initially rotates to

accommodate the stiffener web rotation around the attachment point. As the compressive load is increased, the von Mises stress in the plating reaches and exceeds the yield stress of the material at which point a typical “pitched roof” configuration and plastic mechanism occurs in the plating (see Figure 27). After this point, the total collapse is quite sudden.

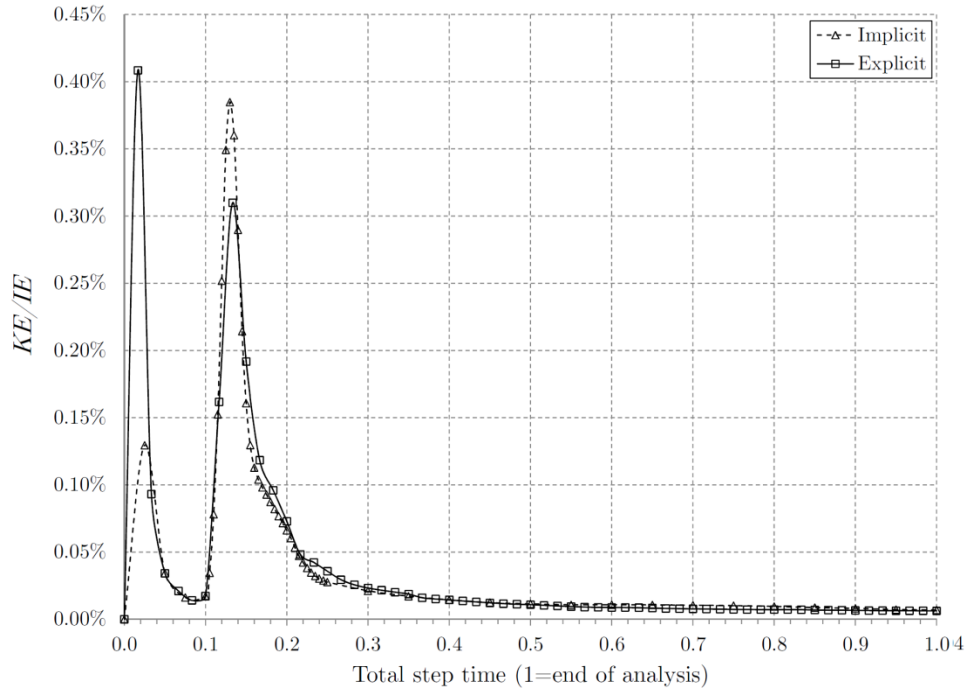


Figure 25: Ratio of kinetic and internal energies for implicit and explicit analyses

The cross-section failure domain is quite narrow. The initial stiffener tripping is governed by the position of geometric imperfections and the tripping locations on adjacent stiffeners. Similar failure domains and collapse mechanisms have been observed in all 1-B NLFE analyses.

5.2 Load Control

Figure 28 and Figure 29 show the sensitivity of loading control for the two quasi-static analyses: implicit and explicit, and for two shell element types: S4 and S4R, respectively. The time integration scheme sensitivity has already been addressed in Section 5.1. Moment control approach resulted in slowly decaying bending moment in the post ultimate strength region, and the moment-curvature curves did not exhibit the characteristic first peak as in the case of curvature controlled loading. Upon inspection, it has been found that the moment distribution across the model was very uneven, even though it should have been constant. Basically, the boundaries at which the moment is applied are too close to the failure domain on the 1-B models, and the measured moment in the middle of the model is affected by the boundaries during the accelerated collapse event. The same model behavior when using moment control has been observed by Shu

and Moan [20]. The problems with moment control do not exist on the 2-H models where the failure domain is sufficiently far away from the boundaries.

Both curvature and moment control analyses yield very similar ultimate bending capacity values, especially when S4 shell elements are used. On sufficiently long models, such as 2-H models, they both simulate equivalent loading sequence and can, therefore, be used interchangeably. The curvature control has been chosen in this project because it provides more control over the inertial forces in the post ultimate strength region.

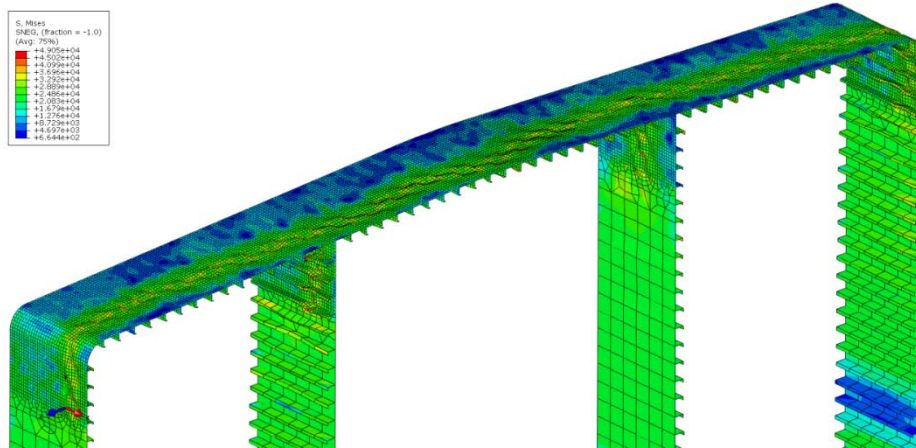


Figure 26: Von Mises stresses in $[N/cm^2]$ at the last increment of the static analysis

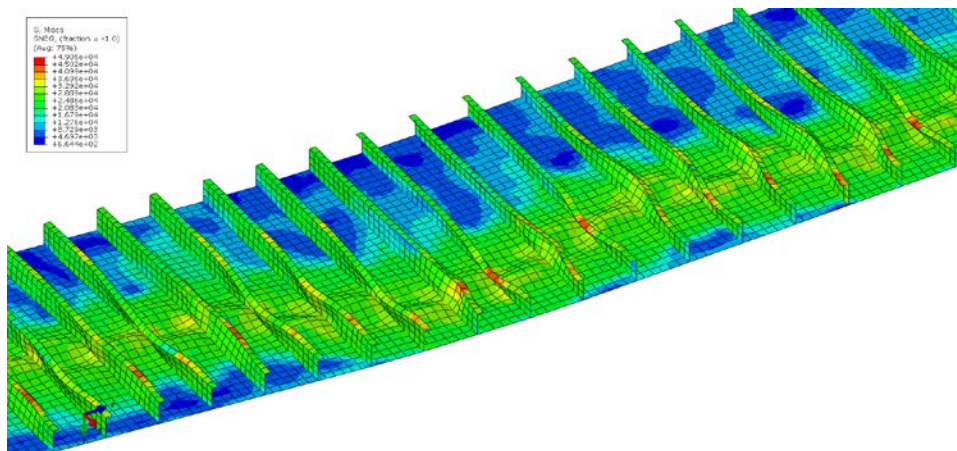


Figure 27: Deck stiffener tripping and “pitched roof” plate configuration

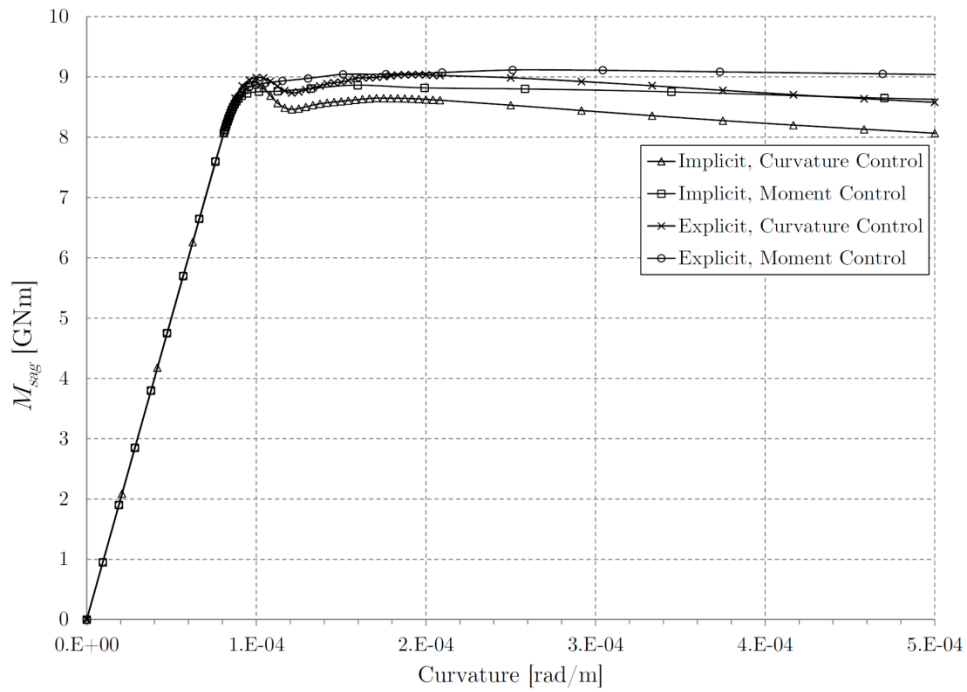


Figure 28: Sensitivity of time integration scheme and loading control for S4 shell elements

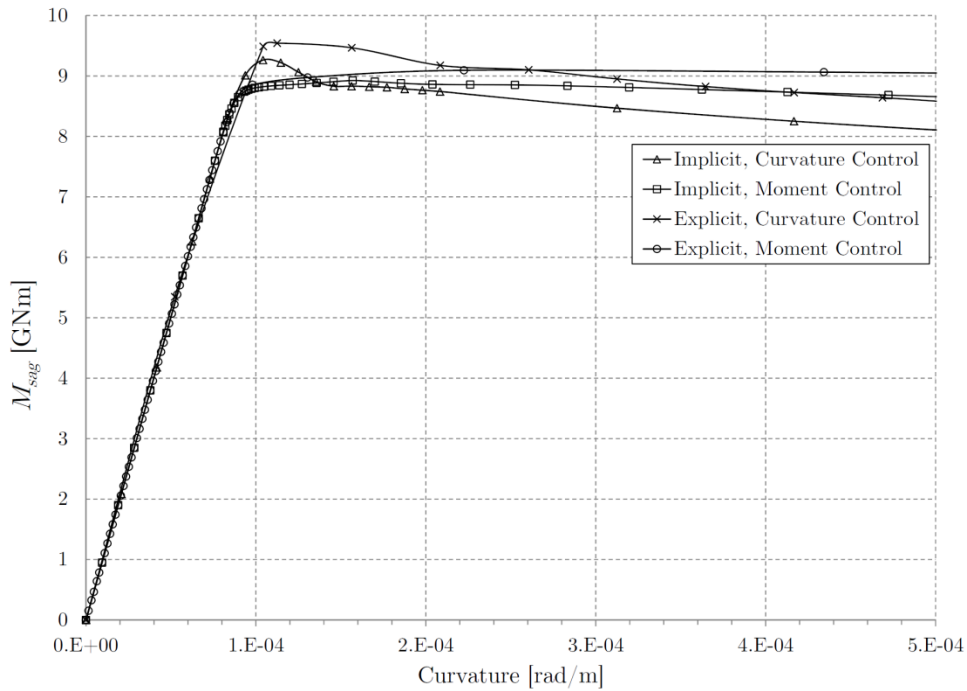


Figure 29: Sensitivity of time integration scheme and loading control for S4R shell elements

5.3 Iteration Algorithm and Element Type Sensitivity

Figure 30 shows sensitivity of the iteration algorithm and element type when using quasi-static implicit analysis with curvature control. It can be concluded that the shell element type has a significant effect on the post ultimate strength behavior of the hull girder, while the choice of iteration algorithm seems to have a much smaller effect on the ultimate and post ultimate strength behavior, especially if full integration shell elements are used. All simulations, except the N-R algorithm with S4R elements, yield a very similar behavior up to the first minima on the moment-curvature curve after which the curves start to differ slightly. The simulation with N-R algorithm and S4R elements initially yields the highest ultimate strength of all the simulations, but after that the hull collapses beyond recovery, unlike in other simulations where there is always some degree of recovery (second maxima in the moment-curvature curve).

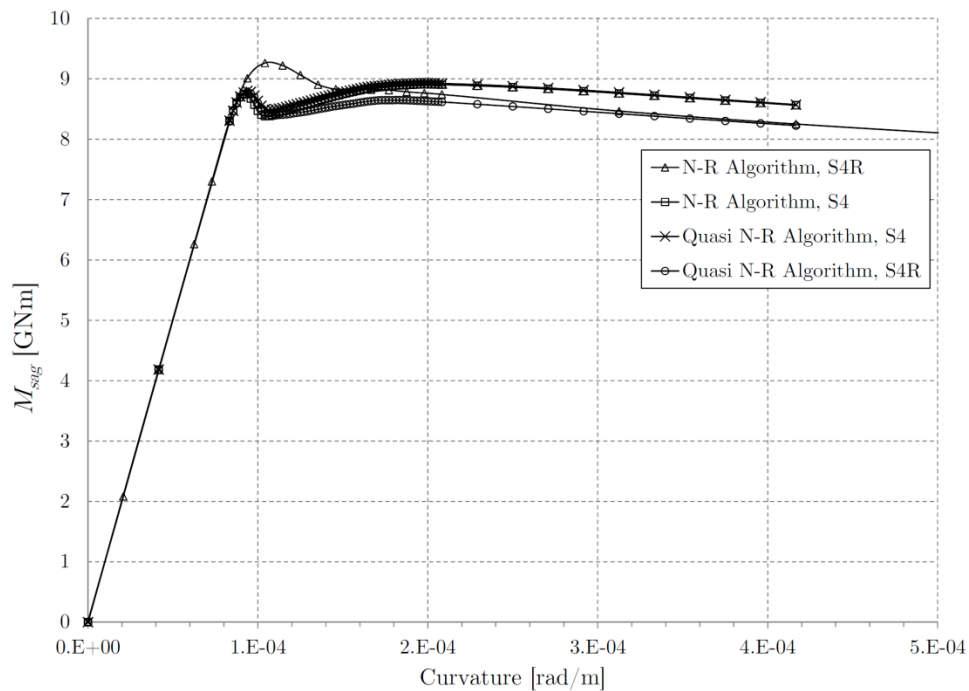


Figure 30: Sensitivity of iteration algorithm and element type. All simulations have been performed using quasi-static implicit analysis with curvature control.

5.4 Conclusion and Final Choice of Analysis Parameters

The quasi-static analysis has been chosen over the static analysis for its greater stability and convergence properties. Static analysis convergence properties were very sensitive to the mesh size. For the chosen mesh size, static analysis could only be run using Riks iteration algorithm.

The choice of implicit vs. explicit time integration scheme is based on CPU time consideration since both methods yield consistently very similar ultimate bending

capacities in all analyses. The explicit method is actually much faster than the implicit method when no beam elements are present in the model. However, the stable time increment of the explicit method becomes extremely small (on the order of $10E-12$) when short beam elements exist in the model. It is worth noting that the stable time step of the explicit analysis can be increased by increasing the mass of the beam elements in the model (mass scaling), or by using the fixed time step corresponding to the stable time step of the shell elements. However, in those cases the convergence or the stability of the analysis is not guaranteed, and one needs to check the energy histories and other variables to ensure that a valid and stable response has been achieved. Another, very conclusive, check is to compare the moment-curvature curve from the NLFEA with that from the linear static analysis. If a stable quasi-static solution has been achieved, then the slope of the linear portion of the moment-curvature curve should exactly match the corresponding slope from the linear static analysis. Figure 31 shows a comparison between quasi-static NLFEA using explicit time integration scheme and the linear static analysis. As it can be observed, the linear slopes match.

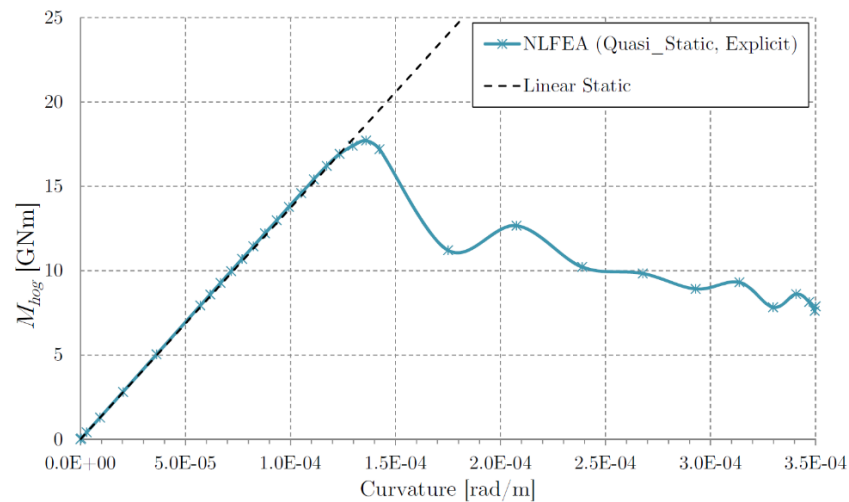


Figure 31: Comparison between the quasi-static explicit NLFEA and the linear static analysis (intact bulk carrier in hogging 2-H model)

The explicit method has been used in this work only in cases where implicit method had convergence problems that could not be stabilized. To achieve consistency, all damaged and intact cases for a particular vessel with a certain direction of the bending moment (sagging or hogging) have been analyzed using the same time integration scheme.

Curvature control has been chosen over moment control for its ability to achieve a proper quasi-static response without accelerating the model end cross sections when the applied moment becomes greater than the ultimate capacity of the hull.

Full integration S4 elements with the full N-R iteration algorithm have been chosen over the reduced integration S4R elements and the quasi N-R algorithm for their superior accuracy. On the other hand, S4R elements and the quasi N-R algorithm have not proved to be any faster compared to the S4 elements and full N-R algorithm.

6. Phase II Results

This section contains the intact and damage ultimate vertical bending moment capacities for the selected single hull FPSO, double hull Suezmax tanker, 180,000 DWT bulk carrier, and the 8500 TEU containership. All the calculations have been performed in ABAQUS using the quasi-static analysis on 2-H models. Table 5 shows the DOF of each FE model in the intact condition. Of course, the FE models representing the damaged conditions have a smaller number of DOFs. Two FE models have been used per intact vessel, depending on the bending moment direction (sagging or hogging). In order to save on computation time, only the compression outer flange of the hull has been fine meshed as stated in Section 4.9.

Table 5: DOF of the 2-H FE models in intact condition (in millions)

	Sagging	Hogging
FPSO	1.29	1.56
Tanker	1.43	2.09
Bulk carrier	1.11	2.27
Containership	1.33	1.59

All the analyses have been performed on the Linux cluster using, on average, 20 Intel Xeon CPU cores. All the analyses have managed to converge in the post ultimate strength region. However, the maximum curvature to which the analysis managed to converge varied between the analyses. Therefore, the total computation time per single NLFEA varied considerably. On average it took 15 hours to complete one NLFEA. A total of eight intact and 266 damaged cases have been analyzed. The results of all of these analyses are presented in this section and the Appendix. However, numerous additional NLFEA have also been performed in order to verify results, test parameters, or fix non-convergence problems.

6.1 Damage Cases

The damage in both collision and grounding has been assumed in a form of a rectangle, as required by IACS CSR. Four different damage breadths, b , and heights, d , have been used generating a total of 16 damaged cases per vessel, per damage type (collision or grounding), and per bending moment direction (sagging or hogging). The default longitudinal damage extent, l , has been taken as spanning across three web frames (3WF), including the removal of the first and the last WF within the damaged area. In the case of the Suezmax tanker with collision damage, two additional longitudinal damage extents have been analyzed spanning one web frame (1WF) and across the entire 2-H model (ALL WF). Each of these three longitudinal extents have been combined with all 16 transverse damage cases, generating a total of 48 damage cases for tanker with collision damage in sagging. Another damage case spanning five web frames (5WF) has been analyzed for the tanker with D6 (see Table 7) collision damage in sagging in order

to complete the analysis of the effect of the longitudinal damage extent. On top of that, two additional damage cases for tanker with collision damage in sagging have been analyzed in order to assess the effect of longitudinal position of the damage. In order to assess the effect of the transverse position of the damage, three additional damage cases for tanker with grounding damage in hogging have been analyzed. In the case of containership, only two damage breadths, instead of four, have been considered for collision cases due to very narrow main deck transverse span between the shell and the inner bulkhead. It is also worth noting that for grounding cases with sagging bending moment and collision cases with hogging bending moment, the damage is defined in the coarser-mesh area of the FE model. Therefore, the damage transverse size parameters in these cases were slightly different than in the cases where the damage has been defined in the fine-mesh area of the model (collision with sagging and grounding with hogging). Also, due to mesh size limitations, only three damage heights across the double bottom, instead of four, have been defined for tanker, bulk carrier, and the containership with grounding damage under sagging bending moment. Table 6 shows the number of analyzed cases for each vessel and damage type.

Table 6: Analyzed cases

	Intact	Collision (SAG)	Collision (HOG)	Grounding (SAG)	Grounding (HOG)
FPSO	2	16	16	16	16
Tanker	2	48+1+2	16	12	16+3
Bulk carrier	2	16	16	12	16
Containership	2	8	8	12	16

The 16 transverse damage extents have been denoted as D1, D2, ... D16. Table 7 shows these transverse damaged cases in a tabular form classified by the b/B and d/D ratios, where b and d are the breadth and depth of the damage, while B and D are the breadth and depth of the vessel. For the vessels with double bottom (Suezmax tanker, bulk carrier, and containership) the d/H ratio has been used instead of d/D , where H is the depth of the double bottom.

Table 7: Damaged case classification by damage size, vessel, damage type, and vertical bending moment direction

FPSO – Collision (SAG & HOG)						FPSO – Grounding (SAG & HOG)													
d/D \ b/B	0.00	0.05	0.10	0.20	0.30	d/D \ b/B	0.00	0.17	0.33	0.60	0.80								
0.00						0.00													
0.26						D1						D2	D3	D4	0.05	D1	D2	D3	D4
0.40						D5						D6	D7	D8	0.10	D5	D6	D7	D8
0.60						D9						D10	D11	D12	0.20	D9	D10	D11	D12
0.81						D13						D14	D15	D16	0.30	D13	D14	D15	D16

Tanker – Collision (SAG & HOG)									
d/D \ b/B	0.00	0.05	0.10	0.20	0.30				
0.00									
0.24						D1	D2	D3	D4
0.37						D5	D6	D7	D8
0.49						D9	D10	D11	D12
0.69						D13	D14	D15	D16

Tanker – Grounding (HOG)									
d/H \ b/B	0.00	0.17	0.33	0.60	0.80				
0.00									
0.25						D1	D2	D3	D4
0.50						D5	D6	D7	D8
0.77						D9	D10	D11	D12
1.00						D13	D14	D15	D16

Tanker – Grounding (SAG)									
d/H \ b/B	0.00	0.17	0.33	0.60	0.80				
0.00									
0.33						D1	D2	D3	D4
0.67						D5	D6	D7	D8
1.00						D9	D10	D11	D12

BC – Collision (SAG & HOG)									
d/D \ b/B	0.00	0.05	0.10	0.20	0.28				
0.00									
0.25						D1	D2	D3	D4
0.40						D5	D6	D7	D8
0.60						D9	D10	D11	D12
0.80						D13	D14	D15	D16

BC – Grounding (HOG)									
d/H \ b/B	0.00	0.17	0.33	0.60	0.80				
0.00									
0.25						D1	D2	D3	D4
0.50						D5	D6	D7	D8
0.80						D9	D10	D11	D12
1.00						D13	D14	D15	D16

BC – Grounding (SAG)									
d/H \ b/B	0.00	0.17	0.33	0.60	0.80				
0.00									
0.33						D1	D2	D3	D4
0.67						D5	D6	D7	D8
1.00						D9	D10	D11	D12

Containership – Collision (SAG & HOG)						
d/D \ b/B	0.00	0.03	0.05			
0.00						
0.25					D1	D2
0.40					D5	D6
0.60					D9	D10
0.80					D13	D14

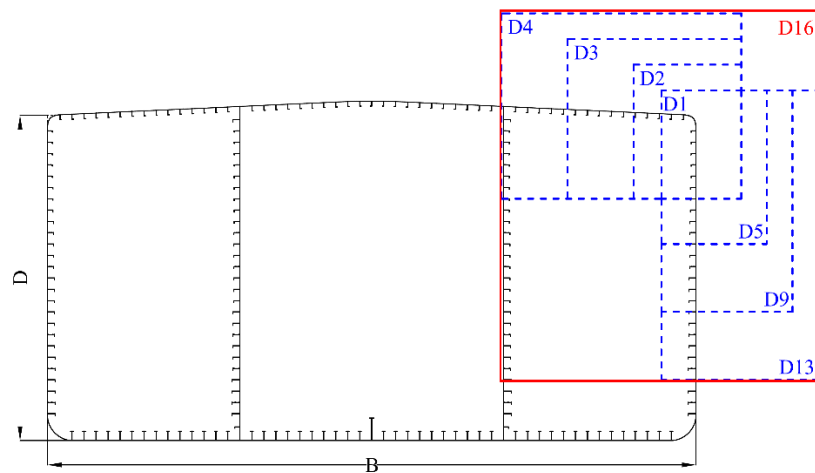
Containership – Grounding (HOG)									
d/H \ b/B	0.00	0.17	0.33	0.60	0.80				
0.00									
0.25						D1	D2	D3	D4
0.50						D5	D6	D7	D8
0.74						D9	D10	D11	D12
1.00						D13	D14	D15	D16

Containership – Grounding (SAG)					
b/B	0.00	0.17	0.33	0.60	0.80
d/H					
0.00					
0.33		D1	D2	D3	D4
0.67		D5	D6	D7	D8
1.00		D9	D10	D11	D12

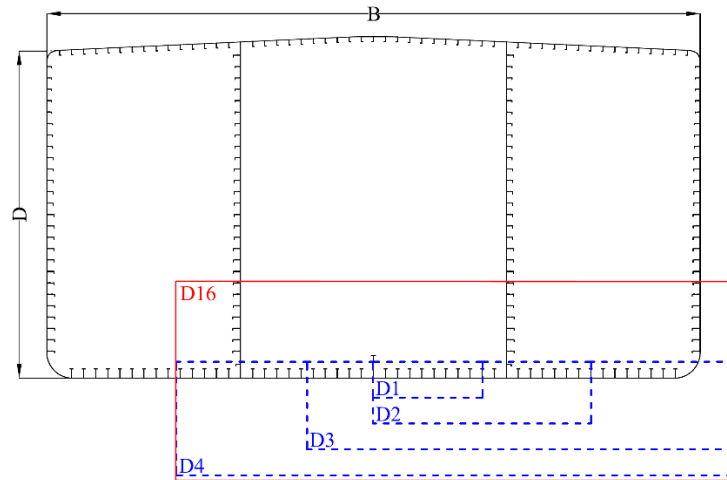
Figure 32 and Figure 33 show graphically the damaged cases for FPSO and tanker, respectively. Blue dashed lines represent damaged cases across the entire b/B and d/D range. The red line denotes the largest transverse damage extent (D16), and the magenta line denotes the IACS damage case (where applicable).

Every collision damage case includes the damage to the deck, as per IACS requirements. The grounding damage cases start at the centerline and include the damage to any longitudinal member that is in the centerline. As the ratio b/B increases above 0.5, the damage is extended to both sides of the vessel, always including the bilge area. In case of the single hull FPSO, increasing the b/B ratio greatly affects the amount of damaged bottom structure, while increasing the d/D ratio has a much smaller effect. For the double hull tanker, increasing the d/H ratio has a significant effect, especially as this ratio reaches one and the entire inner bottom becomes damaged.

Sharp edges of the rectangular damaged area have been retained in order to simulate the sharp edges and stress concentrations present in the hull following a real damage.



a) Collision - SAG



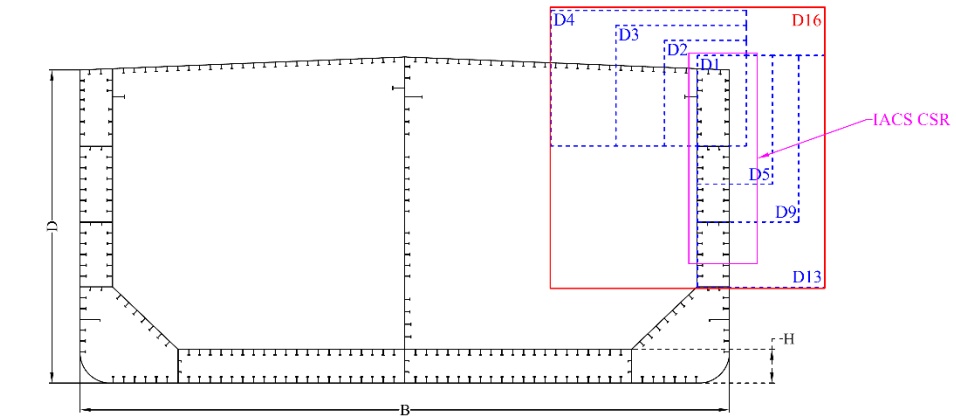
b) Grounding - HOG

Figure 32: Transverse damage extents for the FPSO

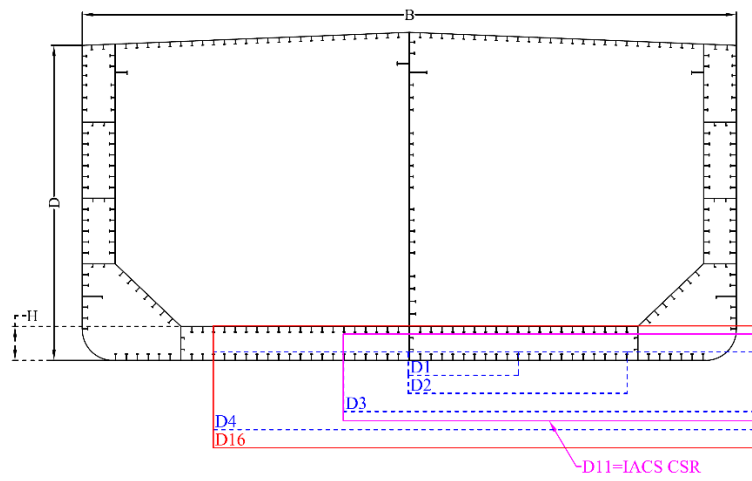
Longitudinally, all the damages have been located at the middle of the model to minimize the effect of the boundary conditions. Figure 34 shows the longitudinal damage extents. The ends of the damage include any transverse structure within the transverse damage extent. The ALL WF spans across the entire 2-H model and, therefore, has no discontinuity in the longitudinal direction. In this case there are no stress concentration areas at the ends of the damage.

In order to assess the effect of the longitudinal position of the damage, the default 3WF D10 collision damage case has been shifted from the middle of the model towards the aft on a tanker under the sagging bending moment condition. Two such additional cases have been analyzed where the collision damage has been shifted two and four web frames aft of the middle of the model, respectively. These shifts required FE model re-meshing in order to shift the fine mesh area aft, as well as re-imposing the geometric imperfections on the fine-meshed area of the model. Figure 35 shows these three longitudinal variations of the collision damage.

In order to assess the effect of the transverse position of the damage, the modified D13 grounding damage on the tanker has been shifted in the transverse direction between two consecutive longitudinal girders (centerline girder and the hopper tank side girder). The idea was to create three damage cases with approximately the same bottom section modulus reduction, but with different transverse positions. D13 damage has been slightly modified not to include the centerline girder. This damage has been denoted as D13* T1, to other transverse position of this damage have then been generated, D13* T2 and D13* T3 as shown in Figure 36. The bottom section modulus reduction differs only slightly between these three damage cases due to small variations in the bottom plating thickness in the transverse direction.



a) Collision - SAG



b) Grounding - HOG

Figure 33: Transverse damage extents for the Suezmax tanker

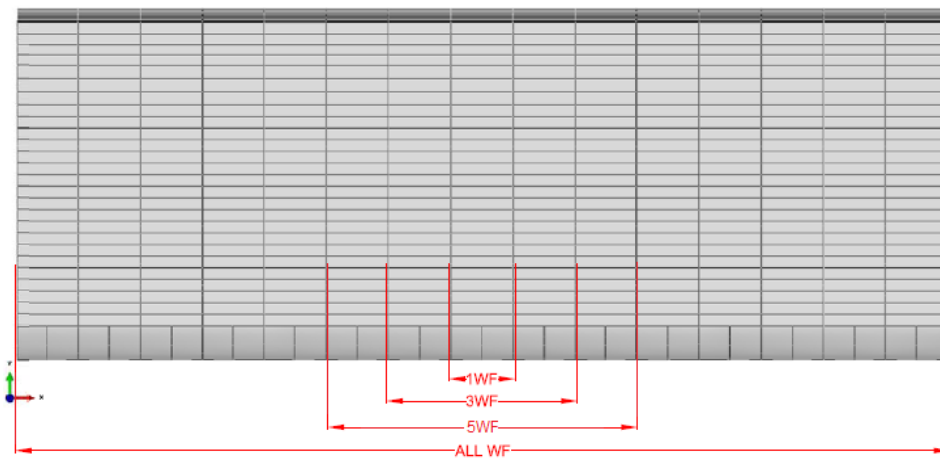


Figure 34: Longitudinal damage extents

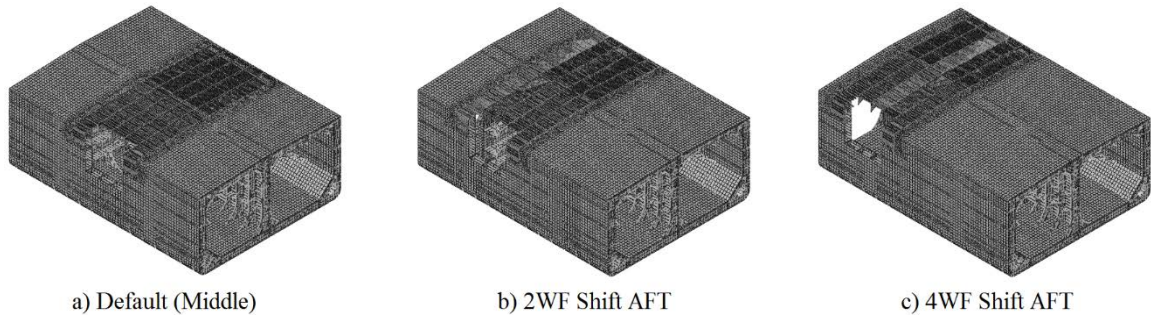


Figure 35: Longitudinal variation of the damage on a tanker with D10 collision damage

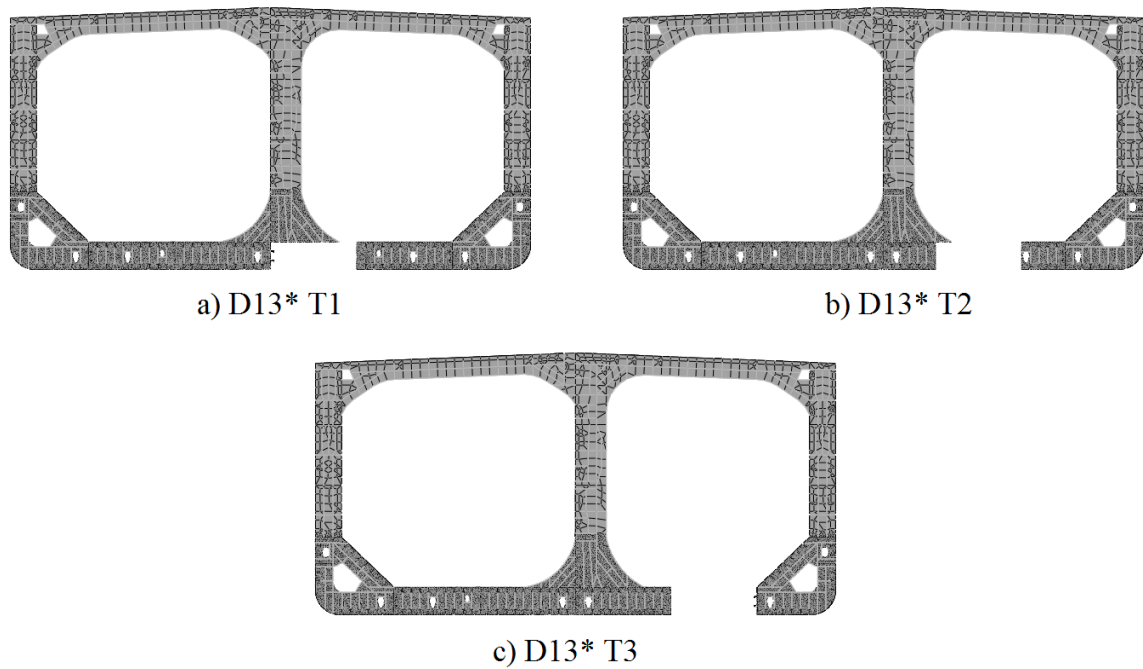


Figure 36: Transverse variation of the damage on a tanker with grounding damage

The following subsections present the summarized NLFEA results for all the intact and damaged cases. For clarity, all moment-curvature plots for damaged cases are given in the Appendix. Intact case has been included on every such plot for comparison purposes.

6.2 Results of NLFEA

6.2.1 Intact Condition

Figure 37 presents the intact moment-curvature curves for FPSO. NLFEA results are compared with the enhanced IIM (EIIM) results. EIIM accounts for the rotation and translation of the neutral axis due to asymmetry in the structure and/or loading.

The ultimate vertical bending moment capacity predicted by the NLFEA is greater by 6.2 % in hogging and by 1.5 % in sagging, compared to the EIIM. However, the prediction of the post ultimate strength behavior of the hull differs between the two methods. Compared to the EIIM, the NLFEA predicts a much sharper drop in the load bearing capacity after the ultimate limit state has been reached.

Figure 38 is similar to Figure 37, but presents the intact results for the Suezmax tanker. The ultimate vertical bending moment capacity predicted by the NLFEA is greater by 6.0 % in hogging and by 2.3 % in sagging, compared to the EIIM. Again, the prediction of the post ultimate strength behavior of the hull differs between the two methods, with NLFEA predicting a much sharper drop in the load bearing capacity after the ultimate limit state has been reached.

Figure 39 and Figure 40 compare the NLFEA and EIIM methods for intact bulk carrier and containership, respectively. For bulk carrier, the ultimate vertical bending moment capacity predicted by the NLFEA is greater by 3.0 % in hogging and by 4.3 % in sagging, compared to the EIIM. For containership, the ultimate vertical bending moment capacity predicted by the NLFEA is greater by 5.2 % in hogging and by 4.8 % in sagging, compared to the EIIM.

IIM and EIIM have been extensively validated against other more sophisticated methods in the intact case, and it is not surprising to see good agreement with NLFEA up to the ultimate strength point.

Currently, an effort is underway at ABS to validate the enhanced IIM (EIIM) used for Rapid Response Damage Assessment (RRDA) against NLFEA for intact as well as damaged cases. The validation has been performed for FPSO, tanker, and bulk carrier vessels under uniaxial and biaxial bending. EIIM consistently yields results closer to the NLFEA compared with the traditional IIM. The improvement is even more evident for damaged cases with highly asymmetric damage where the rotation of the neutral axis is more pronounced. In all the damaged cases with the default longitudinal damage extent, the NLFEA yielded more conservative results compared to the EIIM with the largest discrepancy of 13.59% for the bulk carrier with collision damage. However, if the effects of damage corners are removed by using the ALL WF models, the agreement between EIIM and NLFEA becomes much better. EIIM is essentially a 2-D method without any means of accounting for 3-D effects such as stress concentrations at damage corners. Therefore, it is not surprising that removing those stress concentrations in the ALL WF

model yields a better agreement between NLFEA and EIIM. More information about NLFEA – IIM – EIIM validation can be found in [20].

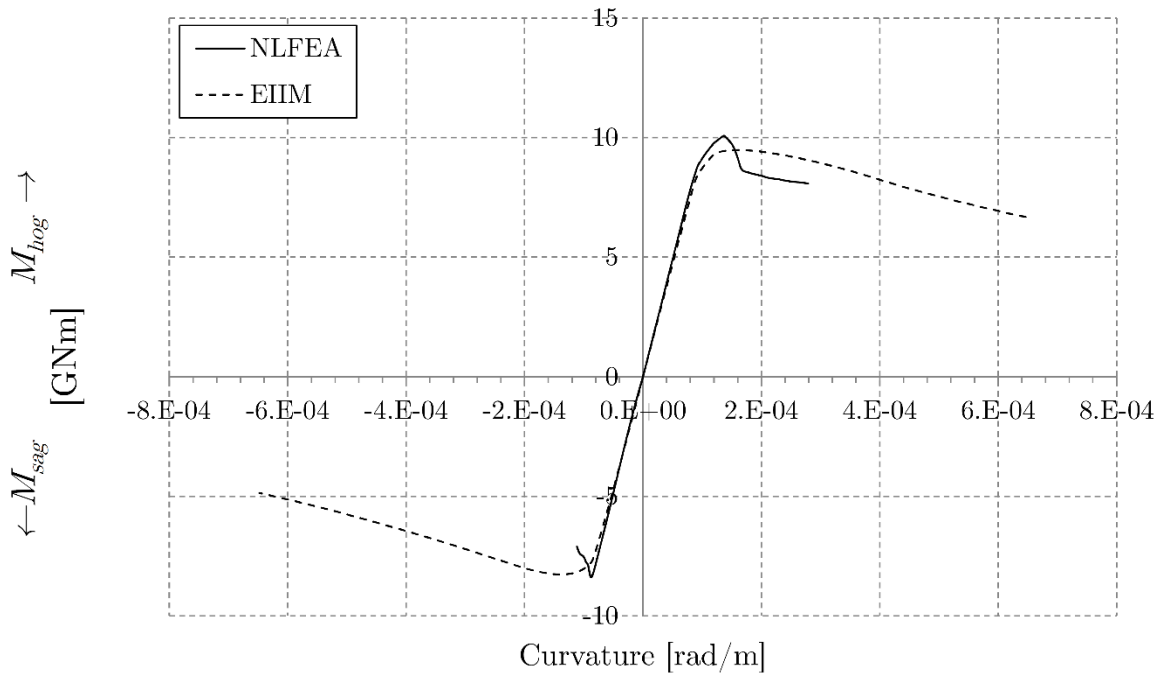


Figure 37: FPSO intact moment-curvature curves

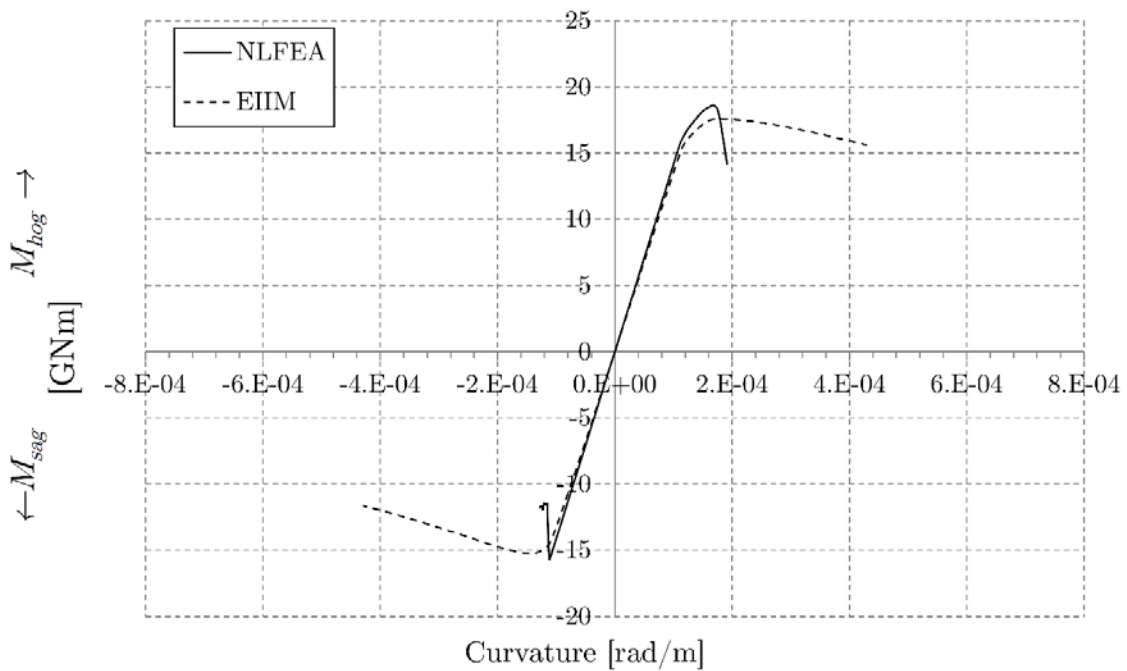


Figure 38: Tanker intact moment-curvature curves

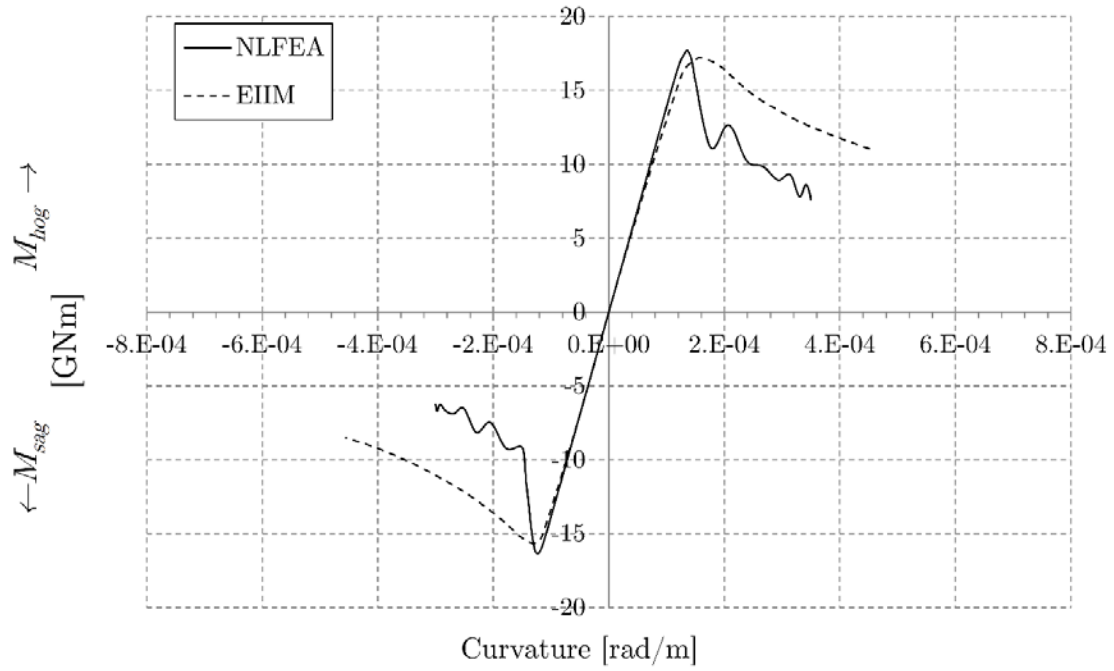


Figure 39: Bulk carrier intact moment-curvature curves

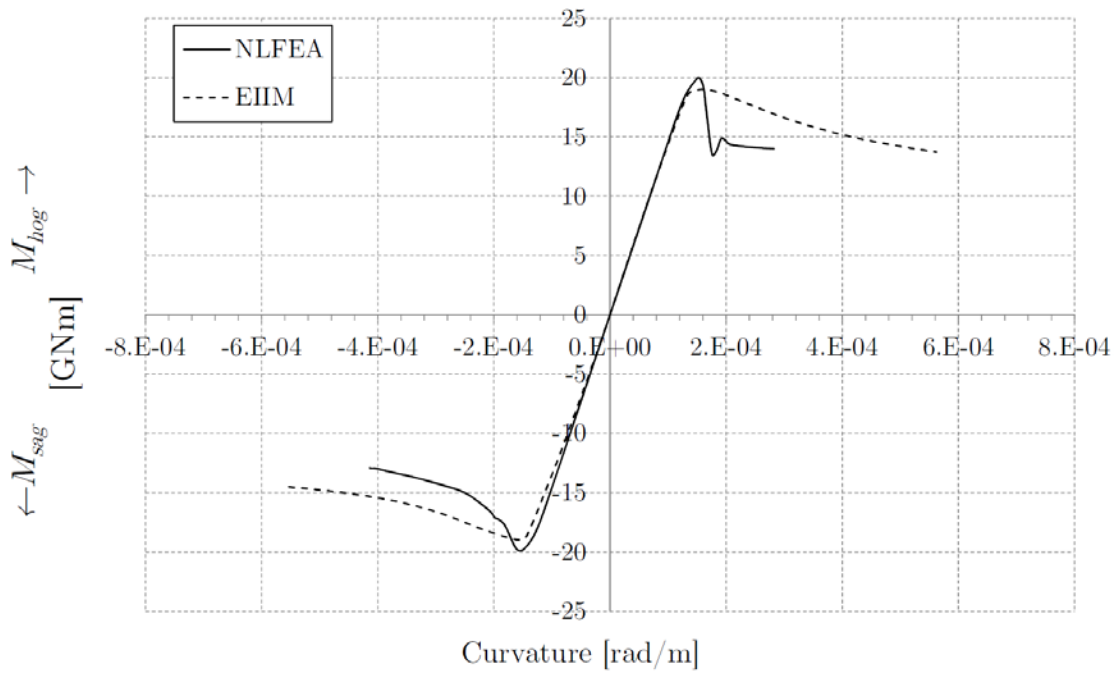


Figure 40: Containership intact moment-curvature curves

6.2.2 Damage Cases

Table 8 to Table 11 show the summary of ultimate strength results for all four analyzed vessels.

Table 8: Summary of NLFEA results for FPSO

(a)

FPSO – Collision (SAG)						
Case	A [m ²]	I_z [m ⁴]	W_D [m ³]	NA_y [m]	NA_z [m]	$M_{u, sag}$ [GNm]
Intact	5.16	463.46	36.90	10.44	0.00	8.389
D1	4.97	441.32	34.05	10.04	-0.88	7.082
D2	4.91	432.12	32.98	9.90	-1.10	6.630
D3	4.80	411.35	30.65	9.58	-1.51	6.334
D4	4.55	370.38	26.27	8.90	-2.17	5.224
D5	4.88	438.52	33.57	9.94	-1.30	6.777
D6	4.83	429.18	32.50	9.79	-1.53	6.351
D7	4.71	408.08	30.16	9.47	-1.96	6.076
D8	4.39	362.93	25.31	8.66	-2.85	4.840
D9	4.74	437.85	33.40	9.89	-2.01	6.555
D10	4.69	428.44	32.31	9.74	-2.25	6.108
D11	4.57	407.16	29.95	9.40	-2.71	5.801
D12	4.14	360.06	24.79	8.48	-4.06	4.313
D13	4.59	436.16	33.52	9.99	-2.80	6.677
D14	4.54	426.89	32.42	9.83	-3.06	6.062
D15	4.43	405.88	30.04	9.49	-3.56	5.708
D16	3.85	358.67	24.91	8.60	-5.56	3.966

(b)

FPSO – Collision (HOG)						
Case	A [m ²]	I_z [m ⁴]	W_D [m ³]	NA_y [m]	NA_z [m]	$M_{u, hog}$ [GNm]
Intact	5.16	463.46	36.90	10.44	0.00	10.068
D1	4.81	438.18	33.81	10.04	-0.94	9.496
D2	4.77	430.86	32.95	9.92	-1.12	9.367
D3	4.65	408.66	30.44	9.58	-1.57	8.843
D4	4.41	369.18	26.18	8.90	-2.23	7.806
D5	4.73	435.61	33.37	9.95	-1.33	9.393
D6	4.69	428.19	32.51	9.83	-1.52	9.201
D7	4.57	405.66	29.98	9.47	-1.99	8.572
D8	4.26	362.39	25.30	8.67	-2.87	7.287
D9	4.61	434.95	33.19	9.90	-2.01	9.141
D10	4.56	427.47	32.32	9.77	-2.21	8.873
D11	4.44	404.74	29.77	9.40	-2.72	8.179
D12	4.03	359.60	24.79	8.49	-4.02	6.683
D13	4.47	433.51	33.31	9.99	-2.77	8.995
D14	4.43	426.13	32.43	9.86	-2.98	8.736
D15	4.31	403.67	29.86	9.48	-3.52	8.055
D16	3.78	358.49	24.89	8.60	-5.37	6.339

(c)

FPSO – Grounding (HOG)						
Case	A [m ²]	I _z [m ⁴]	W _B [m ³]	NA _y [m]	NA _z [m]	M _{u, hog} [GNm]
Intact	5.16	463.46	44.40	10.44	0.00	10.068
D1	4.77	427.37	38.41	11.13	-0.23	8.572
D2	4.48	391.05	33.07	11.82	-0.99	7.415
D3	4.06	328.99	25.27	13.02	-2.18	5.794
D4	3.72	267.09	18.80	14.21	-1.52	4.779
D5	4.77	427.37	38.41	11.13	-0.23	8.506
D6	4.45	387.73	32.59	11.90	-1.07	7.302
D7	3.99	320.05	24.22	13.21	-2.51	5.687
D8	3.62	250.87	17.23	14.56	-1.79	4.560
D9	4.77	427.37	38.41	11.13	-0.23	8.499
D10	4.37	382.26	31.74	12.04	-1.25	7.105
D11	3.84	304.88	22.42	13.60	-3.26	5.187
D12	3.39	220.81	14.43	15.31	-2.44	3.907
D13	4.77	427.37	38.41	11.13	-0.23	8.498
D14	4.32	380.02	31.34	12.13	-1.39	7.006
D15	3.72	297.65	21.50	13.84	-3.87	4.991
D16	3.21	204.39	12.92	15.82	-2.99	3.656

(d)

FPSO – Grounding (SAG)						
Case	A [m ²]	I _z [m ⁴]	W _B [m ³]	NA _y [m]	NA _z [m]	M _{u, sag} [GNm]
Intact	5.16	463.46	44.40	10.44	0.00	8.389
D1	4.89	427.98	38.46	11.13	-0.19	8.212
D2	4.48	391.32	33.05	11.84	-0.97	7.802
D3	4.21	330.48	25.34	13.04	-2.11	6.803
D4	3.85	267.77	18.84	14.21	-1.44	6.107
D5	4.77	430.16	38.56	11.15	-0.18	8.185
D6	4.56	388.68	32.60	11.92	-1.07	7.716
D7	4.14	320.24	24.22	13.22	-2.49	6.462
D8	3.66	250.88	17.22	14.57	-1.76	5.610
D9	4.93	429.49	38.51	11.15	-0.19	8.198
D10	4.44	384.20	31.86	12.06	-1.17	7.626
D11	4.00	307.42	22.60	13.60	-3.25	6.077
D12	3.43	221.13	14.45	15.31	-2.39	5.129
D13	4.88	430.30	38.57	11.16	-0.23	8.198
D14	4.41	381.23	31.40	12.14	-1.39	7.561
D15	3.83	299.16	21.61	13.85	-3.80	5.629
D16	3.24	205.64	12.99	15.83	-2.96	4.533

Table 9: Summary of NLFEA results for Tanker

(a)

Suezmax Tanker – Collision (SAG)						
Case	A [m ²]	I _z [m ⁴]	W _D [m ³]	NA _y [m]	NA _z [m]	M _{u, sag} [GNm]
Intact	7.50	665.51	51.11	10.58	0.01	15.685
D1	7.30	634.52	47.46	10.23	-0.82	12.945
D2	7.00	600.96	43.67	9.84	-1.58	11.513
D3	6.90	570.52	40.55	9.53	-1.99	9.872
D4	6.70	537.98	37.36	9.20	-2.30	9.251
D5	7.20	631.68	47.03	10.17	-1.08	12.464
D6	6.90	594.64	42.78	9.70	-2.09	10.939
D7	6.70	563.59	39.66	9.39	-2.53	9.433
D8	6.60	530.38	36.45	9.05	-2.86	8.799
D9	7.10	630.58	46.78	10.12	-1.49	12.149
D10	6.70	592.05	42.32	9.61	-2.80	10.357
D11	6.60	560.54	39.14	9.28	-3.26	8.923
D12	6.40	526.81	35.91	8.93	-3.62	8.284
D13	7.00	630.34	46.80	10.13	-1.95	11.977
D14	6.50	591.60	42.26	9.60	-3.81	9.921
D15	6.30	560.06	39.06	9.26	-4.31	8.440
D16	6.20	526.22	35.80	8.90	-4.72	7.849

(b)

Suezmax Tanker – Collision (HOG)						
Case	A [m ²]	I _z [m ⁴]	W _D [m ³]	NA _y [m]	NA _z [m]	M _{u, hog} [GNm]
Intact	7.50	665.51	51.11	10.58	0.01	18.645
D1	7.30	635.66	47.51	10.22	-0.82	17.735
D2	7.10	603.26	43.84	9.84	-1.55	16.220
D3	6.90	572.87	40.72	9.53	-1.96	15.190
D4	6.80	540.39	37.55	9.21	-2.28	14.162
D5	7.20	632.82	47.05	10.15	-1.08	17.501
D6	6.90	596.94	42.98	9.71	-2.06	15.693
D7	6.80	565.95	39.83	9.39	-2.50	14.519
D8	6.60	532.80	36.64	9.06	-2.83	13.462
D9	7.10	631.71	46.83	10.11	-1.49	17.178
D10	6.70	594.36	42.48	9.61	-2.76	15.039
D11	6.60	562.91	39.31	9.28	-3.22	13.898
D12	6.40	529.24	36.08	8.93	-3.59	12.851
D13	7.00	631.47	46.81	10.11	-1.94	16.999
D14	6.50	593.91	42.45	9.61	-3.77	14.537
D15	6.30	562.42	39.22	9.26	-4.27	13.358
D16	6.20	528.65	35.96	8.90	-4.68	12.235

(c)

Suezmax Tanker – Grounding (HOG)						
Case	A [m ²]	I _z [m ⁴]	W _B [m ³]	NA _y [m]	NA _z [m]	M _{u, hog} [GNm]
Intact	7.50	665.51	62.90	10.58	0.01	18.645
D1	7.30	634.49	57.68	11.00	-0.13	16.344
D2	7.00	600.26	52.52	11.43	-0.62	15.066
D3	6.60	548.65	45.49	12.06	-1.26	13.096
D4	6.30	497.82	39.20	12.70	-0.80	11.566
D5	7.20	631.40	57.35	11.01	-0.15	16.251
D6	7.00	597.07	52.15	11.45	-0.65	14.971
D7	6.60	542.51	44.69	12.14	-1.37	12.964
D8	6.20	490.94	38.35	12.80	-0.91	11.576
D9	7.20	629.77	57.04	11.04	-0.15	16.188
D10	6.90	595.28	51.90	11.47	-0.65	14.912
D11	6.50	537.07	43.95	12.22	-1.47	12.702
D12	6.20	484.81	37.64	12.88	-1.01	11.252
D13	7.00	609.59	53.66	11.36	-0.31	15.036
D14	6.40	549.81	45.07	12.20	-1.35	12.425
D15	5.80	460.30	34.27	13.43	-2.47	9.732
D16	5.20	351.98	23.54	14.95	-1.55	7.600

(d)

Suezmax Tanker – Grounding (SAG)						
Case	A [m ²]	I _z [m ⁴]	W _B [m ³]	NA _y [m]	NA _z [m]	M _{u, sag} [GNm]
Intact	7.50	665.51	62.90	10.58	0.01	15.685
D1	7.20	631.54	57.31	11.02	-0.15	15.574
D2	7.00	597.19	52.16	11.45	-0.64	15.203
D3	6.60	544.38	44.92	12.12	-1.32	14.383
D4	6.20	493.01	38.61	12.77	-0.86	13.675
D5	7.20	629.71	57.04	11.04	-0.15	15.558
D6	6.90	589.19	50.97	11.56	-0.77	15.042
D7	6.50	538.42	44.10	12.21	-1.43	14.198
D8	6.20	486.30	37.79	12.87	-0.97	13.508
D9	7.00	609.02	53.52	11.38	-0.31	15.369
D10	6.30	539.16	43.66	12.35	-1.59	14.170
D11	5.80	460.21	34.27	13.43	-2.45	12.337
D12	5.20	351.84	23.53	14.95	-1.52	10.449

Table 10: Summary of NLFEA results for Bulk Carrier

(a)

Bulk Carrier – Collision (SAG)						
Case	A [m²]	I_z [m⁴]	W_D [m³]	NA_y [m]	NA_z [m]	M_{u, sag} [GNm]
Intact	6.00	655.57	48.10	11.17	0.00	16.327
D1	5.70	611.46	43.15	10.63	-1.13	12.794
D2	5.60	584.75	40.24	10.27	-1.75	10.893
D3	5.20	519.43	33.75	9.41	-2.89	9.127
D4	4.90	433.38	26.35	8.35	-3.88	7.585
D5	5.60	605.89	42.34	10.49	-1.63	12.226
D6	5.40	579.41	39.47	10.12	-2.26	10.404
D7	5.10	511.67	32.84	9.22	-3.48	8.863
D8	4.80	423.43	25.40	8.13	-4.54	7.290
D9	5.50	605.32	42.21	10.46	-2.06	11.959
D10	5.30	578.70	39.31	10.08	-2.72	10.289
D11	5.00	510.48	32.64	9.16	-3.99	8.783
D12	4.70	421.43	25.15	8.04	-5.11	7.215
D13	5.30	603.78	42.34	10.54	-2.88	11.905
D14	5.10	576.67	39.55	10.22	-3.89	10.153
D15	4.80	509.31	32.75	9.25	-5.28	8.353
D16	4.40	420.96	25.16	8.07	-6.55	6.705

(b)

Bulk Carrier – Collision (HOG)						
Case	A [m²]	I_z [m⁴]	W_D [m³]	NA_y [m]	NA_z [m]	M_{u, hog} [GNm]
Intact	6.00	655.57	48.10	11.17	0.00	17.710
D1	5.80	617.37	43.60	10.64	-1.03	16.539
D2	5.60	588.11	40.39	10.24	-1.70	15.201
D3	5.20	520.68	33.72	9.36	-2.87	12.650
D4	4.90	434.84	26.39	8.32	-3.85	9.969
D5	5.60	611.41	42.73	10.49	-1.55	15.895
D6	5.50	581.76	39.55	10.09	-2.24	14.555
D7	5.10	512.68	32.82	9.18	-3.47	11.883
D8	4.80	424.62	25.41	8.09	-4.52	9.175
D9	5.50	610.86	42.60	10.46	-2.01	15.601
D10	5.40	581.04	39.39	10.05	-2.72	14.219
D11	5.00	511.47	32.60	9.11	-4.01	11.478
D12	4.70	422.59	25.15	8.00	-5.12	8.673
D13	5.40	609.29	42.76	10.55	-2.79	15.477
D14	5.10	578.86	39.57	10.17	-3.83	13.884
D15	4.80	510.32	32.71	9.20	-5.26	10.938
D16	4.50	422.14	25.19	8.04	-6.52	7.964

(c)

Bulk Carrier – Grounding (HOG)						
Case	A [m²]	I_z [m⁴]	W_B [m³]	NA_y [m]	NA_z [m]	M_{u, hog} [GNm]
Intact	6.00	655.57	58.69	11.17	0.00	17.710
D1	5.80	628.67	54.34	11.57	-0.14	15.712
D2	5.60	600.25	50.02	12.00	-0.57	14.337
D3	5.30	554.67	43.74	12.68	-1.22	12.776
D4	5.10	512.59	38.51	13.31	-0.83	11.675
D5	5.80	624.44	53.65	11.64	-0.16	15.488
D6	5.60	592.77	48.91	12.12	-0.64	14.039
D7	5.20	540.62	41.91	12.90	-1.40	12.642
D8	4.90	491.07	35.98	13.65	-0.96	11.477
D9	5.70	619.75	52.88	11.72	-0.18	15.147
D10	5.50	584.37	47.67	12.26	-0.73	13.732
D11	5.10	523.70	39.70	13.19	-1.67	11.670
D12	4.70	465.46	33.06	14.08	-1.15	9.988
D13	5.50	599.19	49.48	12.11	-0.35	13.156
D14	5.00	536.67	40.81	13.15	-1.49	10.504
D15	4.50	443.58	30.26	14.66	-2.71	7.922
D16	3.90	318.81	19.06	16.73	-1.71	5.784

(d)

Bulk Carrier – Grounding (SAG)						
Case	A [m²]	I_z [m⁴]	W_B [m³]	NA_y [m]	NA_z [m]	M_{u, sag} [GNm]
Intact	6.00	655.57	58.69	11.17	0.00	16.327
D1	5.80	625.00	53.74	11.63	-0.15	16.218
D2	5.60	595.10	49.26	12.08	-0.60	16.080
D3	5.30	548.27	42.90	12.78	-1.28	15.385
D4	5.00	502.67	37.32	13.47	-0.87	14.982
D5	5.70	619.73	52.88	11.72	-0.17	16.206
D6	5.50	585.91	47.91	12.23	-0.69	15.926
D7	5.10	531.33	40.68	13.06	-1.50	14.991
D8	4.80	476.02	34.22	13.91	-1.02	14.352
D9	5.50	598.14	49.35	12.12	-0.34	16.102
D10	5.00	536.04	40.73	13.16	-1.46	14.893
D11	4.50	445.06	30.42	14.63	-2.75	12.489
D12	3.90	320.75	19.21	16.70	-1.79	9.751

Table 11: Summary of NLFEA results for Containership

(a)

Containership – Collision (SAG)						
Case	A [m²]	I_z [m⁴]	W_D [m³]	NA_y [m]	NA_z [m]	$M_{u, sag}$ [GNm]
Intact	6.40	691.41	51.64	11.61	0.00	19.893
D1	5.90	618.03	43.04	10.64	-1.87	15.114
D2	5.20	465.66	28.71	8.78	-4.99	10.779
D5	5.90	615.01	42.59	10.56	-2.20	14.696
D6	5.10	455.94	27.72	8.55	-5.75	10.296
D9	5.70	614.44	42.46	10.53	-2.64	14.283
D10	4.90	452.75	27.29	8.41	-6.77	9.756
D13	5.60	612.97	42.57	10.60	-3.23	13.996
D14	4.60	451.98	27.31	8.45	-8.28	9.253

(b)

Containership – Collision (HOG)						
Case	A [m²]	I_z [m⁴]	W_D [m³]	NA_y [m]	NA_z [m]	$M_{u, hog}$ [GNm]
Intact	6.40	691.41	51.64	11.61	0.00	20.006
D1	5.90	620.27	43.28	10.67	-1.83	16.973
D2	5.20	465.67	28.71	8.78	-4.99	10.666
D5	5.90	617.27	42.84	10.59	-2.15	16.607
D6	5.10	455.95	27.72	8.55	-5.75	9.691
D9	5.80	616.71	42.71	10.56	-2.59	16.338
D10	4.90	452.77	27.29	8.41	-6.77	8.809
D13	5.60	615.11	42.81	10.63	-3.19	16.242
D14	4.60	451.92	27.32	8.46	-8.32	7.966

(c)

Containership – Grounding (HOG)						
Case	A [m ²]	I _z [m ⁴]	W _B [m ³]	NA _y [m]	NA _z [m]	M _{u, hog} [GNm]
Intact	6.40	691.41	59.55	11.61	0.00	20.006
D1	6.20	657.10	54.44	12.07	-0.15	16.872
D2	5.90	623.54	49.80	12.52	-0.60	15.287
D3	5.70	585.54	44.90	13.04	-0.85	13.197
D4	5.40	536.79	39.18	13.70	-0.43	11.524
D5	6.10	651.64	53.63	12.15	-0.18	16.433
D6	5.90	612.84	48.33	12.68	-0.71	14.645
D7	5.60	565.63	42.46	13.32	-1.11	12.694
D8	5.30	508.28	36.05	14.10	-0.62	10.948
D9	6.10	647.59	53.04	12.21	-0.20	15.836
D10	5.80	604.72	47.24	12.80	-0.80	13.782
D11	5.50	551.48	40.76	13.53	-1.30	11.916
D12	5.10	486.43	33.71	14.43	-0.78	9.766
D13	5.90	627.41	50.07	12.53	-0.33	14.505
D14	5.40	559.18	41.36	13.52	-1.36	11.952
D15	4.90	469.57	31.68	14.82	-2.26	9.202
D16	4.40	347.16	20.93	16.59	-1.38	6.323

(d)

Containership – Grounding (SAG)						
Case	A [m ²]	I _z [m ⁴]	W _B [m ³]	NA _y [m]	NA _z [m]	M _{u, sag} [GNm]
Intact	6.40	691.41	59.55	11.61	0.00	19.893
D1	6.20	654.76	54.11	12.10	-0.16	19.510
D2	5.90	618.70	49.14	12.59	-0.65	18.687
D3	5.70	577.32	43.90	13.15	-0.95	17.733
D4	5.40	525.41	37.91	13.86	-0.51	16.823
D5	6.10	648.52	53.16	12.20	-0.20	19.396
D6	5.80	606.51	47.49	12.77	-0.78	18.423
D7	5.50	554.11	41.08	13.49	-1.28	17.068
D8	5.20	492.20	34.32	14.34	-0.75	15.888
D9	5.90	627.39	50.07	12.53	-0.33	19.032
D10	5.40	559.17	41.36	13.52	-1.36	17.030
D11	4.90	469.99	31.73	14.81	-2.25	14.406
D12	4.40	348.98	21.07	16.56	-1.39	11.495

In the above tables, A is the cross-section area of the hull, I_z is the moment of inertia around the transverse axis (z), W_D and W_B are the section moduli of the deck and bottom, respectively, NA_y is the vertical position of the neutral axis, and NA_z is the horizontal position of the neutral axis (measured from the centerline).

The main collapse mode in all intact cases and the majority of the damaged cases is the interframe collapse of stiffened panels. Similarly to 1-B models, local stiffener tripping occurs first, and the plate between stiffeners rotates initially to accommodate the stiffener web rotation around the attachment point. As the compressive load is increased, the von Mises stress in the plating reaches and exceeds the yield stress of the material at which point a typical “pitched roof” configuration and plastic mechanism occur in the plating. It is also worth noting that all damaged cases, in which the direction of the bending moment causes compressive stresses in the intact flange of the hull (collision with hogging and grounding with sagging), exhibit interframe collapse modes.

The cross-section failure domain is usually quite narrow and is concentrated between the two web frames, for all vessel types. The initial stiffener tripping is governed by the position of geometric imperfections and the tripping locations on adjacent stiffeners. For damaged cases the failure initiates from the highly stressed region at the corner of the damaged area on the deck or bottom and progresses outwards towards the side plating. Figure 41 to Figure 51 show typical interframe failure domains for all four vessels in various intact and damaged cases. All the figures show von Mises stress distribution at the last converged step of the analysis in the post ultimate strength region. Stresses for FPSO are in N/cm^2 , while the stresses for the other three vessel types are in N/m^2 .

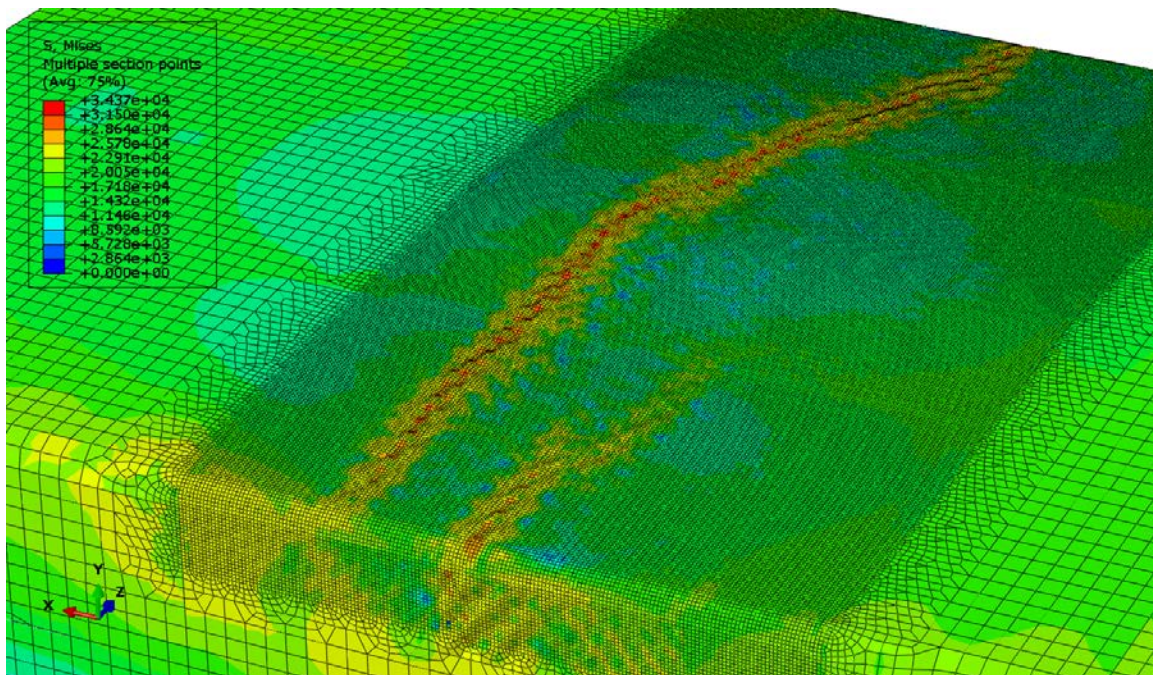


Figure 41: Intact FPSO in sagging

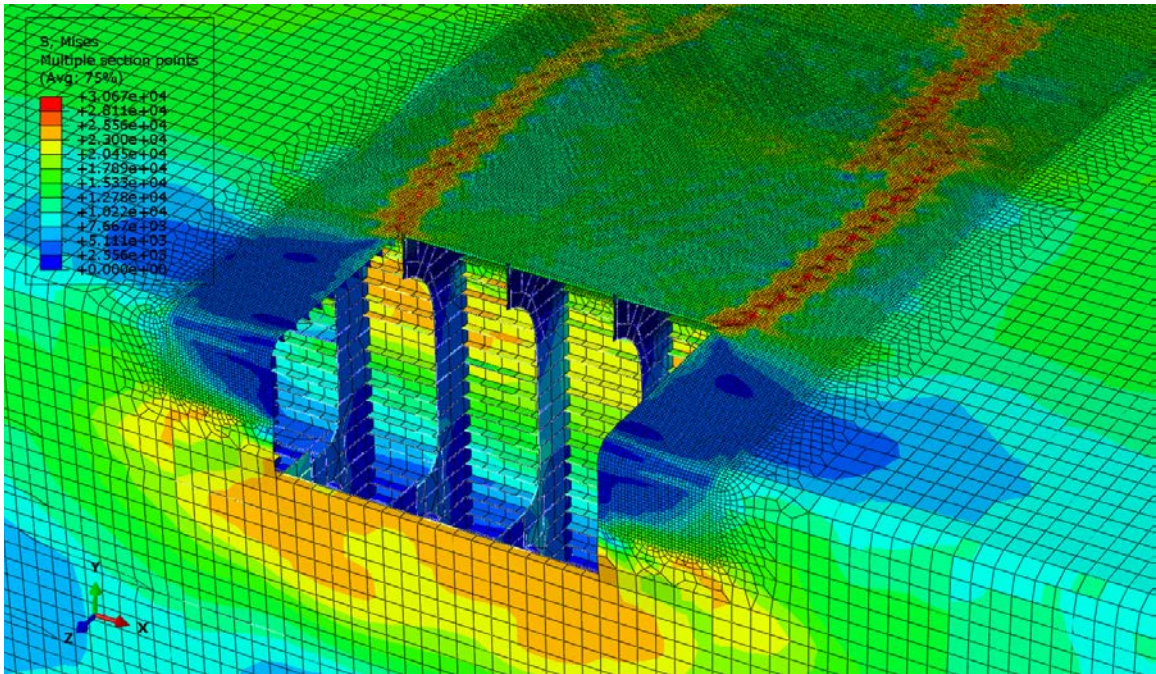


Figure 42: FPSO with D3 collision damage in sagging. Two narrow failure domains stemming from the damage corners can be observed.

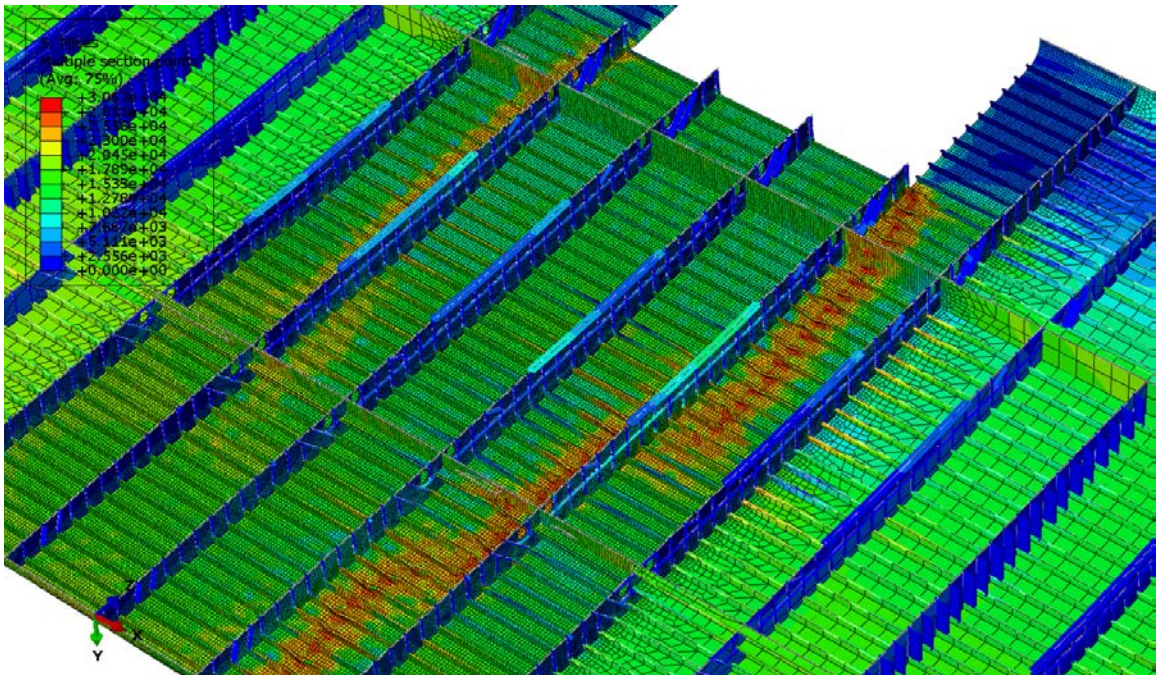


Figure 43: FPSO with D3 collision damage in sagging. Deck is viewed from below.

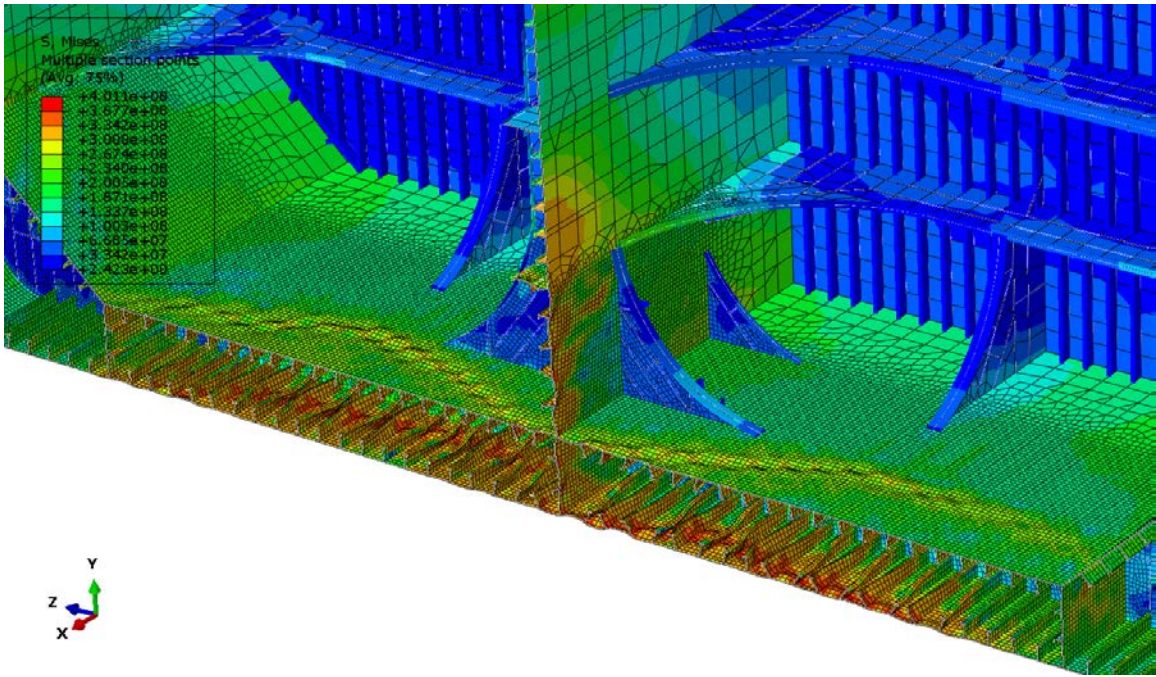


Figure 44: Intact tanker in hogging. The model has been cut to reveal the damage to bottom and inner bottom stiffened panels.

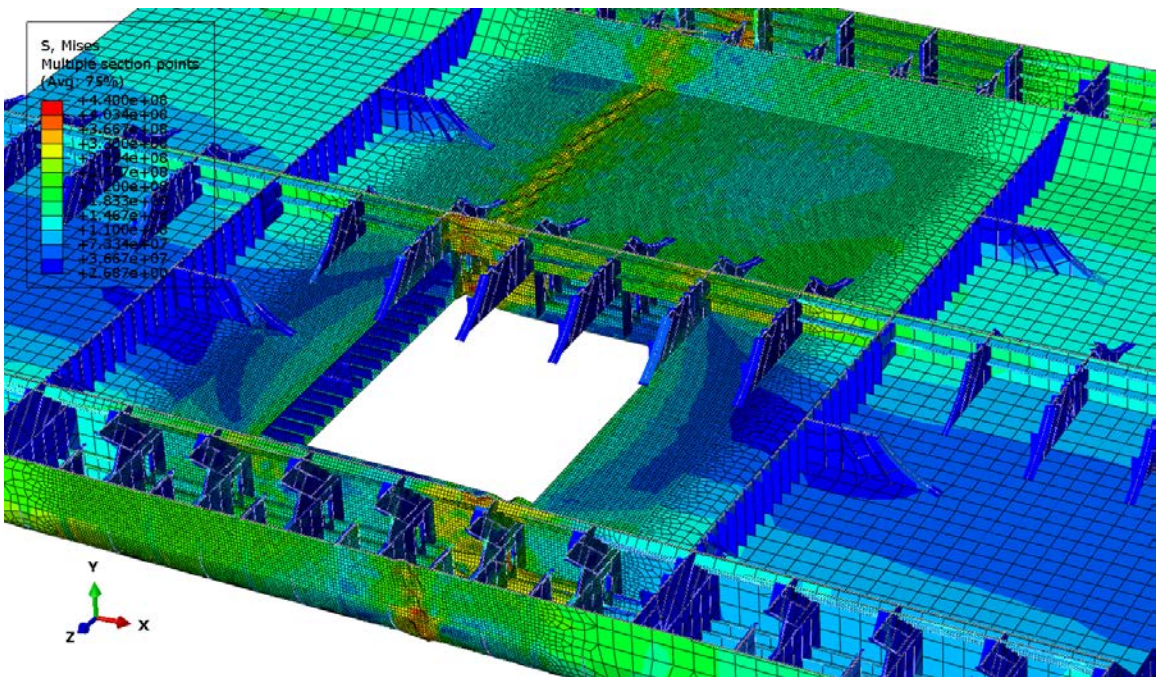


Figure 45: Tanker with D14 grounding damage in hogging.

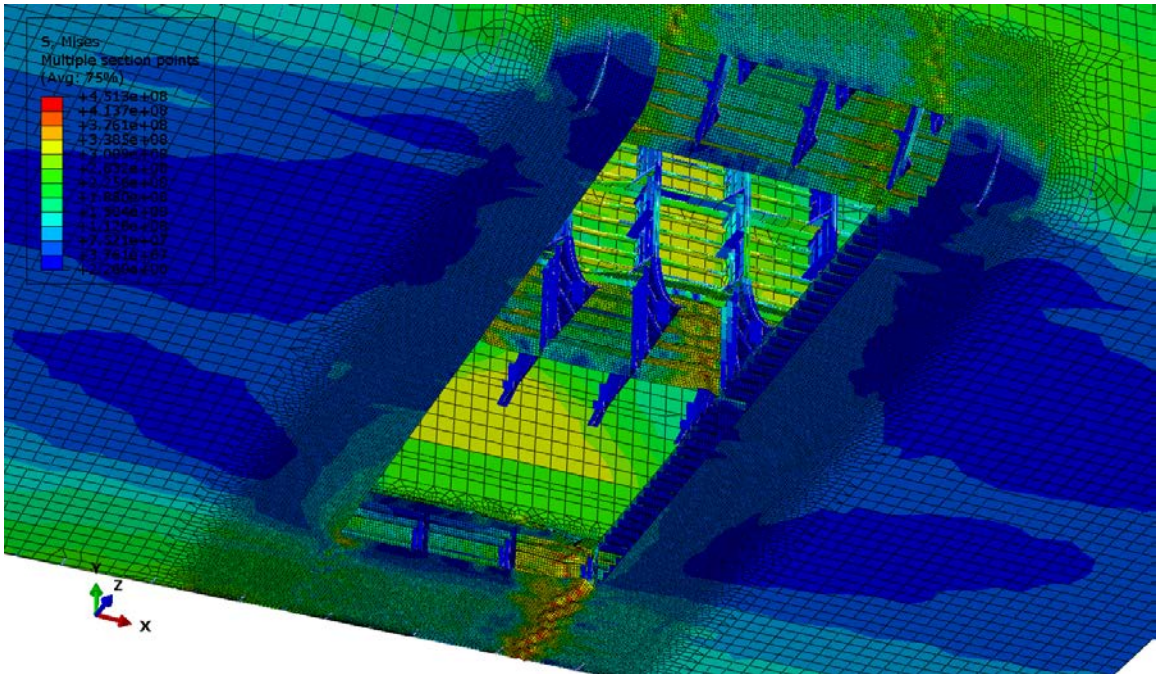


Figure 46: Tanker with D16 grounding damage in hogging.

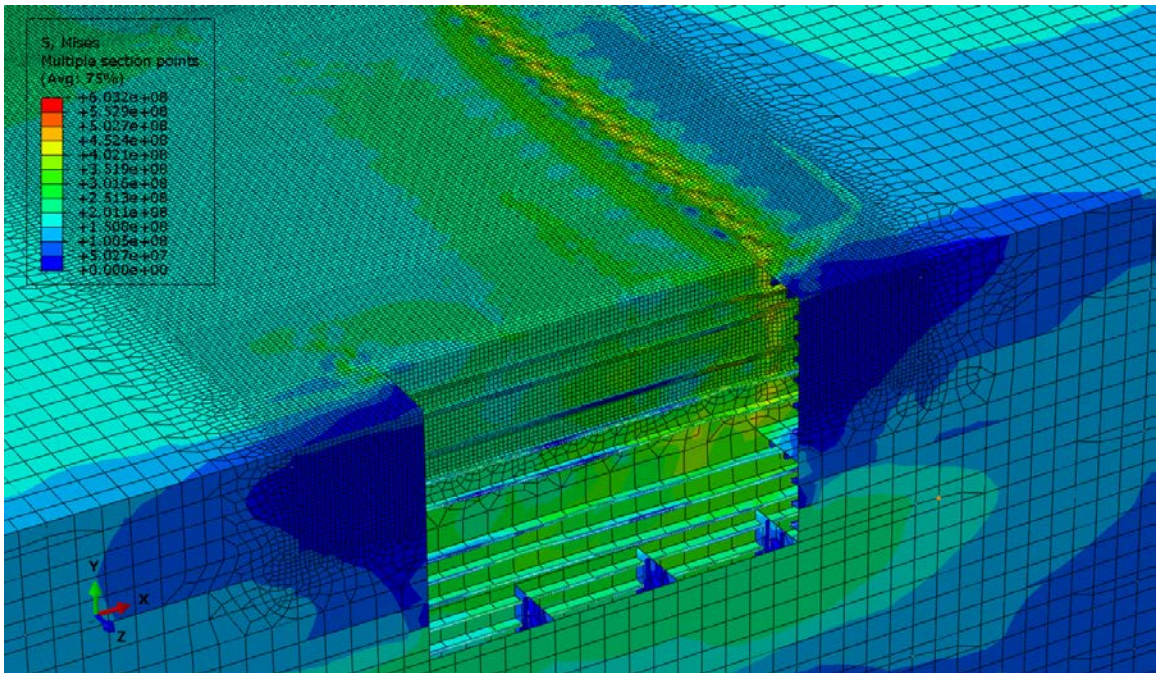


Figure 47: Tanker with D5 collision damage in sagging.

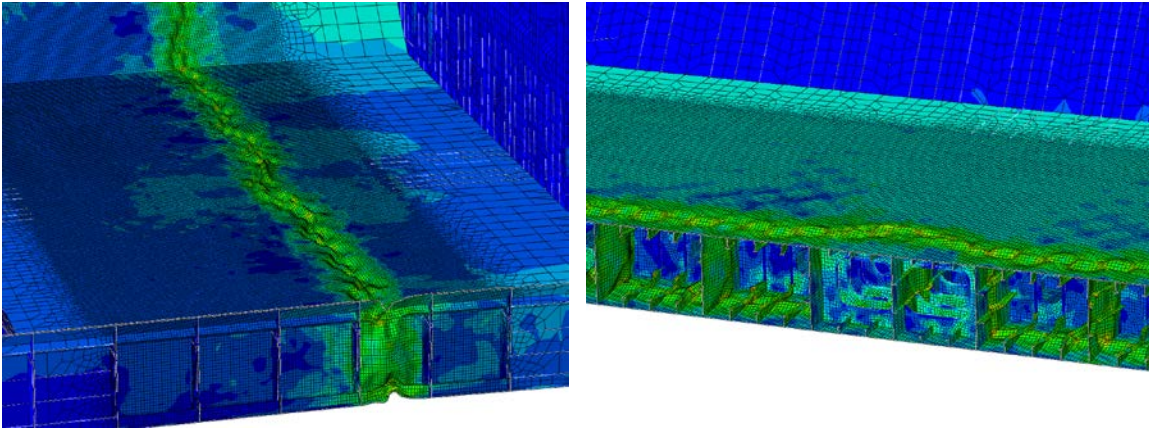


Figure 48: The interframe collapse mode of the intact bulk carrier in hogging

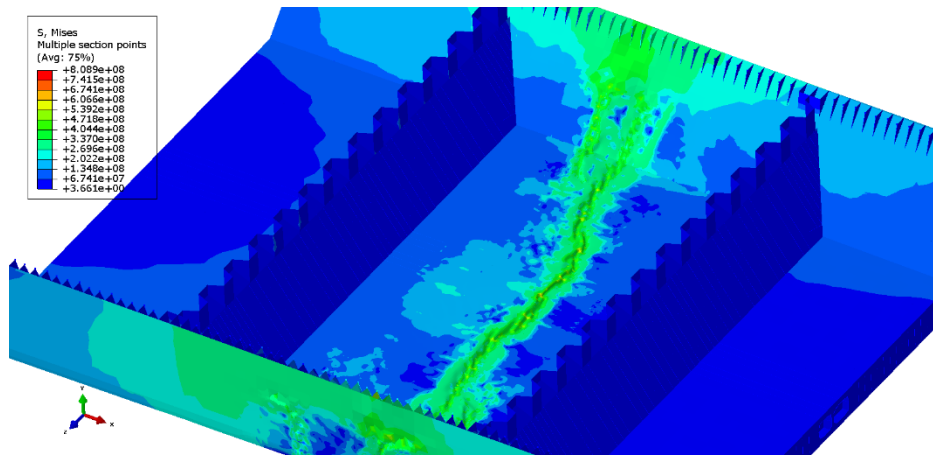


Figure 49: The interframe collapse mode of the bulk carrier with D8 grounding damage in hogging

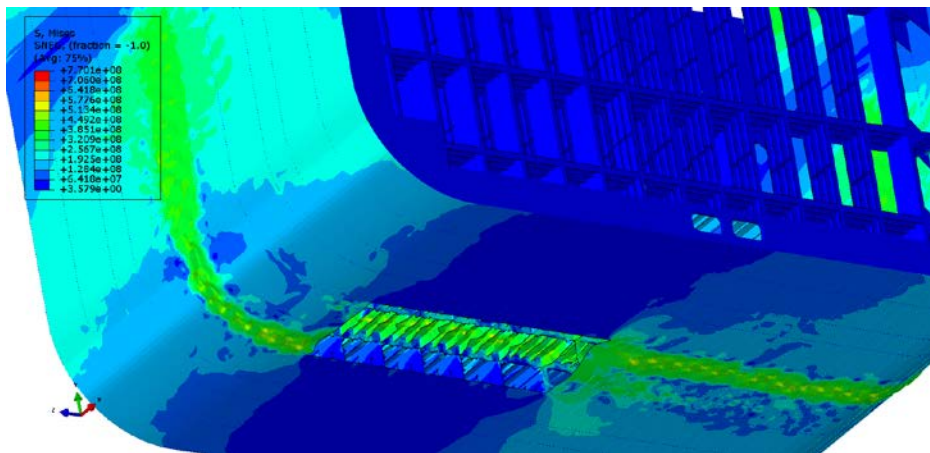


Figure 50: The interframe collapse mode of the containership with D10 grounding damage in hogging

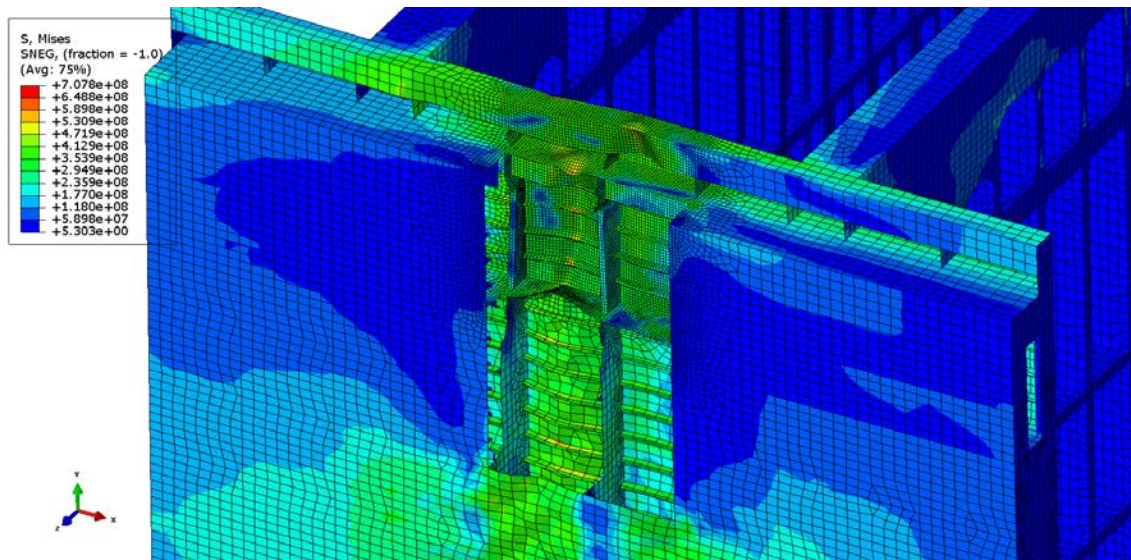


Figure 51: The interframe collapse mode of the containership with D5 collision damage in sagging

Interframe collapse mode supports the application of IIM or EIIM which cannot account for any other collapse mode. There were a few instances where pure interframe collapse has not been observed. This happened on the tanker with collision damages D2, D6, D10, and D14 in sagging and in a few bulk carrier cases with grounding and collision damage. All the tanker cases in which non-interframe failure mode has been observed have the same damage breadth where the inner skin bulkhead has been removed, leaving the deck webs without the end support (see Figure 53). All other collision damage cases either have the inner skin bulkhead intact, or leave a much shorter unsupported cantilever length of the deck webs. Therefore, only collision damage cases D2, D5, D10, and D14 exhibit the overall deck buckling in addition to local stiffener tripping. Figure 52 to Figure 55 show a comparison of the collapse modes between D2 and D4, where D4 does not exhibit overall deck buckling due to a shorter unsupported span of the damaged deck webs.

This is the reason why the moment-curvature curves for tanker D2, D6, D10, and D14 collision damage look quite different compared to the rest of the curves for other damage sizes. The overall buckling of the deck is in the opposite direction to the imposed curvature which increases the geometric stiffness of the hull and slows down the loss of moment bearing capacity. This is especially visible for the longitudinal damage extent of 3WF and ALL WF. The longitudinal damage extent of 1WF is too short for this effect to become noticeable.

The overall deck buckling does not happen for the FPSO because the two longitudinal bulkheads shorten the unsupported length of the deck webs.

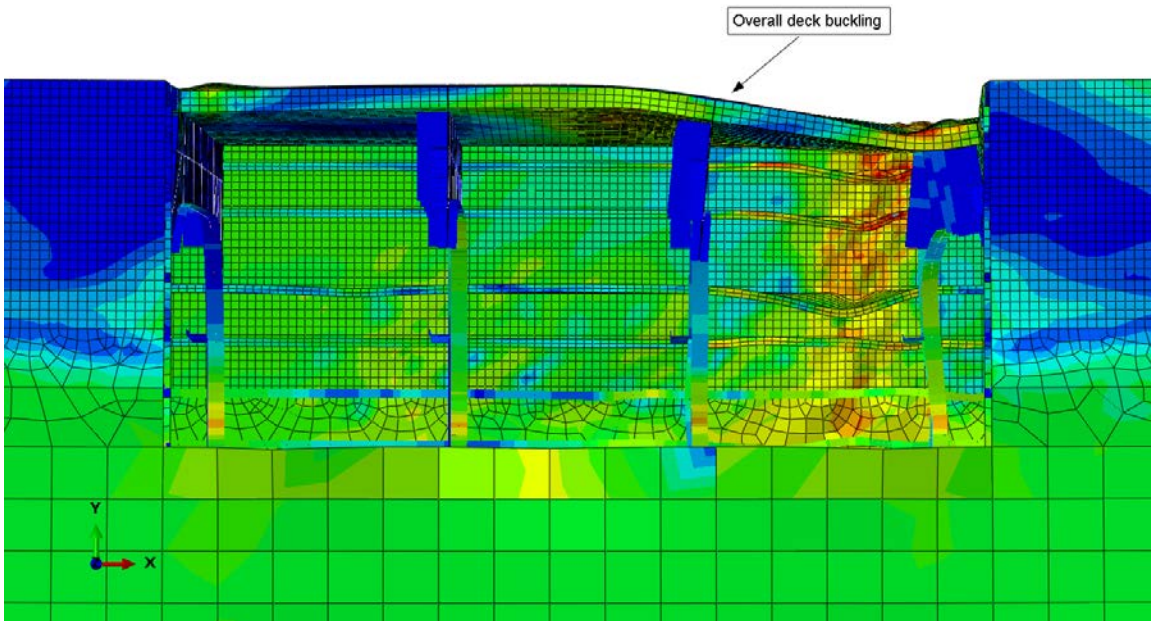


Figure 52: Tanker with D2 collision damage in sagging. Overall deck buckling can be observed.

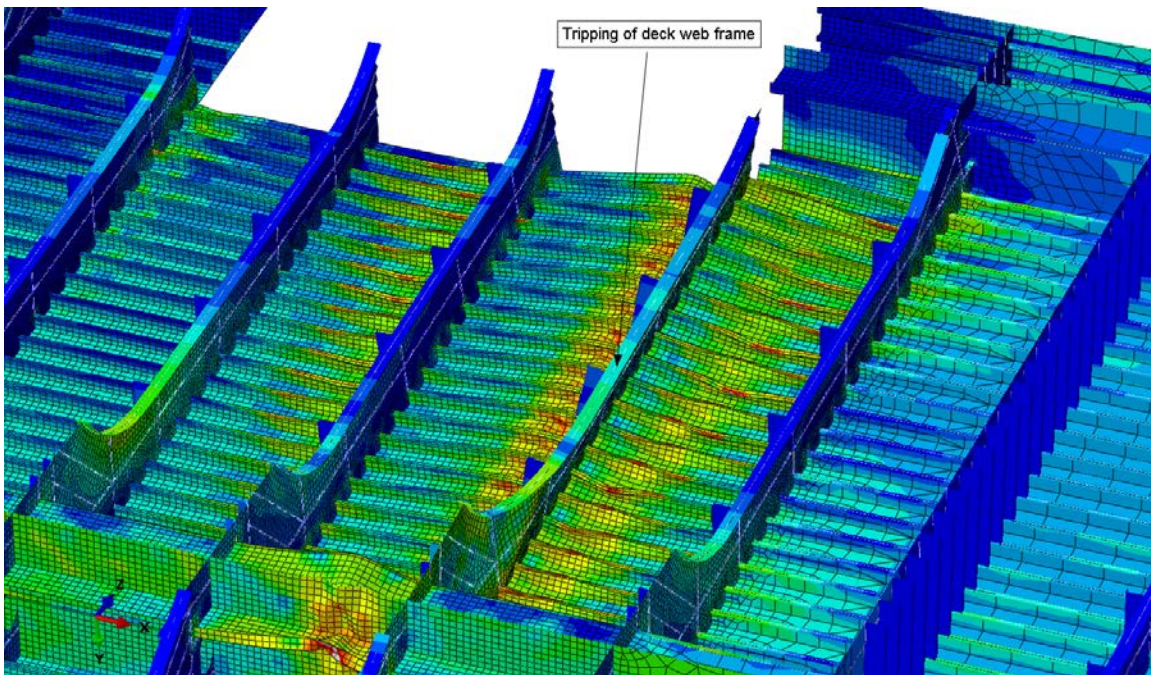


Figure 53: Tanker with D2 collision damage in sagging. Damaged deck web has tripped.

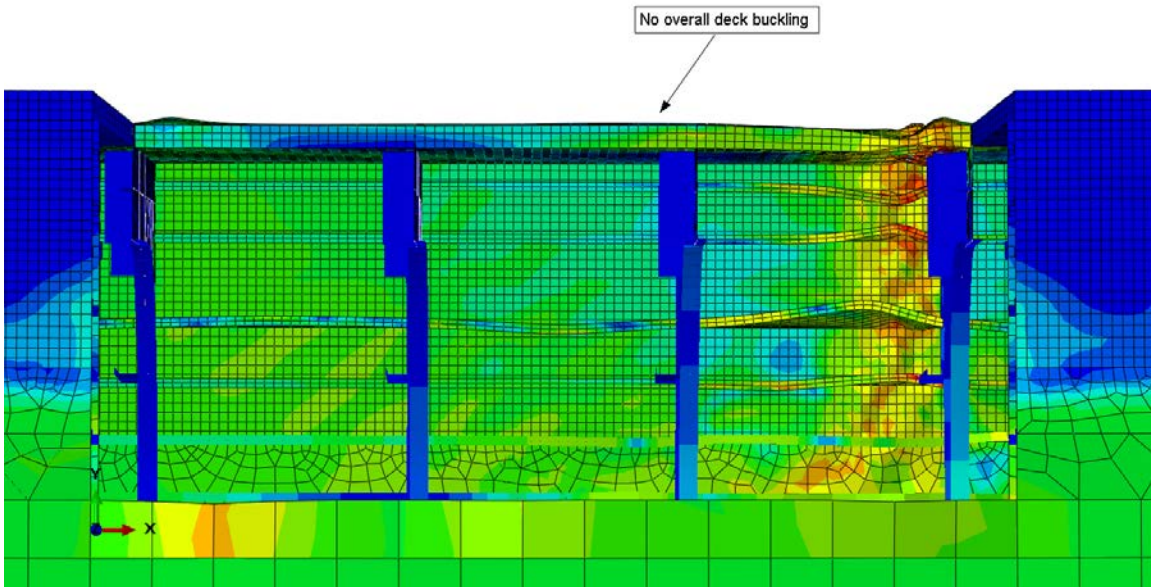


Figure 54: Tanker with D4 collision damage in sagging. There is no overall deck buckling.

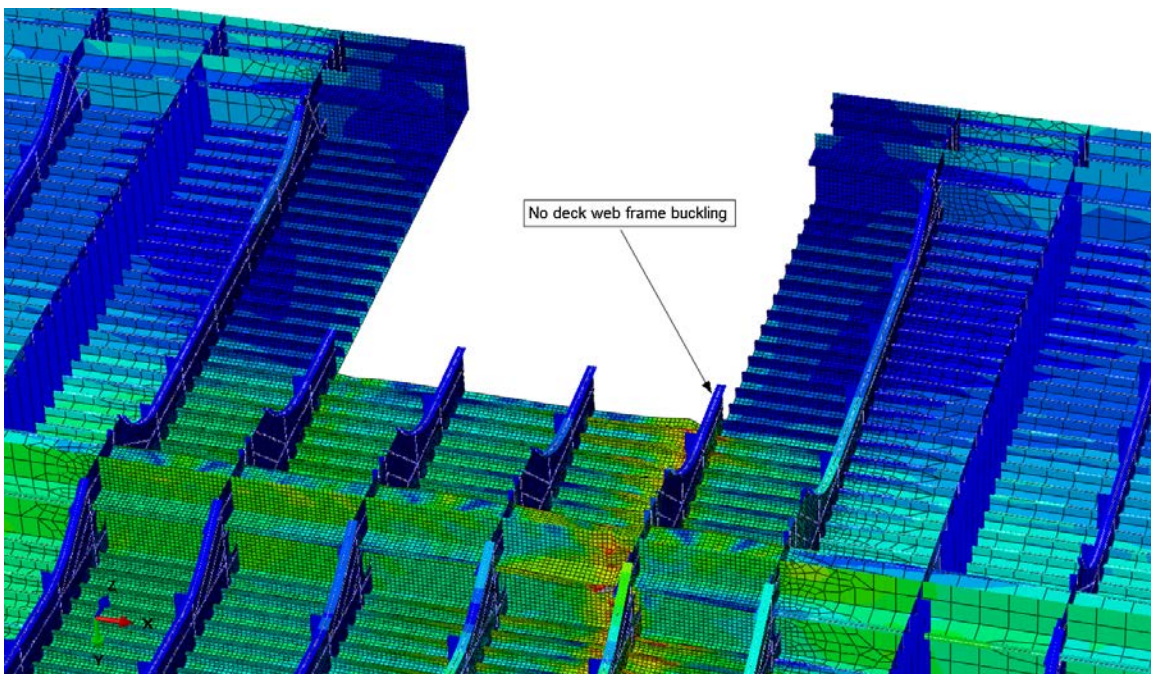


Figure 55: Tanker with D4 collision damage in sagging. Damaged deck webs are completely unstressed.

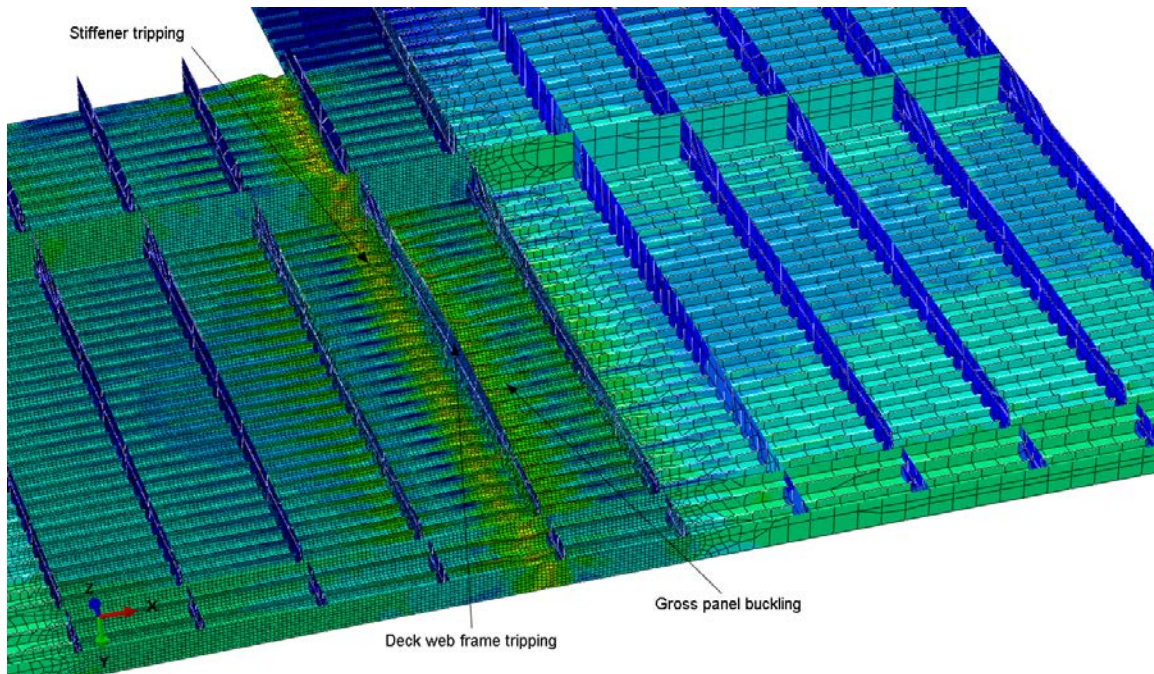


Figure 56: Tanker with D4 collision damage in sagging. Two types of interframe collapse are shown: stiffener tripping and gross panel buckling.

In the case of the tanker with collision damage, where the interframe collapse modes are observed, deck panels located on the other side of the collision damage and adjacent to the panels with stiffener tripping, undergo gross panel buckling. These two types of interframe collapse (stiffener tripping and gross panel buckling) are shown in Figure 56 for the tanker with D4 collision damage in sagging. The initial stiffener tripping and local plate buckling give rise to deck web tripping. The adjacent plating has to rotate in order to accommodate the web frame rotation, and this gives rise to the gross buckling of the panel on the other side of the web frame.

Bulk carrier grounding damage cases D9, D10, D11, and D12 are such where the height of the damage is equal to three quarters of the double bottom height. In such cases, the inner bottom loses the support of bottom girders and floors. Therefore, a large portion of the inner bottom starts to behave as a very large longitudinally stiffened panel, as opposed to strong grillage, and the overall inner bottom buckling starts to occur early in the analysis for hogging bending moment. This is the primary mode of failure and occurs on the damaged side of the vessel. The primary mode of failure on the intact side of the vessel is still interframe collapse of the bottom, inner bottom and double bottom longitudinal girders (see Figure 57). Grounding damage cases with smaller height exhibit pure interframe collapse modes (see Figure 58). On the other two vessels with a double bottom (tanker and containership) overall buckling of the inner bottom does not happen when the grounding damage height reaches three quarters of the double bottom height (see Figure 59). This is mainly due to heavier stiffening of the inner bottom and larger double bottom height of tanker and containership compared to the bulk carrier.

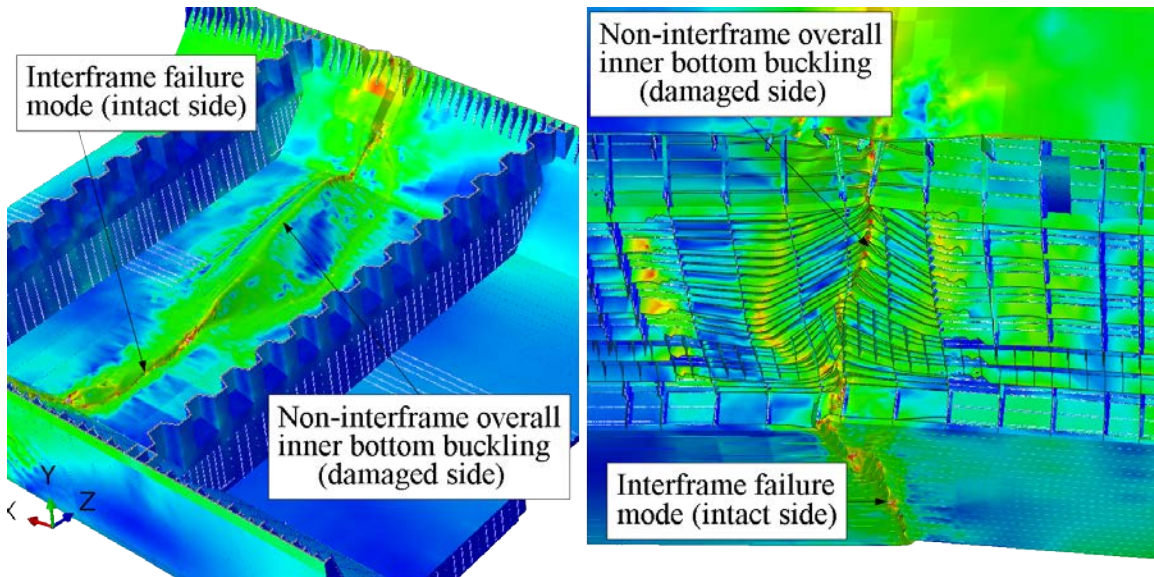


Figure 57: Failure modes on damaged and intact sides of a bulk carrier with grounding damage in hogging

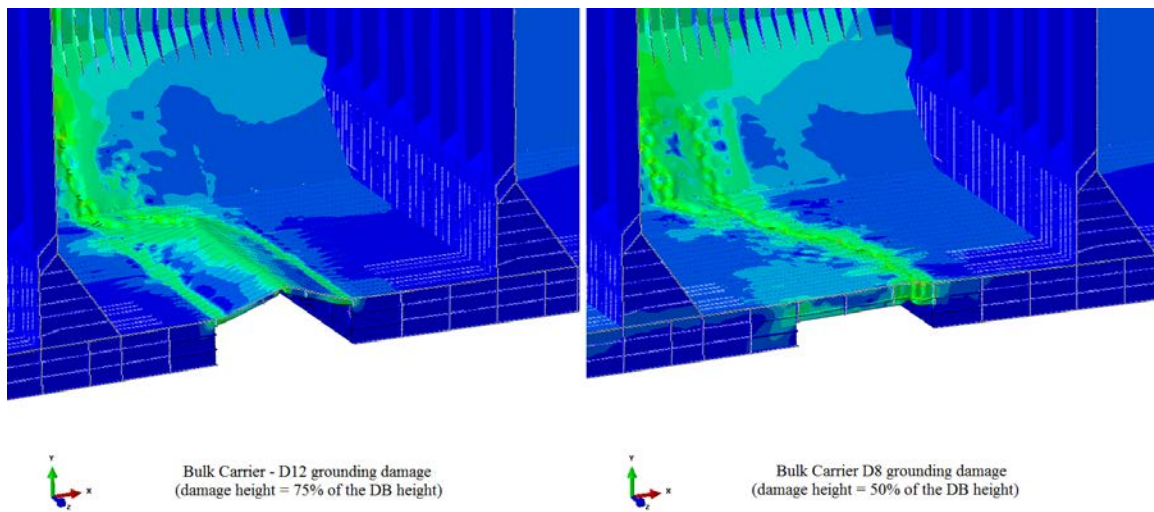


Figure 58: Non-interframe (left) and interframe (right) failure modes on a bulk carrier in hogging with two different damage heights.

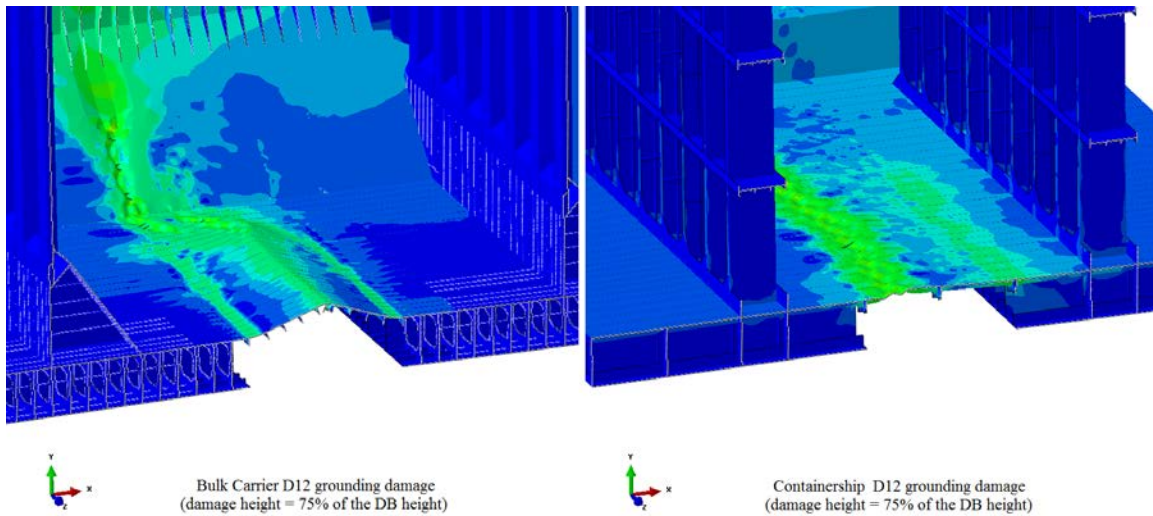


Figure 59: Non-interframe failure mode on a bulk carrier (left) and interframe failure mode on a containership (right) with grounding damage. Both damage heights are 75% of the double bottom height.

Due to very large web frame spacings in the wing tank of the bulk carrier, the default collision damage spans across only one web frame. All the collision damage cases on a bulk carrier resulted in interframe collapse modes. The one on the intact side is characterized by stiffener tripping and plate buckling between stiffeners. The one on the damaged side is characterized by the overall stiffened panel buckling (see Figure 60). However, if the collision damage is extended, there is a chance that the failure mode on the damaged side becomes non-interframe as shown on Figure 61.

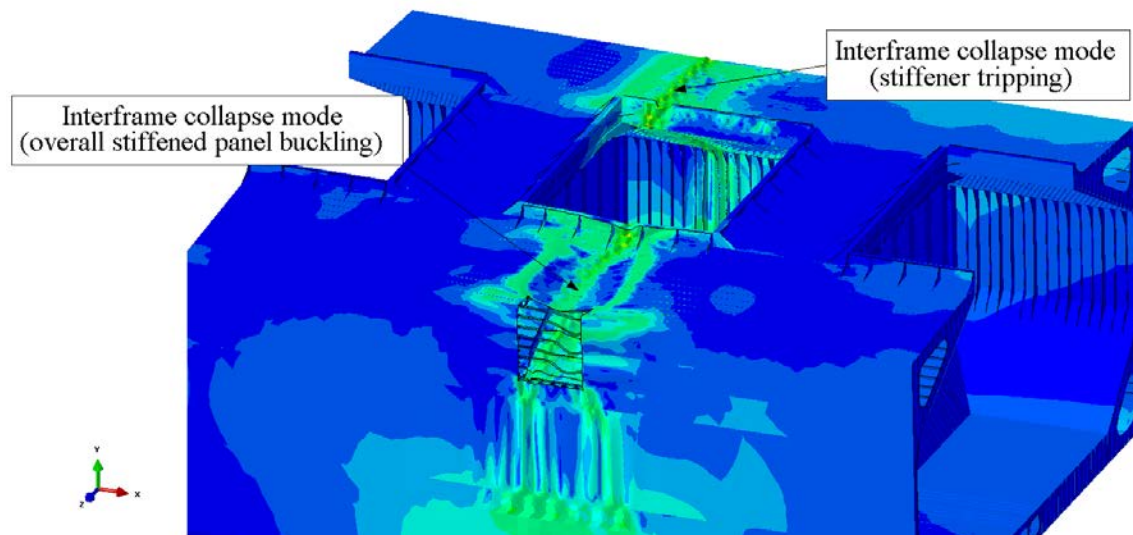


Figure 60: Interframe collapse modes of the bulk carrier with collision damage in sagging

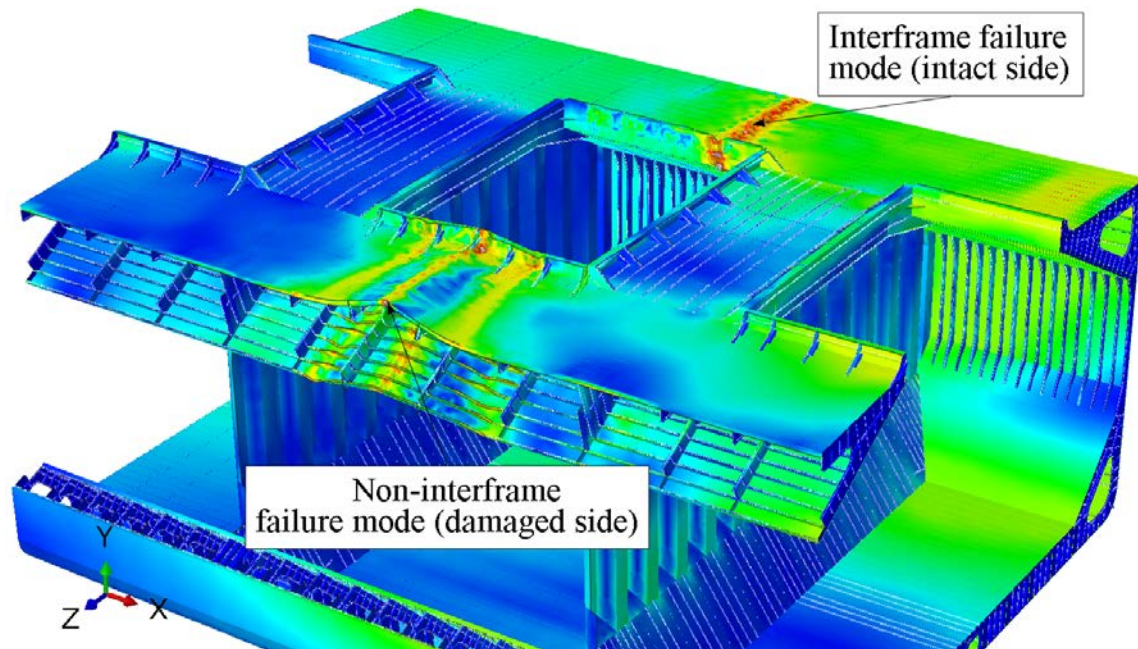


Figure 61: Failure modes on damaged and intact sides of a bulk carrier with collision damage in sagging when the damage length spans across the entire model.

The failure mode on the intact side is always interframe. After overall deck or inner bottom buckling occurs, the load quickly redistributes so that the intact side bears the majority of it. Since the collapse mode on the intact side is still interframe, the interframe collapse assumption is still approximately satisfied.

6.2.3 A Note on the Buckling Capacity of Stiffeners

As the stiffener tripping was observed to be the dominant collapse mode in all intact and the majority of damaged cases, it is important to verify their buckling capacity.

During the NLFE simulations, the curvature of the model is constantly being increased, but the onset of nonlinear behavior occurs well beyond the Rule value of the total vertical bending moment (maximum permissible still water + Rule wave vertical bending moment). For example, Figure 62 shows the moment-curvature curve of the intact containership in hogging. The value of the total Rule bending moment is also given for comparison. It can be seen that the total Rule bending moment is well within the linear portion of the moment-curvature curve. Therefore, the vessel survives the extreme vertical bending moment with 10^{-8} probability of exceedance without any yielding or buckling. Figure 63 shows compressive stresses in the bottom of the containership loaded with the total Rule hogging bending moment. The stiffener compressive stresses are approximately 190 N/mm^2 . Figure 64 shows the same bottom stiffened panels at the onset of buckling (and yielding) when the compressive stress in the bottom stiffeners reaches 350 N/mm^2 . Therefore, the effective buckling utilization factor of the shown bottom stiffeners is approximately equal to $\eta = 190/350 \approx 0.54$, which is well below the

allowable buckling utilization factor of $\eta_{ALLOW} = 1$. A similar conclusion can be drawn for plate buckling.

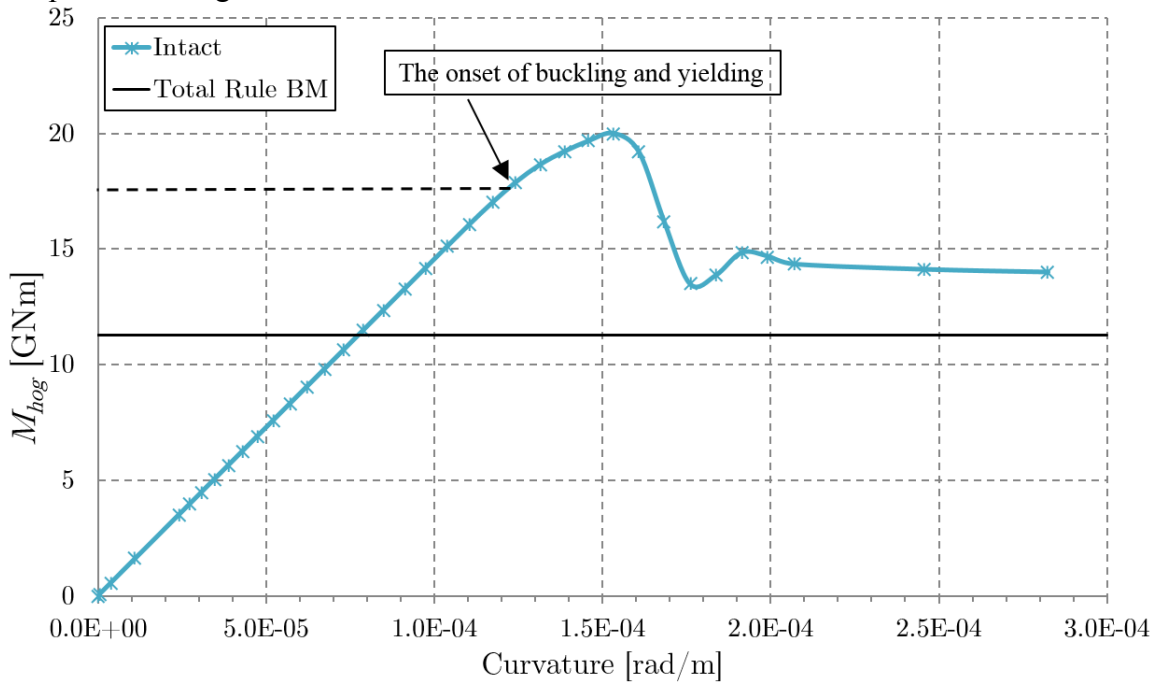


Figure 62: Comparison of the ultimate strength of the containership in hogging and its total Rule hogging bending moment

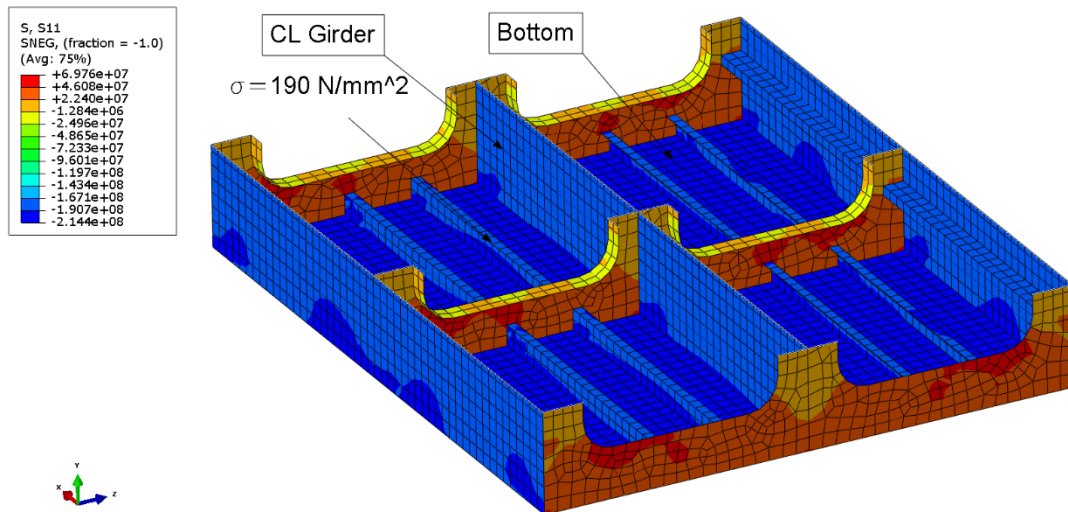


Figure 63: Longitudinal stresses in the x direction in the bottom of the containership at the Rule value of the total bending moment

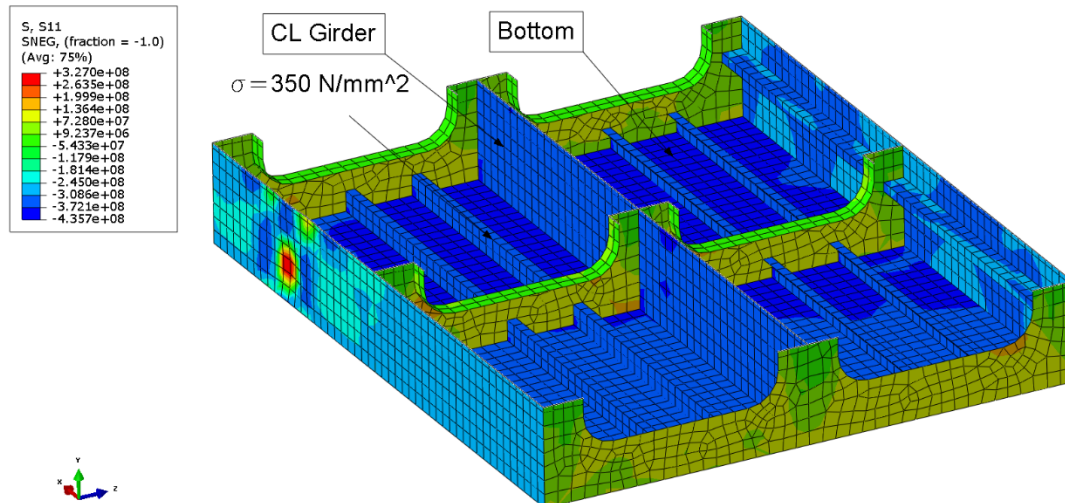


Figure 64: Longitudinal stresses in the x direction in the bottom of the containership at the onset of buckling and yielding

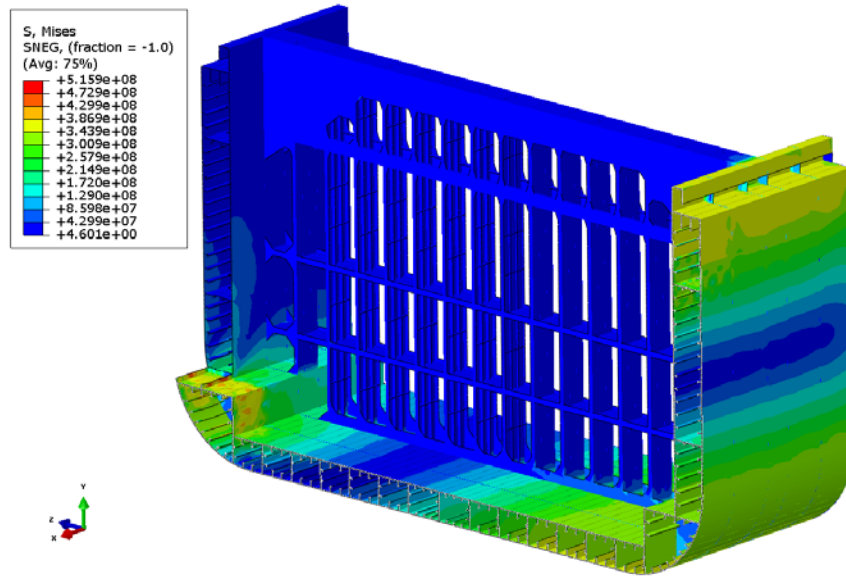
6.2.4 The Ultimate Strength Reduction Factor

Figure 66 to Figure 69 show the ultimate strength reduction factor, $USRF = M_u/M_{u,intact}$, as a function of damage size ratios for each vessel, damage type, and vertical bending moment direction. A 3-D spline has been fitted to this data.

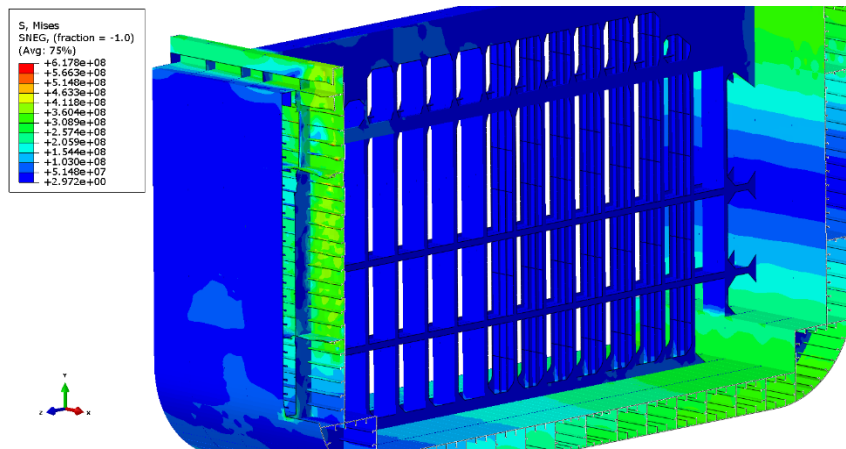
It can immediately be noticed that grounding damage has a more significant effect on the reduction of the hogging ultimate bending moment than it has on the sagging. Also, collision damage reduces the sagging bending moment more significantly than it does the hogging bending moment. These are expected results since, due to buckling, damage will always have more impact on the ultimate strength of the vessel when the hull outer flange, where the damage is located, is under compression.

However, there is one exception to this for the case of containership with collision damage where the damage takes out both the side shell and the inner longitudinal bulkhead (damage cases D2, D6, D10, and D14). In these cases, the ultimate strength in sagging is not governed by the buckling of the deck, hatch coaming, and the shear strake. Rather, the ultimate strength of the section is reached as these structural members start to yield under the compressive load. The buckling of these members, which have large scantlings and form a very rigid engineering passageway, is delayed until the structure is significantly in the post ultimate strength region. Similarly, the deck outer flange yields in tension when the ship is subjected to hogging bending moment, but in this case the ultimate strength of the vessel is governed by the interframe buckling of the intact double bottom. The absence of deck outer flange buckling for damage cases D2, D6, D10, and D14, when the ultimate strength in sagging is reached, explains the fact that, for these cases, collision causes slightly smaller relative reduction of the ultimate sagging bending moment compared to the relative reduction of the ultimate hogging bending moment.

For damage cases D1, D5, D9, and D13, the ultimate strength in sagging is governed by the buckling of the inner longitudinal bulkhead with the weakened support. Figure 65 shows the deformed cross sections of the containership with D13 and D14 collision damages, respectively. Both cases show the instant when the ultimate sagging bending moment has been reached. It can be noticed that the ultimate strength of the D13 case has been reached with significant stiffener tripping and plate buckling on the damaged side. On the other hand, no buckling (on the intact side) can be observed at the ultimate strength point of the D14 case.



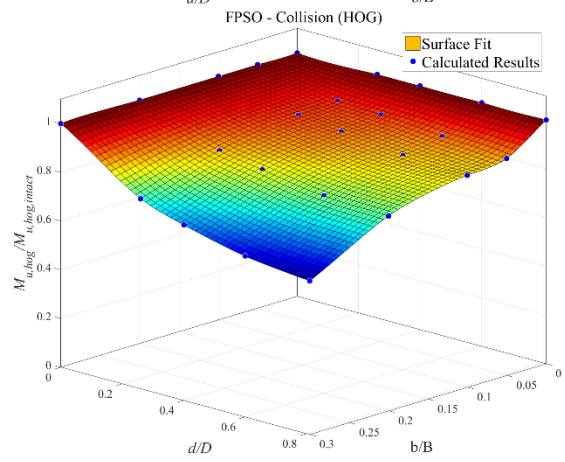
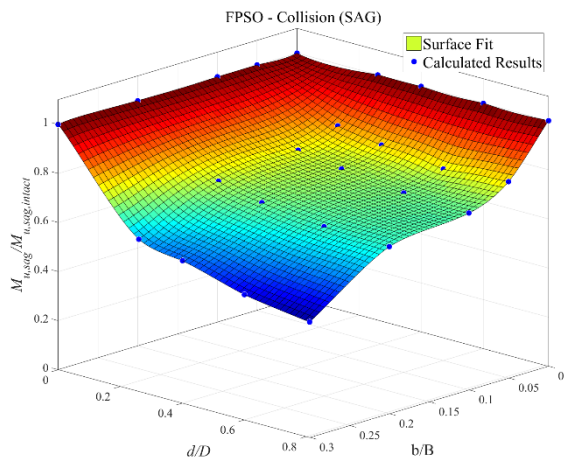
(a)



(b)

Figure 65: Containership D14 (a) and D13 (b) collision cases at the sagging ultimate strength point.

Table 12 to Table 19 show the ultimate bending moment capacity and the *USRF*, respectively, for each vessel and damage type in a tabular fashion.



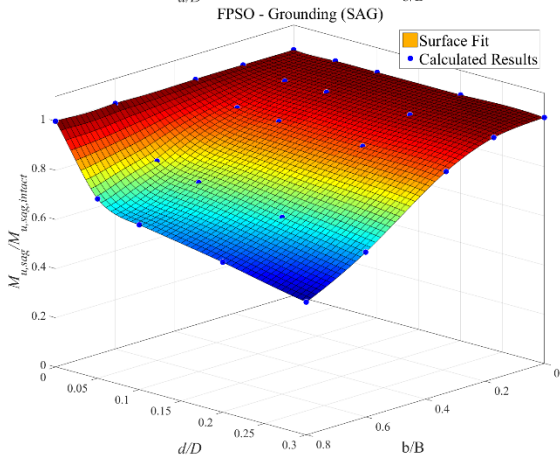
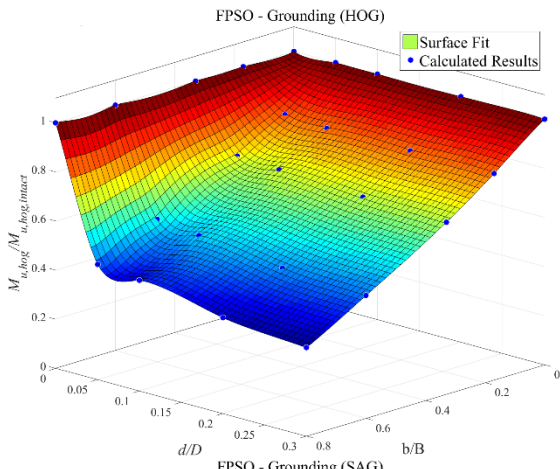


Figure 66: Ultimate strength reduction factor vs. damage size ratios for the FPSO

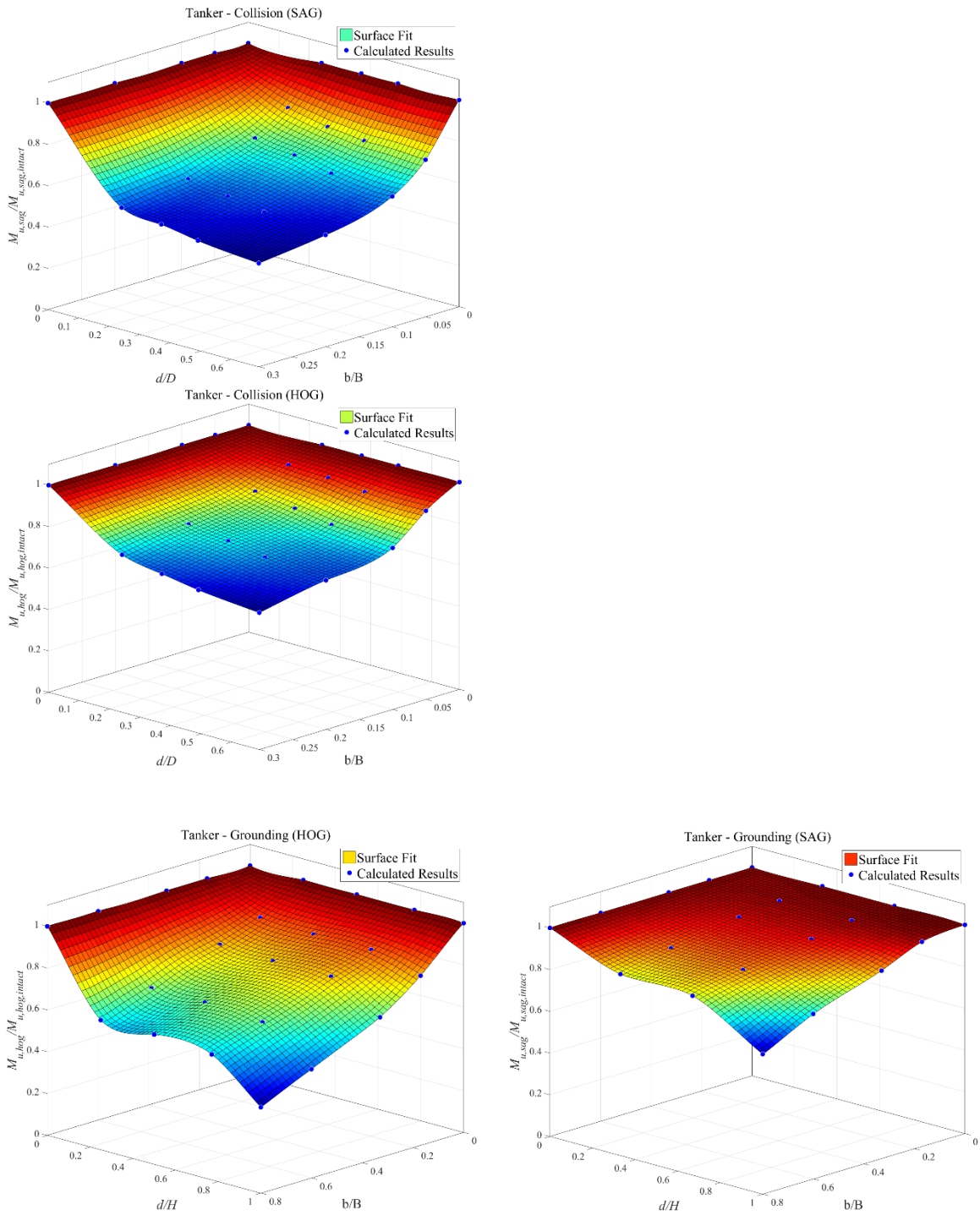
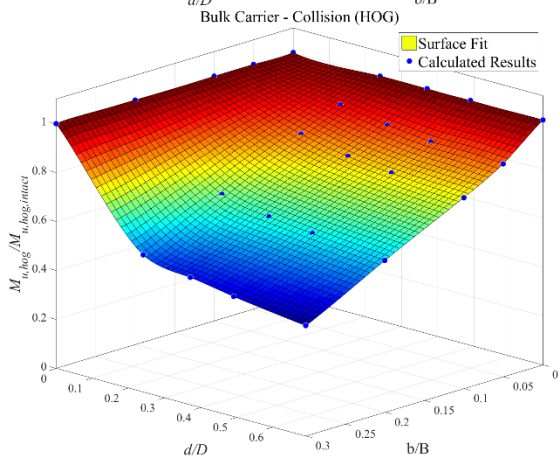
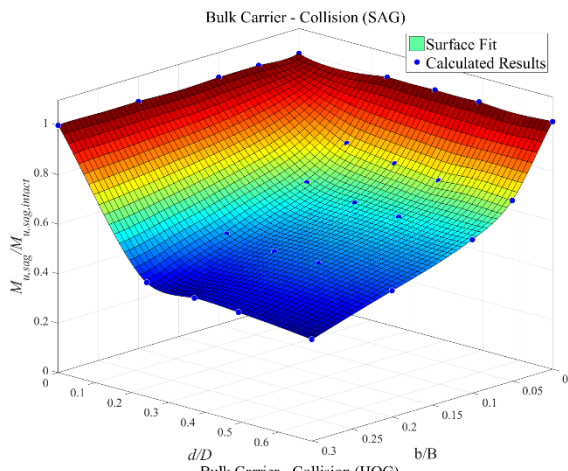


Figure 67: Ultimate strength reduction factor vs. damage size ratios for the Tanker



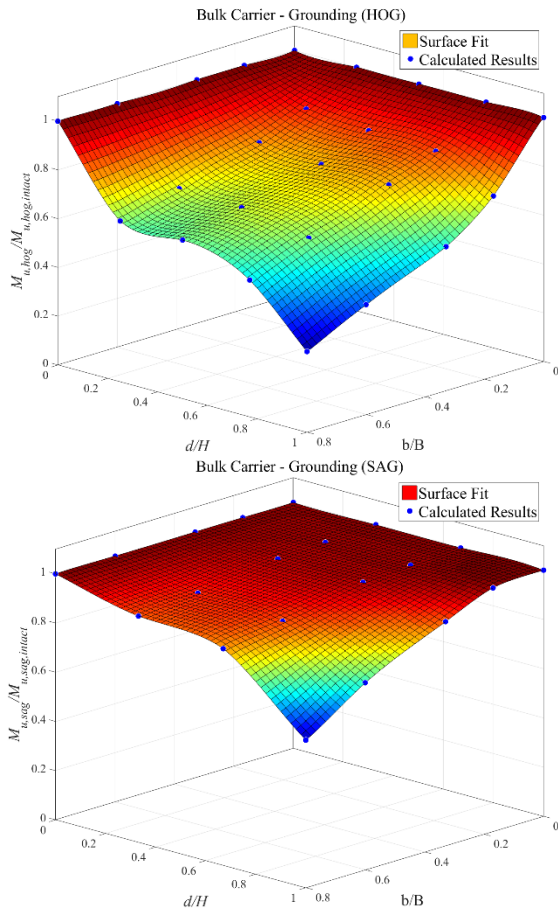
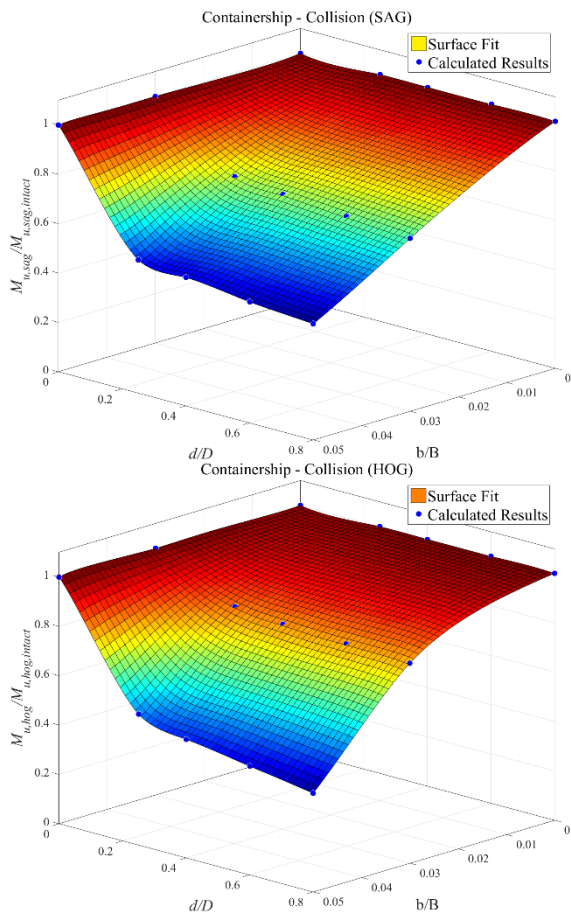


Figure 68: Ultimate strength reduction factor vs. damage size ratios for the Bulk Carrier



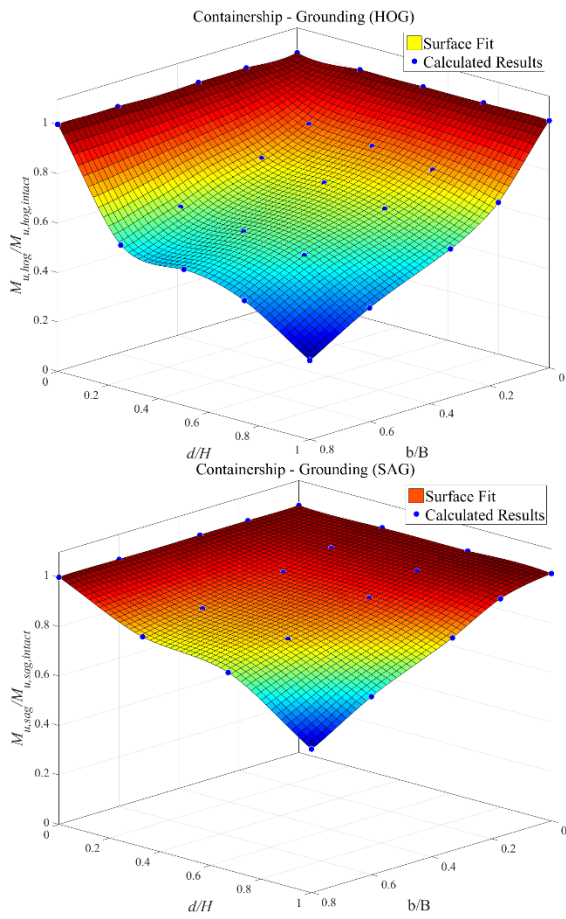


Figure 69: Ultimate strength reduction factor vs. damage size ratios for the Containership

Table 12: Summary of ultimate bending moment capacity in [GNm] for FPSO

FPSO - Collision (SAG)	FPSO - Grounding (HOG)
Survivability of Hull Girder in Damaged Condition	PAGE 85

$d/D \backslash b/B$	0.00	0.05	0.10	0.20	0.30
0.00	8.39	8.39	8.39	8.39	8.39
0.26	8.39	7.08	6.63	6.33	5.22
0.40	8.39	6.78	6.35	6.08	4.84
0.60	8.39	6.56	6.11	5.80	4.31
0.81	8.39	6.68	6.06	5.71	3.97

$d/D \backslash b/B$	0.00	0.17	0.33	0.60	0.80
0.00	10.07	10.07	10.07	10.07	10.07
0.05	10.07	8.57	7.42	5.79	4.78
0.10	10.07	8.51	7.30	5.69	4.56
0.20	10.07	8.50	7.11	5.19	3.91
0.30	10.07	8.50	7.01	4.99	3.66

FPSO - Collision (HOG)					
$d/D \backslash b/B$	0.00	0.05	0.10	0.20	0.30
0.00	10.07	10.07	10.07	10.07	10.07
0.26	10.07	9.50	9.37	8.84	7.81
0.40	10.07	9.39	9.20	8.57	7.29
0.60	10.07	9.14	8.87	8.18	6.68
0.81	10.07	9.00	8.74	8.06	6.34

FPSO - Grounding (SAG)					
$d/D \backslash b/B$	0.00	0.17	0.33	0.60	0.80
0.00	8.39	8.39	8.39	8.39	8.39
0.05	8.39	8.21	7.80	6.80	6.11
0.10	8.39	8.18	7.72	6.46	5.61
0.20	8.39	8.20	7.63	6.08	5.13
0.30	8.39	8.20	7.56	5.63	4.53

Table 13: Summary of ultimate strength reduction factor (*USRF*) for FPSO

FPSO - Collision (SAG)					
$d/D \backslash b/B$	0.00	0.05	0.10	0.20	0.30
0.00	1.00	1.00	1.00	1.00	1.00
0.26	1.00	0.84	0.79	0.76	0.62
0.40	1.00	0.81	0.76	0.72	0.58
0.60	1.00	0.78	0.73	0.69	0.51
0.81	1.00	0.80	0.72	0.68	0.47

FPSO - Grounding (HOG)					
$d/D \backslash b/B$	0.00	0.17	0.33	0.60	0.80
0.00	1.00	1.00	1.00	1.00	1.00
0.05	1.00	0.85	0.74	0.58	0.47
0.10	1.00	0.84	0.73	0.56	0.45
0.20	1.00	0.84	0.71	0.52	0.39
0.30	1.00	0.84	0.70	0.50	0.36

FPSO - Collision (HOG)					
$d/D \backslash b/B$	0.00	0.05	0.10	0.20	0.30
0.00	1.00	1.00	1.00	1.00	1.00
0.26	1.00	0.94	0.93	0.88	0.78
0.40	1.00	0.93	0.91	0.85	0.72
0.60	1.00	0.91	0.88	0.81	0.66
0.81	1.00	0.89	0.87	0.80	0.63

FPSO - Grounding (SAG)					
$d/D \backslash b/B$	0.00	0.17	0.33	0.60	0.80
0.00	1.00	1.00	1.00	1.00	1.00
0.05	1.00	0.98	0.93	0.81	0.73
0.10	1.00	0.98	0.92	0.77	0.67
0.20	1.00	0.98	0.91	0.72	0.61
0.30	1.00	0.98	0.90	0.67	0.54

Table 14: Summary of ultimate bending moment capacity in [GNm] for Tanker

Tanker - Collision (SAG)						Tanker - Grounding (HOG)					
$d/D \backslash b/B$	0.00	0.05	0.10	0.20	0.30	$d/H \backslash b/B$	0.00	0.17	0.33	0.60	0.80
0.00	15.69	15.69	15.69	15.69	15.69	0.00	18.64	18.64	18.64	18.64	18.64
0.24	15.69	12.95	11.51	9.87	9.25	0.25	18.64	16.34	15.07	13.10	11.57
0.37	15.69	12.46	10.94	9.43	8.80	0.50	18.64	16.25	14.97	12.96	11.58
0.49	15.69	12.15	10.36	8.92	8.28	0.77	18.64	16.19	14.91	12.70	11.25
0.69	15.69	11.98	9.92	8.44	7.85	1.00	18.64	15.04	12.43	9.73	7.60

Tanker - Collision (HOG)						Tanker - Grounding (SAG)					
$d/D \backslash b/B$	0.00	0.05	0.10	0.20	0.30	$d/H \backslash b/B$	0.00	0.17	0.33	0.60	0.80
0.00	18.64	18.64	18.64	18.64	18.64	0.00	15.69	15.69	15.69	15.69	15.69
0.24	18.64	17.74	16.22	15.19	14.16	0.33	15.69	15.57	15.20	14.38	13.67
0.37	18.64	17.50	15.69	14.52	13.46	0.67	15.69	15.56	15.04	14.20	13.51
0.49	18.64	17.18	15.04	13.90	12.85	1.00	15.69	15.37	14.17	12.34	10.45
0.69	18.64	17.00	14.54	13.36	12.24						

Table 15: Summary of ultimate strength reduction factor (*USRF*) for Tanker

Tanker - Collision (SAG)						Tanker - Grounding (HOG)					
$d/D \backslash b/B$	0.00	0.05	0.10	0.20	0.30	$d/H \backslash b/B$	0.00	0.17	0.33	0.60	0.80
0.00	1.00	1.00	1.00	1.00	1.00	0.00	1.00	1.00	1.00	1.00	1.00
0.24	1.00	0.83	0.73	0.63	0.59	0.25	1.00	0.88	0.81	0.70	0.62
0.37	1.00	0.79	0.70	0.60	0.56	0.50	1.00	0.87	0.80	0.70	0.62
0.49	1.00	0.77	0.66	0.57	0.53	0.77	1.00	0.87	0.80	0.68	0.60
0.69	1.00	0.76	0.63	0.54	0.50	1.00	1.00	0.81	0.67	0.52	0.41

Tanker - Collision (HOG)						Tanker - Grounding (SAG)					
$d/D \backslash b/B$	0.00	0.05	0.10	0.20	0.30	$d/H \backslash b/B$	0.00	0.17	0.33	0.60	0.80
0.00	1.00	1.00	1.00	1.00	1.00	0.00	1.00	1.00	1.00	1.00	1.00
0.24	1.00	0.95	0.87	0.81	0.76	0.33	1.00	0.99	0.97	0.92	0.87
0.37	1.00	0.94	0.84	0.78	0.72	0.67	1.00	0.99	0.96	0.91	0.86
0.49	1.00	0.92	0.81	0.75	0.69	1.00	1.00	0.98	0.90	0.79	0.67
0.69	1.00	0.91	0.78	0.72	0.66						

Table 16: Summary of ultimate bending moment capacity in [GNm] for Bulk Carrier

BC - Collision (SAG)						BC - Grounding (HOG)					
$d/D \backslash b/B$	0.00	0.05	0.10	0.20	0.30	$d/H \backslash b/B$	0.00	0.17	0.33	0.60	0.80
0.00	16.33	16.33	16.33	16.33	16.33	0.00	17.71	17.71	17.71	17.71	17.71
0.24	16.33	12.79	10.89	9.13	7.59	0.25	17.71	15.71	14.34	12.78	11.68
0.37	16.33	12.23	10.40	8.86	7.29	0.50	17.71	15.49	14.04	12.64	11.48
0.49	16.33	11.96	10.29	8.78	7.21	0.77	17.71	15.15	13.73	11.67	9.99
0.69	16.33	11.90	10.15	8.35	6.70	1.00	17.71	13.16	10.50	7.92	5.78

BC - Collision (HOG)						BC - Grounding (SAG)					
$d/D \backslash b/B$	0.00	0.05	0.10	0.20	0.30	$d/H \backslash b/B$	0.00	0.17	0.33	0.60	0.80
0.00	17.71	17.71	17.71	17.71	17.71	0.00	16.33	16.33	16.33	16.33	16.33
0.24	17.71	16.54	15.20	12.65	9.97	0.33	16.33	16.22	16.08	15.38	14.98
0.37	17.71	15.89	14.55	11.88	9.18	0.67	16.33	16.21	15.93	14.99	14.35
0.49	17.71	15.60	14.22	11.48	8.67	1.00	16.33	16.10	14.89	12.49	9.75
0.69	17.71	15.48	13.88	10.94	7.96						

Table 17: Summary of ultimate strength reduction factor (*USRF*) for Bulk Carrier

BC - Collision (SAG)						BC - Grounding (HOG)					
$d/D \backslash b/B$	0.00	0.05	0.10	0.20	0.30	$d/H \backslash b/B$	0.00	0.17	0.33	0.60	0.80
0.00	1.00	1.00	1.00	1.00	1.00	0.00	1.00	1.00	1.00	1.00	1.00
0.24	1.00	0.78	0.67	0.56	0.46	0.25	1.00	0.89	0.81	0.72	0.66
0.37	1.00	0.75	0.64	0.54	0.45	0.50	1.00	0.87	0.79	0.71	0.65
0.49	1.00	0.73	0.63	0.54	0.44	0.77	1.00	0.86	0.78	0.66	0.56
0.69	1.00	0.73	0.62	0.51	0.41	1.00	1.00	0.74	0.59	0.45	0.33

BC - Collision (HOG)						BC - Grounding (SAG)					
$d/D \backslash b/B$	0.00	0.05	0.10	0.20	0.30	$d/H \backslash b/B$	0.00	0.17	0.33	0.60	0.80
0.00	1.00	1.00	1.00	1.00	1.00	0.00	1.00	1.00	1.00	1.00	1.00
0.24	1.00	0.93	0.86	0.71	0.56	0.33	1.00	0.99	0.98	0.94	0.92
0.37	1.00	0.90	0.82	0.67	0.52	0.67	1.00	0.99	0.98	0.92	0.88
0.49	1.00	0.88	0.80	0.65	0.49	1.00	1.00	0.99	0.91	0.76	0.60
0.69	1.00	0.87	0.78	0.62	0.45						

Table 18: Summary of ultimate bending moment capacity in [GNm] for Containership

Containership - Collision (SAG)				Containership - Grounding (HOG)					
d/D \ b/B	0.00	0.03	0.05	d/H \ b/B	0.00	0.17	0.33	0.60	0.80
0.00	19.89	19.89	19.89	0.00	20.01	20.01	20.01	20.01	20.01
0.25	19.89	15.11	10.78	0.25	20.01	16.87	15.29	13.20	11.52
0.40	19.89	14.70	10.30	0.50	20.01	16.43	14.65	12.69	10.95
0.60	19.89	14.28	9.76	0.74	20.01	15.84	13.78	11.92	9.77
0.80	19.89	14.00	9.25	1.00	20.01	14.50	11.95	9.20	6.32

Containership - Collision (HOG)				Containership - Grounding (SAG)					
d/D \ b/B	0.00	0.03	0.05	d/H \ b/B	0.00	0.17	0.33	0.60	0.80
0.00	20.01	20.01	20.01	0.00	19.89	19.89	19.89	19.89	19.89
0.25	20.01	16.97	10.67	0.33	19.89	19.51	18.69	17.73	16.82
0.40	20.01	16.61	9.69	0.67	19.89	19.40	18.42	17.07	15.89
0.60	20.01	16.34	8.81	1.00	19.89	19.03	17.03	14.41	11.49
0.80	20.01	16.24	7.97						

Table 19: Summary of ultimate strength reduction factor (*USRF*) for Containership

Containership - Collision (SAG)				Containership - Grounding (HOG)					
d/D \ b/B	0.00	0.03	0.05	d/H \ b/B	0.00	0.17	0.33	0.60	0.80
0.00	1.00	1.00	1.00	0.00	1.00	1.00	1.00	1.00	1.00
0.25	1.00	0.76	0.54	0.25	1.00	0.84	0.76	0.66	0.58
0.40	1.00	0.74	0.52	0.50	1.00	0.82	0.73	0.63	0.55
0.60	1.00	0.72	0.49	0.74	1.00	0.79	0.69	0.60	0.49
0.80	1.00	0.70	0.47	1.00	1.00	0.73	0.60	0.46	0.32

Containership - Collision (HOG)				Containership - Grounding (SAG)					
d/D \ b/B	0.00	0.03	0.05	d/H \ b/B	0.00	0.17	0.33	0.60	0.80
0.00	1.00	1.00	1.00	0.00	1.00	1.00	1.00	1.00	1.00
0.25	1.00	0.85	0.53	0.33	1.00	0.98	0.94	0.89	0.85
0.40	1.00	0.83	0.48	0.67	1.00	0.98	0.93	0.86	0.80
0.60	1.00	0.82	0.44	1.00	1.00	0.96	0.86	0.72	0.58
0.80	1.00	0.81	0.40						

Since the amount of hull cross section affected by the damage does not change smoothly with the size of the damage, plots as in Figure 66 to Figure 69 can be misleading. Instead, it may be more appropriate to look at the ultimate strength reduction factor as a function of section modulus reduction factor, $SMRF = W/W_{intact}$. These plots are given in Figure 70 to Figure 73.

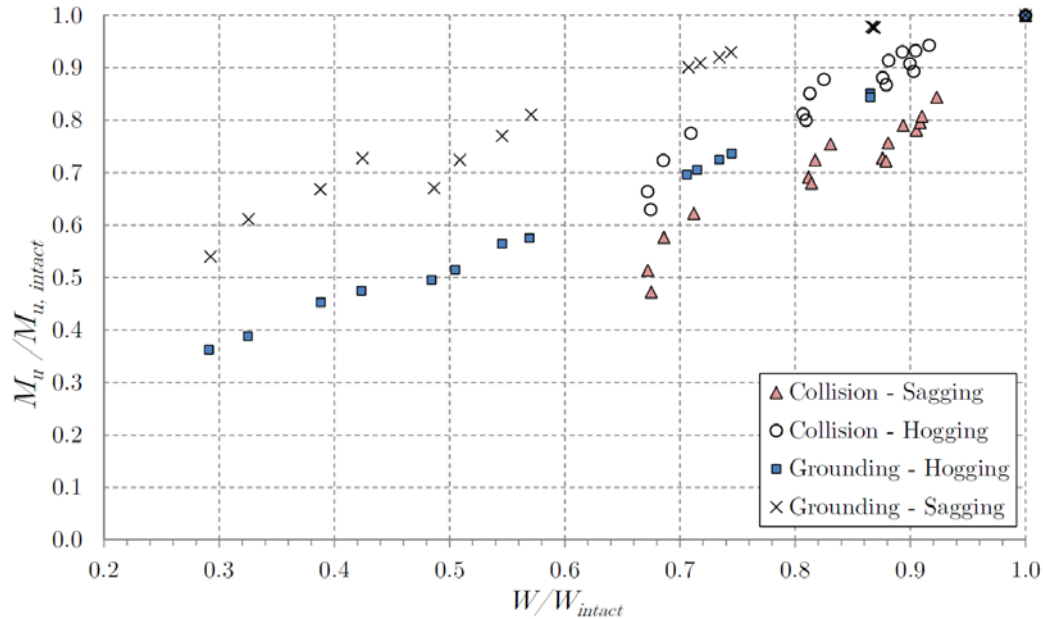


Figure 70: FPSO – ultimate strength reduction factor vs. section modulus reduction factor

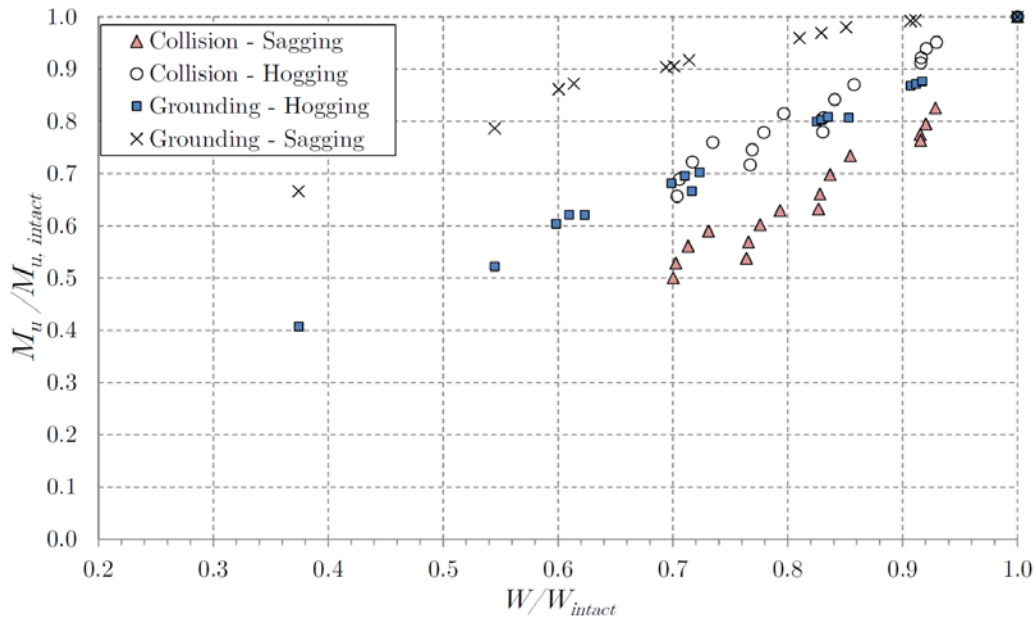


Figure 71: Tanker – ultimate strength reduction factor vs. section modulus reduction factor

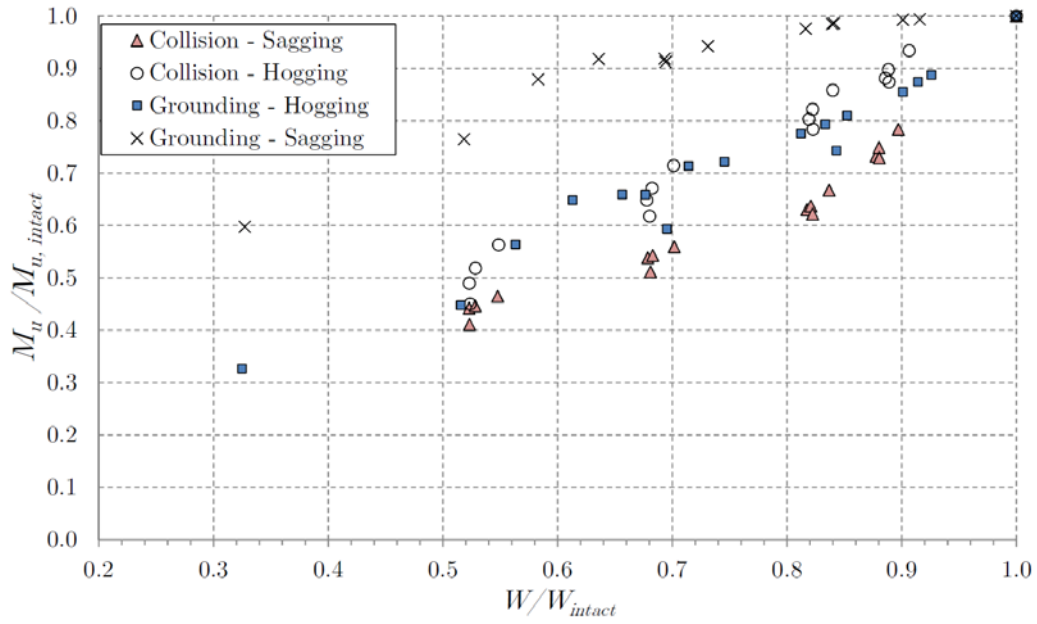


Figure 72: Bulk Carrier – ultimate strength reduction factor vs. section modulus reduction factor

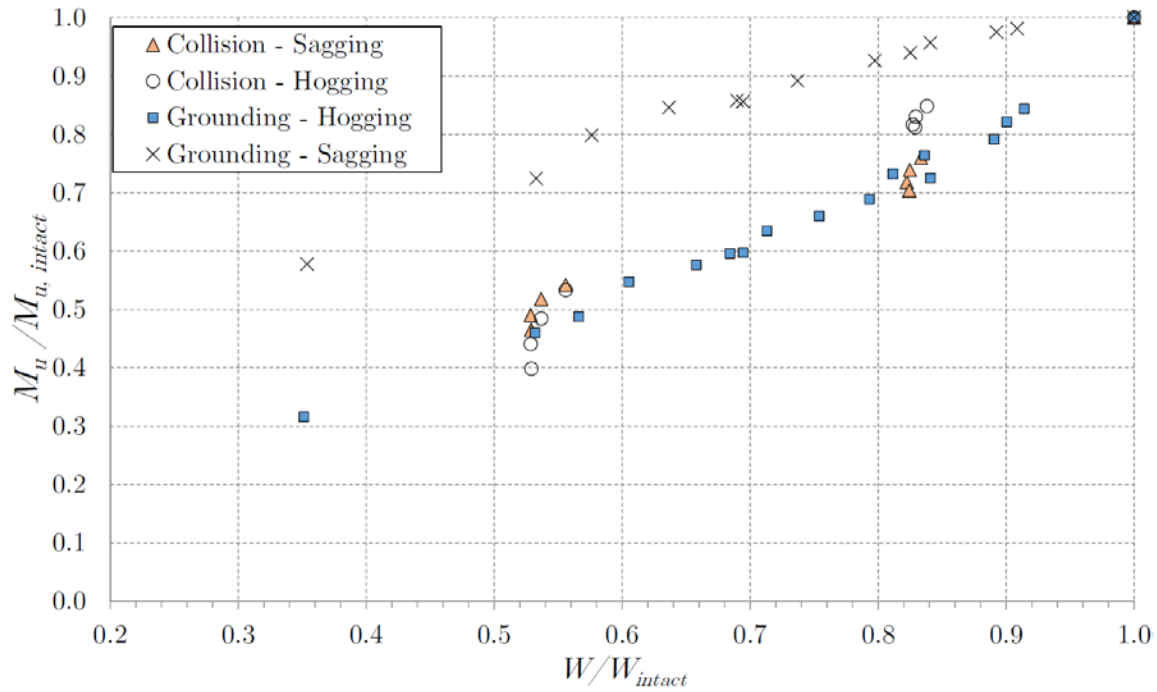


Figure 73: Containership – ultimate strength reduction factor vs. section modulus reduction factor

It is also clearly shown in the above plots that collision damage affects sagging ultimate bending moment more than the hogging, and that the grounding damage affects hogging ultimate bending moment more than it does sagging (except for the containership anomaly that was explained earlier in this subsection). In the case of grounding damage

in hogging, the dependence of $USRF$ vs. $SMRF$ appears to be close to linear, regardless of the vessel. However, more investigation is needed to determine the appropriate fits for the other cases.

6.2.5 Effect of the Longitudinal Damage Extent

As can be seen on Figure 94 to Figure 105, the effect of the longitudinal damage extent is very small. The same conclusion has been obtained by Notaro et al. [16].

The ALL WF case is quite different than the 1WF and 3WF cases because it does not have structural discontinuities at the ends of the damage where the stress concentrations will initialize the collapse failure. Instead, the collapse usually happens at the middle of the model and the ALL WF case yields slightly higher ultimate bending moment capacities compared to the 1WF and 3WF cases. Figure 74 shows the effect of the longitudinal damage extent.

This demonstrates the sensitivity of NLFEA to the existence of structural discontinuities and stress concentration areas that can lead to earlier development of failure mechanisms and different overall collapse sequence. This also points out a potential difficulty in modeling the real-world damage scenarios using NLFEA in emergency situations.

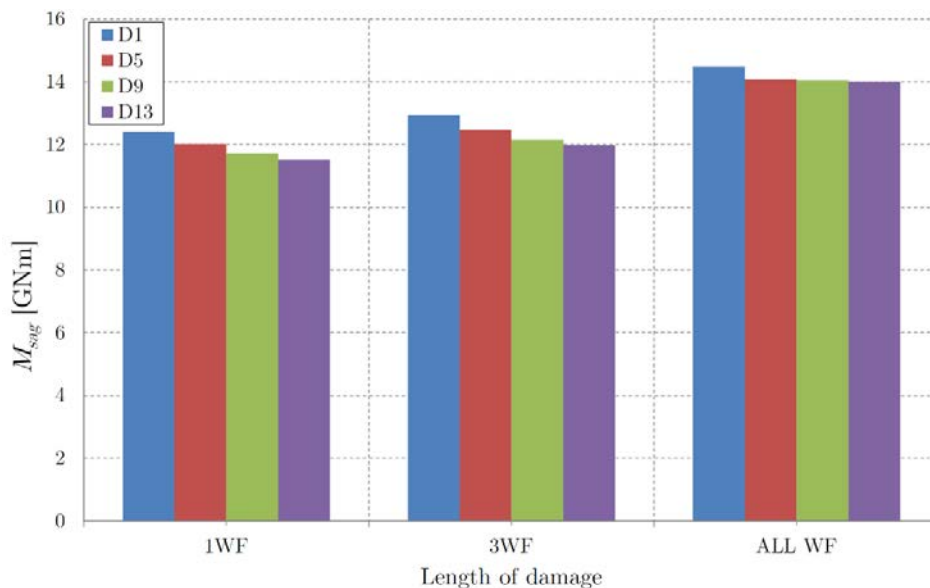


Figure 74: Tanker – Collision Damage - The effect of longitudinal damage extent

For a tanker with D6 collision damage, another damage extent spanning five web frames has also been analyzed. Figure 75 shows the moment-curvature curves for all three damage extents, each having stress concentrations at the damage ends (1WF, 3WF, and 5WF).

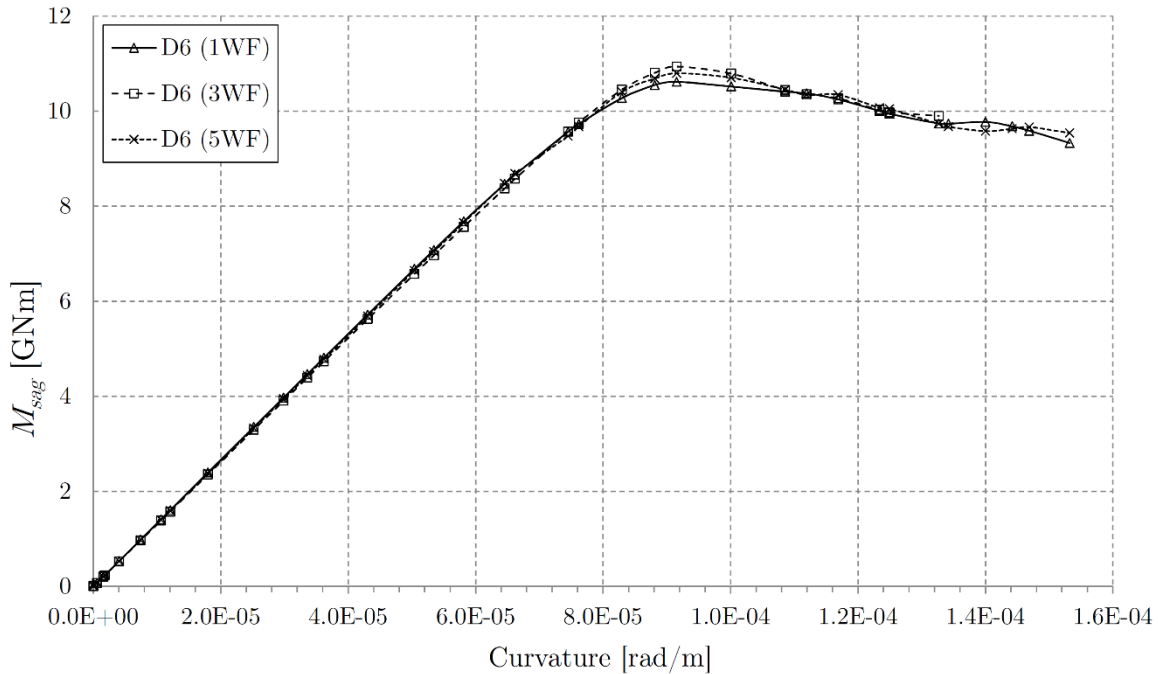


Figure 75: Tanker – D6 Collision Damage - The effect of longitudinal damage extent (each damage has sharp corners at its ends)

Table 20 shows the ultimate strength values for these three D6 longitudinal damage extent variations.

Table 20: Ultimate strength values for the three variations in the longitudinal extent of the D6 collision damage

	M _{u,sag} [GNm]	Difference [%]
D6 (3WF) - Default	10.939	-
D6 (1WF)	10.620	-2.9%
D6 (5WF)	10.799	-1.3%

It is interesting to note that the residual strength of the smallest longitudinal damage extent case (1WF) is smaller compared to residual strengths of both 3WF and 5WF cases. This can be explained by different distribution of initial imperfections around the damage corners that trigger slightly different collapse sequence. Also, for the 1WF case the ends of the damage, where the failure domains form, are close to each other. Therefore, the failure domains on both sides of the damage start to interact triggering a slightly earlier collapse.

6.2.6 Effect of the Longitudinal Position of the Damage

As mentioned in Section 6.1 and shown in Figure 35, three longitudinal positions of the collision damage have been investigated on a tanker in sagging. The 2WF and 4WF shifts aft also included the damage to the transverse bulkhead. However, the effect of the longitudinal position of the damage is quite small. Figure 76 shows the moment-curvature curves of the default case, as well as the 2WF and 4WF shift cases. The largest difference in the ultimate strength between all three cases is 3 %. This could very well have been caused by a slightly different pattern of imperfections used in these three cases. It should also be pointed out that the scantlings of all the longitudinal members are constant over the entire length of the model. Had this not been the case, the differences in the ultimate strength could have been larger.

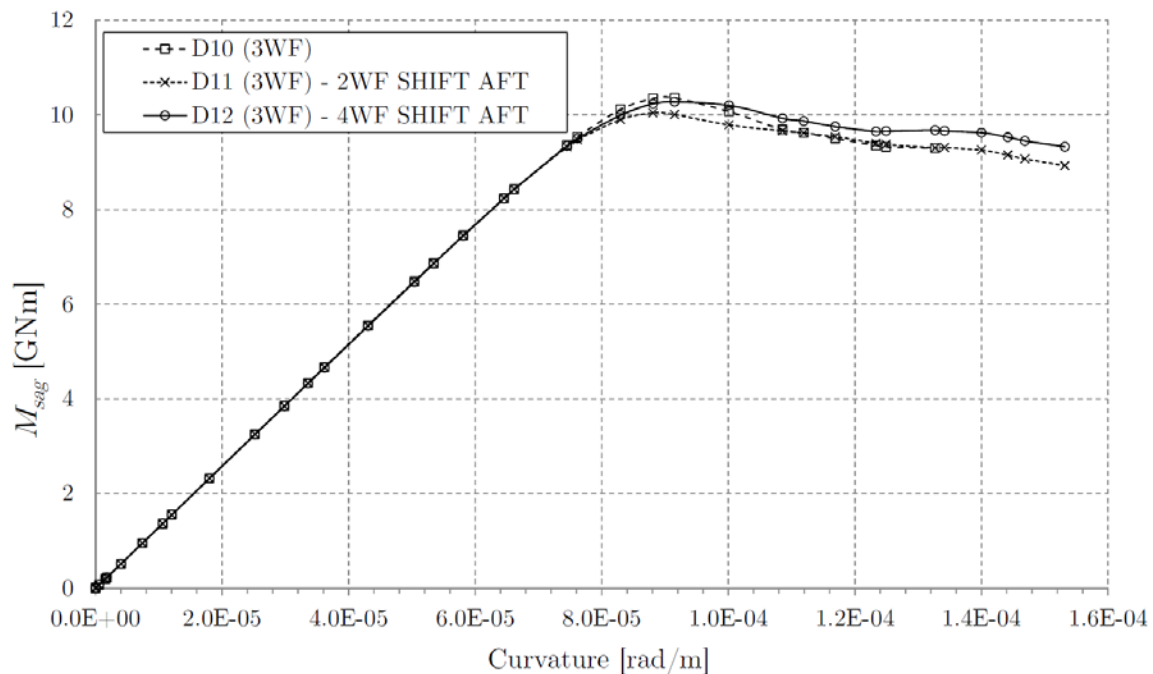


Figure 76: Tanker – D10 Collision Damage - The effect of longitudinal position of the damage

Table 21: Ultimate strength values for the three variations in the longitudinal position of the collision damage

	$M_{u,sag}$ [GNm]	Difference [%]
D10 - Default	10.357	-
D10 - 2WF SHIFT AFT	10.042	3.0%
D10 - 4WF SHIFT AFT	10.276	0.8%

6.2.7 Effect of the Transverse Position of the Damage

As mentioned in Section 6.1 and shown in Figure 36, three transverse positions of the grounding damage have been investigated on a tanker in hogging. All three damage cases have approximately the same bottom section modulus reduction, but different transverse positions. The effect of the transverse position of the damage is small. Figure 77 shows the moment-curvature curves of all three damage cases. The largest difference in the ultimate strength between all three cases is 3.6 %. As with the variation in the longitudinal position of the damage, this could have been caused by a slightly different pattern of imperfections used in these three cases or due to the small variation in the bottom shell plate thickness in the transverse direction. It should also be pointed out that the transverse location of the damage could potentially play a significant role if bi-axial bending (vertical and horizontal) is applied. This could be a topic of further investigation.

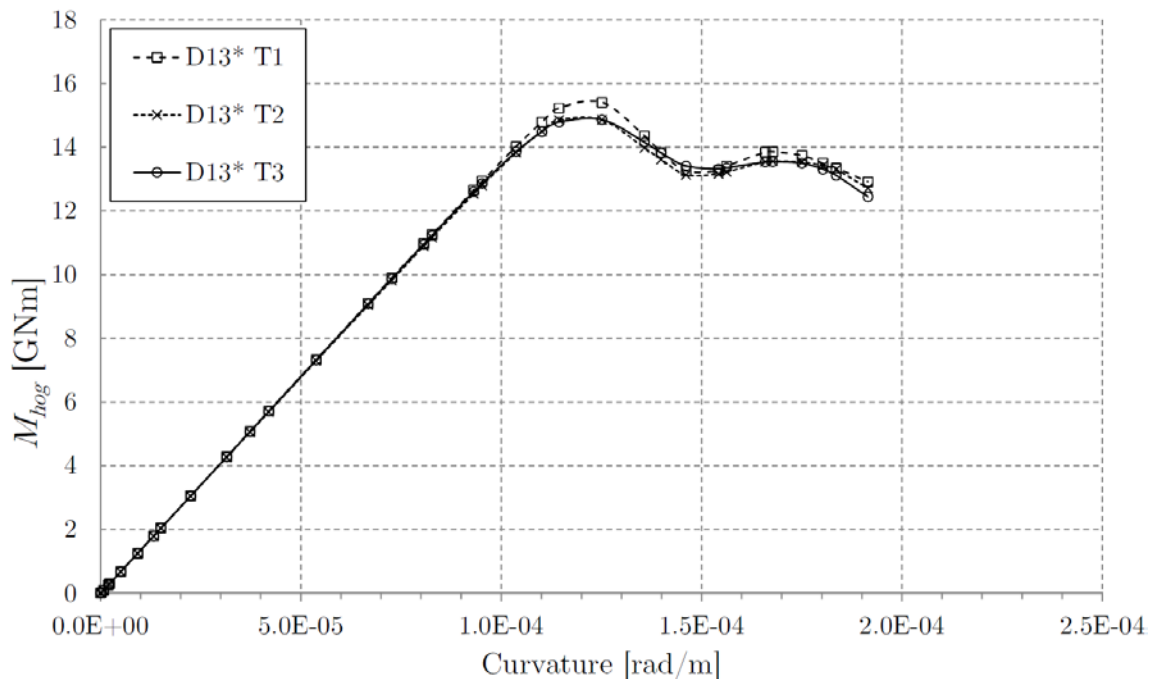


Figure 77: Tanker – D10 Collision Damage - The effect of longitudinal position of the damage

Table 22: Ultimate strength values for the three variations in the transverse position of the collision damage

	$M_{u,hog}$ [GNm]	Difference [%]
D13* T1	15.410	-
D13* T2	14.861	3.6%
D13* T3	14.864	3.5%

7. Summary and Conclusions

Nonlinear finite element analysis (NLFEA) has been used to investigate the reduction of ultimate vertical bending moment capacity of a vessel following damage due to collision and grounding. NLFEA is generally considered as the most sophisticated and time-consuming method for ultimate strength calculations. It accounts for material and geometric nonlinearities and has the ability to correctly represent the load redistribution in the structure undergoing collapse. NLFEA is very challenging due to the number of different parameters that have to be accurately controlled during the analysis in order to achieve a stable solution.

The 2-H CAD and FE models of four vessels have been generated: single hull FPSO, double hull Suezmax tanker, 180,000 DWT bulk carrier, and 8500 TEU containership. The 1-B FE model of the FPSO has also been generated and used in the sensitivity study with respect to model and analysis parameters. This study required 17 NLFEA simulations on the 1-B FE model. As a result, dynamic quasi-static analysis with full integration S4 shell elements and full Newton-Raphson algorithm has been chosen for the 2-H NLFE simulations. Both implicit and explicit time integration schemes have been used.

NLFEA results are presented in tabular and graphical manner in this report.

A total of eight intact and 266 residual strength analyses have been conducted on the 2-H models of the four selected vessels for systematically varied damage type, damage size, damage location, and the vertical bending moment direction. On average, one such analysis took 15 hours to complete on a cluster with 20 processor cores. The guidance provided in this report is useful for avoiding needless repetition of NLFE analyses because of the modeling that did not fit the problem. All the NLFEA results have been presented in graphic and tabular fashions. This very large collection of ultimate strength results can be used to calibrate the Rule residual strength requirements, or to validate more efficient methods. It can also be used to quickly estimate the ultimate strength reduction factor of a vessel, based on its type and damage parameters. It is important to note that, although each of the analyzed vessels presents a “typical sample” of its category, generalization of these results to other vessels should be made with caution.

The following additional conclusions can be also drawn from these analyses:

- The NLFEA results agree well with the enhanced incremental iterative method (EIIM) for intact hull structures. The agreement between these two methods for damaged structures is the object of an ongoing investigation at ABS.
- The dominant mode of collapse for all intact and the majority of damaged cases is the interframe stiffener tripping followed by the local plate yielding and buckling.
- Non-interframe collapse mode has been observed in only four collision cases on the tanker and in four grounding cases on the bulk carrier.
- In the case of the tanker with collision damage that resulted in long unsupported cantilever deck webs (damages D2, D6, D10, and D14), overall deck buckling occurs as the primary mode of failure on the damaged side.

- Overall inner bottom buckling is the dominant mode of collapse for the bulk carrier with grounding damage that affects three quarters of the double bottom in the vertical direction (damages D9, D10, D11, D12). Smaller grounding damage will not cause overall buckling of the inner bottom, but will cause interframe collapse mode instead. No overall inner bottom collapse has been observed on the other two vessels with double bottom (tanker and containership) in any grounding damage case.
- For the tanker with collision damage, in addition to the stiffener tripping, gross panel buckling also occurs on panels on the other side of the deck web.
- In case of grounding damage in hogging, the dependence of the ultimate strength reduction factor vs. the section modulus reduction factor appears to be close to linear, regardless of the vessel type. However, more investigation is needed to determine the appropriate fits for the other cases.
- Length of the damage extent has a negligible effect on the ultimate bending capacity as long as the discontinuities at damage ends are included in the model.
- The existence of sharp damage corners causes stress concentrations which have a negative effect on the residual strength of the vessel. This needs to be taken into account when using 2-D methods that cannot take such 3-D effects into account.
- The longitudinal and transverse location of the damage have marginal effect on the vertical ultimate bending moment provided that the section modulus reduction caused by the damage stays unchanged.

7.1 Recommendations for Future Work

This work forms a basis for residual strength Rule requirements calibration based on the reliability analysis. It should also be used for calibrating and improving more simple methods for residual strength calculations, such as the EIIM method.

8. References

- [1] C. S. Smith, "Influence of Local Compressive Failure on Ultimate Longitudinal Strength of Ship's Hull," in *Proceedings of the International Symposium on Practical Design in Shipbuilding*, Tokyo, 1977.
- [2] IACS, Common Structural Rules for Bulk Carriers and Oil Tankers – External Release 1, London: International Association of Classification Societies, 2014.
- [3] J. B. Caldwell, "Ultimate Longitudinal Strength," *Transactions of the Royal Institution of Naval Architects*, vol. 107, pp. 411-430, 1965.
- [4] J. K. Paik and A. E. Mansour, "A Simple Formulation for Predicting the Ultimate Strength of Ships," *Journal of Marine Science and Technology*, vol. 1, no. 1, pp. 52-62, 1995.
- [5] Y. Ueda and S. M. H. Rashed, "An Ultimate Transverse Strength Analysis of Ship Structures," *Journal of the Society of Naval Architects of Japan*, vol. 136, pp. 309-324, 1974.
- [6] J. K. Paik, *The Intelligent Super-Size Finite Element Method: Theory and Practice*, Busan: Department of Naval Architecture and Ocean Engineering, Busan National University, 2006.
- [7] O. Hughes and J. K. Paik, *Ship Structural Analysis and Design*, Jersey City, NJ: The Society of Naval Architects and Marine Engineers, 2010, pp. 8.1-8.22.
- [8] J. K. Paik and A. K. Thayamballi, *Ultimate Limit State Design of Steel Plated Structures*, Chichester: John Wiley & Sons, LTD, 2003.
- [9] P. Wriggers, *Nonlinear Finite Element Methods*, Heidelberg: Springer-Verlag, 2008.
- [10] J. K. Paik and A. K. Thayamballi, *Ship-Shaped Offshore Installations: Design, Building, and Operation*, Cambridge: Cambridge University Press, 2007.
- [11] J. M. Gordo and C. G. Soares, "Interaction Equation for the Collapse of Tankers and Containerships Under Combined Bending Moments," *Journal of Ship Research*, vol. 41, no. 3, p. 230-240, 1997.
- [12] E. Riks, "The Application of Newton's Method to the Problem of Elastic Stability," *Journal of Applied Mechanics*, vol. 39, p. 1060, 1972.
- [13] Simulia, *Abaqus 6.13 User's Manual*, Providence, RI: Dassault Systèmes Simulia Corp., 2012.
- [14] E. Lehmann, "Discussion on Report of Committee III. 1: Ultimate Strength," in *Proceedings of 16th ISSC*, pp. 121-131, 2006.
- [15] H. K. K. Amlashi and T. Moan, "Ultimate Strength Analysis of a Bulk Carrier Hull Girder Under Alternate Hold Loading Condition—A Case Study: Part 1: Nonlinear Finite Element Modelling and Ultimate Hull Girder Capacity," *Marine Structures*, vol. 21, no. 4, p. 327-352, 2008.
- [16] Notaro, G., Kippenes, J. et al., "Residual Hull Girder Strength of Ships with Collision or Grounding Damages," in *Proceedings of the 11th International Symposium on Practical Design of Ships and Other Floating Structures*, Rio de Janeiro, RJ, Brazil, 2010.

- [17] Z. Liu and J. Amdahl, "Numerical and Simplified Analytical Methods for Analysis of the Residual Strength of Ship Double Bottom," *Ocean Engineering*, vol. 52, pp. 22-34, 2012.
- [18] E. Steen, T. K. Østvold, et al., PULS User's Manual, Høvik, Norway: Det Norske Veritas, 2001.
- [19] T. K. Østvold, E. Steen and G. Holtsmark, "Nonlinear Strength Analysis of a Bulk Carrier - a Case Study," in *Proceedings of the 9th International Symposium on Practical Design of Ships and Other Floating Structures*, Hamburg, 2004.
- [20] M. Petricic and E. VanDerHorn, "Assessment of the Residual Hull Girder Ultimate Strength of Damaged Vessels Subjected to Vertical and Horizontal Bending Using Nonlinear Finite Element Analysis," in *The Damaged Ship III Conference*, London, UK, 2015.
- [21] ABS, Guide for Assessing Hull-Girder Residual Strength for Bulk Carriers, New York, NY: American Bureau of Shipping, 1995.
- [22] ABS, Guide for Assessing Hull-Girder Residual Strength for Tankers, New York, NY: American Bureau of Shipping, 1995.
- [23] S. Rusaas, "Final Publishable Paper - Tech. rep. 0-00-X-2003-03-0," HARDER Consortium, 2003.
- [24] MARIN, PRECAL V 4.0 User's Manual, Wageningen, The Netherlands: MARitime Research Institute Netherlands, 2000.
- [25] SAIC, NLOAD3D Nonlinear 3D Seakeeping and Load Prediction Program User Documentation Version 1.9.3, Bowie, Maryland: Science Applications International Corporation, 2012.
- [26] Z. Shu and T. Moan, "Ultimate Hull Girder Strength of a Bulk Carrier Under Combined Global and Local Loads in the Hogging and Alternate Hold Loading Condition Using Nonlinear Finite Element Analysis," *Journal of Marine Science and Technology*, vol. 17, no. 1, pp. 94-113, 2012.
- [27] M. Petricic, "Residual Strength of a Hull Girder in Damaged Condition (Work in Progress)," American Bureau of Shipping, Houston, TX, 2014.

9. APPENDIX

9.1 FPSO – Collision Damage (Sagging)

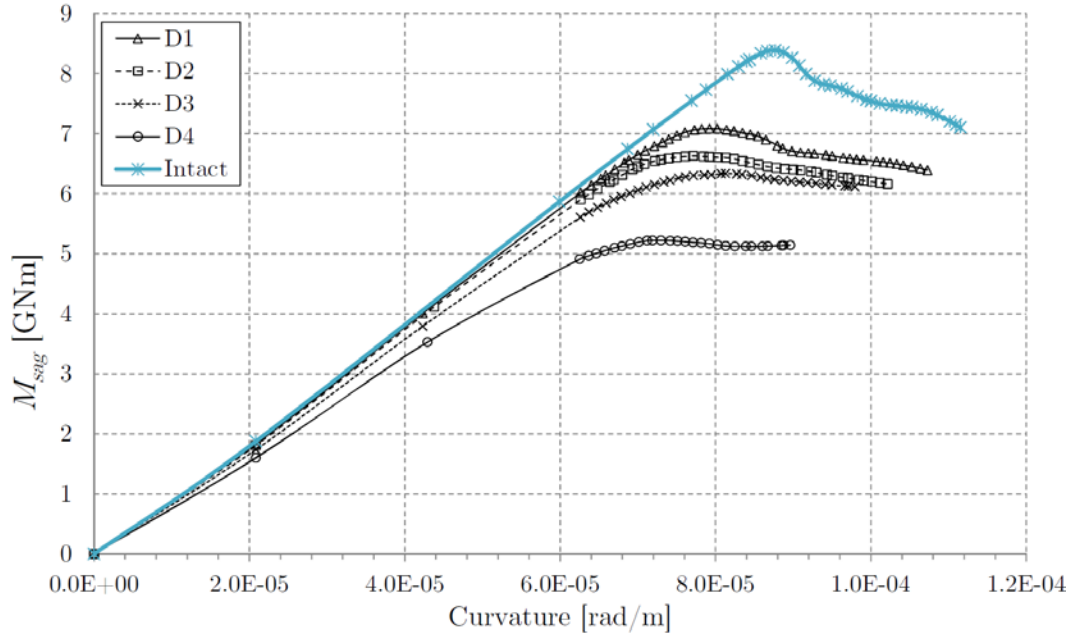


Figure 78: FPSO – Collision Damage D1-D4 (Sagging)

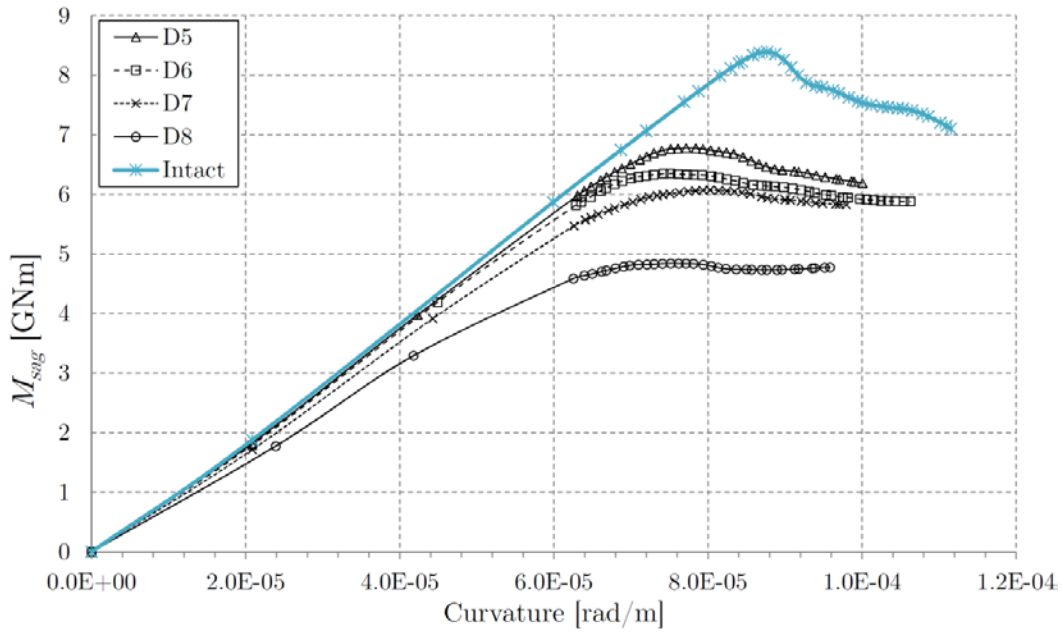


Figure 79: FPSO – Collision Damage D5-D8 (Sagging)

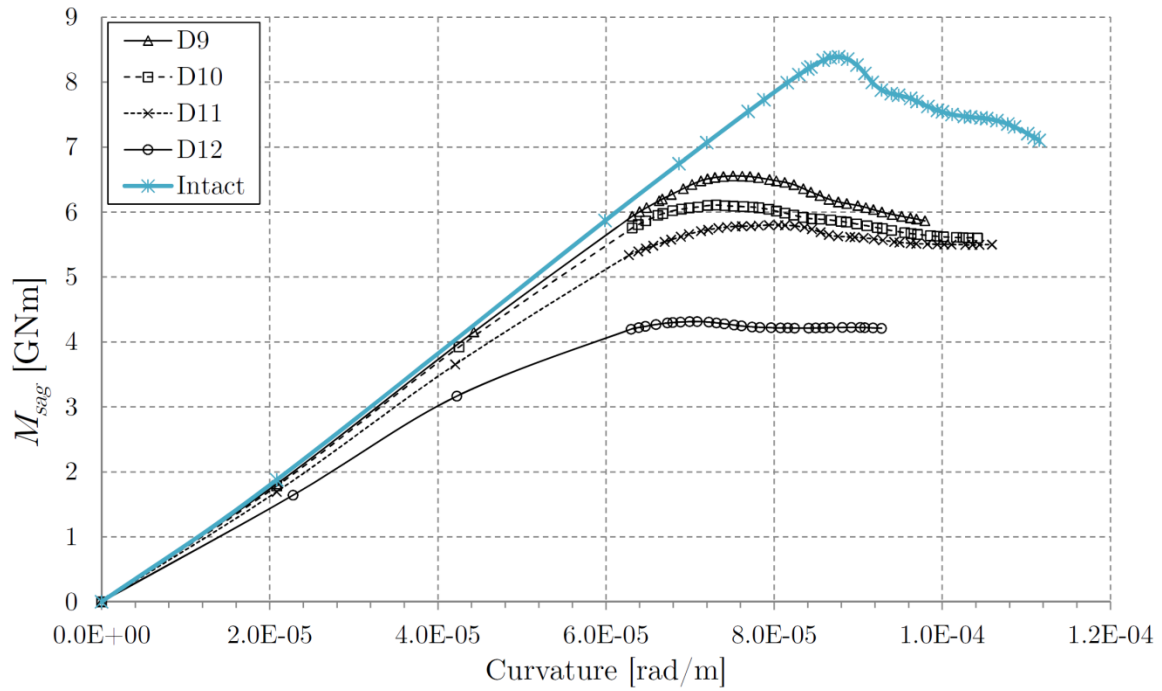


Figure 80: FPSO – Collision Damage D9-D12 (Sagging)

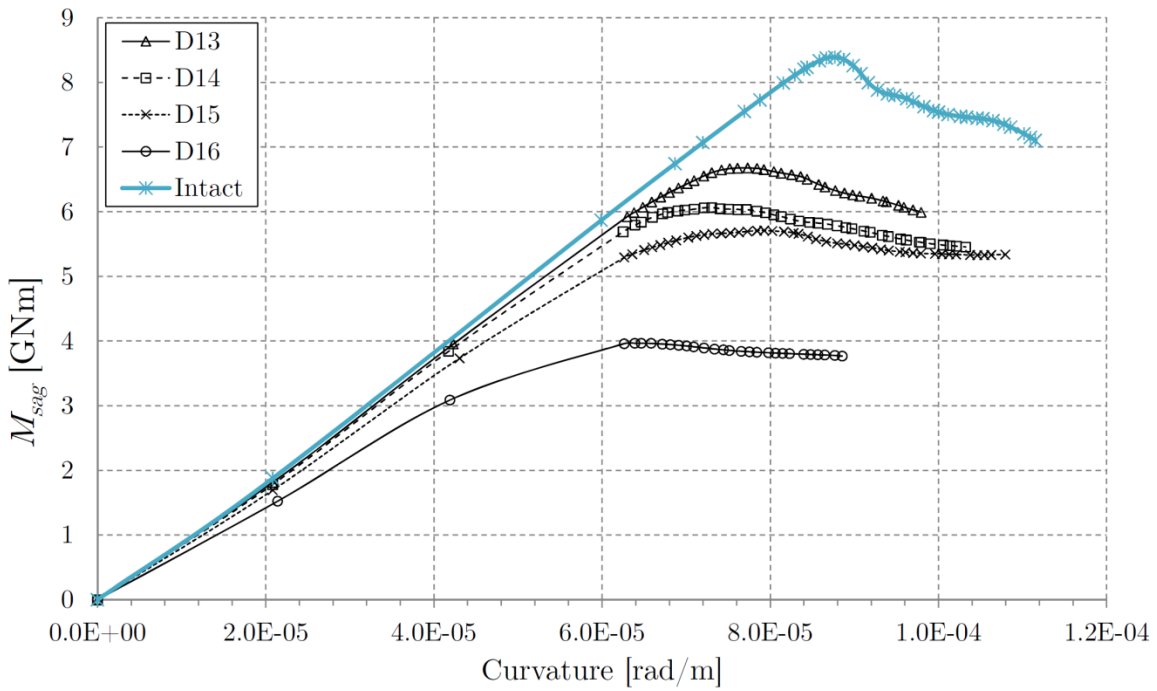


Figure 81: FPSO – Collision Damage D13-D16 (Sagging)

9.2 FPSO – Collision Damage (Hogging)

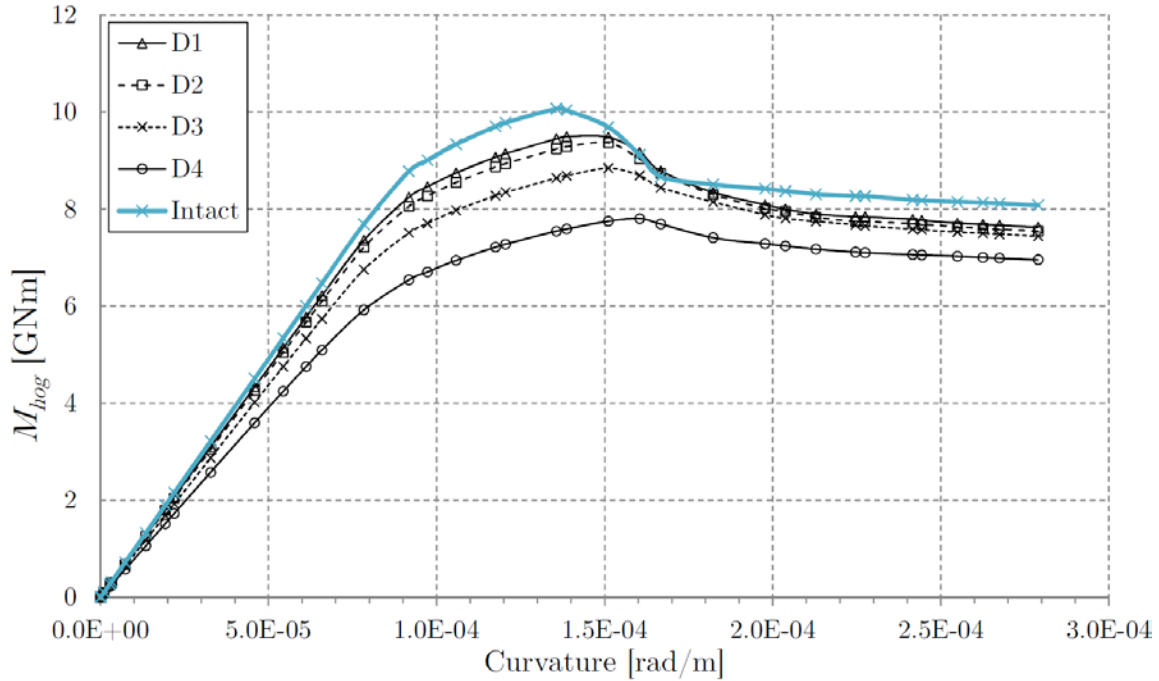


Figure 82: FPSO – Collision Damage D1-D4 (Hogging)

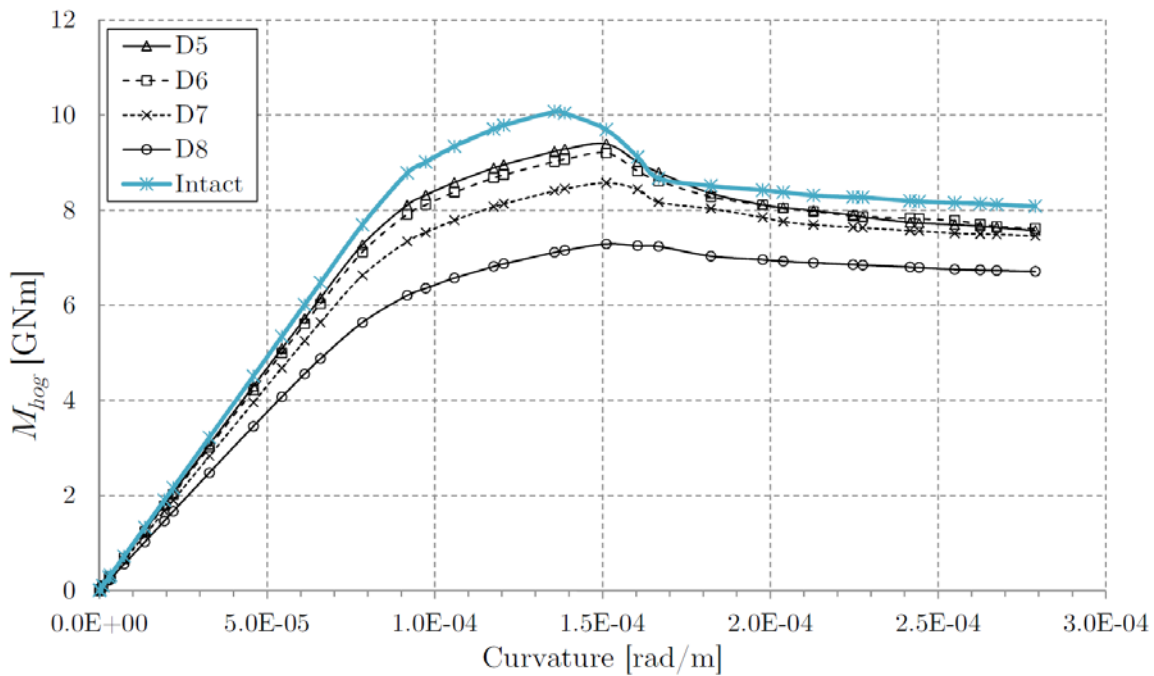


Figure 83: FPSO – Collision Damage D5-D8 (Hogging)

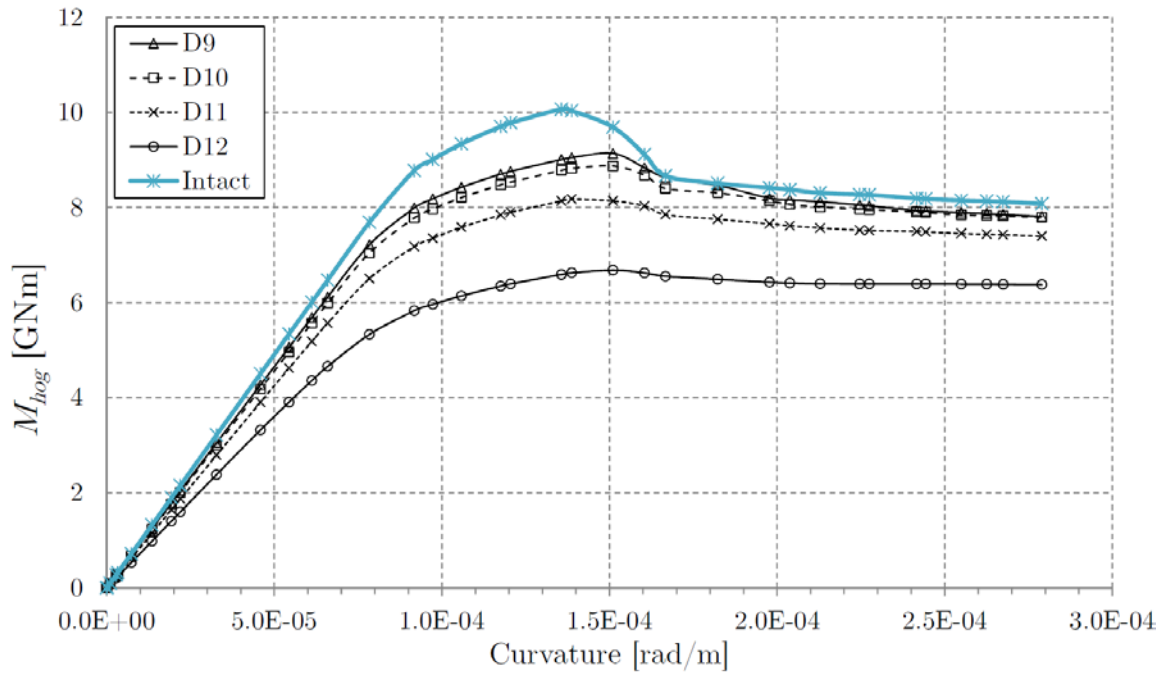


Figure 84: FPSO – Collision Damage D9-D12 (Hogging)

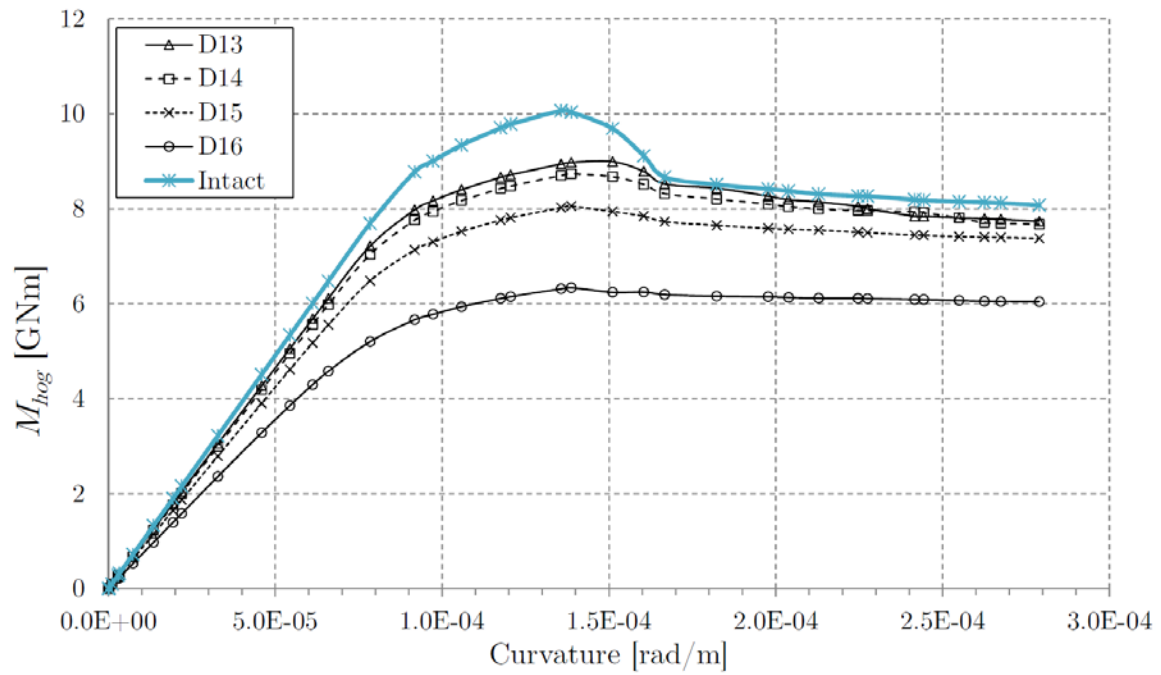


Figure 85: FPSO – Collision Damage D13-D16 (Hogging)

9.3 FPSO – Grounding Damage (Hogging)

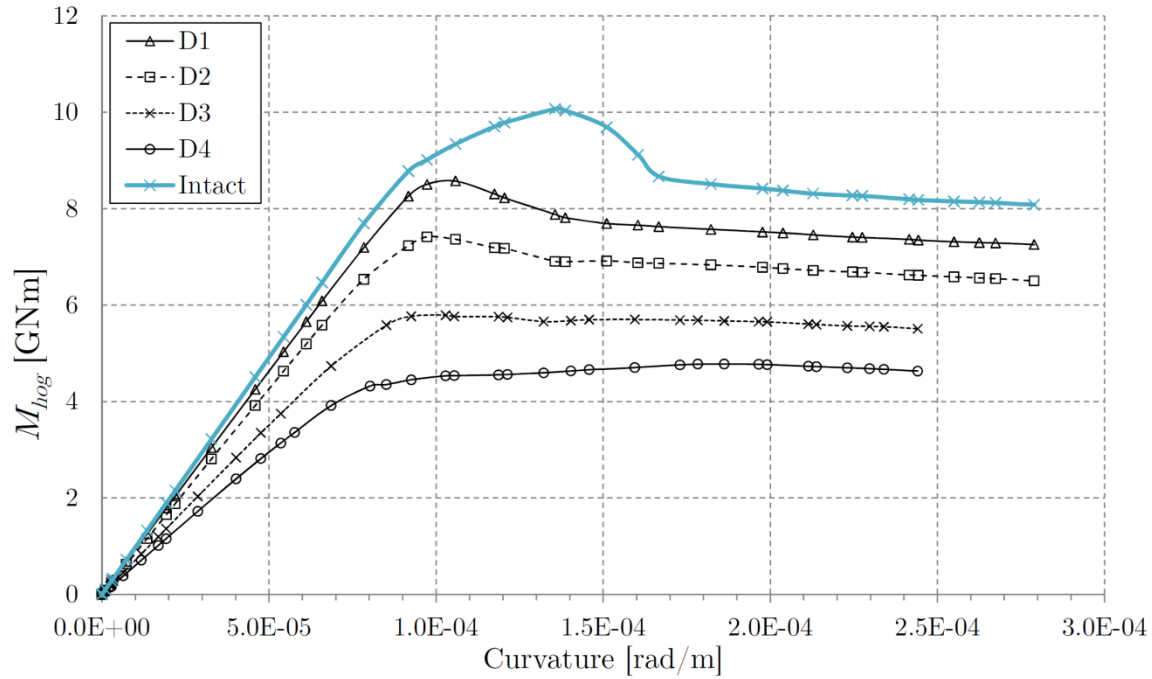


Figure 86: FPSO – Grounding Damage D1-D4 (Hogging)

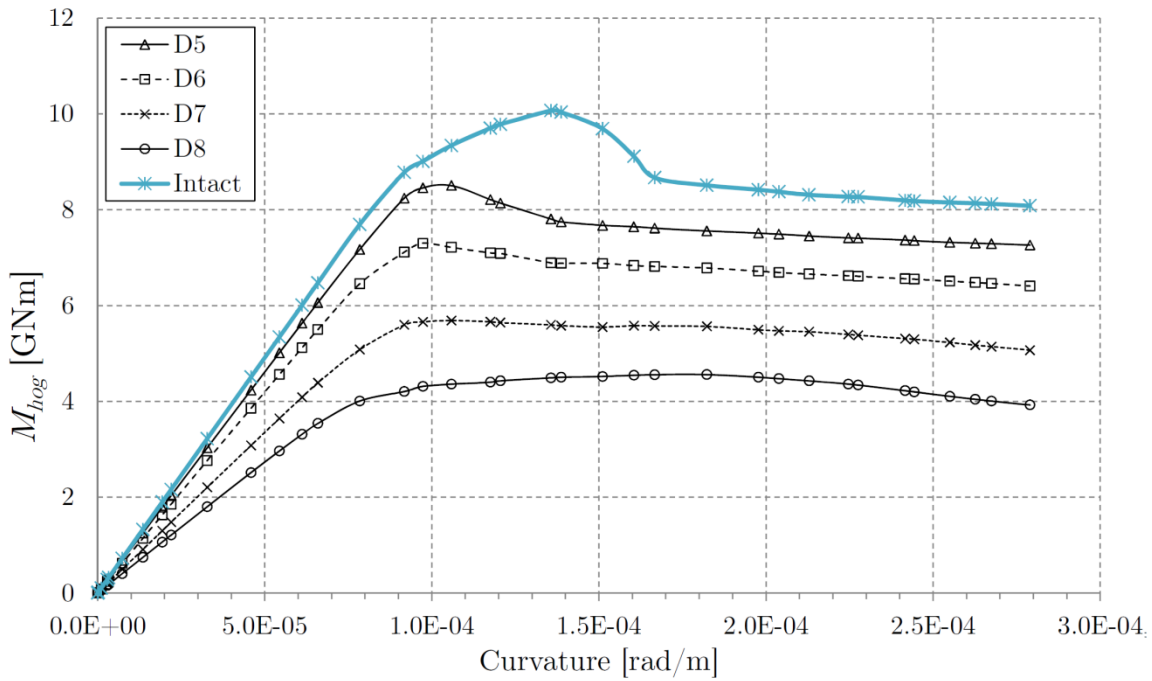


Figure 87: FPSO – Grounding Damage D5-D8 (Hogging)

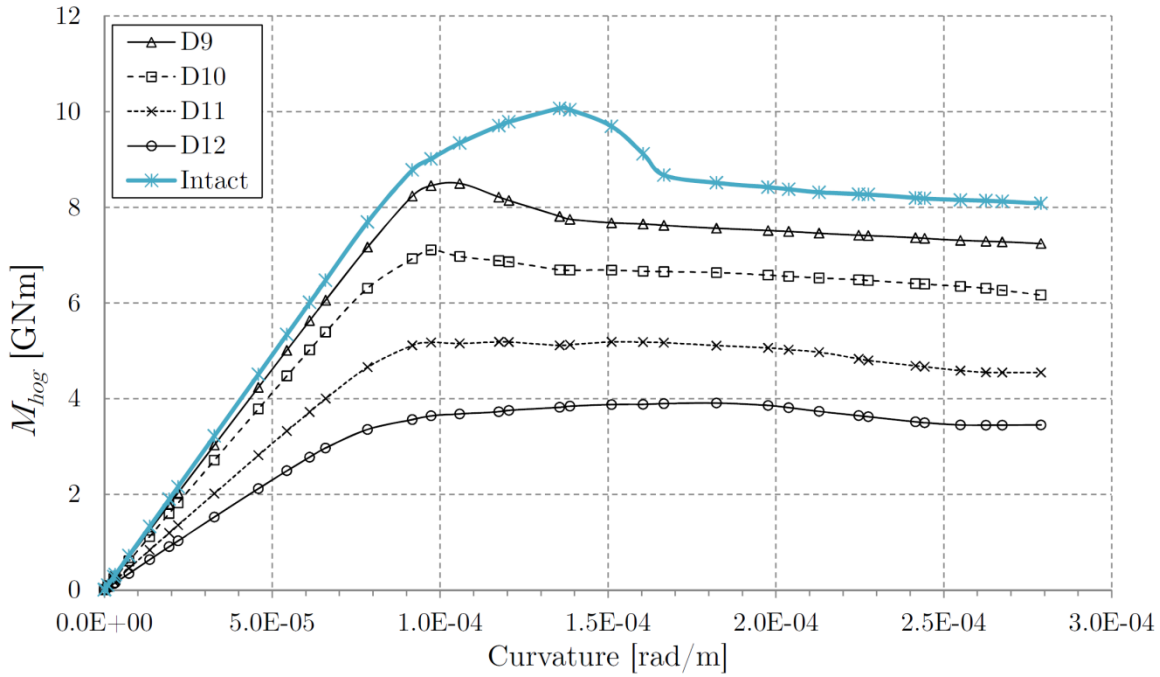


Figure 88: FPSO – Grounding Damage D9-D12 (Hogging)

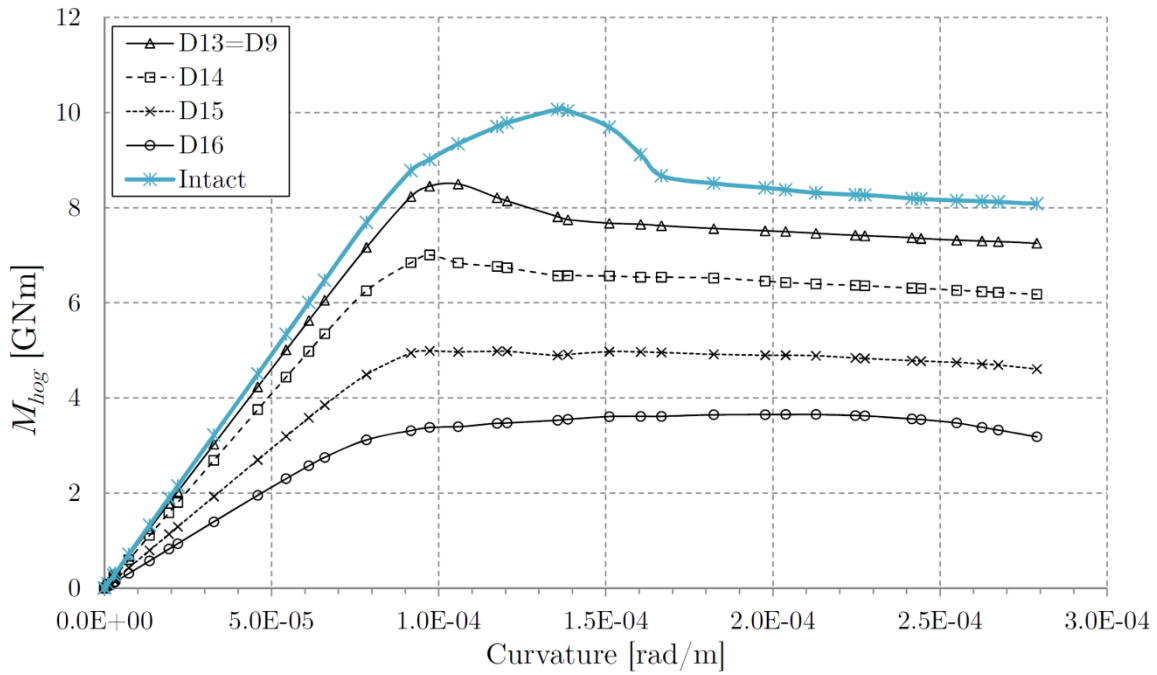


Figure 89: FPSO – Grounding Damage D13-D16 (Hogging)

9.4 FPSO – Grounding Damage (Sagging)

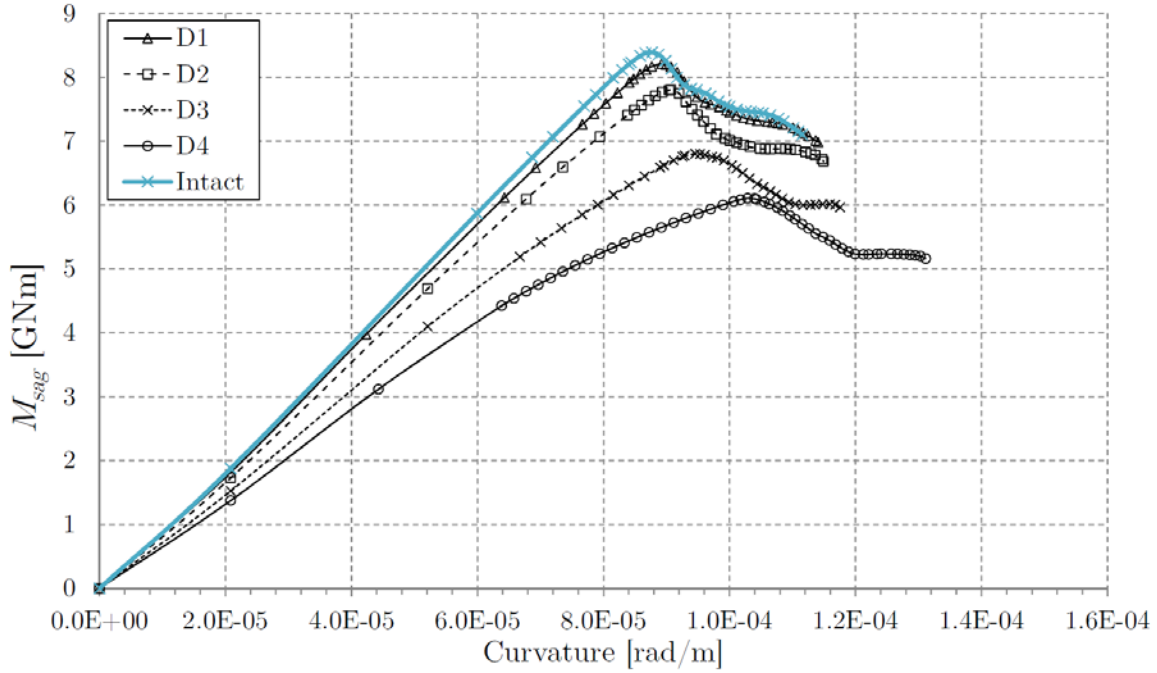


Figure 90: FPSO – Grounding Damage D1-D4 (Sagging)

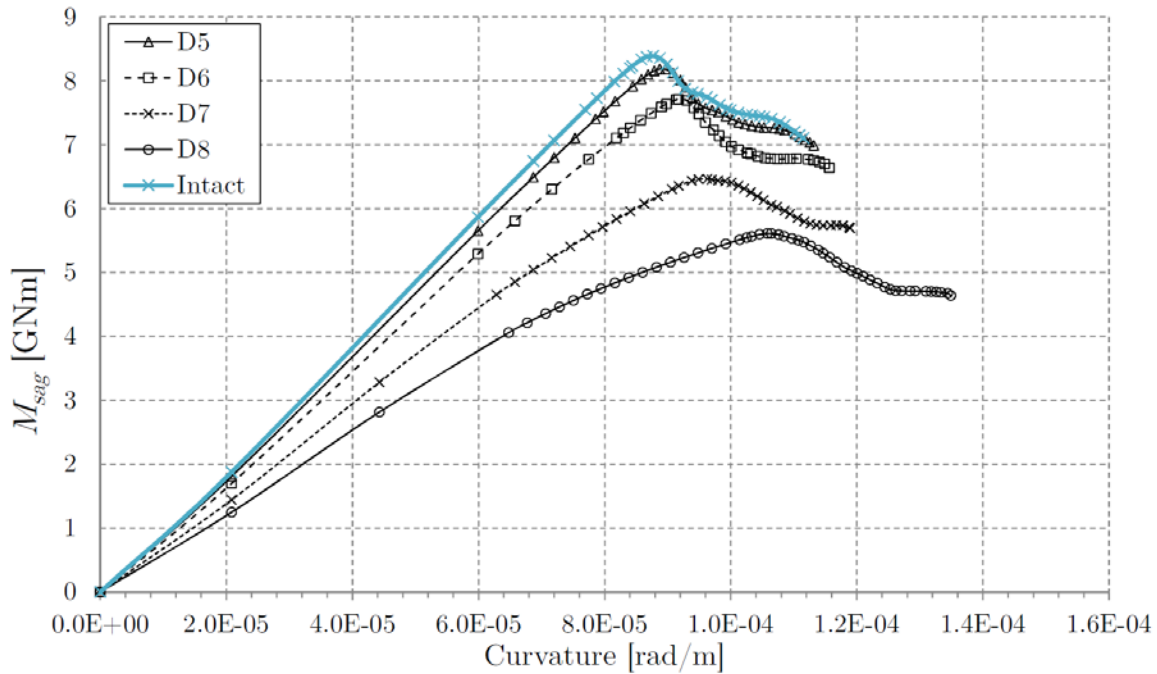


Figure 91: FPSO – Grounding Damage D5-D8 (Sagging)

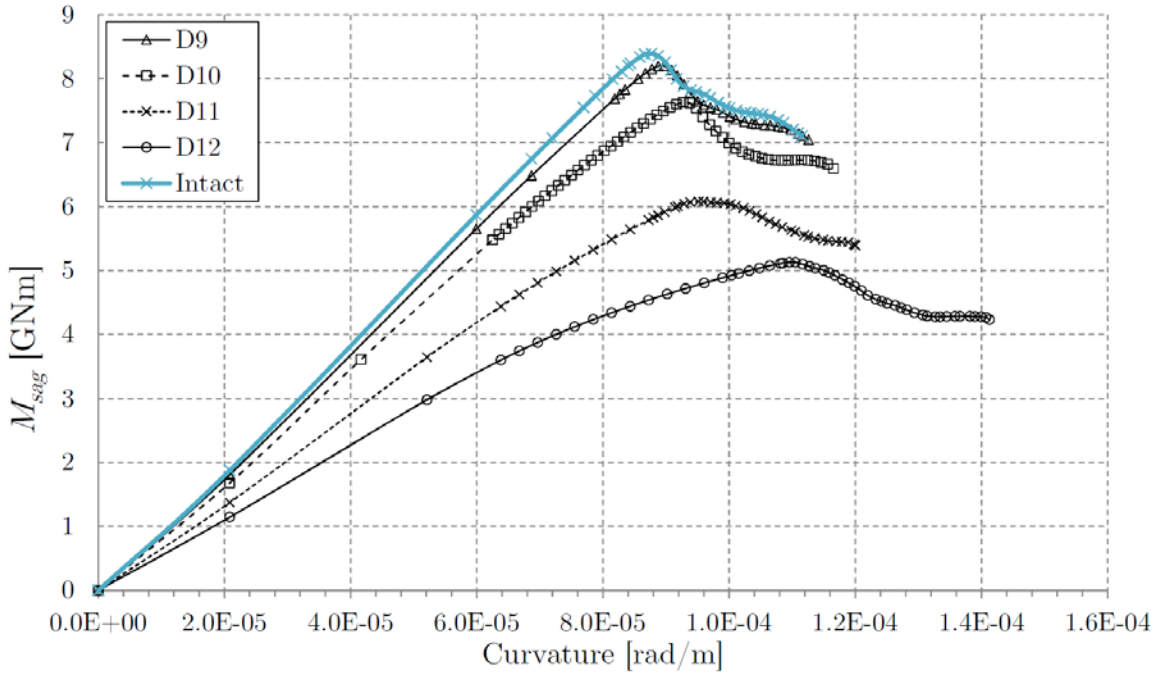


Figure 92: FPSO – Grounding Damage D9-D12 (Sagging)

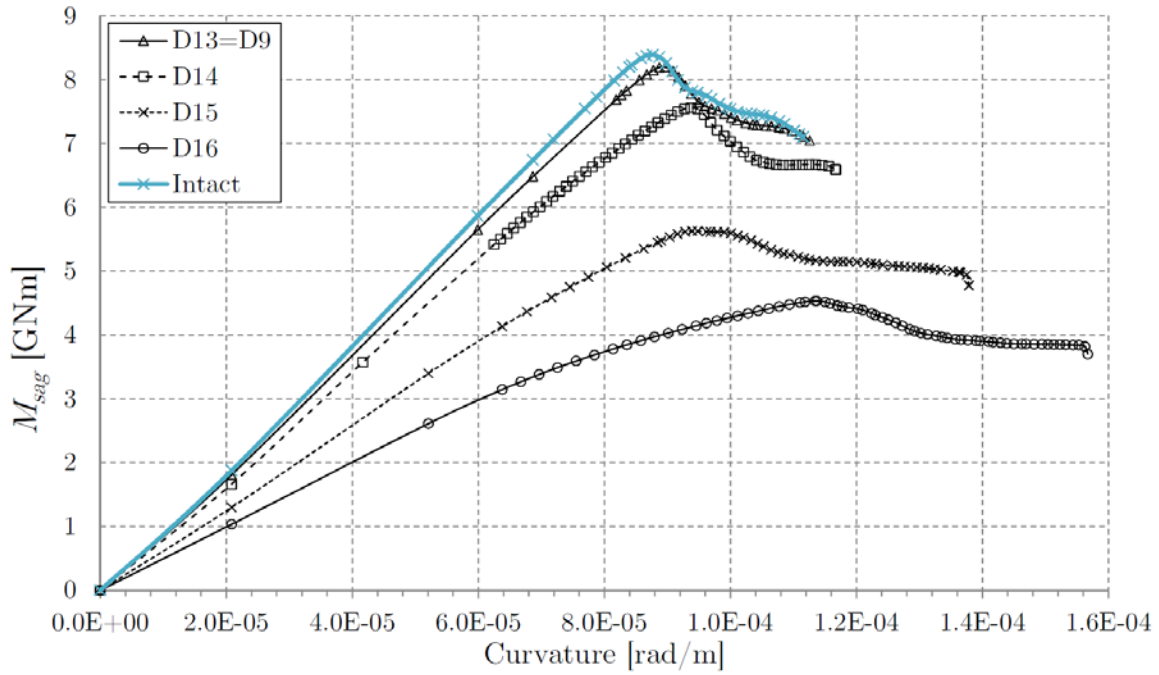


Figure 93: FPSO – Grounding Damage D13-D16 (Sagging)

9.5 Tanker – Collision Damage (Sagging - 1WF)

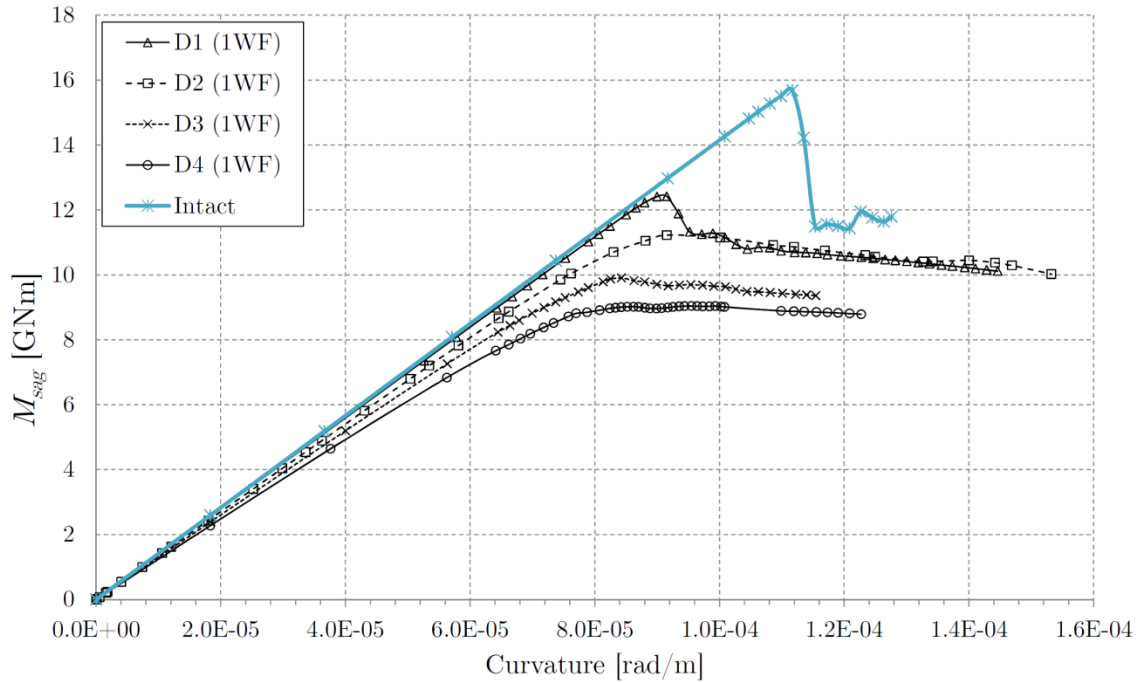


Figure 94: Tanker – Collision Damage D1-D4 (Sagging - 1WF longitudinal extent)

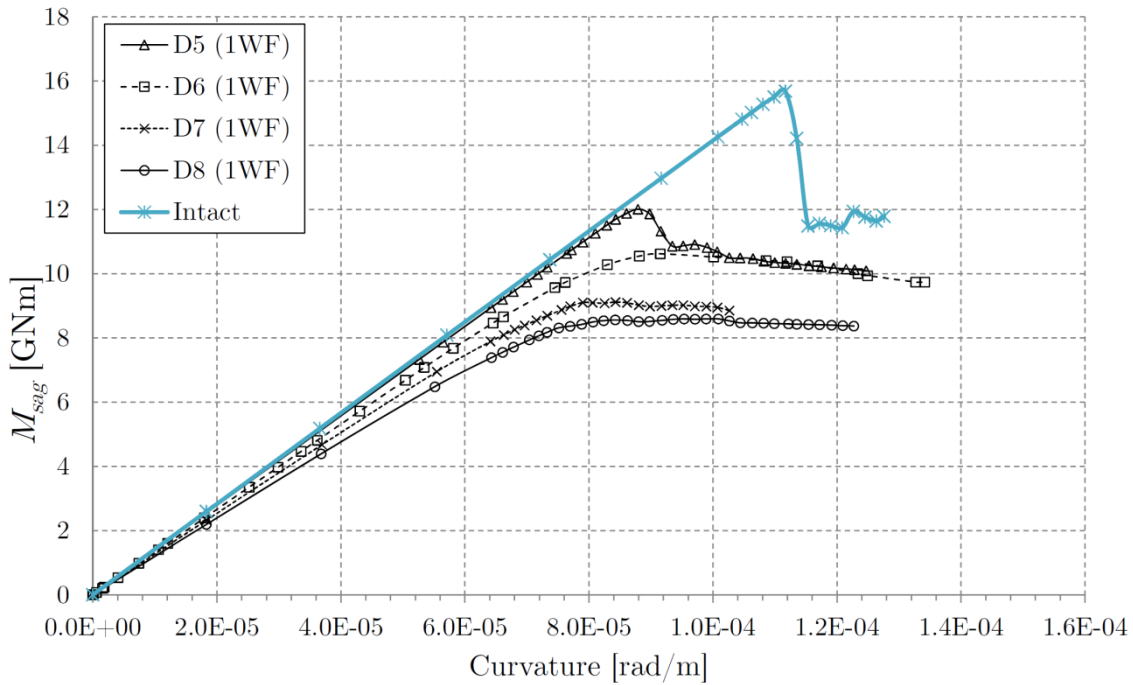


Figure 95: Tanker – Collision Damage D5-D8 (Sagging - 1WF longitudinal extent)

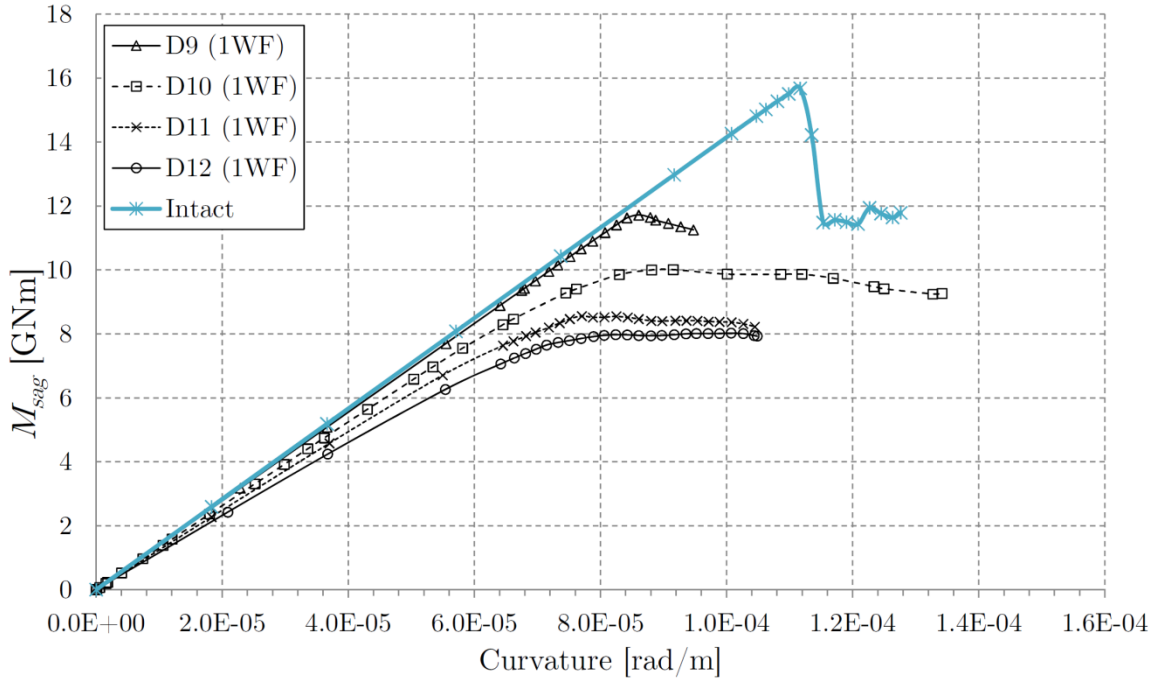


Figure 96: Tanker – Collision Damage D9-D12 (Sagging - 1WF longitudinal extent)

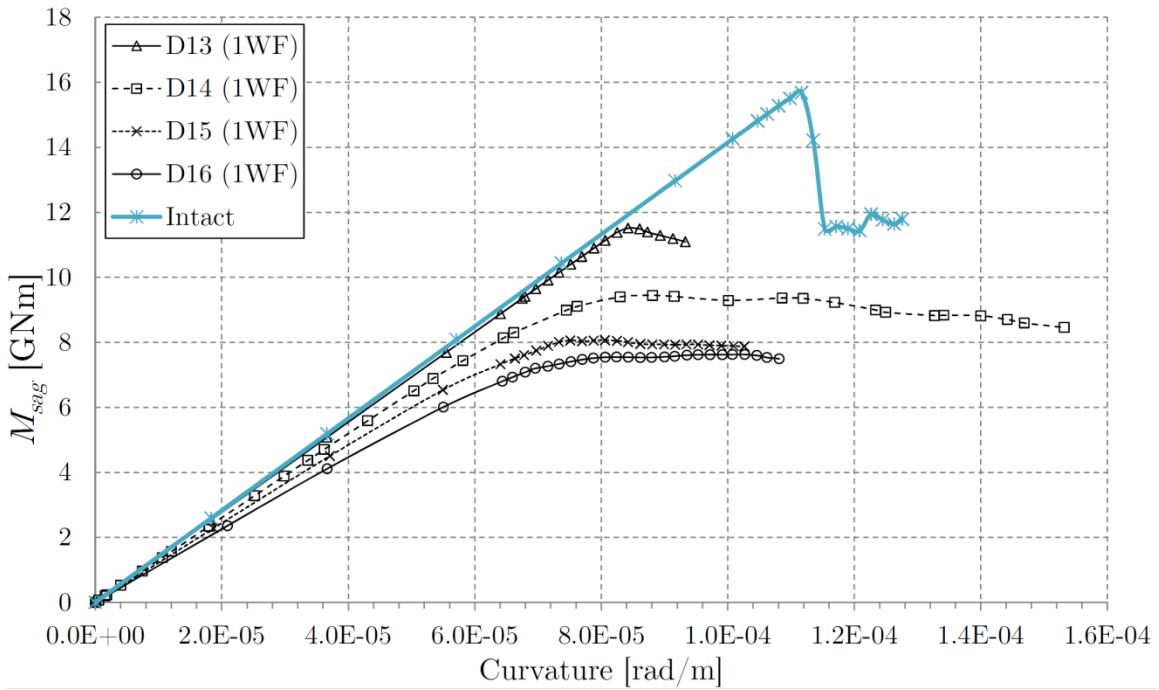


Figure 97: Tanker – Collision Damage D13-D16 (Sagging - 1WF longitudinal extent)

9.6 Tanker – Collision Damage (Sagging - 3WF)

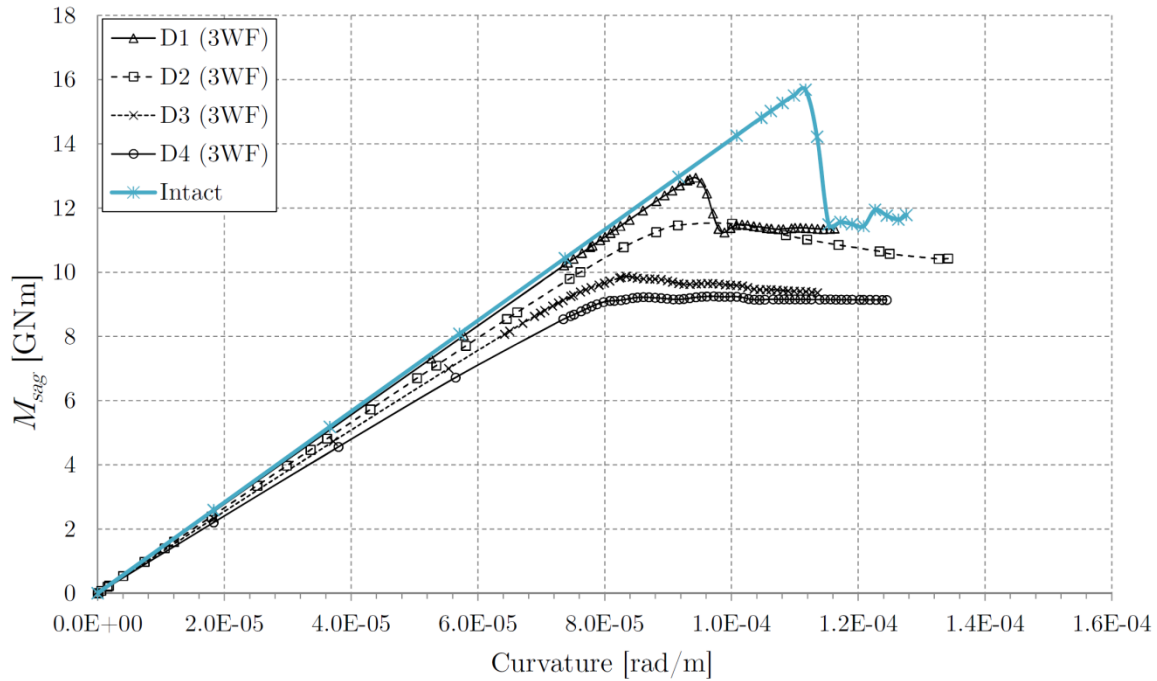


Figure 98: Tanker – Collision Damage D1-D4 (Sagging - 3WF longitudinal extent)

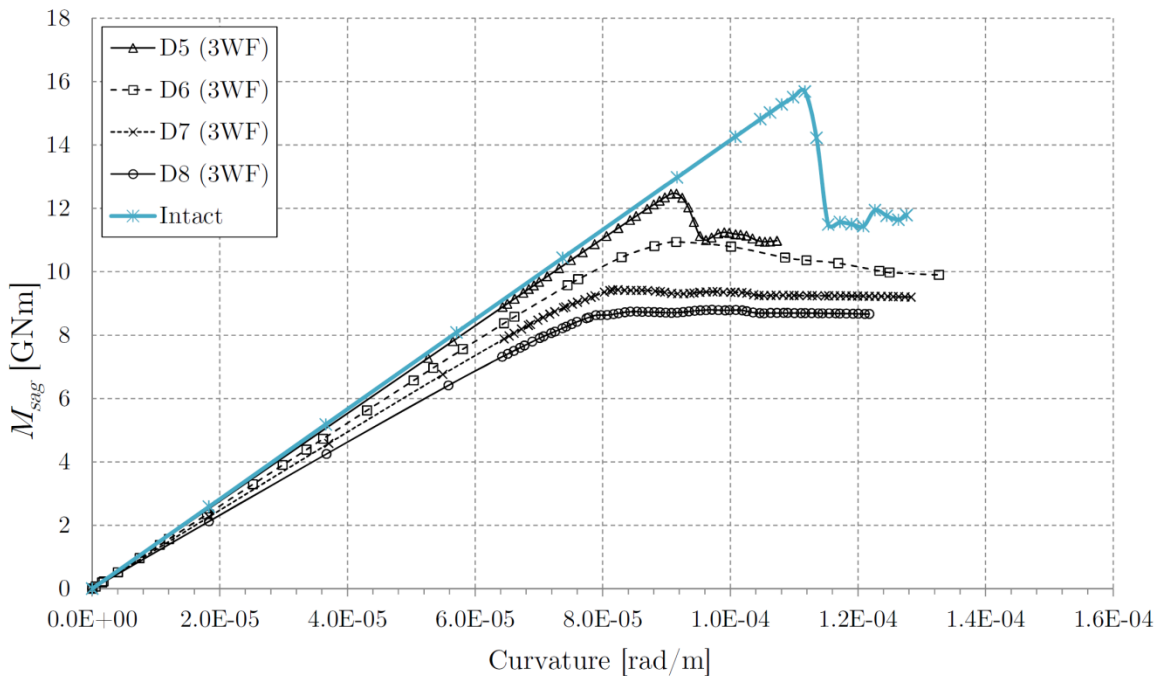


Figure 99: Tanker – Collision Damage D5-D8 (Sagging - 3WF longitudinal extent)

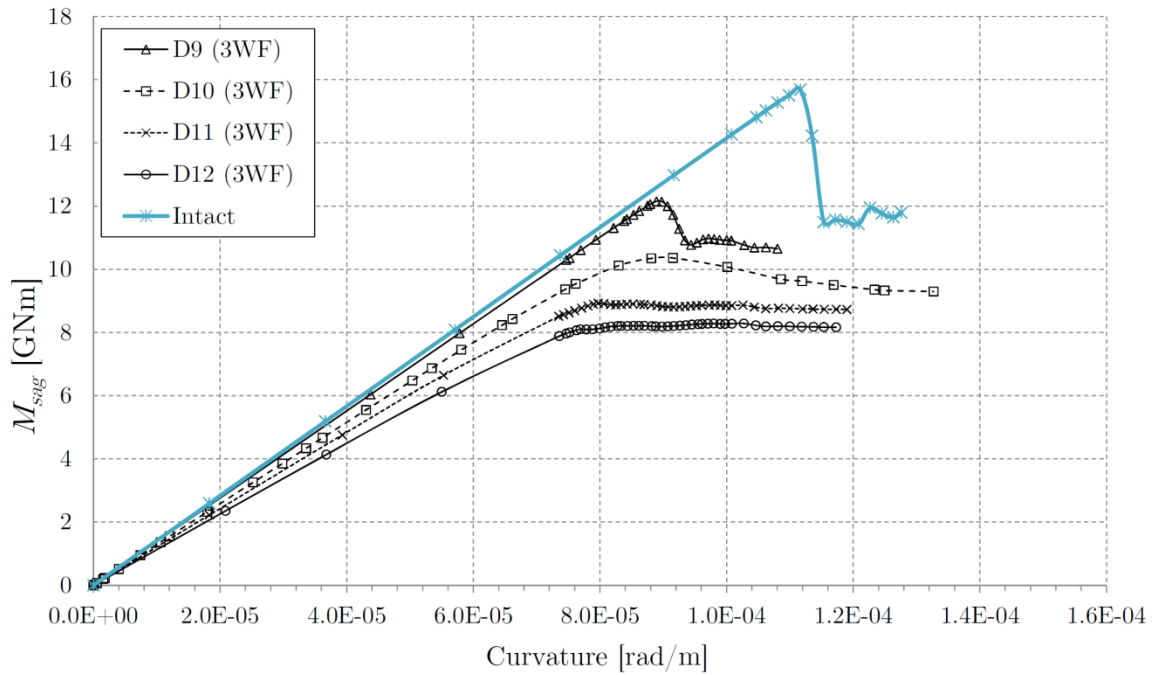


Figure 100: Tanker – Collision Damage D9-D12 (Sagging - 3WF longitudinal extent)

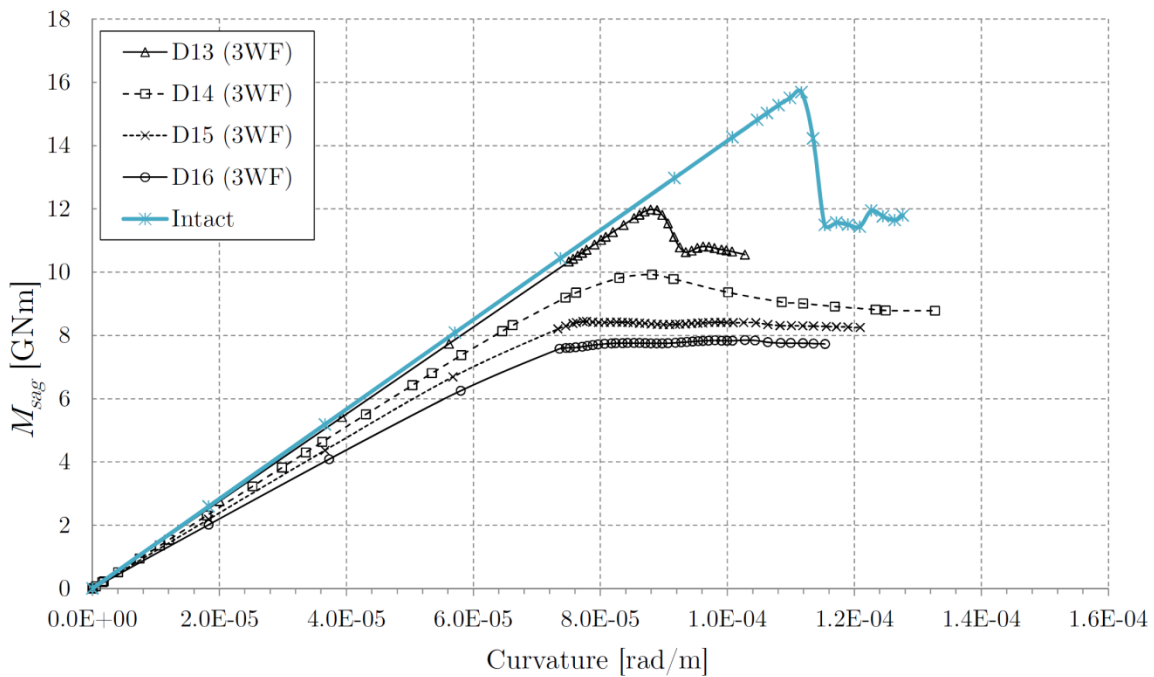


Figure 101: Tanker – Collision Damage D13-D16 (Sagging - 3WF longitudinal extent)

9.7 Tanker – Collision Damage (Sagging - ALL WF)

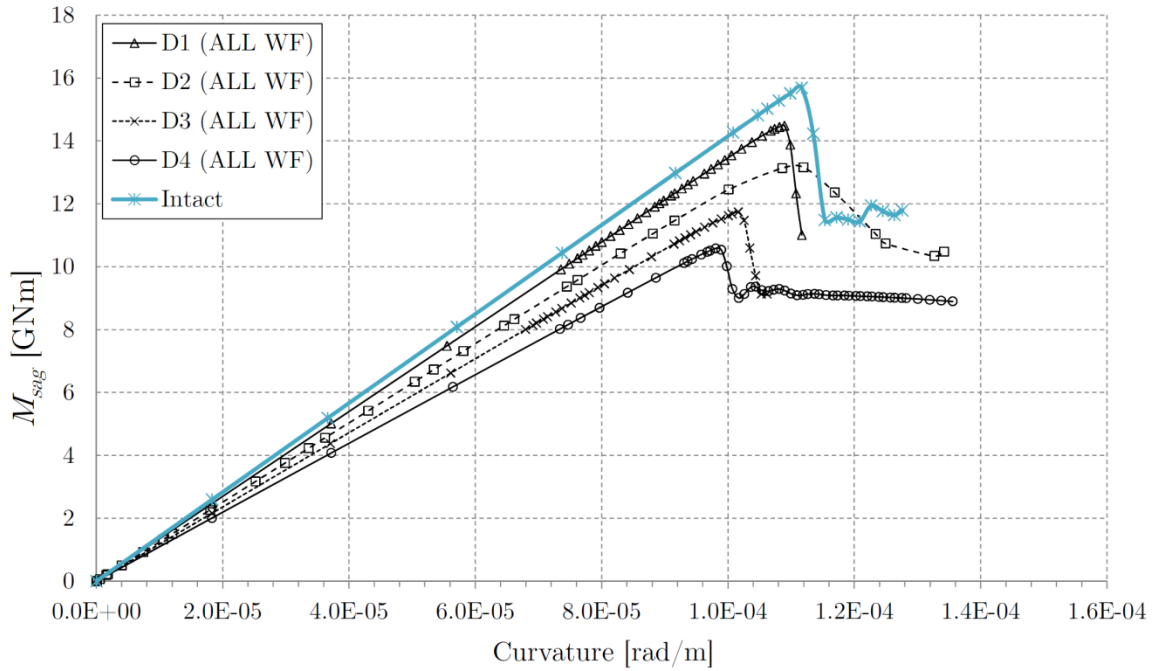


Figure 102: Tanker – Collision Damage D1-D4 (Sagging - ALL WF longitudinal extent)

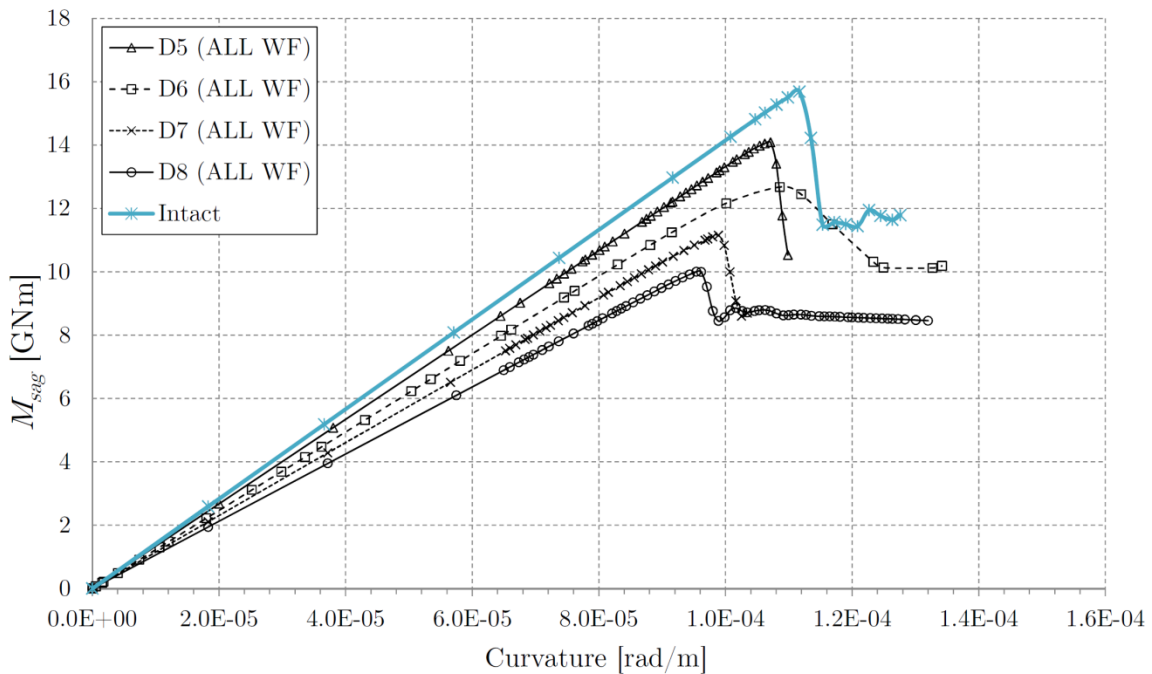


Figure 103: Tanker – Collision Damage D5-D8 (Sagging - ALL WF longitudinal extent)

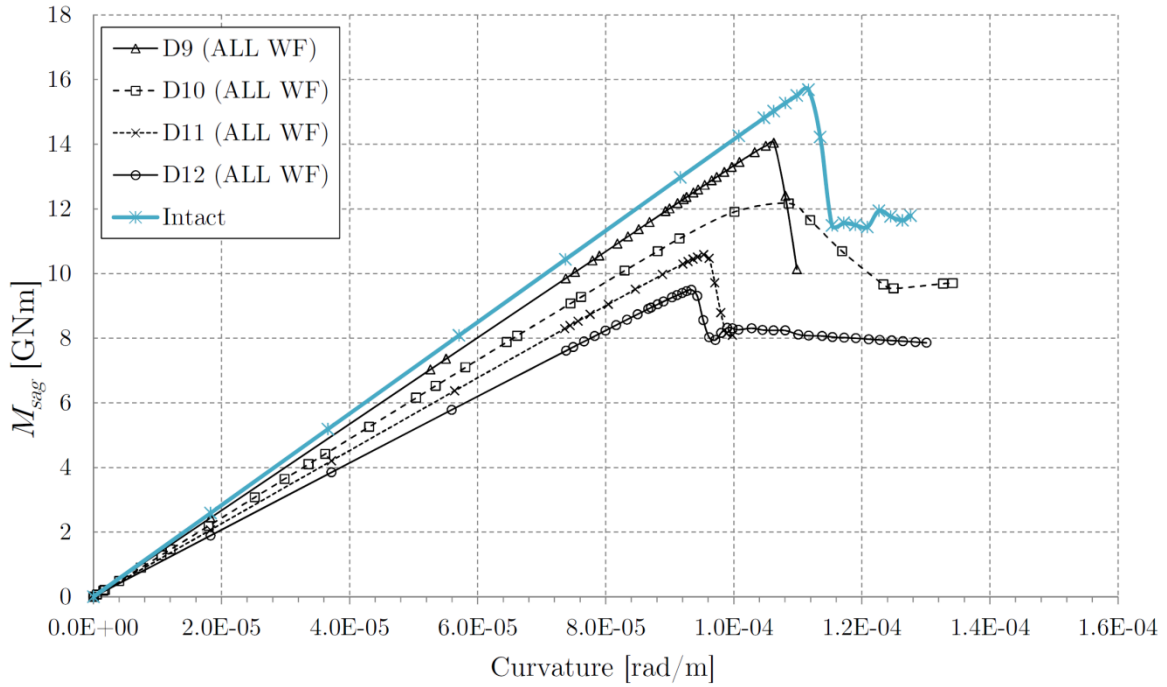


Figure 104: Tanker – Collision Damage D9-D12 (Sagging - ALL WF longitudinal extent)

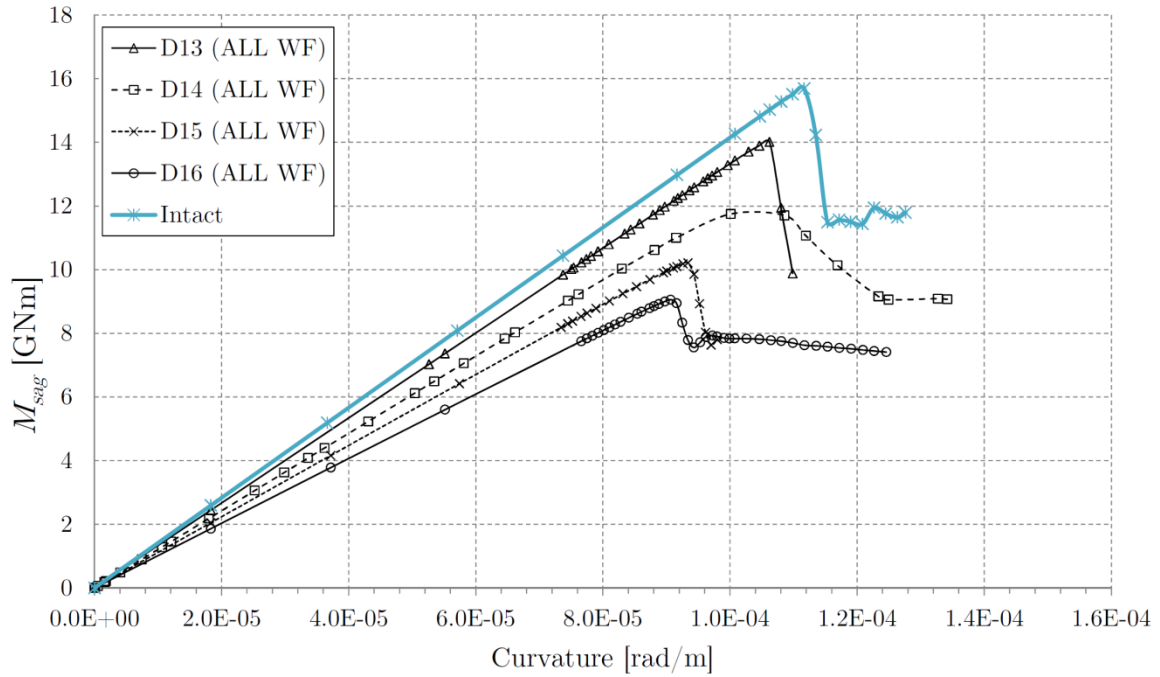


Figure 105: Tanker – Collision Damage D13-D16 (Sagging - ALL WF longitudinal extent)

9.8 Tanker – Collision Damage (Hogging - 3WF)

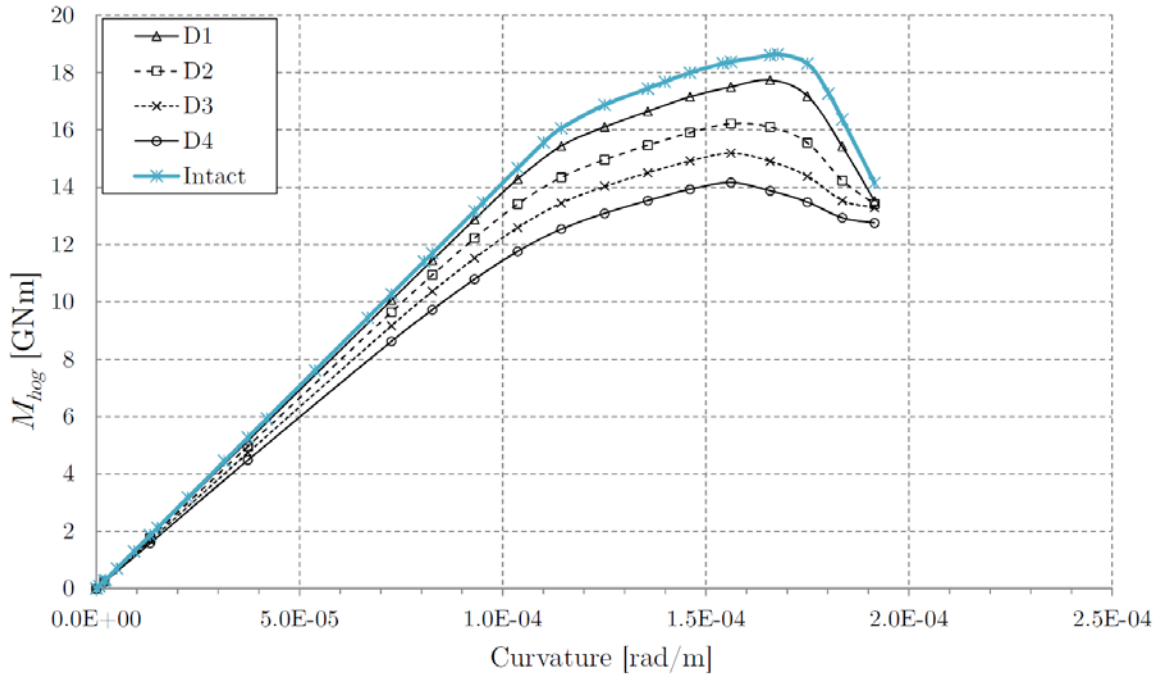


Figure 106: Tanker – Collision Damage D1-D4 (Hogging - 3WF longitudinal extent)

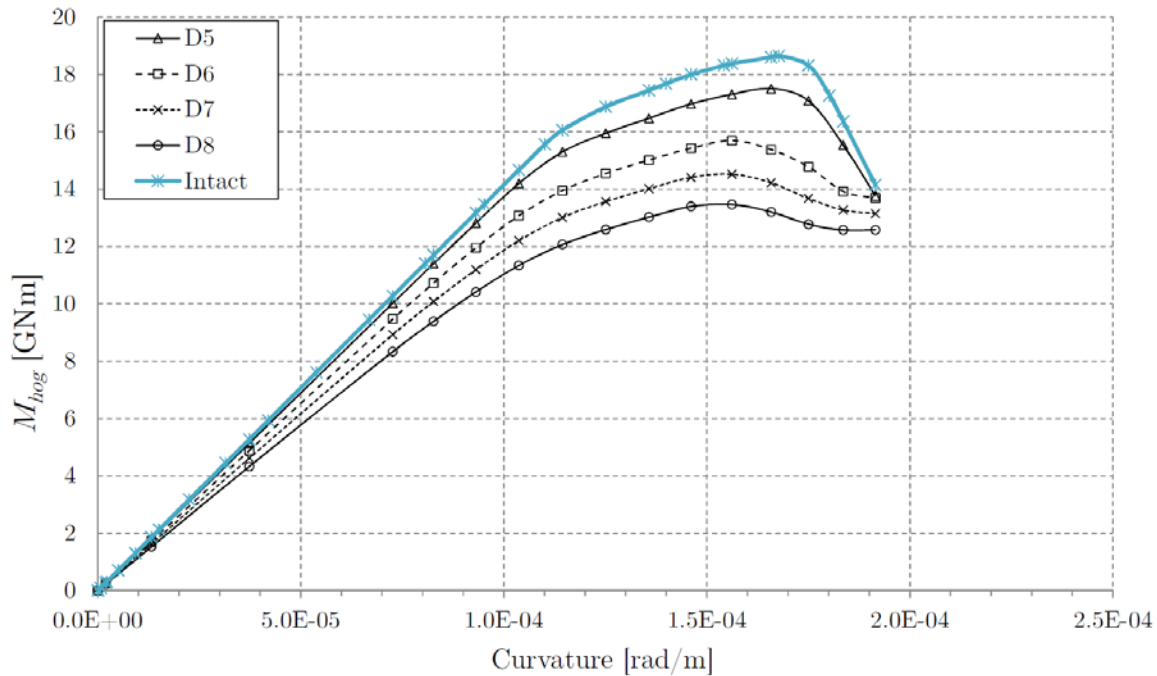


Figure 107: Tanker – Collision Damage D5-D8 (Hogging - 3WF longitudinal extent)

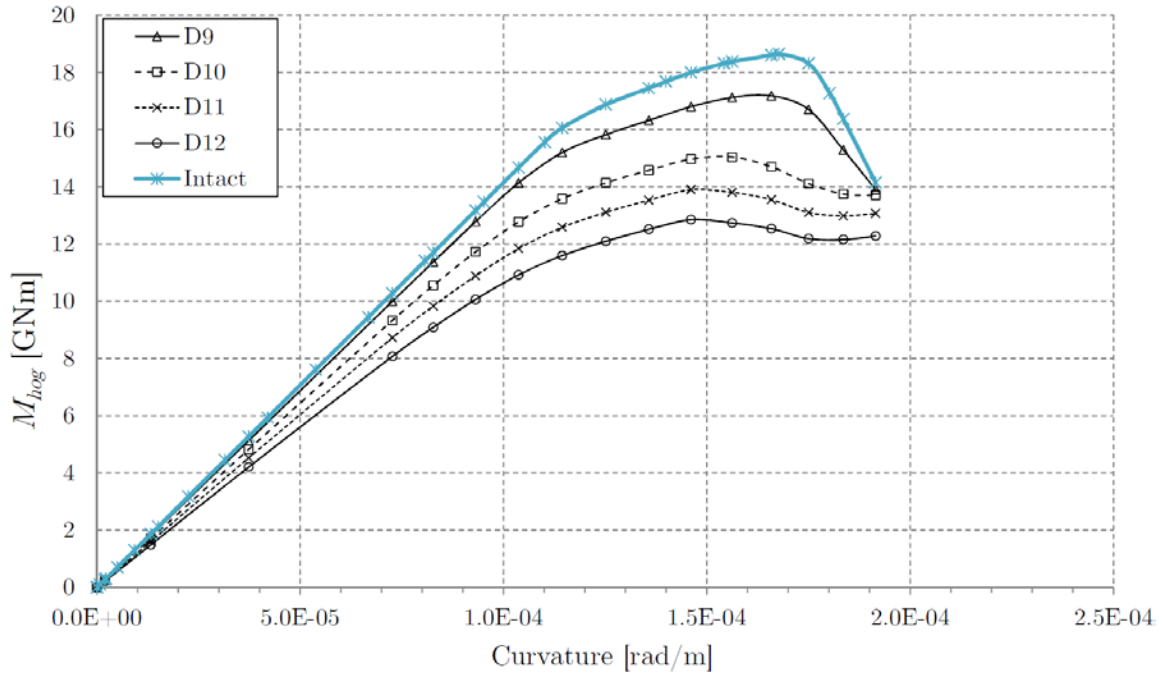


Figure 108: Tanker – Collision Damage D9-D12 (Hogging - 3WF longitudinal extent)

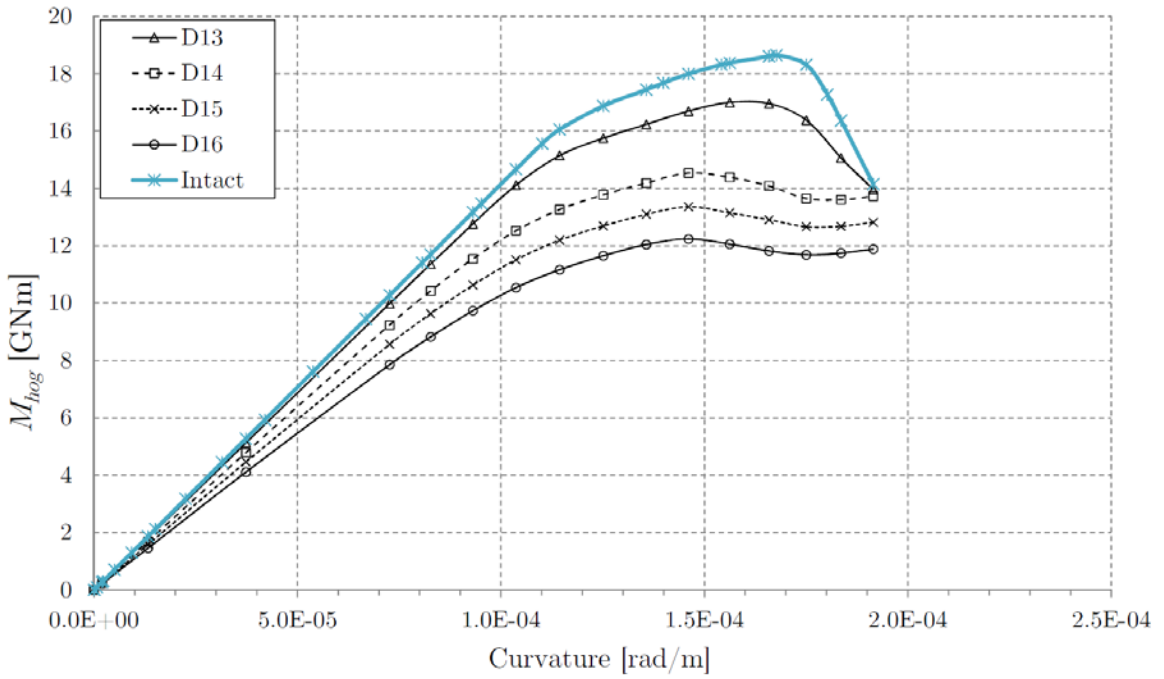


Figure 109: Tanker – Collision Damage D13-D16 (Hogging - 3WF longitudinal extent)

9.9 Tanker – Grounding Damage (Hogging)

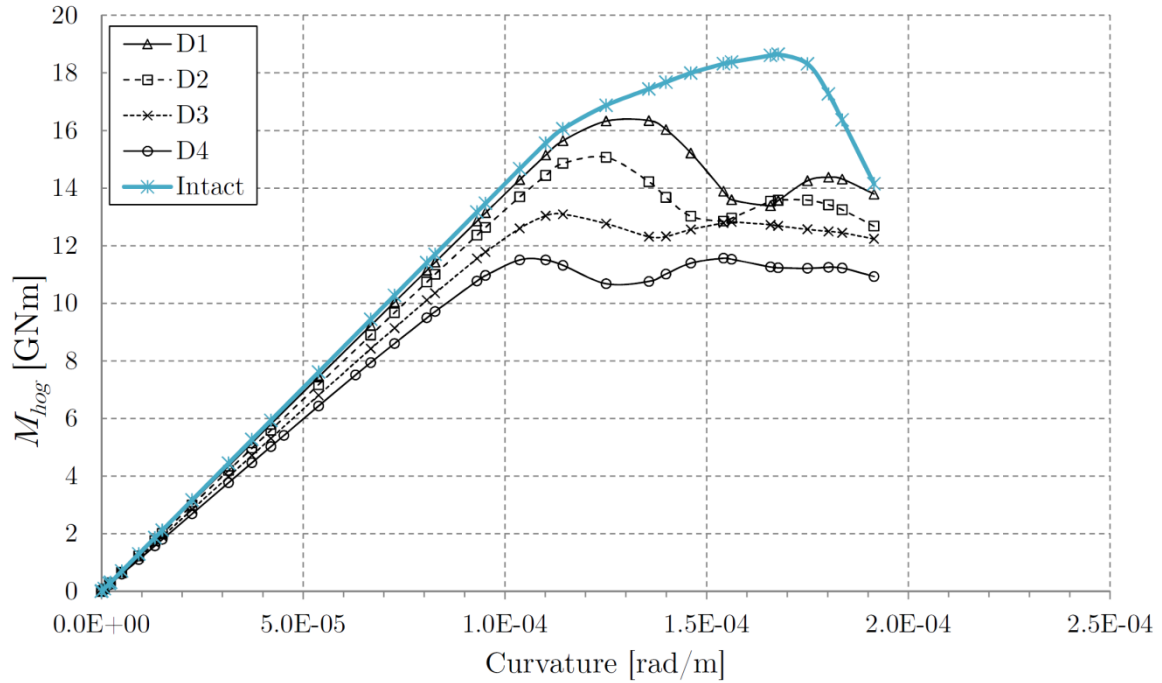


Figure 110: Tanker – Grounding Damage D1-D4 (Hogging)

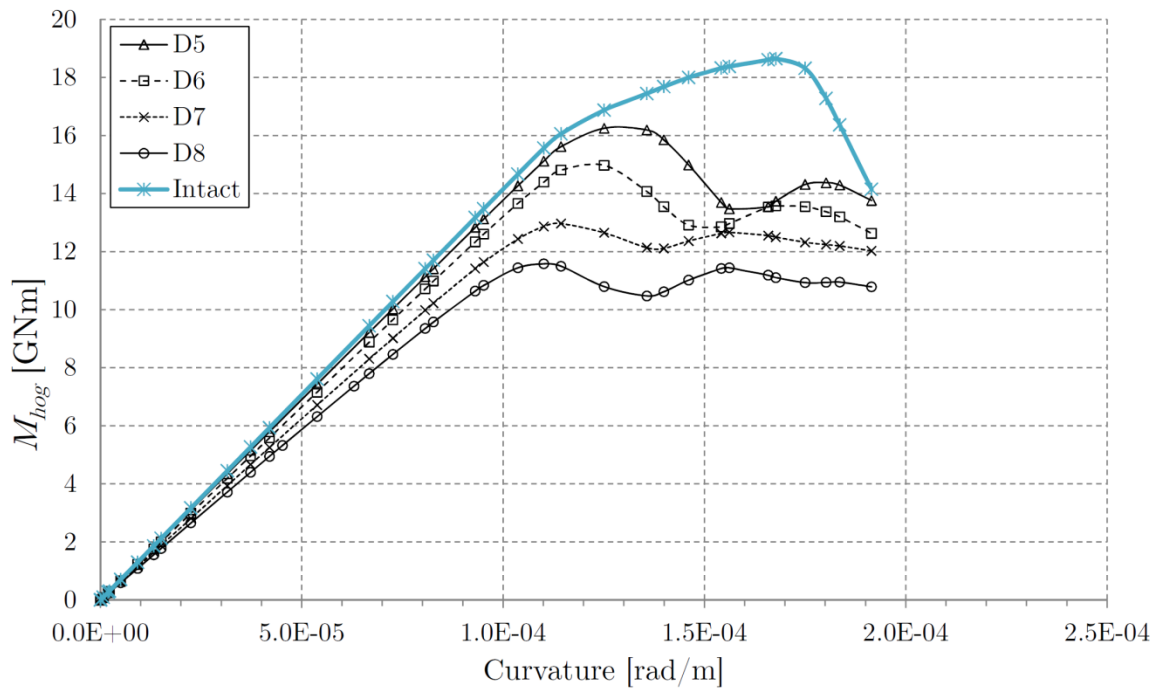


Figure 111: Tanker – Grounding Damage D5-D8 (Hogging)

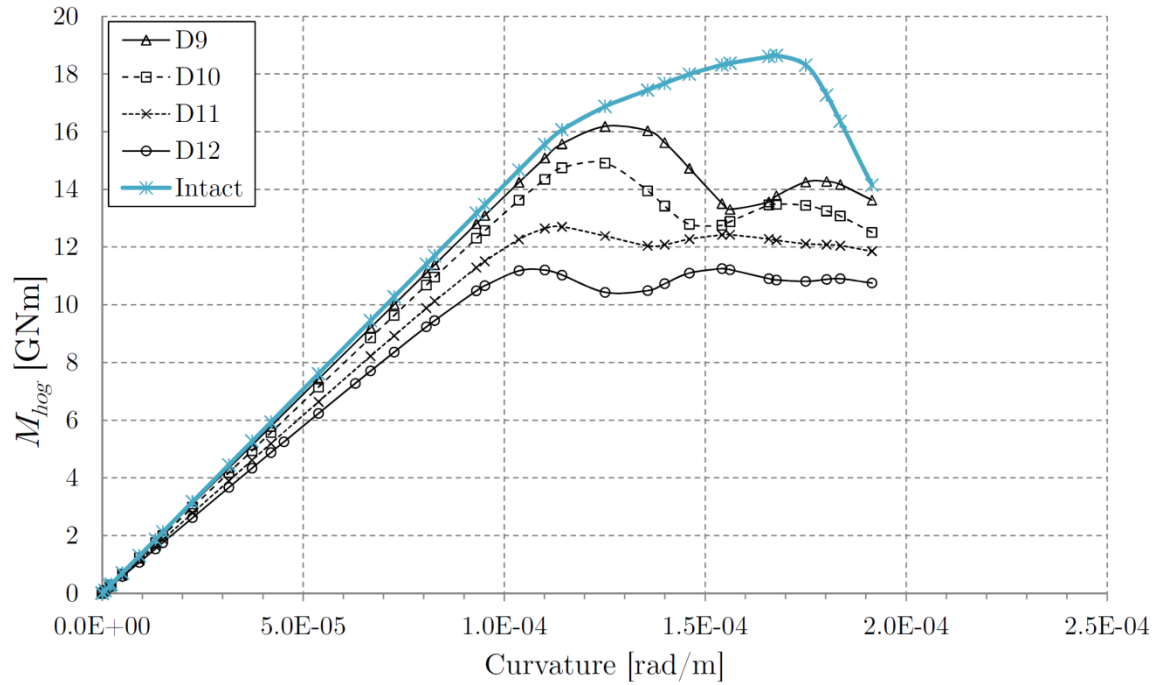


Figure 112: Tanker – Grounding Damage D9-D12 (Hogging)

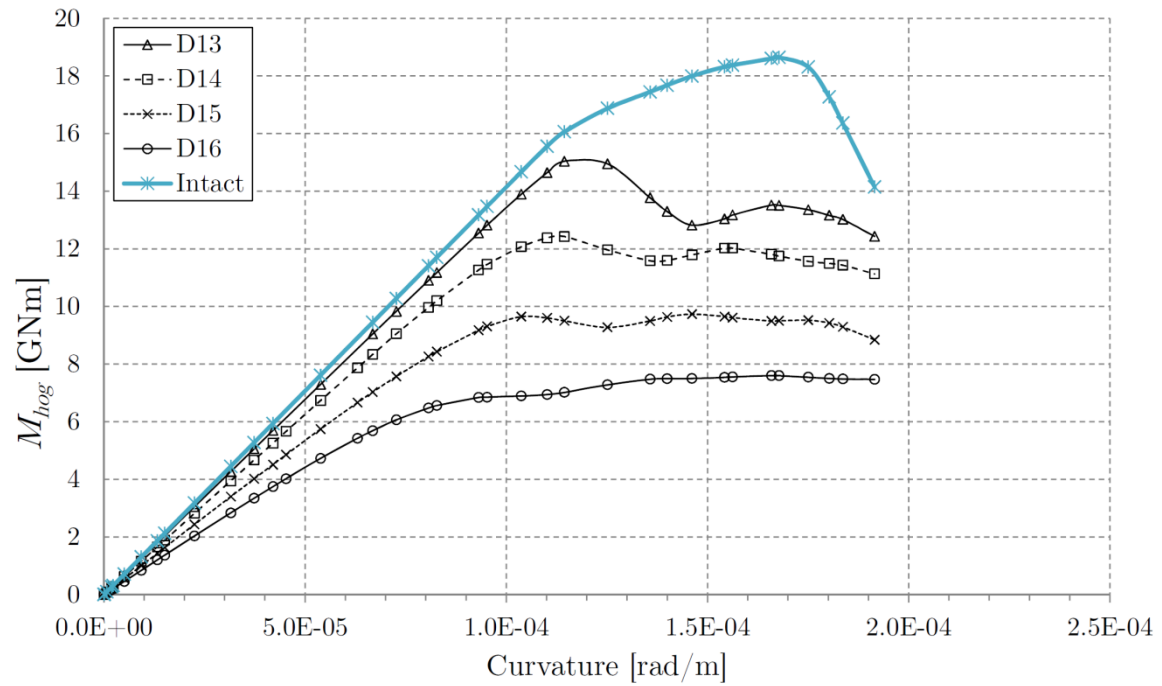


Figure 113: Tanker – Grounding Damage D13-D6 (Hogging)

9.10 Tanker – Grounding Damage (Sagging)

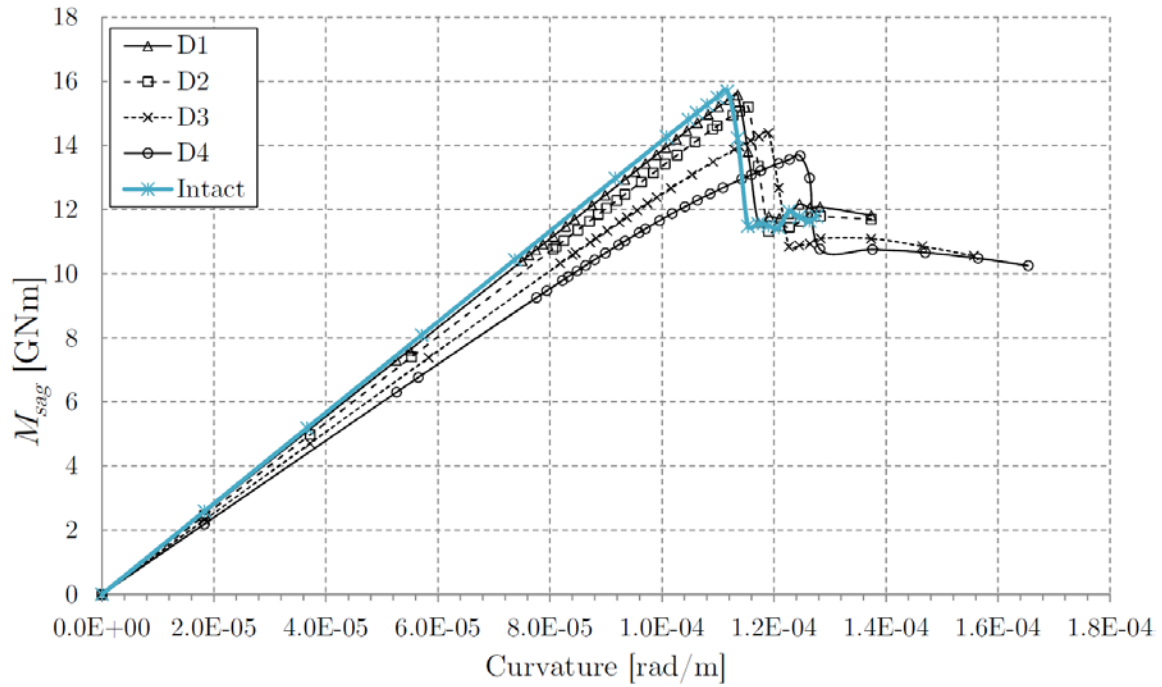


Figure 114: Tanker – Grounding Damage D1-D4 (Sagging)

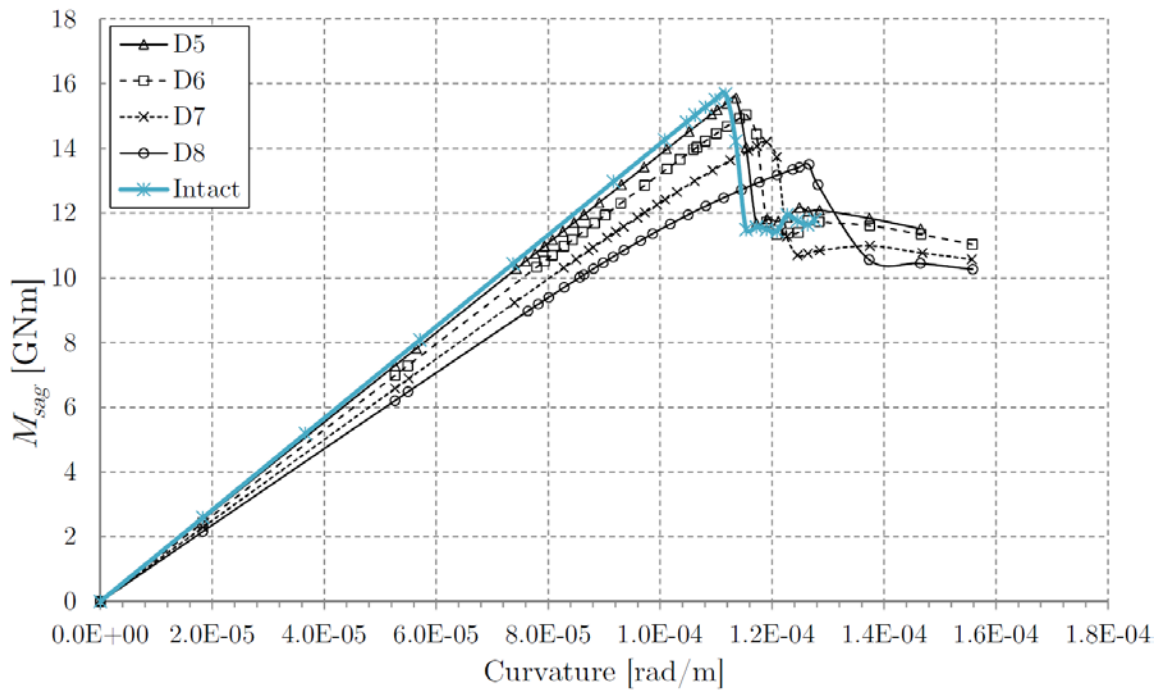


Figure 115: Tanker – Grounding Damage D5-D8 (Sagging)

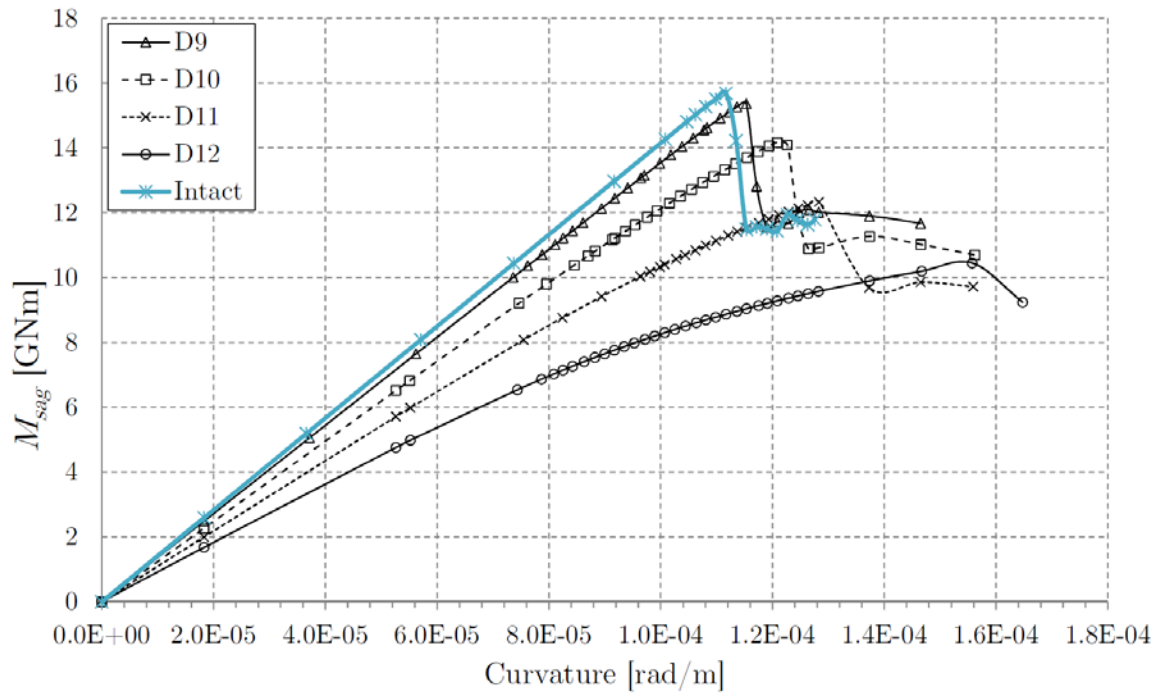


Figure 116: Tanker – Grounding Damage D9-D12 (Sagging)

9.11 Bulk Carrier – Collision Damage (Sagging)

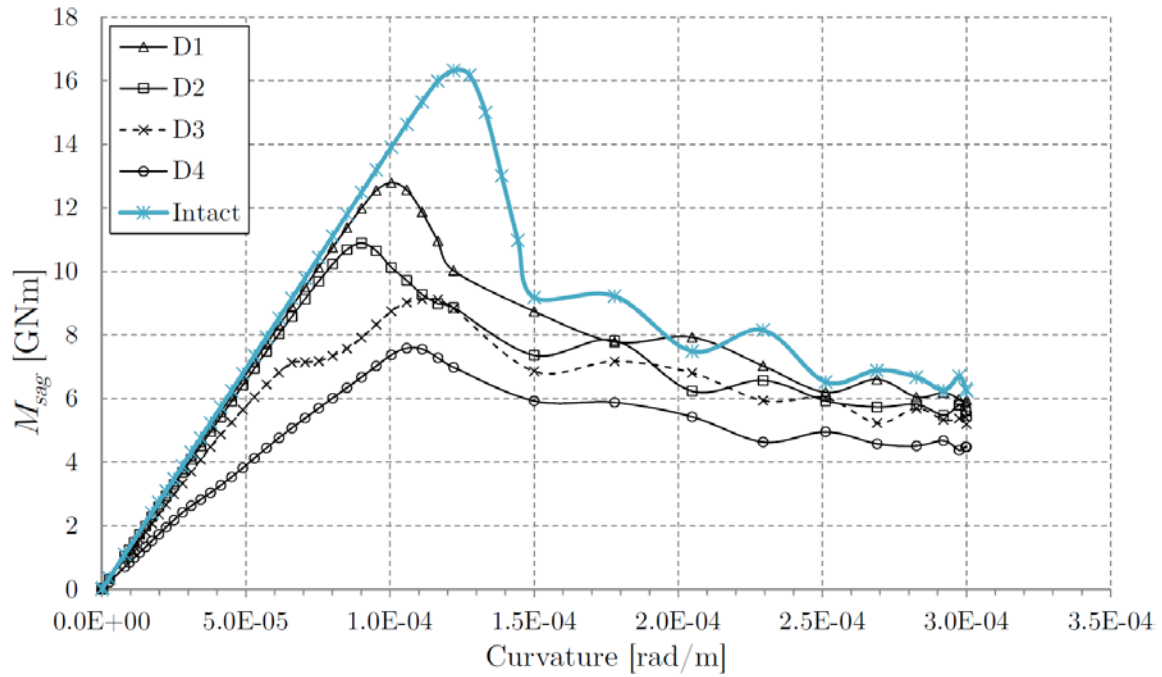


Figure 117: Bulk Carrier – Collision Damage D1-D4 (Sagging)

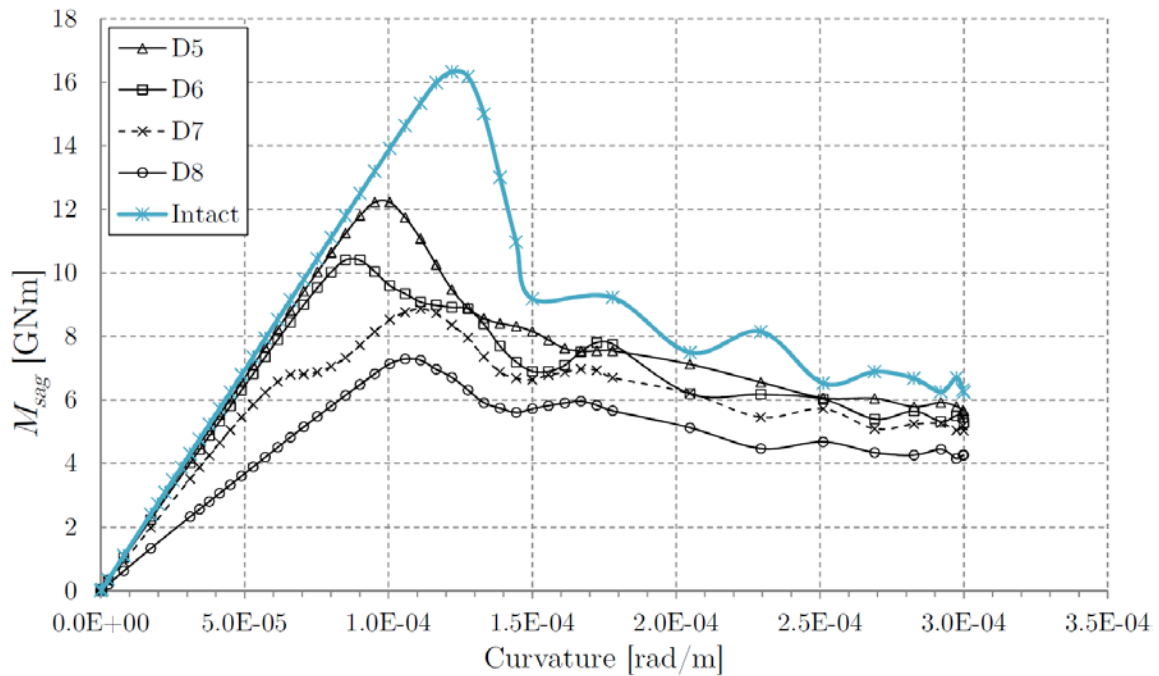


Figure 118: Bulk Carrier – Collision Damage D5-D8 (Sagging)

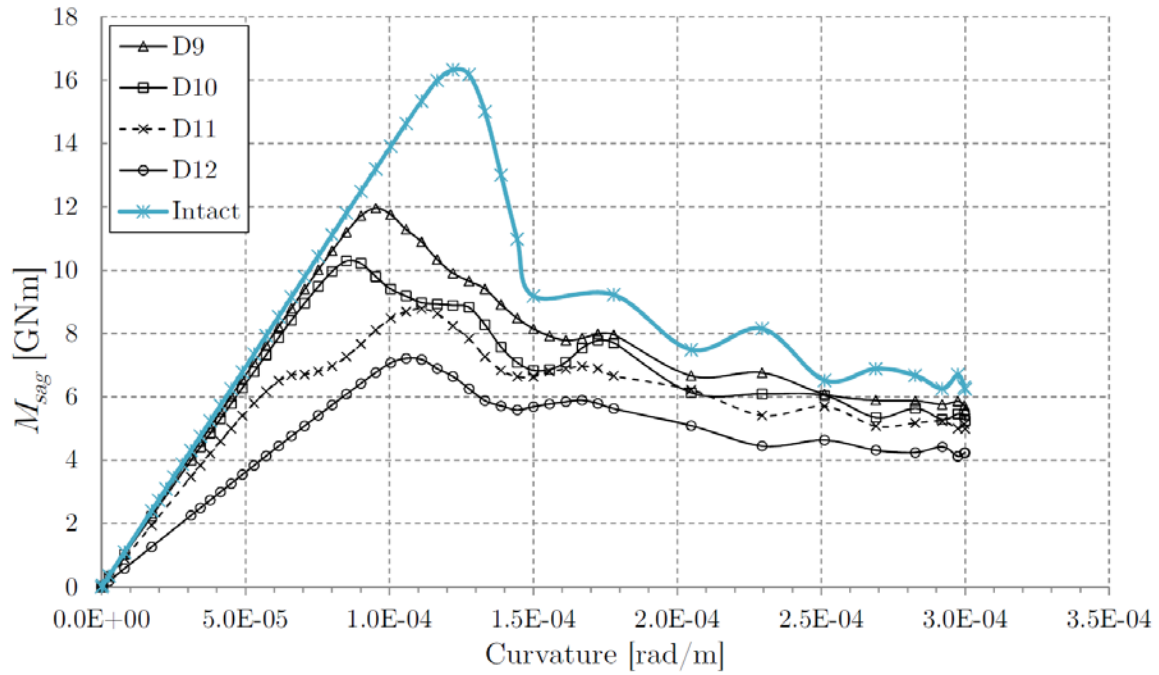


Figure 119: Bulk Carrier – Collision Damage D9-D12 (Sagging)

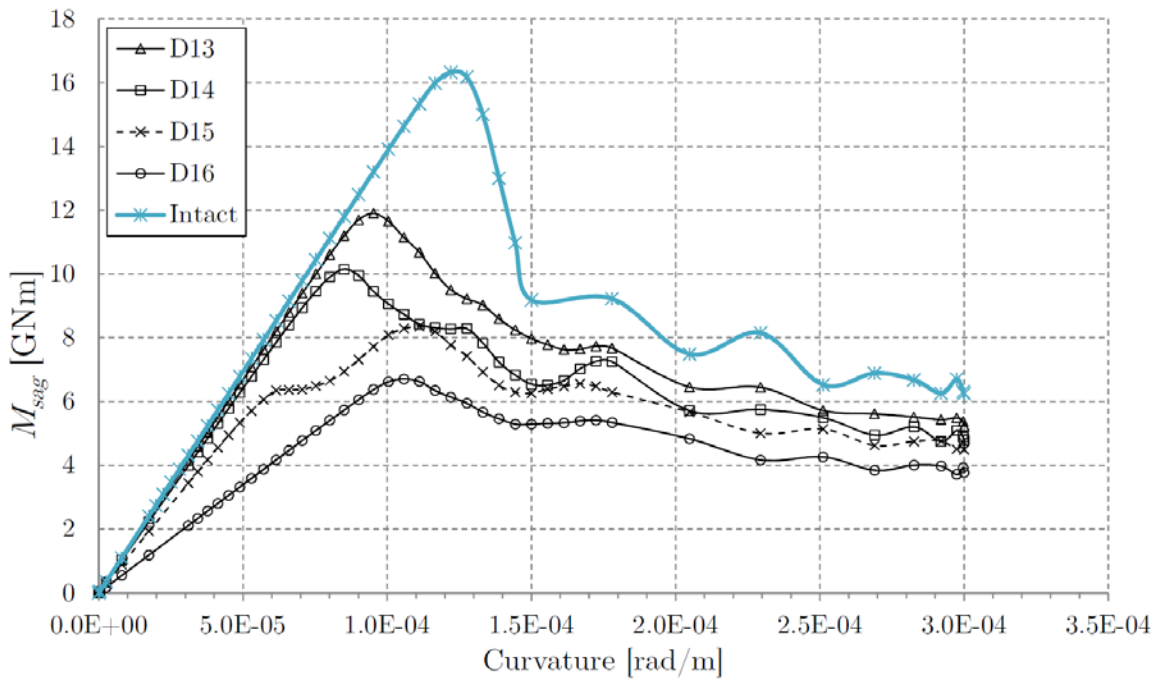


Figure 120: Bulk Carrier – Collision Damage D13-D16 (Sagging)

9.12 Bulk Carrier – Collision Damage (Hogging)

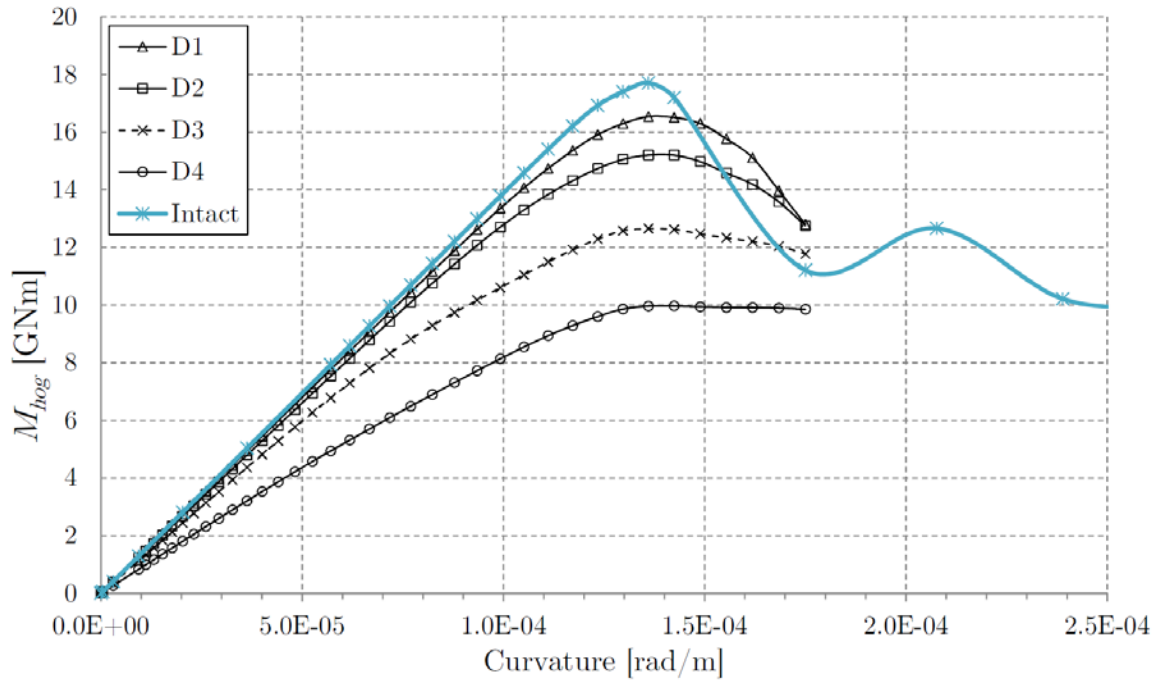


Figure 121: Bulk Carrier – Collision Damage D1-D4 (Hogging)

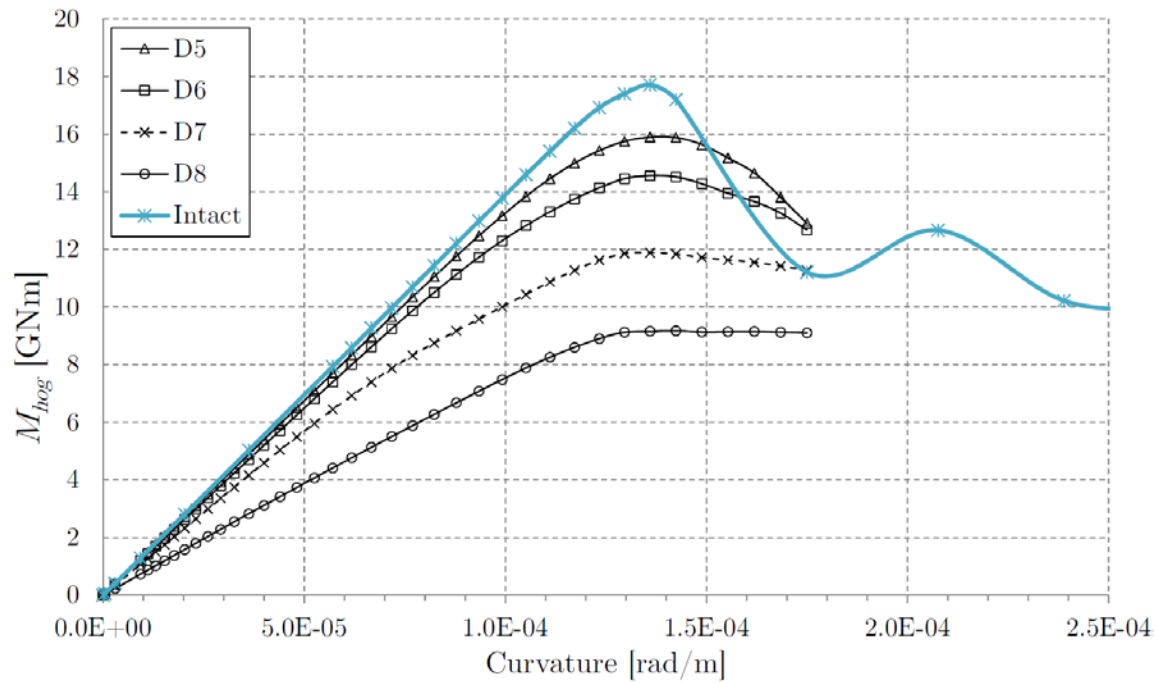


Figure 122: Bulk Carrier – Collision Damage D5-D8 (Hogging)

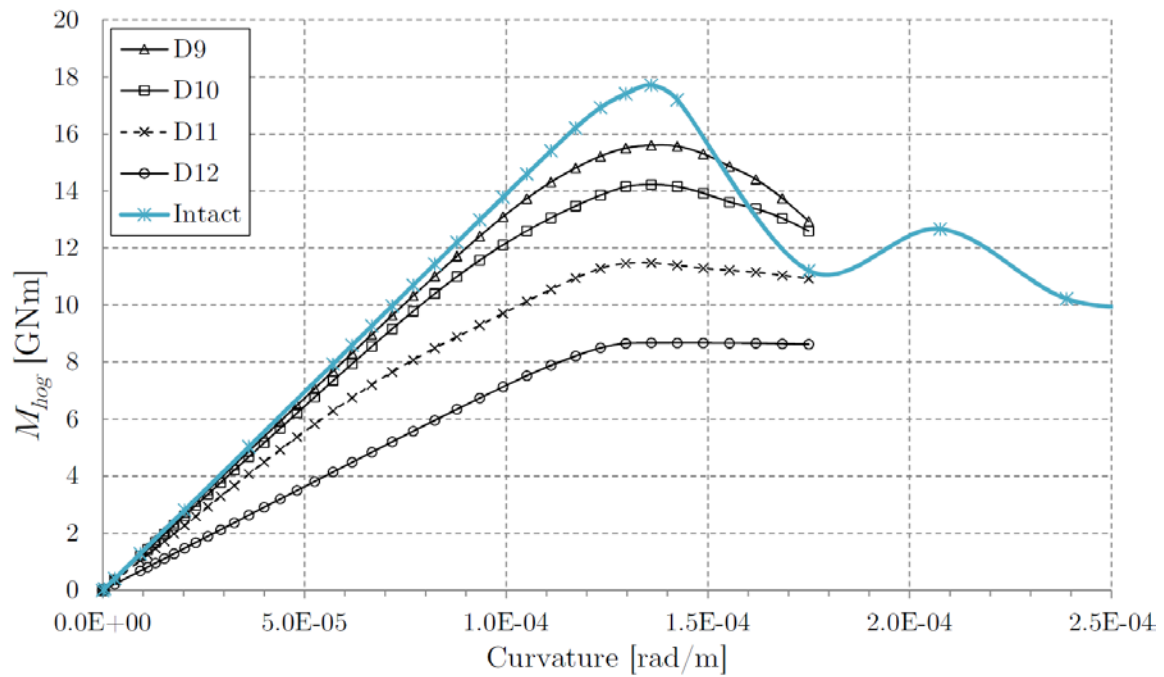


Figure 123: Bulk Carrier – Collision Damage D9-D12 (Hogging)

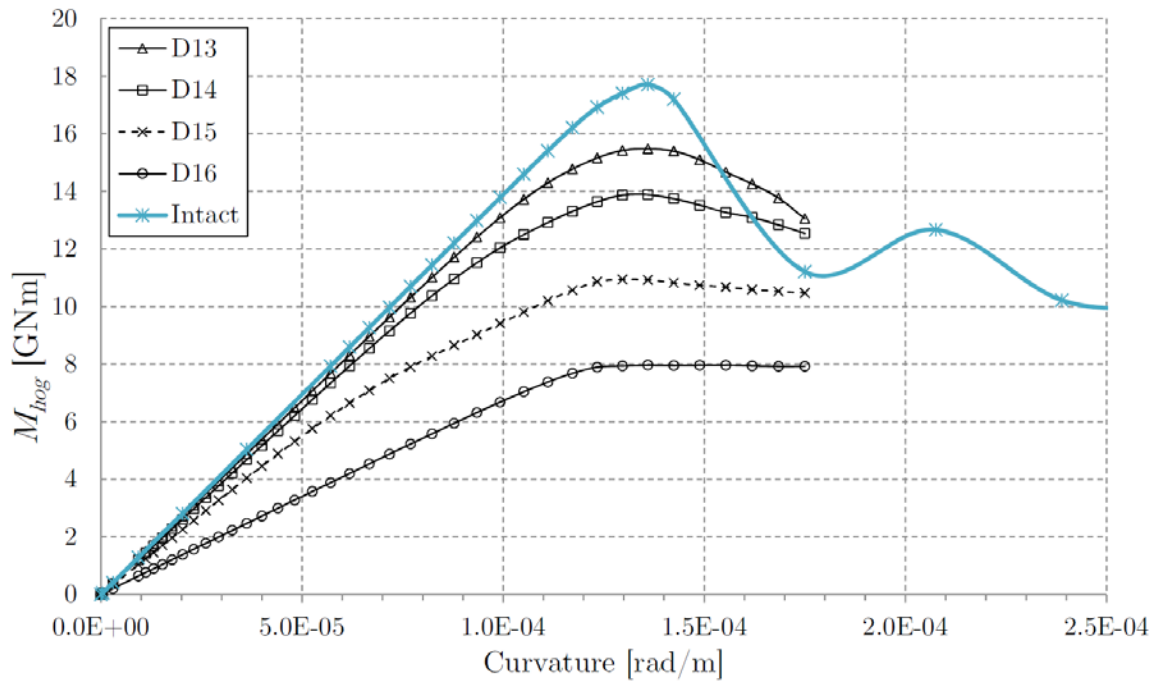


Figure 124: Bulk Carrier – Collision Damage D13-D16 (Hogging)

9.13 Bulk Carrier – Grounding Damage (Hogging)

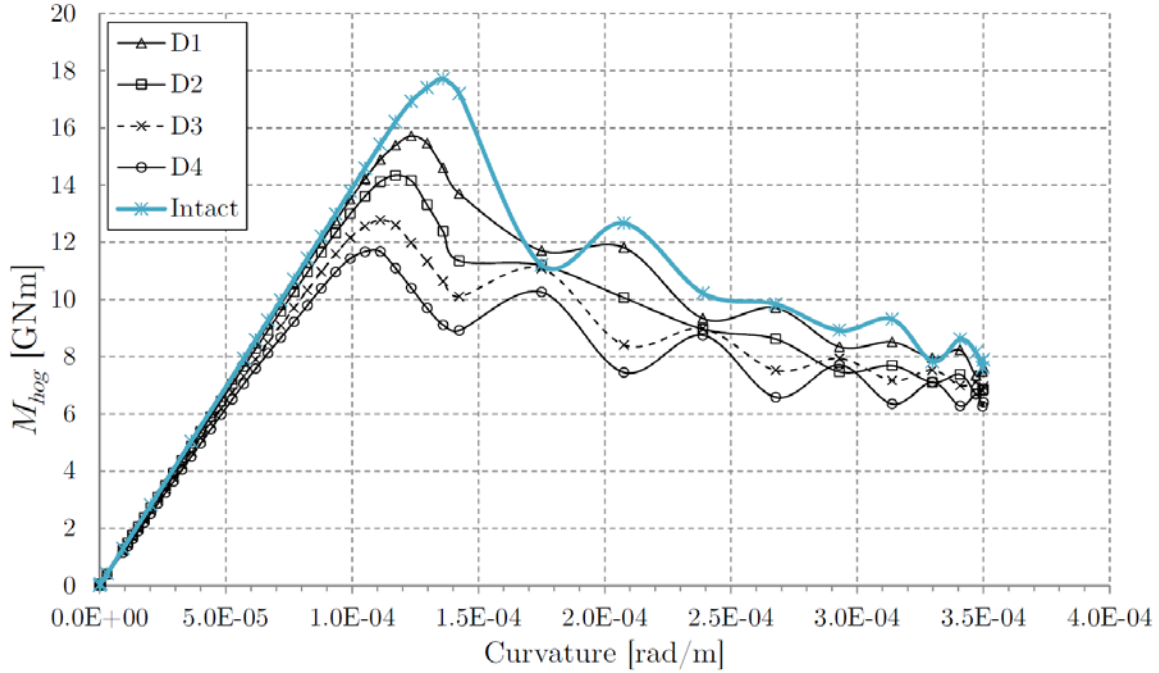


Figure 125: Bulk Carrier – Grounding Damage D1-D4 (Hogging)

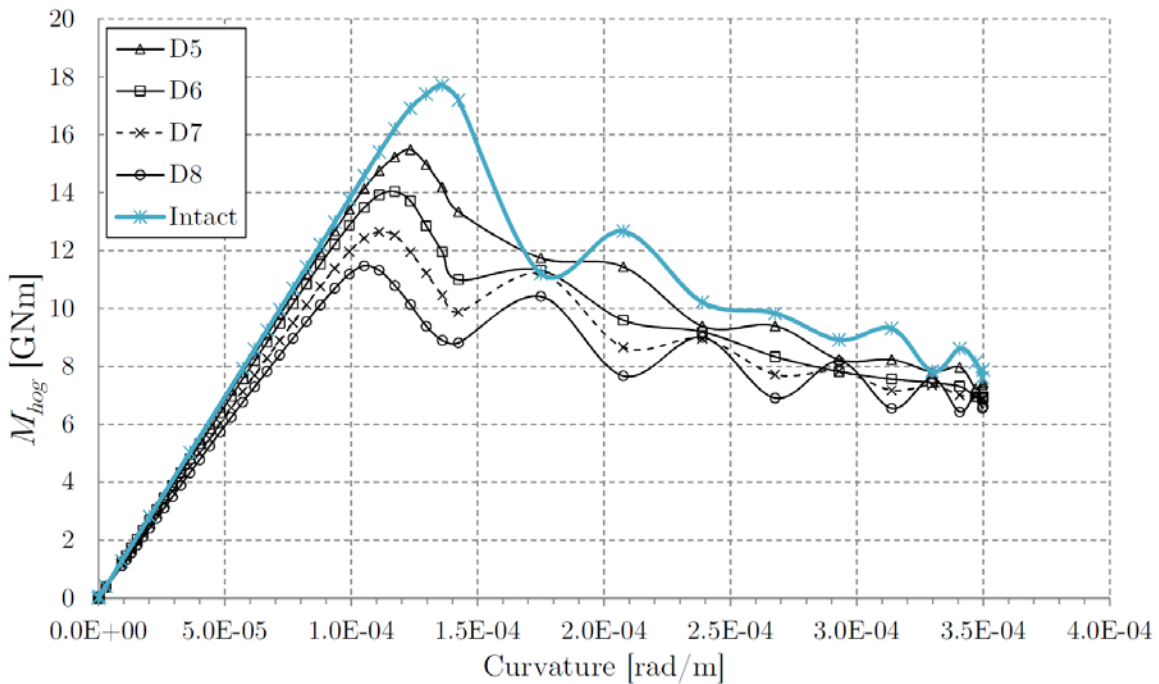


Figure 126: Bulk Carrier – Grounding Damage D5-D8 (Hogging)

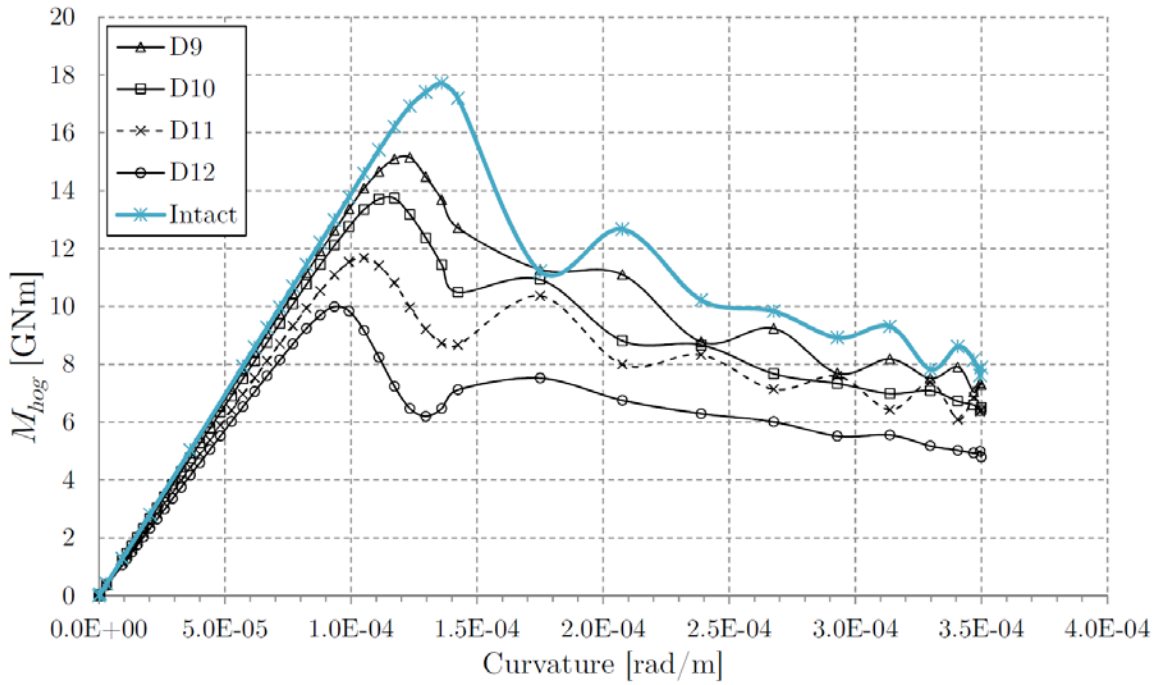


Figure 127: Bulk Carrier – Grounding Damage D9-D12 (Hogging)

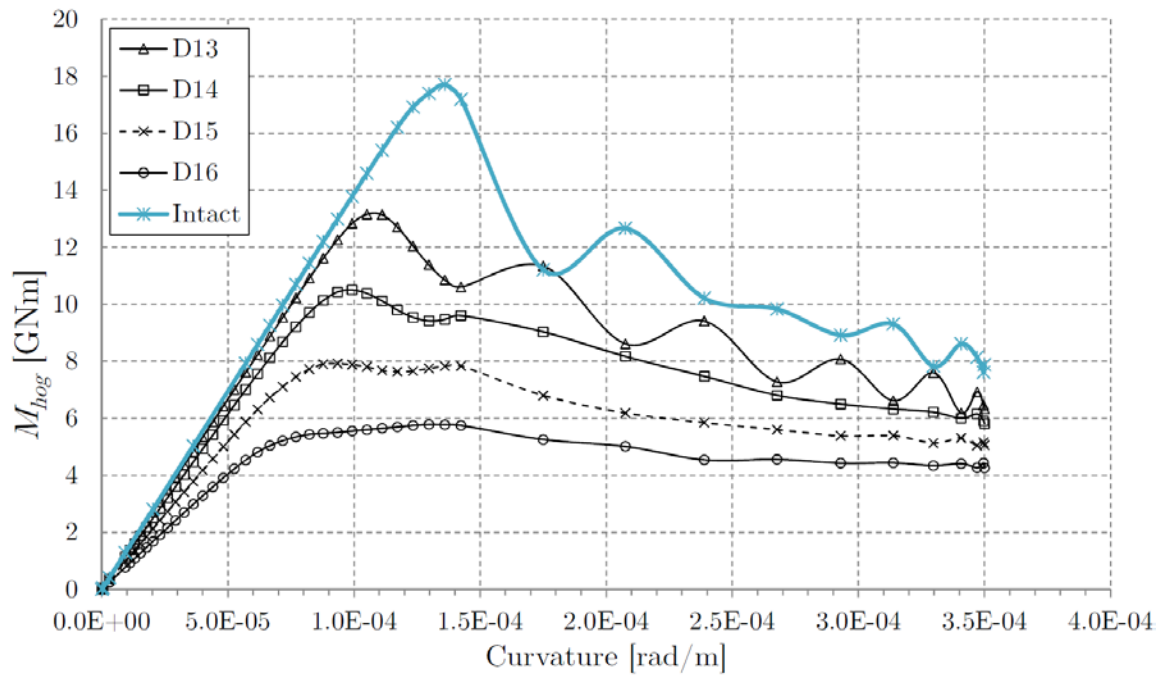


Figure 128: Bulk Carrier – Grounding Damage D13-D16 (Hogging)

9.14 Bulk Carrier – Grounding Damage (Sagging)

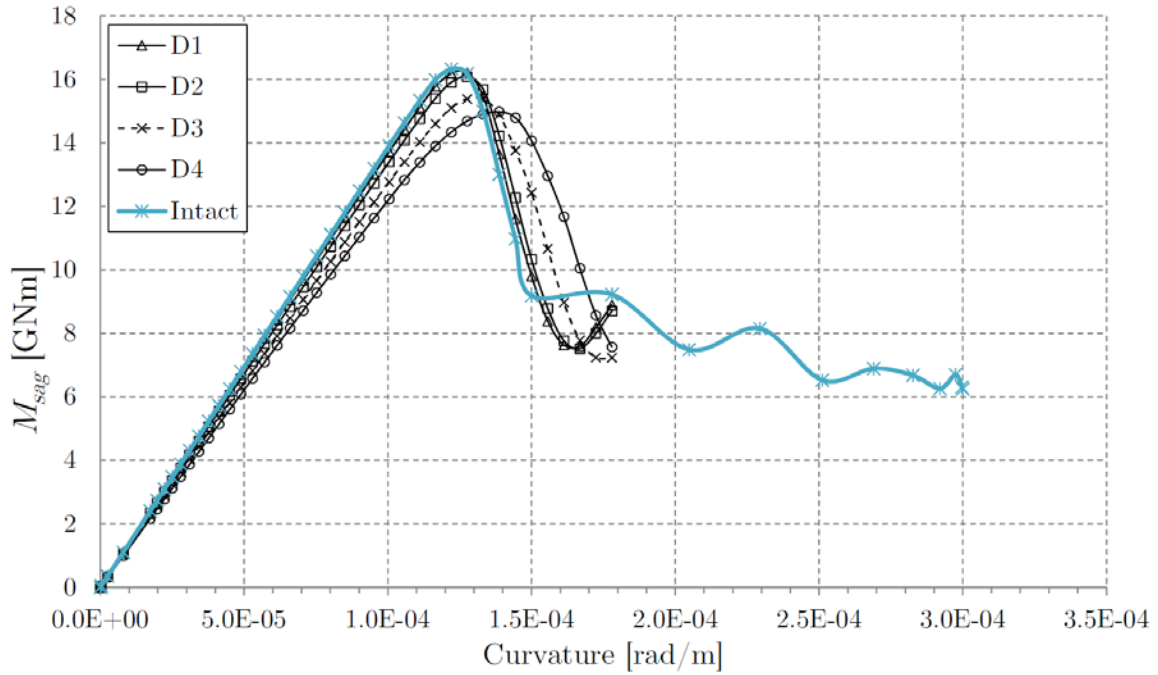


Figure 129: Bulk Carrier – Grounding Damage D1-D4 (Sagging)

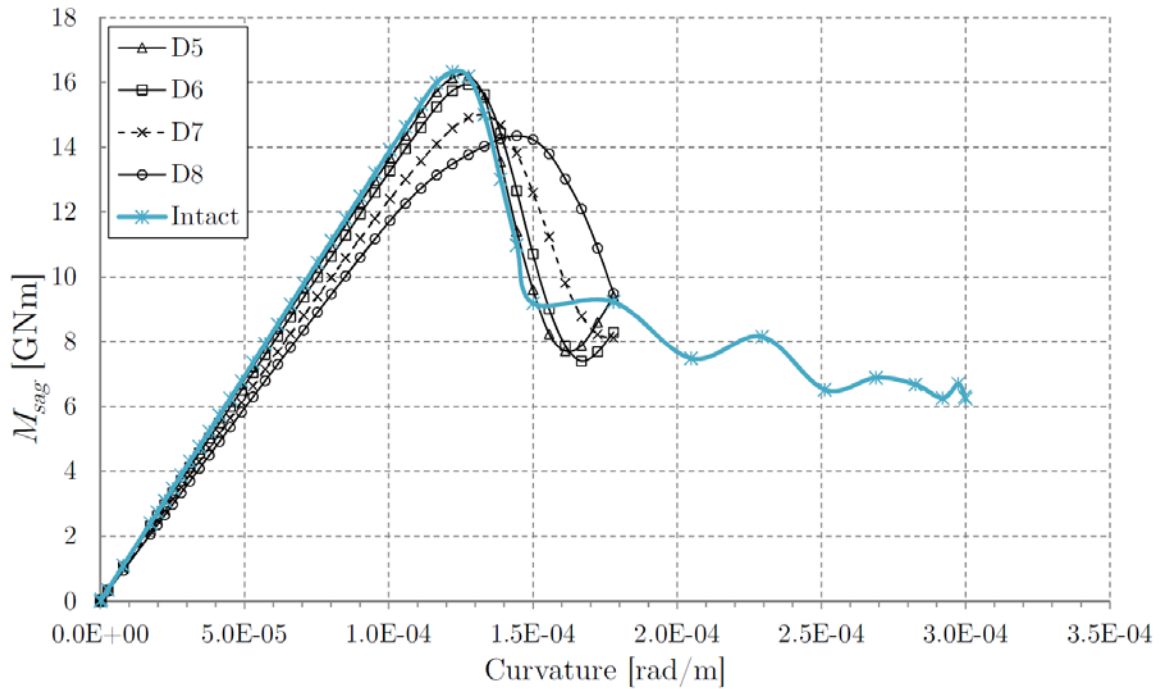


Figure 130: Bulk Carrier – Grounding Damage D5-D8 (Sagging)

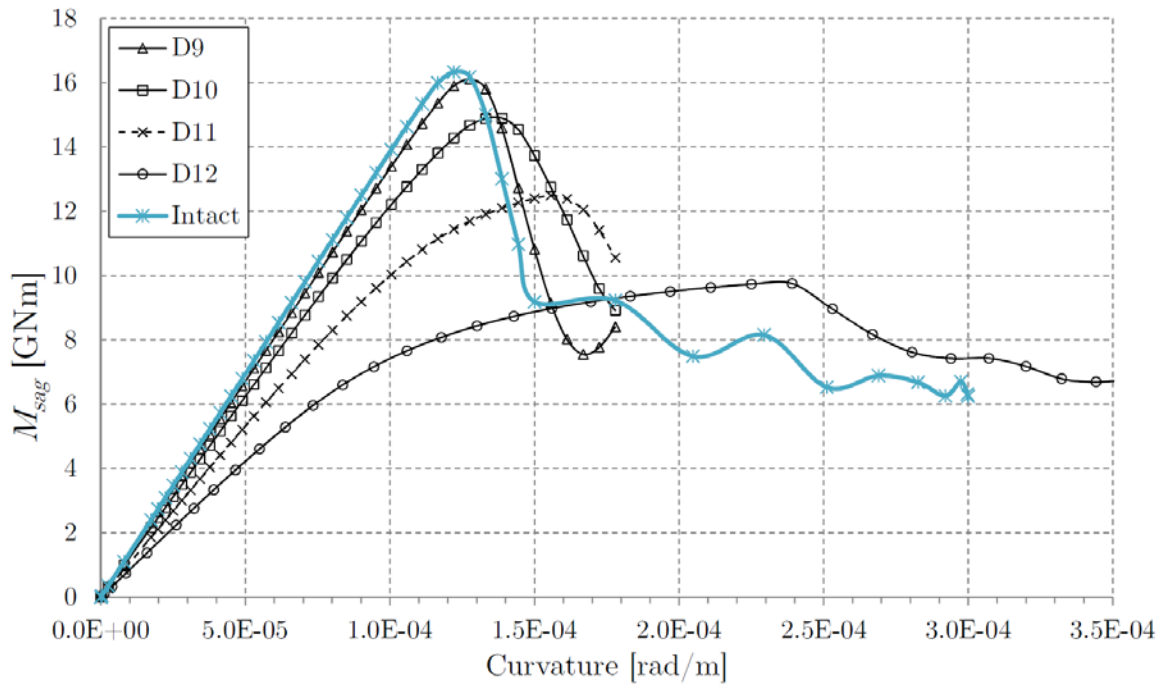


Figure 131: Bulk Carrier – Grounding Damage D9-D12 (Sagging)

9.15 Containership – Collision Damage (Sagging)

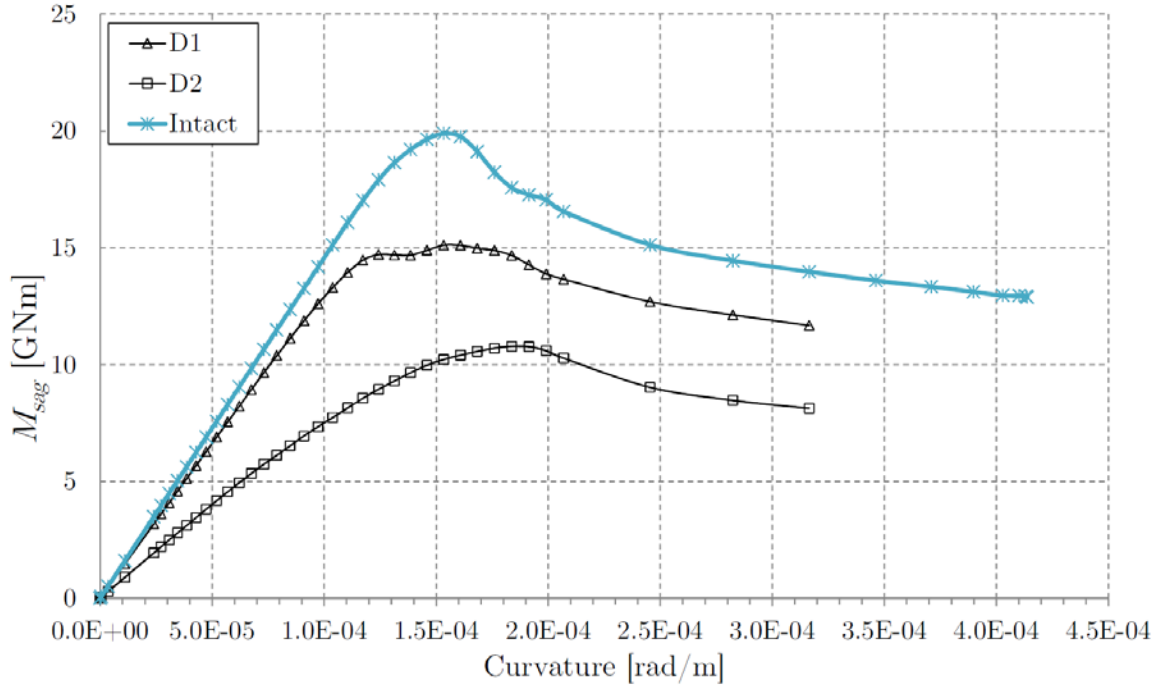


Figure 132: Containership – Collision Damage D1-D2 (Sagging)

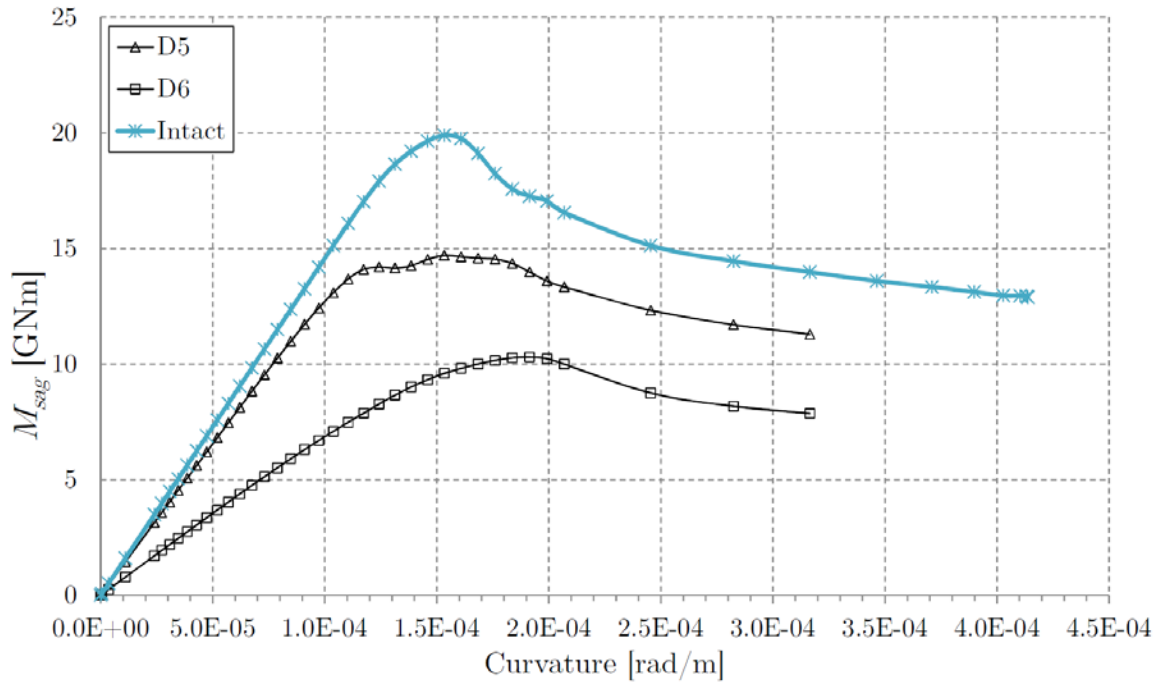


Figure 133: Containership – Collision Damage D5-D6 (Sagging)

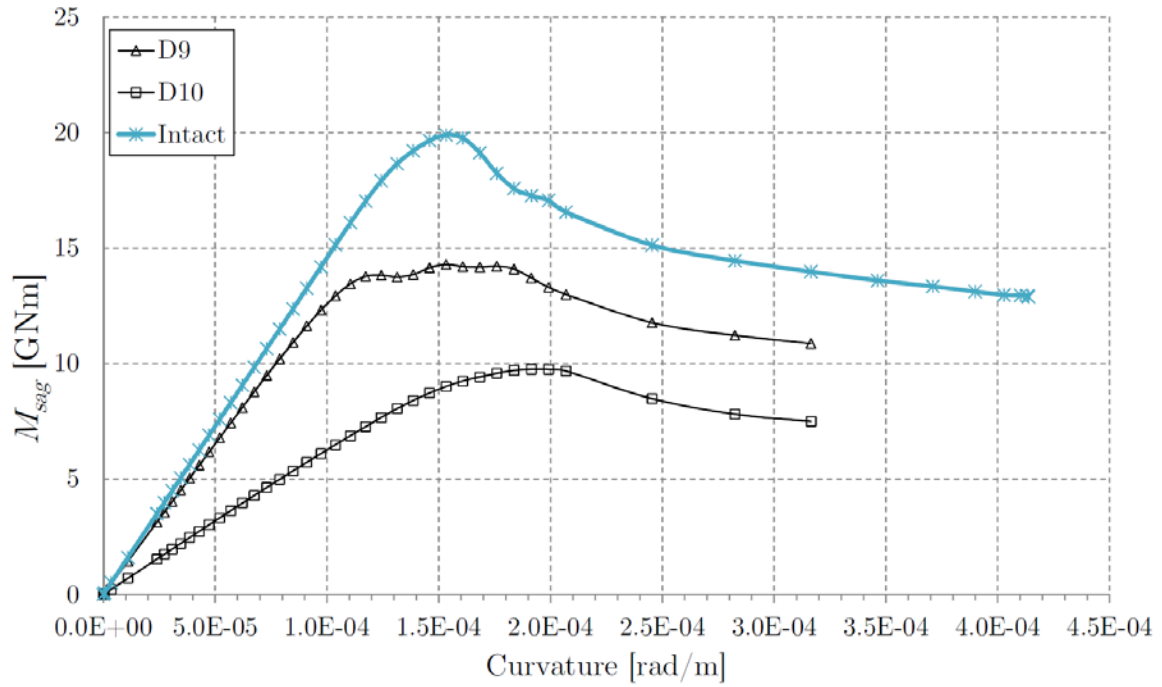


Figure 134 Containership – Collision Damage D9-D10 (Sagging)

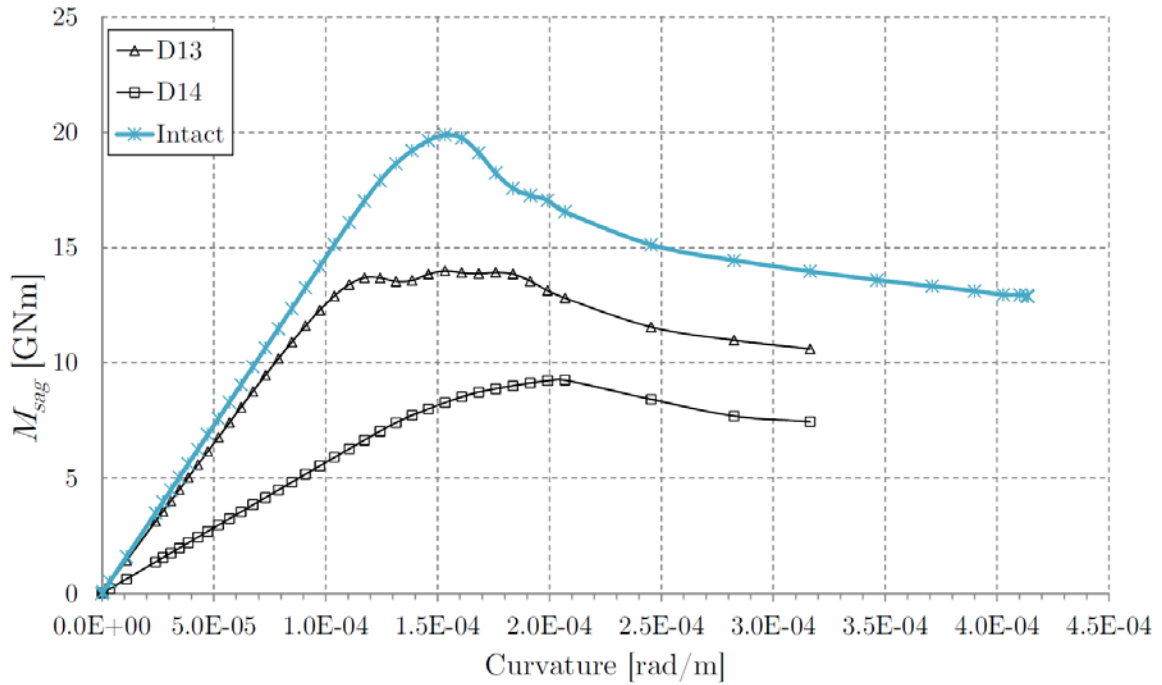


Figure 135: Containership – Collision Damage D13-D14 (Sagging)

9.16 Containership – Collision Damage (Hogging)

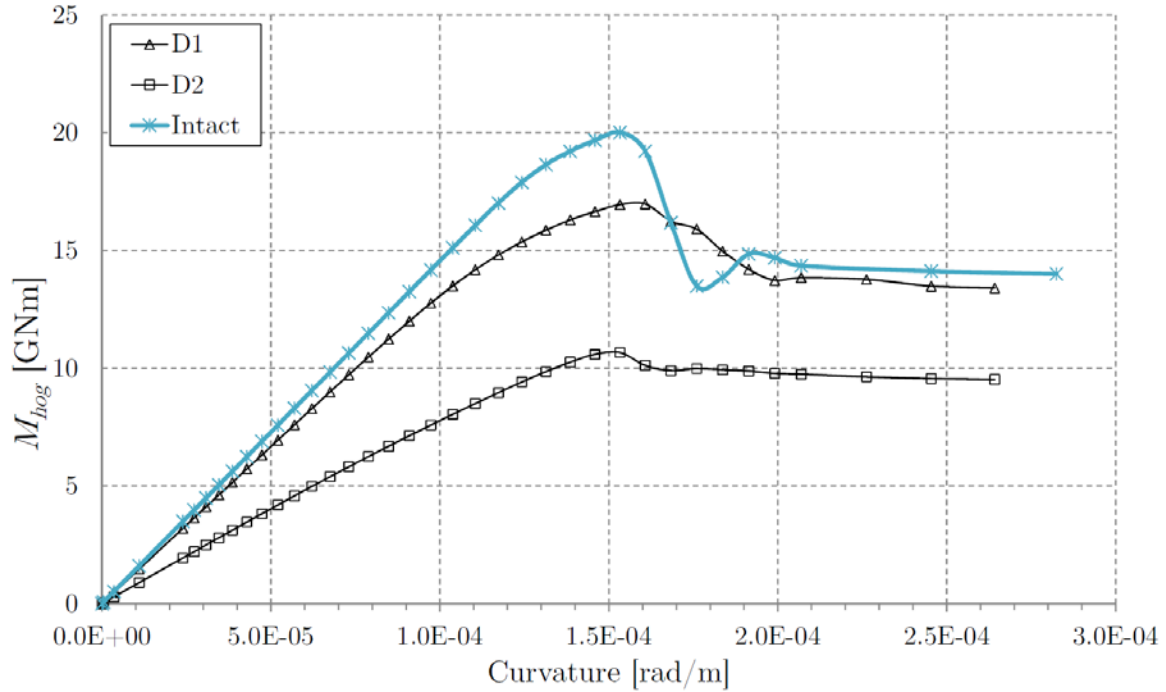


Figure 136: Containership – Collision Damage D1-D2 (Hogging)

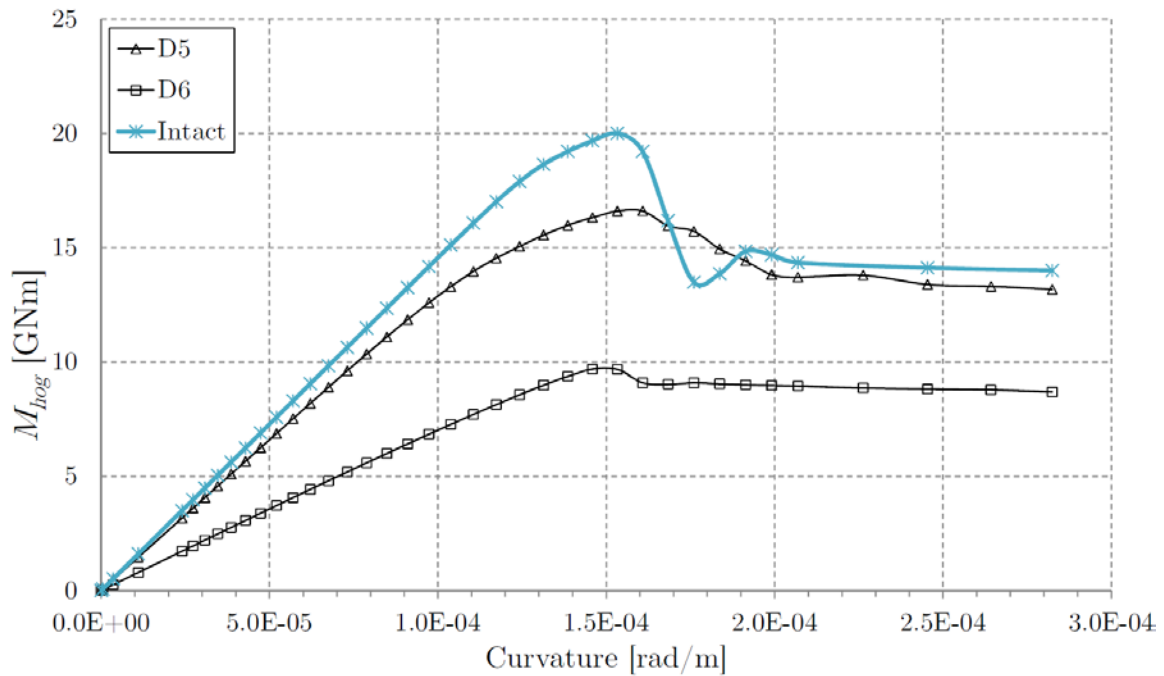


Figure 137: Containership – Collision Damage D5-D6 (Hogging)

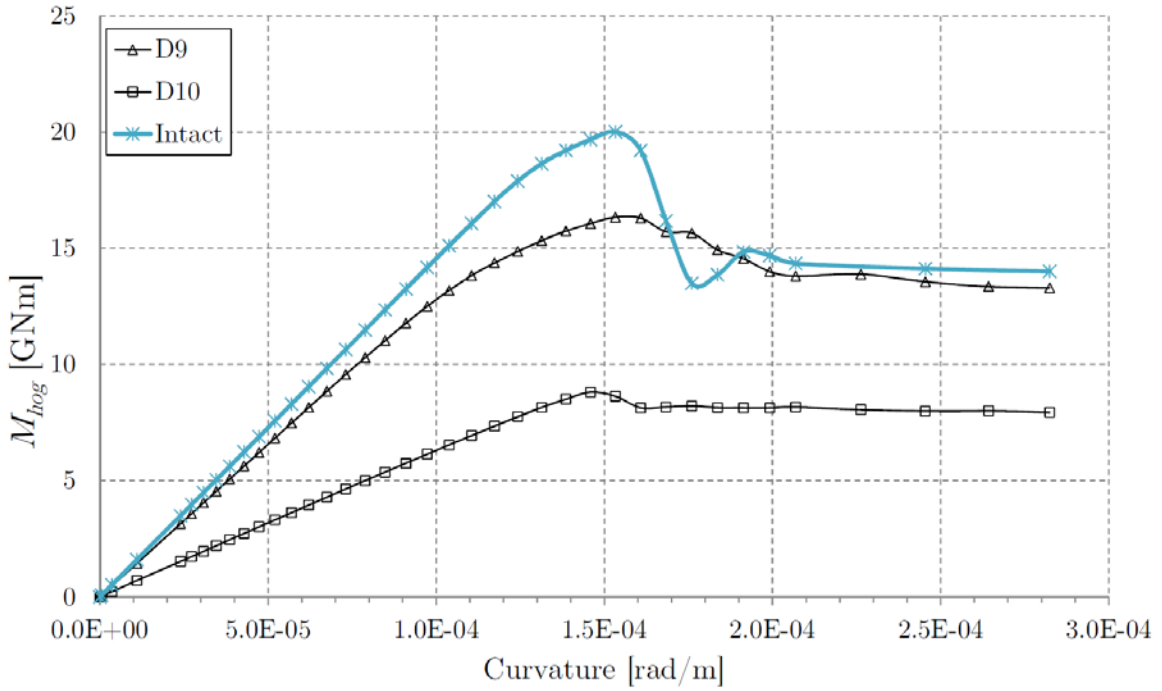


Figure 138: Containership – Collision Damage D9-D10 (Hogging)

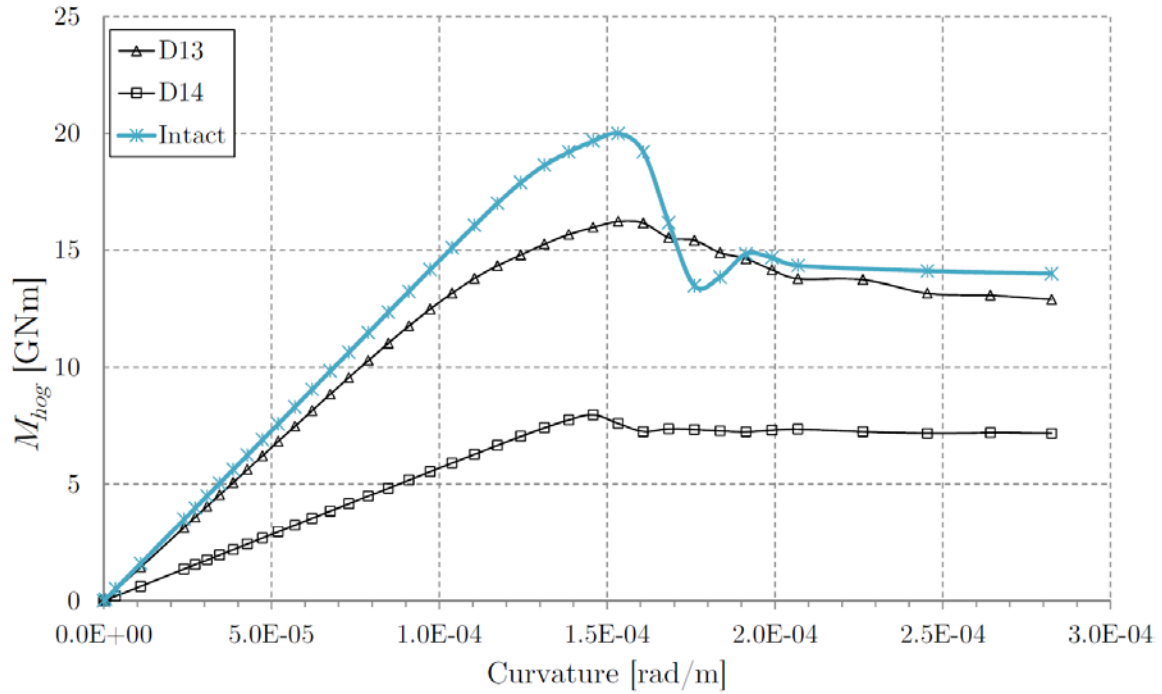


Figure 139: Containership – Collision Damage D13-D14 (Hogging)

9.17 Containership – Grounding Damage (Hogging)

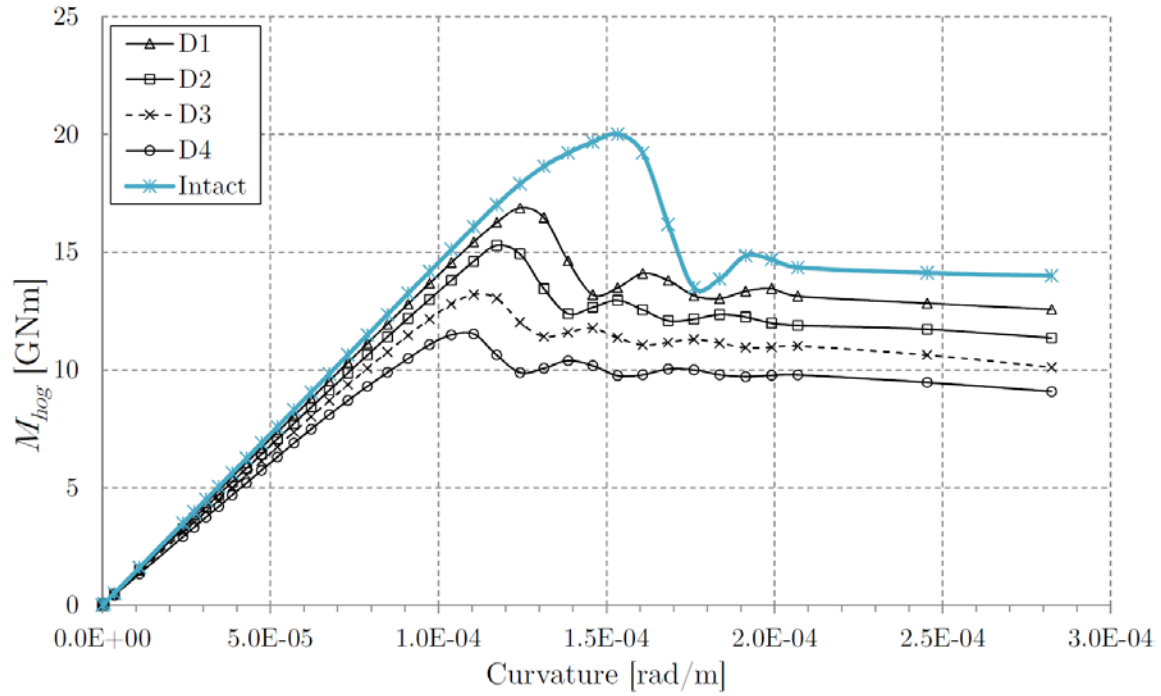


Figure 140: Containership – Grounding Damage D1-D4 (Hogging)

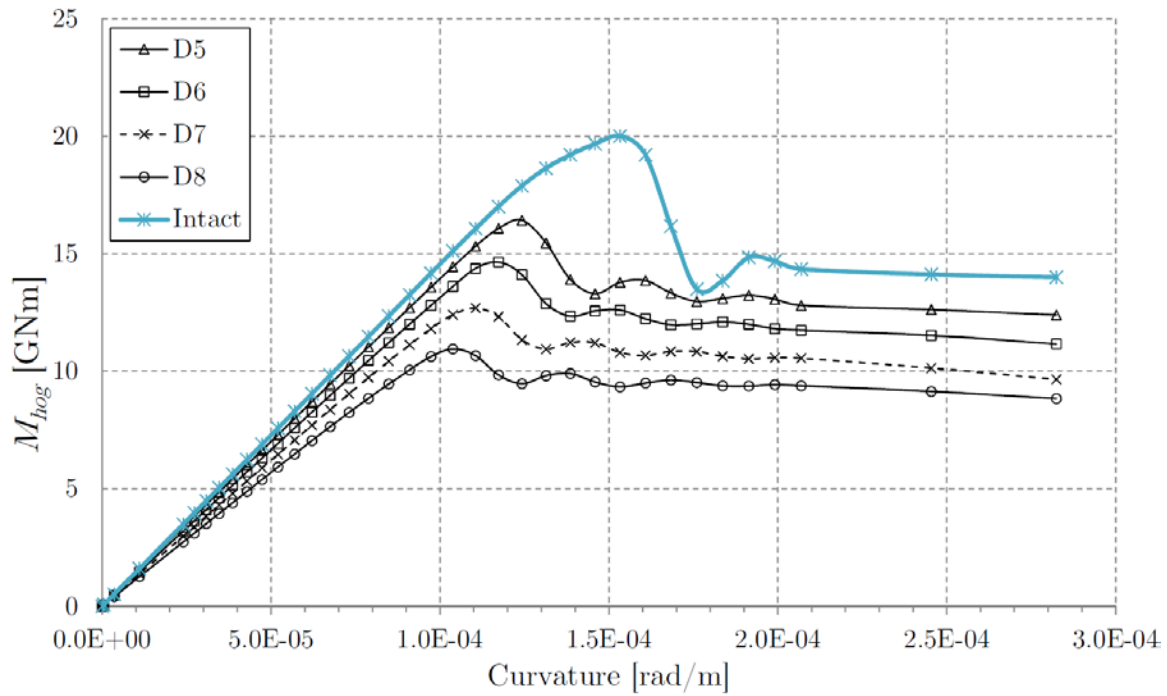


Figure 141: Containership – Grounding Damage D5-D8 (Hogging)

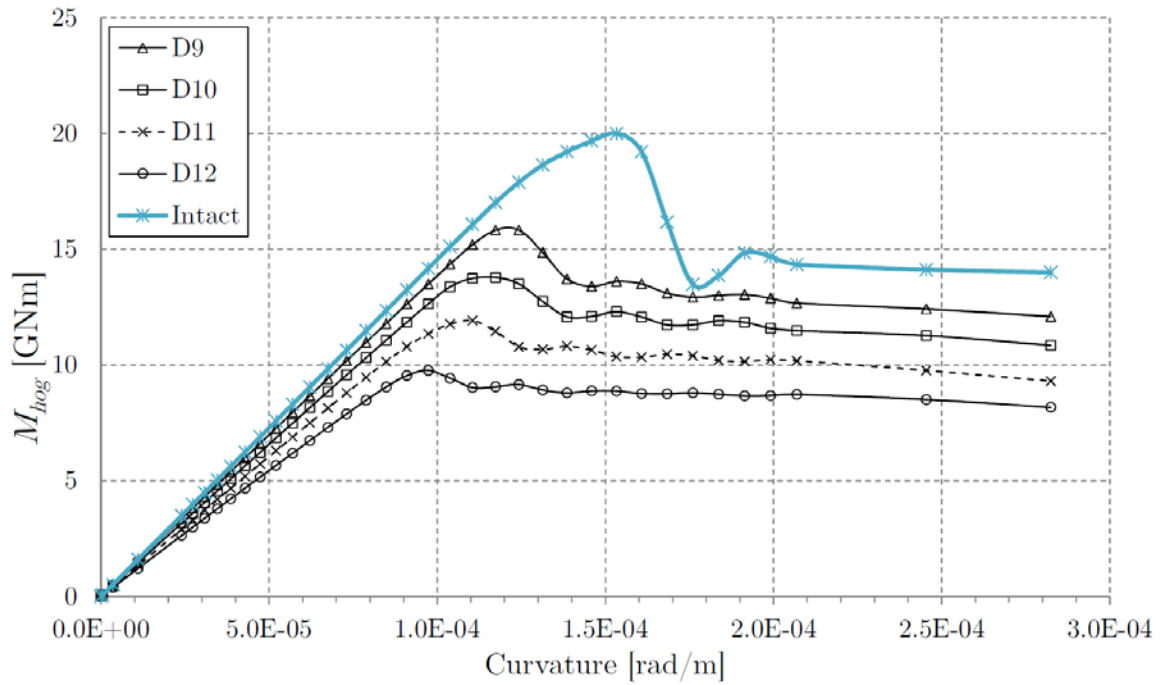


Figure 142: Containership – Grounding Damage D9-D12 (Hogging)

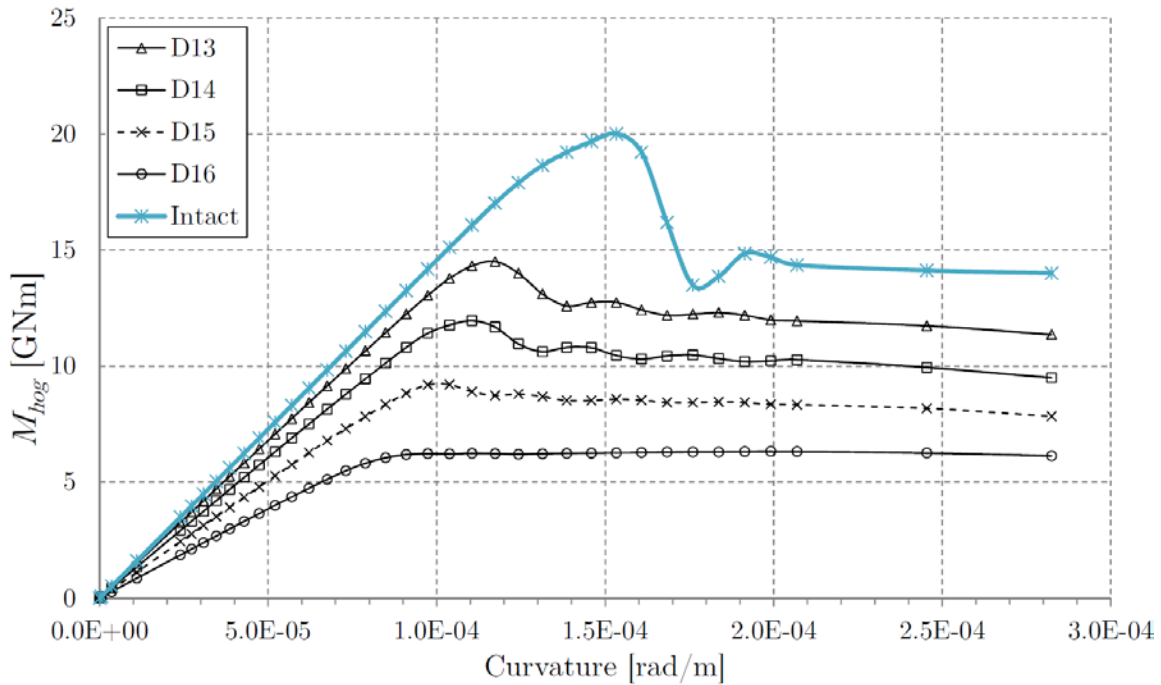


Figure 143: Containership – Grounding Damage D13-D16 (Hogging)

9.18 Containership – Grounding Damage (Sagging)

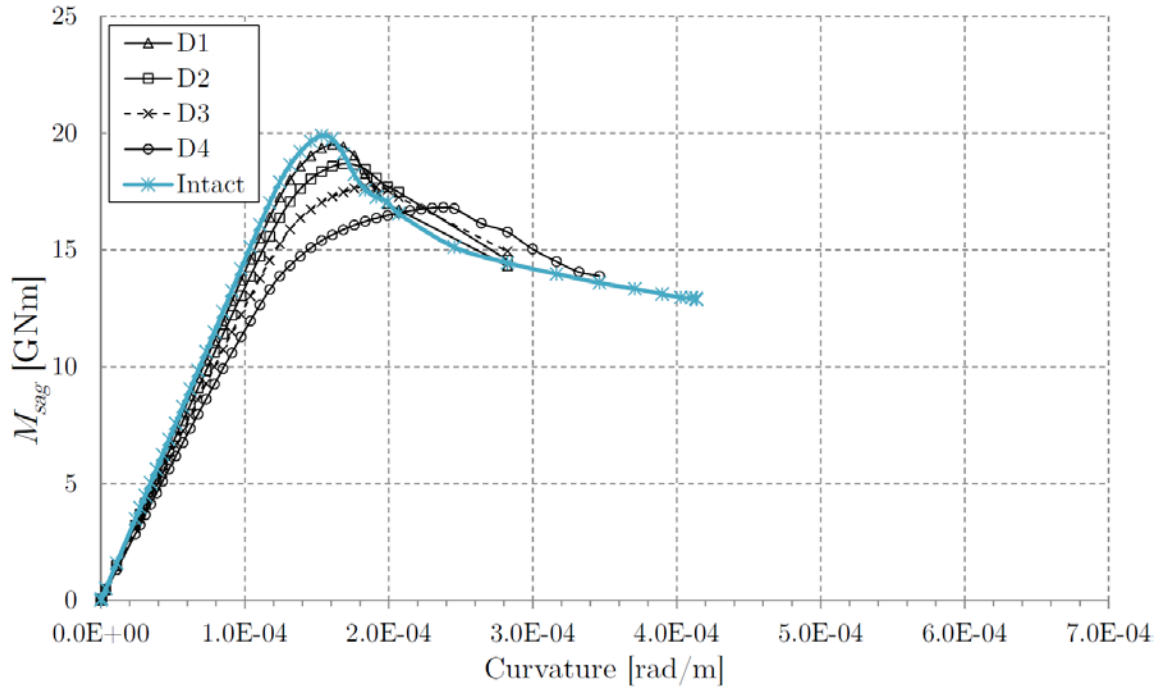


Figure 144: Containership – Grounding Damage D1-D4 (Sagging)

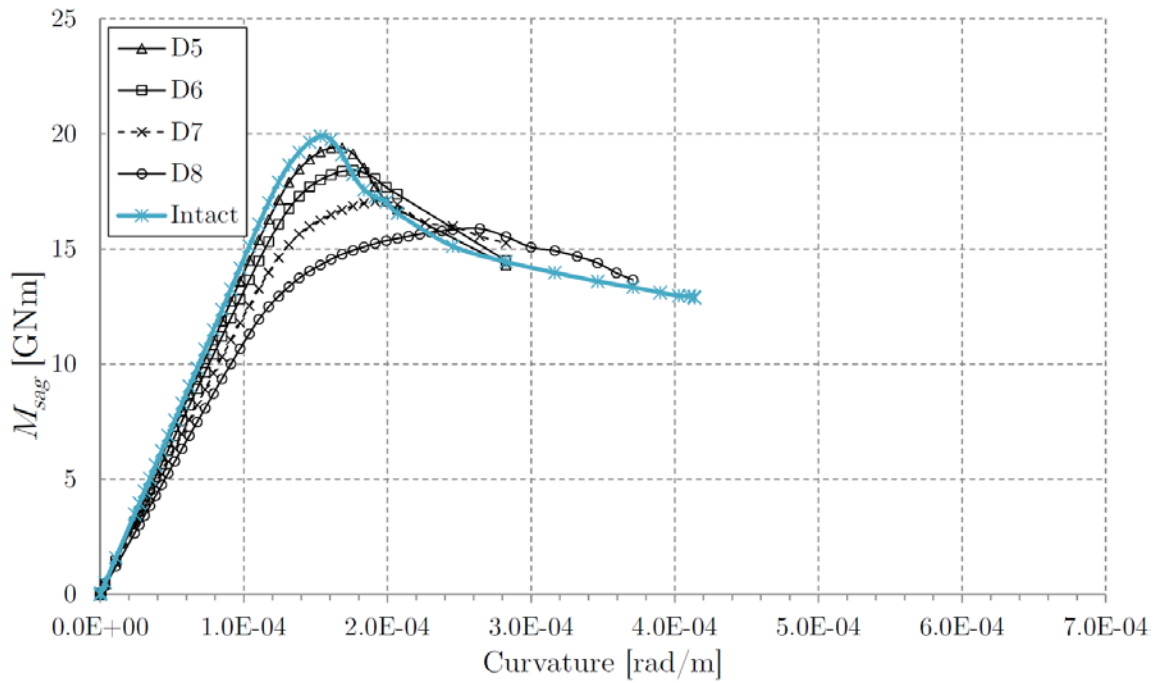


Figure 145: Containership – Grounding Damage D5-D8 (Sagging)

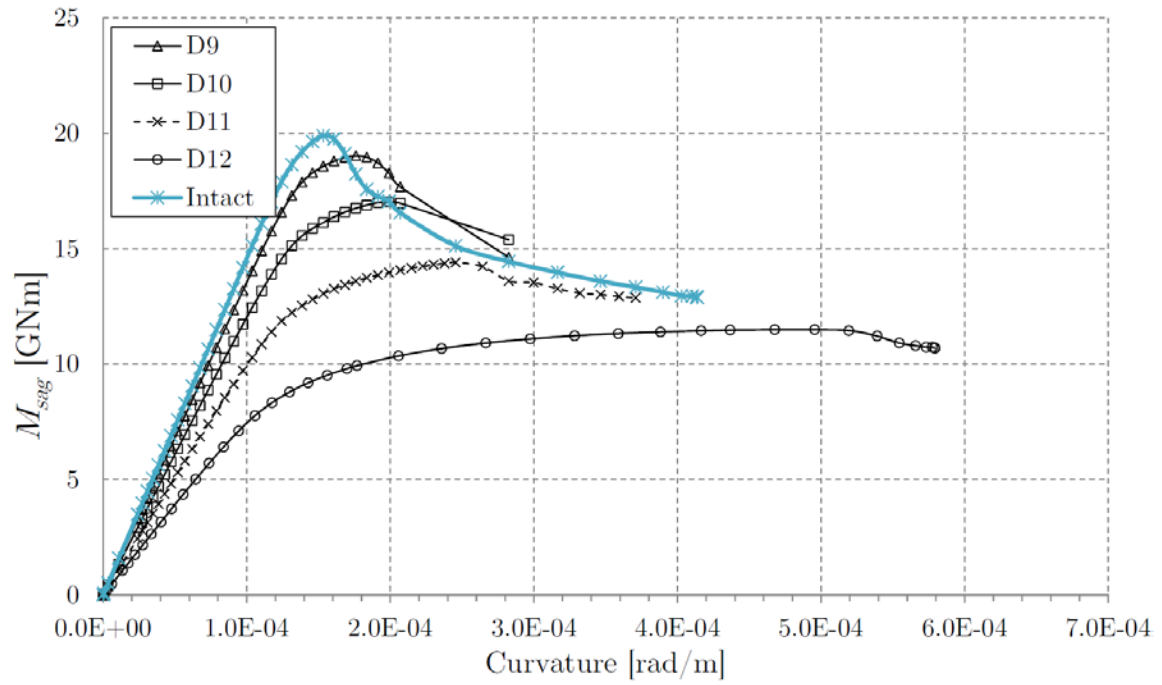


Figure 146: Containership – Grounding Damage D9-D12 (Sagging)

SHIP STRUCTURE COMMITTEE LIAISON MEMBERS

LIAISON MEMBERS

American Society of Naval Engineers	Captain Dennis K. Kruse (USN Ret.)
Bath Iron Works	Mr. Steve Tarpay
Colorado School of Mines	Dr. Stephen Liu
Edison Welding Institute	Mr. Rich Green
International Maritime Organization	Mr. Igor Ponomarev
Int'l Ship and Offshore Structure Congress	Dr. Alaa Mansour
INTERTANKO	Mr. Dragos Rauta
Massachusetts Institute of Technology	
Memorial University of Newfoundland	Dr. M. R. Haddara
National Cargo Bureau	Captain Jim McNamara
National Transportation Safety Board - OMS	Dr. Jack Spencer
Office of Naval Research	Dr. Yapa Rajapaksie
Oil Companies International Maritime Forum	Mr. Phillip Murphy
Samsung Heavy Industries, Inc.	Dr. Satish Kumar
United States Coast Guard Academy	Commander Kurt Colella
United States Merchant Marine Academy	William Caliendo / Peter Web
United States Naval Academy	Dr. Ramswar Bhattacharyya
University of British Columbia	Dr. S. Calisal
University of California Berkeley	Dr. Robert Bea
Univ. of Houston - Composites Eng & Appl.	
University of Maryland	Dr. Bilal Ayyub
University of Michigan	Dr. Michael Bernitsas
Virginia Polytechnic and State Institute	Dr. Alan Brown
Webb Institute	Prof. Roger Compton

RECENT SHIP STRUCTURE COMMITTEE PUBLICATIONS

Ship Structure Committee Publications on the Web - All reports from SSC 1 to current are available to be downloaded from the Ship Structure Committee Web Site at URL:

<http://www.shipstructure.org>

SSC 445 – SSC 393 are available on the SSC CD-ROM Library. Visit the National Technical Information Service (NTIS) Web Site for ordering hard copies of all SSC research reports at

URL: <http://www.ntis.gov>

SSC Report No.	Report Bibliography
SSC 471	Structural Load Prediction for High-Speed Planing Craft Akers, R.H. 2015
SSC 470	Finite Element Modeling Methods: Vibration Analysis For Ships Spence, J. H.; Favini, E. A.; Page, C. A. 2015
SSC 469	Strength And Fatigue Testing Of Composite Patches For Ship Plating Fracture Repair Karr, D.G.; Baloglu, C.; Cao, T.J.; Douglas, A.; Nielsen, K.; Ong, K.T.; Rohrback, B.; and Si, N. 2015
SSC 468	Development of a Structural Health Monitoring Prototype for Ship Structures Grisso, B.L 2013
SSC 467	Incorporation of Residual Stress Effects in a Plasticity and Ductile Fracture Model for Reliability Assessments of Aluminum Ship Hayden, M.J.; Gao, X.; Zhou, J.; Joyce, J.A. 2013
SSC 466	Mean Stress Assessment in Fatigue Analysis and Design Yuen, B.K.; Koko, T.S.; Polezhayeva, H.; Jiang, L 2013
SSC 465	Predictive Modeling Impact of Ice on Ship and Offshore Structures Bueno A. 2012
SSC 464	Design and Detailing for High Speed Aluminum Vessels Design Guide and Training Mish, W Jr.; Lynch, T.; Hesse, E.; Kulis, J.; Wilde, J.; Snyder, Z.; Ruiz, F. 2012
SSC 463	Marine Composites NDE, Inspection Techniques for Marine Composite Construction Greene, E 2012
SSC 462	Review of Current Practices of Fracture Repair Procedures for Ship Structures Wang, G, Khoo, E., ABS Corporate Technology 2012
SSC 461	Structural Challenges Faced By Arctic Ships, Kendrick A., Daley C. 2011
SSC 460	Effect of Welded Properties on Aluminum Structures, Sensharma P., Collette M., Harrington J. 2011
SSC 459	Reliability-Based Performance Assessment of Damaged Ships, Sun F., Pu Y., Chan H., Dow R.S., Shahid M., Das P.K. 2011